

Lawrence Daniel Howard Wood

FLUID DYNAMICS AND PULMONARY VENTILATION

THE EFFECT OF GAS PHYSICAL PROPERTIES AND FLOW RATE
ON PULMONARY VENTILATION AND GAS EXCHANGE

A thesis
presented to
McGill University

In Partial Fulfilment of
the Requirements for the Degree of
Doctor of Philosophy

by

Lawrence Daniel Howard Wood

1974

Praise to You, Lord, King of eternal glory.

ACKNOWLEDGEMENTS

During the course of the work reported in this thesis, I received abundant assistance without which progress would have been impossible. I am especially grateful to Dr. A. Charles Bryan for his stimulating and enthusiastic guidance during the early portion of this project; to Dr. Peter T. Macklem for his kindness, encouragement, supervision, financial support and particularly, for being a continual source of inspiration; and to Drs. Nick Anthonisen, Bjorn Bake, Ludwig Engel, Harold Menkes and J. Milic-Emili, as well as my supervisors, for the many stimulating conversations which fashioned most of the ideas presented herein.

I am also grateful to:

Drs. Paul Despas and Ludwig Engel and Mr. Peter Griffin for their assistance during the studies of lower pulmonary resistance.

Dr. Bjorn Bake for his equal participation in the investigation of regional distribution of inspired gas, and Mr. Brian Murphy, for performing a major part of the mathematical and electronic analysis of lung models in that study.

Drs. Henry Levison, T. R. Weng and S. K. Bau for collaboration in the studies of gas exchange; Miss Anita Liwanag and W/O Bill Burgess for performing gas and blood analyses; and Capt. Bill Lewis and W/O Bill Burgess for performing the tonometry studies.

The Surgeon-General and Officers commanding the Canadian Forces Institute of Environmental Medicine and the Naval Personnel Research Unit, for providing permission, facilities and technical assistance

during studies of exercise in hyperbaric conditions; and
Sgts. Murray Grieve and Eric Cox for constructing the
breathing circuit and operating the recording equipment
used during those investigations.

Mrs. Louise Murphy and Mrs. Sonya Olien for typing this manuscript.

Mr. Lionel Bartlett and W/O Tom Sproule for preparing illustrations,
and the Photography Sections of C.F.I.E.M., the Royal
Victoria Hospital, and the Health Sciences Centre, Winnipeg
for reproductions.

ABSTRACT

Gas transport between the atmosphere and alveoli is influenced by gas physical properties and flow rate (\dot{V}). These parameters were varied to study several mechanisms underlying the dynamics of pulmonary ventilation.

In living human and canine lungs, lower pulmonary resistance (R_{lp}) increased with gas density (ρ) and \dot{V} . In the dogs, flow in peripheral airways ($ld < 4$, mm) was laminar, so the effects of ρ and \dot{V} on R_{lp} occurred in central airways, where higher Reynolds numbers (Re) and the frequently branching pattern of bronchi prevent the growth of laminar boundary layers. Airways resistance was best explained by the equation $R = K \dot{V}^a \rho^a \mu^{1-a}$. The exponent 'a' reflects the proportion of inertial to viscous losses, and changes from 1.0 to zero according to the reduction in Re between glottis and peripheral airways. In healthy subjects breathing air at ambient pressures in excess of 4 Ata, maximum aerobic capacity was lowered by expiratory compression of intrathoracic airways. During submaximal exercise, CO_2 retention occurred at depth. These effects were due to increased ρ , so that healthy subjects breathing dense gas resembled patients with obstructive lung disease.

The regional distribution of gas inspired by seated subjects changed with \dot{V} according to differences in regional time constants (RC).

By increasing RC , greater ρ increased the \dot{V} dependence of regional distribution. This dynamic redistribution of ventilation occurs during quiet breathing, and is opposed by forces generated by the mechanical interaction of lung and chest wall. Concentration differences between upper (U) and lower (L) lung regions influenced the expired concentration vs volume relationship such that 'closing volume' is systematically underestimated when $U/L < 2$. Since the alveolar plateau was horizontal when $U/L \doteq 2$, its usual upward slope probably represents sequential emptying of parallel intraregional units having concentration differences $> 2:1$. Greater ρ improved pulmonary oxygen exchange by reducing intraregional \dot{V}_A/Q variance. Impaired inter-gas diffusion conceivably increased alveolar stratification of O_2 , thereby matching stratified perfusion. Alternatively, by enhancing mechanisms responsible for intraregional cardiogenic gas mixing, greater ρ reduced parallel inhomogeneity.

RESUME

Le transport des gaz entre l'atmosphère et les alvéoles est influencé par les propriétés physiques des gaz et le débit (\dot{V}). Nous avons modifié ces paramètres pour étudier plusieurs mécanismes responsables de la dynamique de la ventilation pulmonaire.

Chez l'homme et chez le chien, les résistances pulmonaires inférieures (R_{lp}) augmentent avec la densité (ρ) et \dot{V} . Chez le chien, le débit dans les voies aériennes périphériques (diamètre < 4 mm) est laminaire, de telle sorte que les effets de ρ et \dot{V} sur R_{lp} surviennent dans les voies aériennes centrales, où le nombre de Reynold (Re) élevé et la multiplicité des divisions bronchiques empêche le développement d'un écoulement laminaire. Les résistances des voies aériennes sont le mieux décrites par l'équation: $R = K \dot{V}^a \rho^a \mu^{1-a}$. L'exposant 'a' reflète le rapport entre les pertes liées à l'inertie et celles dues à la viscosité, et change de 1.0 à zéro selon la réduction de Re entre la glotte et les voies aériennes périphériques. Chez les sujets sains respirant de l'air à plus de 4 Ata, la capacité aérobie maximale diminue par la compression expiratoire des voies aériennes intrathoraciques. A l'exercice sousmaximal, il survient une rétention de CO_2 en profondeur. Ces effets sont liés à la ρ accrue, et ces sujets sains respirant un gaz dense ressemblent aux malades atteints d'un syndrome obstructif pulmonaire.

Chez le sujet assis la distribution régionale du gaz inspiré varie avec \dot{V} selon les différences des constantes de temps régionales (RC). En

augmentant RC, la densité accrue augmente la dépendance de la distribution régionale vis à vis \dot{V} . Cette redistribution dynamique de la ventilation survient en respiration calme, et est contrée par les forces produites par l'interaction mécanique du poumon et de la cage thoracique. Les différences de concentration entre le sommet (S) et la base (B) pulmonaire influence la relation concentration expirée/volume de sorte que le 'volume de fermeture' est systématiquement sous-estimé quand $S/B < 2$. Comme le plateau alvéolaire est horizontal quand $S/B \approx 2$, sa pente ascendante usuelle représente probablement la vidange séquentielle d'unités parallèles intrarégionales ayant des différences de concentration $> 2:1$. Une ρ augmentée améliore les échanges pulmonaires d'oxygène en réduisant la variation intrarégionale des $\dot{V}A/Q$. Une diffusion inter-gaz altérée augmente vraisemblablement la stratification alvéolaire de l'oxygène, s'ajustant ainsi à la perfusion stratifiée. L'alternative serait qu'en augmentant les mécanismes responsables du mélange gazeux intrarégional cardiogénique, une ρ accrue réduirait l'inhomogénéité parallèle.

LIST OF TABLES

TABLE		PAGE
1	Exponents Relating Resistance to Gas Physical Properties and Flow Rate	19
2	Geometric and Hydraulic Parameters of the Human Airway	22
3	Gas Physical Properties	24
4	Lung Volumes and Catheter Position During Resistance Measurements	88
5	Arterial Blood Gas Tensions	89
6	Coefficients of Variation	94
7	Effect of Gas Physical Properties and Flow Rate on R_{lp}	97
8	Effect of Gas Physical Properties on Partitioned Resistance	100
9	Effect of Flow Rate on Partitioned Resistance	102
10	Partitioned Resistance at 65% VC Pre Vagotomy	103
11	Partitioned Resistance at 35% VC Pre Vagotomy	104
12	Partitioned Resistance at 65% VC Post Vagotomy	105
13	Partitioned Resistance at 35% VC Post Vagotomy	106
14	Effect of Gas Physical Properties and Flow Rate on Human R_{lp}	118
15	Exponents Relating Gas Physical Properties and Flow Rate to R law	122
16	Physical Characteristics and Lung Volumes	128
17	Regional Counts at Equilibration (% of Total)	137
18	Results of Gas and Blood Analysis	182
19	The Effect of Gas Density on Pulmonary Gas Exchange	183

TABLE**PAGE**

20	Gas Density and Gas Exchange During Cardiac Catheterisation	184
21	Flow Rates and Resistances at Expiratory Flow Limitation	197
22	Cardio-Respiratory Parameters During Exercise (ACB)	202
23	Cardio-Respiratory Parameters During Exercise (LW)	203

LIST OF FIGURES

FIGURE		PAGE
1	Airways resistance per generation and bronchial P-V relationships as calculated from three fluid dynamic theories.	33
2	Relationship between regional and overall lung volumes.	43
3	Average regional ^{133}Xe concentration measured in eight vertical lung regions following bolus inspiration from different lung volumes.	45
4	Expired concentration versus volume curves from two subjects who inhaled ^{133}Xe bolus from RV while standing erect.	49
5	Effect of sequential emptying on regional lung volumes.	51
6	Schematic diagram of experimental apparatus.	86
7	Photograph of Poly viso recording of \dot{V} , P_c and P_p during forced oscillation at two lung volumes.	87
8	Values of R_c measured during air oscillations at 0.5 lps versus R_c predicted from values measured at 1 and 2 lps according to equation 1 and 2.	92
9	Comparison of resistance at 1 lps between air and SF_6 for central and peripheral airways.	99
10	Exponent 'a' versus airway generation.	111
11	Relationship between Reynold's number and exponent 'a' in lower pulmonary airways.	120
12	Flow oscillations during panting at 80 bpm.	125
13	Schematic diagram of breathing apparatus.	130
14	Volume distribution of 2 ml ^{133}Xe bolus injected at mouthpiece and measured in extra thoracic trachea during inspirations at 0.2 and 2.0 lps.	133
15	Representative records of inspiratory flow rate and inspired volume from three bolus inhalations in Subject J.H.	135

FIGURE

PAGE

- 16 Plot of duplicate measurements of $\dot{V}_r(\text{alv})$ for all subjects and counter positions. 138
- 17 $\dot{V}_r(\text{alv})$ in the upper and lower lung regions plotted against \dot{V}_I for fourteen ^{133}Xe boli in one subject. 139
- 18 Mean \pm SE $\dot{V}_r(\text{alv})$ for 7 subjects at 6 vertical lung regions, against \dot{V}_I . 140
- 19 Mean \pm SE $\dot{V}_r(\text{alv})$ for seven subjects plotted against counter distance from the lung top during quasi-static inspiration and at 1.5 lps. 141
- 20 Ventilation ratio (V_U/V_L) of average $\dot{V}_r(\text{alv})$ for the upper two regions to the average $\dot{V}_r(\text{alv})$ of the lower two regions plotted against \dot{V}_I . 143
- 21 Mean \pm SE V_U/V_L for 7 seven subjects plotted against \dot{V}_I . 144
- 22 V_U/V_L plotted against step \dot{V}_I applied to lung models. 148
- 23 V_U/V_L of non-linear lung model having equal resistances, plotted against step \dot{V}_I of air or SF_6 . 149
- 24 Change in relative tidal volumes of two compartments of simple lung models, and corresponding changes in C_{dyn} , plotted against sinusoidal breathing frequency. 157
- 25 Calculated $C_{\text{dyn}}/C_{\text{st}}$ of a two compartment lung model at infinite cycling frequency versus ratio of compartment time constants. 160
- 26 V_U/V_L of linear model, against \dot{V}_I applied as a step and as a ramp. 163
- 27 V_U/V_L against ramp \dot{V}_I of dead space, bolus, and tidal volume for linear model. 165
- 28 Mouth count rate versus lung volume, recorded during three vital capacity expirations in subject J.H. 169
- 29 Relationship between expired count rate ratio ($R_V/.5VC$) and pre-expiratory upper to lower concentration ratio. 170

FIGURE		PAGE
30	Relationship between phase IV (ZVC) and upper to lower concentration ratio.	171
31	Expiratory pressure-flow curves at 75%VC in one subject at 1, 4 and 10 Ata.	196
32	Relationship between lung volume and P_{Lmax} in two subjects at 1, 2, 4 and 10 Ata.	198
33	Maximum flow-static recoil relationships in two subjects at 1, 4 and 10 Ata.	199
34	Relationships of transpulmonary pressure and expiratory flow to lung volume during maximum exercise at 1, 4 and 10 Ata in one subject.	200
35	Relationships of transpulmonary pressure and expiratory flow to lung volume during maximum exercise and maximum voluntary ventilation at 1, 4 and 10 Ata in one subject.	201
36	Distribution of constant current applied to electronic analog of two compartment lung model.	219
37	Schematic illustration of airways pressure drop at onset of flow limitation.	222
38	Relationship between \dot{V}_{max} and P_{Lmax} for 2 subjects at 1, 2, 4 and 10 Ata.	224
39	Relationship between \dot{V}_{max} and downstream flow resistive pressure drop at 1, 2, 4 and 10 Ata.	225

TABLE OF CONTENTS

<u>SECTION</u>	<u>PAGE</u>
ACKNOWLEDGEMENTS	
ABSTRACT	
LIST OF TABLES	
LIST OF FIGURES	
I. INTRODUCTION	1
II. PULMONARY RESISTANCE	3
A. Equation of Motion for the Lungs	
1. Definition of Pulmonary Resistance	
2. Measurement of Pulmonary Resistance	4
a. Interruption of Respiratory Flow	
b. Subtraction of P_{el}	5
c. Pulmonary Resonance	
d. Resistive Work done on the Lungs	
e. Airways Resistance	
3. Components of Pulmonary Resistance	6
B. Pulmonary Tissue Resistance	
C. Airways Resistance	9
1. Principles of Fluid Dynamics	
a. Laminar Flow	
b. Flow in the Entry Length	10
c. Turbulent Flow	12
d. Additional Factors affecting Resistance to Flow in Pipes	13
e. Flow in a Venturi Tube	16

SECTION**PAGE**

2. Application of Fluid Dynamic Principles to Airway Morphometry	18
a. Morphometry of the Respiratory Tract	20
b. Physical Properties of Respiratory Gases	21
c. Rohrer's Calculation of Airways Resistance	25
d. Flow Visualization Studies	29
e. Calculation of Bronchial Resistance from Entry Length Theory	31
3. Observed Effects of Gas Physical Properties and Flow Rate	35
III. INTRAPULMONARY DISTRIBUTION OF INSPIRED GAS	41
A. Quasi-static Distribution	
1. Uneven $\Delta V/V_0$ Between Vertical Lung Regions	
a. Different V_0	
b. Different ΔV	44
c. Sequential Ventilation	46
2. Uneven $\Delta V/V_0$ Within Small Lung Regions	54
a. Series Inhomogeneity	55
b. Parallel Inhomogeneity	66
3. Summary	68
B. Dynamic Distribution of Ventilation	69
1. Mechanical Time Constants of Pulmonary Units	70
2. Effect of Breathing Frequency on the Intrapulmonary Distribution of Ventilation	72
a. Evidence for Asynchronous Ventilation	
b. Factors Promoting Synchronous Ventilation	74

SECTION**PAGE**

- 3. Effect of Flow Rate on Ventilation Distribution 76
 - a. Expiratory Flow
 - b. Inspiratory Flow 80

IV. EXPERIMENTS 84

- A. The Effect of Gas Physical Properties and Flow Rate on Canine Lower Pulmonary Resistance
 - 1. Introduction
 - 2. Methods
 - a. Experimental Procedure
 - b. Data Analysis 90
 - c. Calibration Techniques 93
 - d. Calculation of Gas Physical Properties and Reynold's Numbers 95
 - 3. Results 96
 - 4. Discussion 107
 - 5. Summary and Conclusions 114
- B. The Effect of Gas Physical Properties and Flow Rate on Human Lower Pulmonary Resistance 115
 - 1. Introduction
 - 2. Methods
 - 3. Results 117
 - 4. Discussion 119
 - 5. Summary and Conclusions 126
- C. The Effect of Flow Rate on the Regional Distribution of Inspired Gas 127
 - 1. Introduction
 - 2. Methods

SECTION**PAGE**

a. Experimental Procedure	127
b. Preliminary Experiments	132
3. Results	134
4. Discussion	142
a. Lung Model Studies	146
b. Equality of Regional Resistances	152
c. Effects of Regional Resistances on Regional Ventilation in Normal Subjects	155
5. Summary and Conclusions	164
D. The Influence of Regional Concentration Differences on the Expired Concentration vs volume Relationship	167
1. Introduction	
2. Methods	
3. Results	168
4. Discussion	172
5. Summary and Conclusions	176
E. The Effect of Gas Density on Pulmonary Gas Exchange in Man	177
1. Introduction	
2. Methods	
3. Results	181
4. Discussion	
5. Summary and Conclusions	190
F. Exercise Ventilatory Mechanics at Increased Ambient Pressure	192
1. Introduction	

SECTION**PAGE**

2. Methods	192
a. IVPV Relationships at Rest	
b. Exercise Studies	194
3. Results	195
4. Discussion	204
a. IVPV Relationships at Rest	
b. Exercise Studies	206
5. Summary and Conclusions	209
G. Appendix	211
1. The Effect of Periodic Flow on Airways Resistance	
2. Estimate of Regional Resistance from Regional Lung Expansion	213
3. Distribution of Inspired Gas in a Two-Compartment Lung Model	214
a. Constant Flow	
b. Ramp Flow	215
c. Experimental Flow	217
4. Frictional Resistance to Flow Downstream from EPP	221
V. CONCLUSIONS	227
BIBLIOGRAPHY	

CHAPTER I

INTRODUCTION

In his recent undersea explorations, man has encountered new disturbances of his internal environment. One physical consequence of increased ambient pressure is increased density of respiratory gases. During an earlier study relating gas density and expiratory flow (164), basic questions arose regarding the effect of hyperbaric conditions on exercise capacity, airways resistance, distribution of ventilation and pulmonary gas exchange. A review of contemporary literature revealed several studies proposing mechanisms underlying these aspects of pulmonary dynamics. To the extent that these mechanisms were in effect, the behaviour of the lung when exposed to variations in gas physical properties and flow rate was predictable. The studies reported in this thesis employed experimental methods and designs selected to detect the predicted behaviour.

Thus, this project has two general objectives; to provide empirical information regarding alterations and limitations of pulmonary function produced in the hyperbaric environment, and, from these changes to elucidate mechanisms underlying normal pulmonary dynamics at 1 Ata. The former aim is of potential value to future undersea development, since awareness of physiologic problems occasionally leads to technical solutions or appropriate precautions. Better definition of pulmonary dynamics in health may be of particular value in interpreting the battery of sensitive tests generated by recent interest in early detection of lung disease. The scope of the project is broad, in the sense that diverse

aspects of pulmonary function were investigated with a corresponding variety of experimental methods. Some integration results from interrelationships between airways resistance, pulmonary ventilation and gas exchange, but the prime unifying feature is the common investigative approach of varying gas physical properties and flow rate. Although gas viscosity (μ) is a relevant fluid dynamic parameter, far greater changes on gas density (ρ) were employed, so gas physical properties in these studies refer principally to gas density and kinematic viscosity (μ/ρ).

For the sake of continuity, complete individual experiments are presented in separate sections of Chapter IV. Where components of these studies interfere with orderly progression, they are presented in the appendix. Chapters II and III contain a review of selected aspects of pulmonary resistance and intrapulmonary distribution of ventilation thought relevant to the experimental studies. In Chapter II, an attempt is made to correlate newer theories of flow resistance and the classical description of Rohrer. In Chapter III, the elastic properties of lung regions responsible for static distribution are reviewed as a basis for understanding published distinctions between i.) sequential and asynchronous behaviour, ii.) static and dynamic behaviour, and iii.) regional and intraregional behaviour. Chapter V outlines the conclusions of this project which are considered to be contributions to original knowledge.

CHAPTER II

PULMONARY RESISTANCE

A. Equation of Motion for the Lungs

1. Definition of Pulmonary Resistance

The cyclic motion of air between the atmosphere and the gas exchanging surfaces of the lung is driven by pressures generated by the respiratory muscles. A rigorous analysis relating lung motion to the applied pressures according to Newton's equation of motion is the basis of contemporary understanding of the mechanics of pulmonary ventilation (99, 135). The pressure applied across the lung (P_L) is the difference between airway opening pressure (P_{AO}) and pressure in the pleural space (P_{pl}).

$$P_L = P_{AO} - P_{pl}$$

Transpulmonary pressure is opposed by an equal and opposite pressure which may be elastic (P_{el}), frictional (P_{fr}) and inertial (P_{in}).

$$P_L = P_{el} + P_{fr} + P_{in}$$

Elastic pressures are the product of the distending volume of the lung (V_L) and its elastance, usually expressed as the reciprocal of pulmonary compliance ($1/C_L$). The static balance of lung and chest wall recoil determines the resting volume of the lung, so volume change (V_T) occurs about a resting elastic pressure (P_{el0}). Frictional pressure is proportioned to pulmonary flow (\dot{V}) by the pulmonary resistance (R_L) and inertial pressure is related to volume acceleration (\ddot{V}) by pulmonary inertance (I_L).

$$P_L = P_{el0} + V_T/C_L + R_L\dot{V} + I_L\ddot{V}$$

The temporal relationships of these pressures are simplified because normal breathing approximates a sinusoidal change of volume. Thus, the first de-

derivative of volume change, \dot{V} , leads V_T by 90° and has the amplitude ωV_T litres per second (lps), where ω is equivalent to $2\pi \times$ respiratory frequency (f). Similarly, the second derivative (\ddot{V}) leads volume by 180° and is $\omega^2 V_T$ lps²

$$P_L - P_{el0} = \Delta P_L = V_T/C_L + R_L \omega V_T + I_L \omega^2 V_T \quad (1)$$

This equation of lung motion may be represented on x and y coordinates by the circular motion of volume. P_{el} , P_{fr} and P_{in} are scaled to V_T according to equation 1, and are in phase with V_L , \dot{V} and \ddot{V} respectively. P_L is the vector sum of these pressures.

Pulmonary resistance may be defined as the change of that component of P_L in phase with flow per unit change in flow. This flow resistive pressure (P_{fr}) represents the energy lost as heat of friction between moving elements during pulmonary flow.

2. Measurement of Pulmonary Resistance

Several methods are currently employed to isolate P_{fr} and solve the equation of lung motion for R_L . These depend on accurate measurements of P_{pl} . Direct estimates have been obtained through a needle sampling pressure in a small intrapleural air pocket. The anatomic location of the esophagus in the pleural space allows an indirect estimate of P_{pl} from an air-containing esophageal balloon. These and other techniques were comprehensively reviewed by Agostoni (1).

a. Interruption of Respiratory Flow. During quiet breathing, P_{in} is negligible (96), and P_L is the vector sum of P_{el} and P_{fr} . When flow is suddenly interrupted ($\omega = 0$), P_L becomes equal to P_{el} , so the change in P_L must be P_{fr} (50).

$$P_L = V_T/C_L + R\dot{V}$$

$$\text{when } \dot{V} = 0, \quad P_L' = V_T/C_L$$

$$\text{therefore } P_L - P_L' = P_{fr} = R\dot{V}$$

b. Subtraction of P_{el} . Since the elastic pressure is in phase with lung volume, an increasing proportion of the volume signal may be subtracted from P_L until the corrected signal is in phase with flow (104).

$$P_L - V_T/C_L = P_{fr} = R\dot{V}$$

c. Pulmonary Resonance. As ω increases, \dot{V} increases rapidly until P_{in} equals P_{el} at the resonant frequency (f_0) of the lungs (38). Since the pressures are 180° out of phase, their vector sum is zero and P_L equals P_{fr} . Solving equation 1 for the resonant frequency gives

$$f_0 = \frac{1}{2\pi\sqrt{1/CL}}$$

d. Resistive Work Done on the Lungs. The area of a simultaneous plot of P_L against V_T is the resistive work (W) done on the lungs per breath. Assuming a sinusoidal breathing pattern and constant resistance throughout the cycle, R_L may be calculated according to Nisell (110) from the equation

$$R = \frac{2Wt}{\pi^2 V_T^2} \quad (2)$$

where t is the period of the respiratory cycle.

e. Airways Resistance. A quite different approach to resistance measurement involves the estimation of alveolar pressure (P_{alv}) during ventilation from the associated change in alveolar volume. When a subject breathes while sitting in an airtight box, the box pressure changes with changes in body volume. Body volume changes to the extent that changes in alveolar pressure cause compression and expansion of alveolar gas. Box pressure also changes to the extent that the temperature and number of molecules of alveolar gas change. DuBois et al. (37) observed that rapid shallow breathing through a heated flow metre minimized the exchange of heat, water vapor and respiratory gases in relation to the change of alveolar pressure, so that box pressure changes could be calibrated for P_{alv} . Neglecting inertia, P_{alv} differs from P_{ao} by the product of flow rate and the coefficient of airways

resistance (R_{aw}), so box pressure is in phase with flow and their relationship may be solved for R_{aw} . Mead (98) demonstrated that the volume change of a constant pressure plethysmograph may be similarly calibrated for alveolar pressure. Jaeger and Otis (71) modified this method to measure R_{aw} during quiet breathing by having the subject rebreath a gas mixture containing 5% CO_2 saturated at body temperature and pressure (BTPS).

3. Components of Pulmonary Resistance

Two distinct components are arranged in series and contribute separately to the total frictional pressure loss. Airways resistance, $\frac{P_{ao} - P_{alv}}{V}$, is influenced by airway geometry and the physical properties of the fluid. Lung tissue resistance $\frac{P_{alv} - (P_l - P_{ol})}{V}$ is determined by tissue viscosity and the nonideal elastic properties of pulmonary tissue.

B. Pulmonary Tissue Resistance

Resistance of pulmonary tissues (R_t) may be estimated by subtracting airways resistance (R_{aw}) from pulmonary resistance (R_l). Early investigators (13, 34, 95) estimated the nonelastic work done on lungs ventilated with gases of different physical properties, reasoning that only R_{aw} could be affected by such a change. Fry et al. (50) pointed out that quantitative estimates of R_t from the effects of gas physical properties on R_{aw} necessitate an equal distribution of turbulent flow along the airway for each gas. They theorized that this condition was satisfied for equal flow rates and lung volumes by gases of equal kinematic viscosity, so that R_{aw} varied directly with gas viscosity. By extrapolating values of R_l measured on such gases to zero viscosity, McIlroy et al. (94) measured a mean R_t in six healthy subjects of 0.6 cm H_2O/lps . Their subjects inspired 500 ml of the gas mixture to FRC, and measurements were obtained during a subsequent inspiration of about one litre of the same gas from FRC. The influence of volume

history and tidal volume on pulmonary pressure volume hysteresis may account for this relatively large estimate of tissue resistance (see below).

A second approach is to measure R_t during plethysmographic measurements of R_{aw} . Marshall and DuBois (86) found R_t to exceed R_{aw} by 0.10 to 0.35 cm H₂O/lps in 12 healthy adults during rapid shallow breathing ($V_T < 300$ ml, at 100 bpm), giving a mean value for R_t of 0.21. Jaeger and Otis (71) reported mean \pm s.d. values for R_{aw} ($1.21 \pm .29$) and R_t ($1.69 \pm .44$) measured simultaneously during quiet breathing in 9 healthy adults, giving a value for R_t of 0.48 cm H₂O/lps. With the same method, Bachofen and Scherrer (5) reported significant differences of R_t between groups of 10 adult men ($.29 \pm .12$), 7 adult women ($.50 \pm .15$) and 10 children ($1.02 \pm .32$). In the same groups, mean dynamic pulmonary compliance (C_{dyn}) values were 260, 160 and 94 ml/cm H₂O respectively and mean vital capacities were 5, 4 and 2 liters respectively. A similar relationship of R_t to lung volume and pulmonary compliance was observed by Bachofen (3), who measured R_t in subjects of different size, breathing with different tidal volumes and at different end expiratory positions. When mean flow rate and FRC remained constant, R_t increased with tidal volume. For the same tidal volume, R_t increased more than three times when subjects breathed at high lung volumes where C_{dyn} was diminished. Doubling the flow rate when tidal volume and FRC were unchanged did not appreciably increase the nonelastic work performed on lung tissue, so that R_t calculated from equation 2 decreased.

These observations suggested that pulmonary tissue does not behave as a flow resistance but as a nonideal elastic element exhibiting pressure-volume hysteresis. The area of such a hysteresis loop represents the amount of energy which is not recovered when an elastic element is distended and released. Bachofen and Hildebrandt (4) demonstrated in excised cat, dog and monkey lungs that the area (A) of pressure-volume hysteresis loops is relat-

ed to tidal volume and pressure amplitude (ΔP_L).

$$A = KV_T \Delta P_L \quad (3)$$

The hysteresis constant, K , was 0.12 and varied little with lung volume, lung size, tidal volume or species, but decreased slightly with cycle frequency. A remarkably similar value for K (0.10) was obtained from dynamic tissue pressure-volume curves in human subjects, supporting the conclusion that R_t is mainly an index of nonflow resistive pulmonary hysteresis.

The effect of pulmonary hysteresis on R_t values calculated from P-V loops is readily apparent, and provides an explanation for the dependence of R_t upon pulmonary compliance, lung volume and tidal volume. Less obvious is the influence of hysteresis on R_t estimates from pressure-flow curves. Consideration of the corresponding P-V plots suggests that the high R_t values of McElroy et al. (94), the lower values observed during panting (96) and the negligible values during forced oscillation (82) are not inconsistent. A quantitative estimate of this effect may be obtained using equations 2 and 3 and assuming a hysteresis constant of 0.1. Consider a healthy adult with values of C_L and R_L at FRC of 200 ml/cm H₂O and 2.0 cm H₂O/lps respectively. Tidal oscillations of 1,000, 100 or 40 ml at sinusoidal frequencies of 10, 100 or 240 breaths per minute respectively, give peak to peak flow oscillations of 1.0 lps. In the first case, the elastic pressure excursion is 5 cm H₂O, the hysteresis area calculated from equation 3 is 500 g.cm, and the tissue resistance due to hysteresis alone is 0.6 cm H₂O/lps. Similar solutions for the second and third cases give R_t values of .06 and .025 cm H₂O/lps. Thus, decreasing the tidal volume at the same flow rate causes a similar reduction in the calculated resistance of lung tissue.

It should be noted that for a given V_T and C_L , the resistive work done against lung tissue is independent of frequency. Thus, increasing the frequency serves only to decrease the work per unit flow, and the resistance

calculated from eq. 2. This underlines the suggestion of Bachofen (3) that lung tissue resistance would be better expressed as work per breath than pressure per unit flow. In these terms, lung tissue resistance accounts for 30% of the resistive work per breath done on the lungs during quiet breathing (case 1 above), but only 3% during panting (case 2). During rapid oscillations (4 cps) as in the study of Macklem and Mead (82) the resistive work on pulmonary tissue is negligible.

C. Airways Resistance

1. Principles of Fluid Dynamics

Several recent studies examine the flow regime in the human airway. An attempt is made in this section to relate these contributions to basic principles of fluid dynamics as found in a standard reference (126).

a. Laminar Flow. In 1939, Hagen observed that the weight of water per second (W) flowing steadily through straight smooth walled cylinders was related to the height (h) of the water head.

$$h = aW + bW^2 \quad (4)$$

The coefficient, a , varied directly with pipe length (l) and water viscosity (μ) and inversely with the fourth power of the radius (r). The second term, W^2 , which became insignificant for long pipes, was not influenced by viscosity and was considered to represent the pressure required to impart kinetic energy to the fluid. Two years later Poiseuille independently demonstrated that flow (\dot{V}) in capillary tubes was proportional to the applied pressure (P), r^4 and $1/(\mu l)$, although this relationship ceased to hold for short lengths from the tube entrance. Expressed in c.g.s. units, the empirical Hagen-Poiseuille equation for the frictional pressure drop (P) in long tubes is

$$P_{fa} = \frac{8\mu l \dot{V}}{r^4} \quad (5)$$

where l and r are in cm, \dot{V} in cm^3/sec , μ in $\text{cm H}_2\text{O}\cdot\text{sec}$, and P in $\text{cm H}_2\text{O}$.

When fluid is considered to flow in parallel laminae, Newton's law of friction states that fluid viscosity exerts a force opposing the flow of one layer over another.

$$T = \mu \, du/dy \quad (6)$$

The shear stress (T) is proportional to the shear strain, which is the velocity gradient between laminae (du/dy). The solution of equation 6 for flow in tubes of circular cross-section when velocity at the wall is zero is

$$u(y) = P(r^2 - y^2)/4\mu l \quad (7)$$

where P is the frictional pressure drop in a tube of radius, r and length, l and y is the radial distance from the tube axis.

It follows that the velocity distribution of fluid laminae has the shape of a paraboloid of rotation where peak velocity (u_0) is in the centre of the tube ($y = 0$) and is twice the average velocity (\bar{u}). Furthermore, the solution of equation 7 for P coincides exactly with the Hagen-Poiseuille equation, which verifies Newton's law of friction for these conditions. Accordingly the velocity at the tube wall is zero and the pressure drop is proportioned to the velocity gradient across the tube. The boundary layer is the radial distance from zero velocity at the wall to u_0 , so that for a given flow, boundary layer thickness determines the velocity gradient and pressure drop. When the boundary layer thickness is equal to the tube radius, the change in velocity occurs over the maximal available radial distance, so that the frictional pressure drop described by equation 5 is the lowest possible per unit flow.

b. Flow in the Entry Length. As noted by Hagen and Poiseuille, the pressure drop near the tube entrance does not conform to equation 5. According to Olsen et al (113), this discrepancy is explained as follows. Fluid laminae are considered to enter a tube with constant velocity \bar{u} .

Since the velocity at the wall is zero, layers near the wall have a high shear on the outside and low shear on the inside. They decelerate and, since total flow is constant, central layers accelerate until the distribution of shear across the tube is uniform. As a result, the boundary layer thickness approaches the pipe radius asymptotically as axial distance (x) from the entrance increases. The entry length (L) is the axial distance from the entrance to the site of a fully developed parabolic velocity profile, and can be determined from the equation

$$L = .02875 Re \cdot d \quad (8)$$

Re denotes the dimensionless Reynolds number, which may be considered to relate inertial to viscous forces in the fluid, and d is tube diameter.

$$Re = (d \rho u) / \mu = (4 \rho \dot{V}) / (\pi d \mu) \quad (9)$$

Accordingly when Re is 100, L is approximately equal to three tube diameters. The pressure drop in the entry length (P_e) exceeds that associated with a parabolic velocity profile (P_{1a}) by the pressure required to accelerate core molecules from \bar{u} to u_0 . The accelerative pressure (P_{ca}) is related to fluid density and change in gas velocity according to the Bernouilli equation.

$$P_{ca} = \frac{1}{2} \rho (\bar{u}^2 - u_0^2) \quad (10)$$

Since \bar{u} is equal to $\dot{V} / \pi r^2$ and u_0 when $x = L$ is equal to $2\bar{u}$, it follows that

$$P_e = \frac{8L\mu\dot{V}}{\pi r^4} + \frac{1.5\rho\dot{V}^2}{\pi^2 r^4} \quad (11)$$

The form of this equation is similar to the empirical equation of Hagen (equation 4). From a variation of equation 11, Olsen et al. (113) calculate that P_e for the entire entry length exceeds P_{1a} by a factor of 1.63.

Pedley et al. (119, 121) consider that the additional pressure drop within the entry length is due to the increased shear rate associated with a thin boundary layer. When $x \ll L$ they assume that the velocity profile within the boundary layer is linear, and outside the boundary layer in the axial core it is blunt and of magnitude u_0 . In these conditions, the growth of the

boundary layer ($r\delta$) is described by the equation

$$r\delta = \left(\frac{2\mu x}{\rho u_0} \right)^{.5} \quad (12)$$

From dimensional analysis of boundary layer growth according to equation 12, the energy dissipation in the entry length was calculated.

$$P_e/P_{1a} = \frac{C}{4\sqrt{2}} \left(\frac{d}{x} \cdot Re \right)^{.5} \quad (13)$$

where C is a constant determined by the velocity profile entering the tube. When P_e/P_{1a} was measured in a branched tube model, it decreased progressively from 5.09 to 1.47 as distance from the bifurcation increased. In the entire segment between branches, this ratio decreased from 3.65 to 1.91 as Re decreased from 699 to 177. The variation of P_e/P_{1a} with d/x and Re was adequately described by equation 13 when C was 1.85, confirming that the entry length theory correctly describes the pressure flow relations in branched tubes. By combining equations (5, 9 and 13) the pressure drop in branched tubes is expressed:

$$P_e = K(\rho \mu)^{.5} v^{1.5} \quad (14)$$

where K is a geometric constant, equal to $.508Cx \cdot 5/r^4$ when c.g.s. units are used. Thus, P_e is more dependent on gas density and flow rate than P_{1a} , reflecting the additional pressure drop required to accelerate core molecules in the entry length.

c. Turbulent Flow. A different flow pattern is frequently observed in pipes, where secondary motions perpendicular to the principal fluid motion occur. The transition from laminar to turbulent flow is facilitated by increased tube diameter and fluid velocity and decreased kinematic viscosity; that is, by increased Re. When Re exceeds a critical value of 2000 (Re_c), inertial disturbances introduced into laminar flow by the pipe entrance or wall irregularities grow with time. At much lower Re ($<1/6 Re_c$), such disturbances die out locally whereas between this value and Re_c , they persist proportional to Re (135).

Secondary motions blunt the velocity profile by sweeping kinetic energy from the core toward the walls of the tube. Consequently, the shear rate and pressure drop are increased. The pressure drop caused by turbulent flow (P_{tu}) in smooth walled tubes has been found proportional to a factor of tube geometry, $\frac{1}{r}$, and fluid kinetic energy.

$$P_{tu} = \lambda \frac{1}{r} \cdot \frac{\rho u^2}{2} \quad (15)$$

where λ is the resistance coefficient equal to $\frac{0.67}{Re^{.75}}$. Dividing equation 15 by equation 5 reveals that P_{tu} exceeds the pressure drop for laminar flow in the same pipe by the factor, $4.2 \times 10^{-3} \times Re^{.75}$. When Re is 10,000, P_{tu} is about four times P_{la} . Pedley et al. (119, 121) calculate that most of this increase is due to the blunt velocity profile of turbulent flow, and point out that the pressure drop in frequently branching tubes may be relatively unchanged by the development of core turbulence. By substituting for λ , u , and Re in equation 15

$$P_{tu} = .2 \left(\frac{\rho \cdot 75 \mu \cdot 25^{1.75}}{L^{4.75}} \right) \quad (16)$$

d. Additional Factors Affecting Resistance to Flow in Pipes. The classical flow regimes discussed above occur during continuous flow in straight rigid tubes of circular cross section having smooth dry walls. Several variations on these conditions may influence the pressure drop. In general these variations tend to increase the pressure losses by enhancing inertial disturbances of the velocity profiles. Such disturbances are proportional to Re , and tend to alter laminar, entry length, and turbulent flow equations in the direction of purely accelerative pressure losses. Thus, the pressure drop becomes more dependent on flow rate and gas density and less dependent on gas viscosity than predicted for steady flow through smooth walled pipes.

(1) Flow Oscillations. In conditions of steady laminar flow through a single conducting element, velocities near the centre of the tube exceed those near the wall. When the pressure driving flow is sinusoidally oscillated at increasing frequencies, core flow eventually begins to lag the applied pressure due to the inertia of central molecules. In such circumstances, a greater proportion of the flow occurs near the walls where the shear rate is high, so that total flow per unit pressure decreases relative to steady flow conditions. The magnitude of this disturbance of the boundary layer relative to its steady flow thickness may be calculated according to Watersley (167) from the equation

$$\alpha = r\sqrt{\omega/\nu} \quad (17)$$

where r is tube radius (cm), ω angular frequency (sec^{-1}) and ν is gas kinematic viscosity (cm^2/sec). When the dimensionless parameter α exceeds a value of 1.0, oscillatory resistance exceeds that during steady flow. By this analysis, sinusoidal breathing at 10 cycles per minute causes a significant increase over resistance to steady laminar flow in the trachea and large bronchi (25).

However, the boundary layer of flow in frequently branching tubes is much less than the tube radius. According to Schroter and Sudlow (145) equation 17 may be rewritten to solve for an analogous parameter, β , by substituting boundary layer thickness for radius.

$$\beta = r\delta\sqrt{\omega/\nu} \quad (18)$$

It follows that those features of flow in the bronchial tree which increase resistance to steady flow by promoting a thin boundary layer also cause this resistance to be less affected by flow oscillations. For $\beta > 1.0$ during air breathing, $r\delta$ must exceed 2.8 mm when the breathing frequency is 20 bpm, and during forced oscillations at 4 and 10 cycles per second, $r\delta$ must exceed .8 and .5 mm respectively. Assuming $u_0 = \bar{u}$, boundary layer thickness

for a given steady flow rate may be estimated using measured bronchial dimensions (Table 1) and equation 12. Even though this assumption underestimates u_0 , the boundary layer thickness when flow oscillations are 1.0 lps does not approach the values necessary for $\beta > 1$ until frequency is 10 cycles per second. Combining equations 12 and 18, one obtains

$$\beta = \left(\frac{2 \omega x}{u_0} \right)^{.5} \quad (19)$$

Inspection of equations 17 and 19 reveals that the effect of oscillatory flow in the entry length (β) differs in several respects from its effect (α) on fully developed laminar flow. The term β is independent of gas physical properties and varies inversely with the square root of flow rate. It seems reasonable to conclude that airways resistance is virtually independent of breathing frequency up to 10 cycles per second regardless of the flow amplitude or gas breathed. This conclusion does not take account of flow redistribution among parallel airways (see Chapter III).

(2) Wall Roughness. Schroter and Sudlow (145) pointed out that the maximum size of a protuberance which will not alter the laminar flow characteristic in a pipe may be estimated according to Schiller:

$$E / r \leq \frac{4 \text{ to } 5}{Re^{.5}}$$

where E is the height of the protuberance and r is the pipe radius. Thus, surface irregularities must exceed 15% of the tube radius in order to disrupt laminar flow when Re is 10^3 , suggesting little effect of bronchial roughness in these conditions. It is less clear what effect the same irregularities may have on thin boundary layers. It seems possible that a 1 mm protuberance in the trachea ($r = 10$ mm) may not influence a fully developed parabolic velocity profile but may disturb a boundary layer less than 1 mm thick. Furthermore, Pedley et al. (121) cite the possibility of Taylor-Görtler vortices associated with flow over concave surfaces as promoting transition from

laminar to turbulent boundary layers. If either factor is operative in the airway, the pressure losses will tend to exceed the predictions for flow in smooth walled tubes.

The effect of a liquid film lining the inner surface of conducting tubes was examined by Clarke et al. (27). Their results suggest that when the stream of air flowing through a liquid lined airway remained laminar, there is very little increase in resistance above that predicted from narrowing of the lumen by the liquid layer. When Re was sufficiently high, waves developed in the surface film, associated with a very large increase in resistance. Wave formation occurred at lower Re for thicker liquid layers and lower liquid viscosities. The authors conclude that the thin surface layers present in healthy lungs probably have a negligible effect on flow resistance at all but the highest flow rates.

Major effects of airway distensibility on resistance seems unlikely since radial velocities are necessarily small relative to axial velocities (145). The sharpness and elastic stability of the bifurcation spur may also influence the airway velocity profiles, but no theoretical or empirical estimates of their possible contribution are available.

e. Flow in a Venturi Tube. The classical patterns of pipe flow discussed above are described by fixed relationships among the pressure drop, gas physical properties and flow rate. The variable flow patterns in a well studied fluid velocity metre bear considerable similarity to those in human upper airways (69). A Venturi tube consists of a straight cylinder having a central circular constriction. For an ideal fluid, the lateral pressure difference (ΔP) between the tube and the constriction is purely inertial and equals the increased kinetic pressure of the constricted stream. The velocity of the ideal fluid may be calculated from the Bernoulli equation

$$u = \left(\frac{2 \Delta P}{\rho} \right)^{.5}$$

Because real fluids are viscous, there is a component of ΔP due to viscous shear, and calculations of ideal velocity overestimate the true velocity, which is equal to the total flow (\dot{V}) divided by the cross-sectional area (A) of the constriction. The ratio of ideal to true velocities is the coefficient of discharge (C_d)

$$C_d = \frac{\dot{V}}{A \sqrt{2 \Delta P \rho}} \quad (20)$$

The inertial (ideal) component of ΔP increases with Re , and a logarithmic plot of C_d against Re demonstrates a characteristic pattern. When $Re < 10$, $\log C_d$ increases linearly as $\log Re$, with a slope of 0.5.

$$C_d = K \cdot Re^{.5} \quad (21)$$

Substituting equations 9 and 20 for Re and C_d , and solving for ΔP

$$\Delta P = K \mu \dot{V} \quad (22)$$

Thus, for low Re , the pressure drop varies directly as gas viscosity and flow rate and is independent of gas density. These pressure losses are almost entirely viscous, and similar to the losses of fully developed laminar pipe flow. At very high Re ($> 10^4$), ΔP becomes completely inertial and C_d is equal to 1.0. Solving equation 20 for $C_d = 1.0$,

$$P = K'' \rho \dot{V}^2 \quad (23)$$

where $K'' = \frac{8}{\pi^2 D^4}$. Thus ΔP varies as the kinetic energy of the gas independently of gas viscosity. In the intermediate range ($10 < Re < 10^4$), the logarithmic C_d versus Re plot is curvilinear. As Re increases, the slope progressively decreases from 0.5 to zero. Substituting for C_d and Re in the middle range of Re , where $C_d \propto Re^{.25}$,

$$P = K_3 (\rho \mu)^{.5} \dot{V}^{1.5} \quad (24)$$

The form of this equation is identical to equation 14, describing flow in the entry length. Similarly, when Re is higher, C_d becomes proportioned to $Re^{.125}$, and the resulting equation resembles equation 16 describing turbulent pipe flow.

$$P = K_4 \rho^{.75} \mu^{.25} V^{1.75} \quad (25)$$

In addition to providing a better description of upper airways resistance than any of the classical flow regimes, this Venturi tube model offers a unifying concept for the variety of flow conditions existing throughout the human airway during normal breathing. Inspection of equations 22, 24, 25 and 23 reveals that ΔP is related to gas physical properties and flow rate according to the general equation

$$\Delta P = K_5 V^{a+1} \rho^a \mu^{1-a} \quad (26)$$

The exponent, 'a', increases progressively with Re due to the increasing influence of fluid inertia on the pressure drop. This relationship is also true for the classical flow regimes as indicated in Table 1. It seems reasonable to conclude that the continuously changing flow patterns in the Venturi tube pass through velocity profiles identical to those of laminar, entry length, turbulent and office flow as Re increased. Conversely, it may be argued that departures from airways resistance calculations based on classical flow regimes will be systematic, in the sense that the exponent, 'a', will change according to the prevailing Re and exponents of gas physical properties will change according to equation 26.

2. Application of Fluid Dynamic Principles to Airway Morphometry

In general, the experimental investigations of a certain problem in research has to precede the theoretical considerations. If however, the possibilities of an experimental investigation are so slight, as they are in this case, it may be permissible to make a theoretical reconstruction of the event to begin with. The flow of air in the respiratory tract is a purely physical event, the laws of which are fairly well known. If these laws are applied to this special case with consideration of all possible factors, we may assume with a high degree of probability that we approach the real conditions very closely.

With these remarks, Rohrer (135) introduced the classic paper that has been the foundation of our understanding of airways resistance for over fifty years. Relatively recent measurements have directed attention to several errors in Rohrer's calculations, arising in good part from the lack

TABLE 1Exponents Relating Resistance to Gas Physical Properties and Flow Rate

<u>Flow Regime</u>	<u>Eq. *</u>	<u>\dot{V}</u>	<u>μ</u>	<u>ρ</u>
Venturi Tube	26	a	1-a	a
Laminar	5	0	1.0	0
Entry Length	14	0.5	.5	.5
Turbulent	16	0.75	.25	.75
Orifice	23	1.0	0	1.0

* Corresponding descriptive equation as numbered in the text.

of empirical checks for the complicated theories. Nevertheless, his approach implies an underlying physical basis for a physiologic parameter, and should serve as a model for hypotheses relating the available fluid dynamic principles to airway dimensions.

a. Morphometry of the Respiratory Tract. Airways differ markedly from straight smooth walled cylinders of circular cross section. The pathway from the mouth to the extra-thoracic trachea (135) bends sharply downward at the pharynx, where the width considerably exceeds the anterior-posterior diameter. At the glottis, the cross section is irregularly reduced to about 1.0 cm² before increasing to three times that area in the U-shaped trachea. For such irregular passages, the effective pathway for flow is less than the total cross section and the hydraulic diameter (D_h) may be calculated if the cross sectional area and circumference are known.

$$D_h = 4 \frac{\text{area}}{\text{circumference}} \quad (27)$$

Below the carina, the airway branches repeatedly. At least two excellent studies (62, 159) provide the dimensions of these airways obtained from casts of excised human lungs fixed at about 75% of total lung capacity. Although these dimensions provide a guide to the calculation of bronchial resistance, very few resistance measurements have been made in the same conditions to validate the calculations. Most resistance measurements are obtained at FRC in living human subjects where few detailed measurements of airway dimensions are available.

If respiratory flow is laminar, the frictional pressure drop per unit length of an airway is proportional to the flow rate divided by the fourth power of the radius (see Eq. 5). When two airway segments are connected in series, the total pressure drop is the arithmetic sum of the frictional loss in each. When a bronchus branches into two daughter airways, the resistance due to parallel flow beyond the bifurcation (R_D) is calculated from the in-

verse sum of daughter resistances (R_1, R_2).

$$\frac{1}{R_D} = \frac{1}{R_1} + \frac{1}{R_2}$$

If the daughter bronchi have equal dimensions, resistance per unit length decreases beyond a bifurcation when the branching coefficient (ratio of total daughter to parent cross sectional areas) exceeds $\sqrt{2}$. Weibel (159) observed that the branching coefficient increased progressively from .9 at the carina to 2 at the most peripheral bifurcation, and that the length of daughter branches varies between .81 and .87 of the parent length. Accordingly, Green (59) calculated that the resistance per unit length of the bronchial tree begins to decrease at generation 9, and the resistance per generation is maximum at generations 4 to 8 beyond which it falls off rapidly. These calculations, illustrated in figure 4, are qualitatively similar to estimates of Horsfield and Cumming (63) who also assumed laminar flow in an asymmetric model of airway morphology (62).

Inspection of equation 9 reveals that, for a given flow in a dichotomous bronchial tree where the branching coefficient is 1, Re in the parent bronchus exceed daughter Re by a factor of $\sqrt{2}$. Similarly, beyond generation 9, Re decrease by more than a factor of two in each succeeding generation. Table 2 shows that with relatively low flow rates, Re in the upper airways and large bronchi suggest turbulence, and it is not until the eighth generation that Re fall below 100. In the intermediate bronchi the length to diameter ratios range from 2.5 to 6.0 (62), so that all bronchial segments between branch points are shorter than their entry lengths calculated from equation 8.

b. Physical Properties of Respiratory Gases. The usual inspired gas is air, which may be considered as a mixture of 21% oxygen (O_2) in nitrogen (N_2). This is rapidly warmed to $37^\circ C$ and saturated with water vapor (H_2O) so that at 1.0 atmosphere of absolute ambient pressure (Ata), the inspired gas contains by volume about 74% N_2 , 20% O_2 and 6% H_2O . Pulmonary gas exchange

Table 2

Geometric and Hydraulic Parameters of the Human Airway

Site	Airway Dimensions ⁺				Flow Parameters [*]			
	<u>G</u>	<u>L</u>	<u>d</u>	<u>A</u>	<u>U</u>	<u>Re</u>	<u>rδ</u>	<u>B</u>
Pharynx		10	1.2	1.12	450	3240		
Glottis		.50	.80	.50	1000	4800		
Trachea	0	12	1.8	2.54	200	2160		
Main Bronchi	1	4.76	1.22	2.33	215	1580	.086	1.06
Lobar Bronchi	2	1.90	.83	2.13	235	1170	.052	.64
	6	.90	.28	3.96	125	210	.049	.60
	8	.64	.19	6.95	72	82	.054	.66
	15	.20	.07	113	5	2	.035	.43

+ Tracheo-bronchial from Weibel (159); Upper airway from Rohrer (135).

G: Airway generation.

L: Length of airway segment (cm).

d: Diameter of airway segment (cm).

A: Total cross-section area (cm²).

* Calculated for flow (\dot{V}) of $\pm .5$ lps at 4 cps (air).

\bar{U} : Average velocity = \dot{V}/A (cm/sec).

Re: Reynold's number = $\bar{U} \rho d / \mu$

$r\delta$: Boundary layer thickness = $(2 \mu x / \rho U_0)^{.5}$, where $x = L$ and $U_0 = \bar{U}$, (cm).

B: Wormersley's parameter, modified for frequently branching tubes, = $(2 \omega x / U_0)^{.5}$.

alters the inspire by removing O₂ and adding carbon dioxide (CO₂) in approximately equal volumes. Accordingly, the alveolar gas expired after the central airways are washed out contains about 6% CO₂ and 14% O₂. During re-breathing and shallow rapid panting, the flowing gas must approximate the alveolar fractions.

The physical properties of these gases which influence the energy dissipation during flow are the viscosity (μ) and the specific gravity, or density (ρ). The viscosity of a fluid may be regarded as the internal coefficient of friction of the molecules, indicating the amount of force required for molecules to slide over each other and their container during mass flow. The c.g.s. units are dynes/cm.sec, or poises, and can be converted from force to pressure units (cm H₂O.sec), by dividing by the acceleration of gravity ($g = 980 \text{ cm/sec}^2$). The dynamic viscosity increases with temperature according to Sutherland's factor, and is independent of the ambient pressure over a wide range from 1.0 Ata (128). Values at 37°C for individual respiratory gases are compiled in Table 3. Due to molecular interaction, the dynamic viscosity of a gas mixture is usually higher than that calculated from the fractional volumes and viscosities of the components. The viscosity of respiratory gas mixtures may be estimated by comparing the pressure drop across a pneumotachograph for a fixed flow rate of the mixture with that for the same flow of air (94).

Gas density is the mass of gas per unit volume and varies directly as the ambient pressure and inversely as the absolute temperature. The c.g.s. units are grams/cm³, which can be converted to pressure units (cm H₂O.sec²/cm²) by dividing by g (70). The density of a gas mixture may be calculated from the fractional volumes and densities of the components (128). The ratio of μ to ρ is the kinematic viscosity (ν) of the gas which has the c.g.s. units of cm²/sec. This characteristic is important to

Table 3Gas Physical Properties⁺

<u>Gas</u>	<u>ρ</u>	<u>μ</u>	<u>ν</u>
He	.16	2.02	1.250
H ₂ O	.71	1.00	.141
N ₂	1.09	1.81	.166
O ₂	1.24	2.10	.169
CO ₂	1.72	1.57	.091
SF ₆	5.34	1.20	.025
<u>Mixtures</u> [*]			
HeO ₂	.43	2.10	.490
Air	1.12	1.87	.167
SF ₆ O ₂	4.26	1.60	.038

+ Values at 37°C, 1 Ata as listed by Radford (128) or in the Handbook of Physics and Chemistry.

ρ : density (g/L $\times 10^{-3}$)

μ : viscosity (Poises $\times 10^{-4}$)

ν : kinematic viscosity (cm²/sec)

* 14% O₂, 6% CO₂, and 6% H₂O in He, N₂ or SF₆. Values for density calculated from components, air viscosity from Rohrer (135), and HeO₂ and SF₆O₂ viscosities relative to air measured with a pneumotachygraph (104).

the dynamics of flow in that it indicates the ratio of viscous to inertial forces present in the fluid itself.

c. Rohrer's Calculation of Airways Resistance

(1) Rohrer's Equation. Recognizing that flow through tubes may be laminar or turbulent, Rohrer (135) calculated the critical velocity (u_c) for transition to turbulence in various airways, assuming Re_c to be 1290. From equation 9,

$$u_c = \frac{1290}{d} \times \nu \quad (28)$$

He then calculated the density and viscosity of inspired and expired air, carefully correcting for body temperature, humidification and respiratory quotient.

$$\mu = 1.873 \times 10^{-7} \text{ cm H}_2\text{O}\cdot\text{sec}$$

$$\rho = 1.117 \times 10^{-6} \text{ cm H}_2\text{O}\cdot\text{sec}^2/\text{cm}^2$$

$$\nu = .1677 \text{ cm}^2/\text{sec}$$

Using measured airway diameters (mm), equation 28 was solved for u_c in metres/sec. For dimensional equivalence, d should have been expressed in cm and u_c in cm/sec. This error overestimated u_c by a factor of ten, so that air velocity at all but maximum flow rates was thought to be less than u_c . Rohrer concluded that "tubular" flow in the respiratory system was laminar, and accordingly that part of the pressure drop was calculated from Hagen-Poiseuille equation (eq. 5).

In addition to the pressure losses due to tubular flow, Rohrer considered the disturbances in flow pattern induced by the local constriction of the glottis and changes of flow direction in the nose, pharynx and bronchi. These disturbances add eddies which grow with time when $u > u_c$ and persist proportional to Re when $u_c > u$. With repeated disturbances, the flow pattern may appear turbulent at velocities as low as one-sixth u_c ($Re = 215$). Below this lower limiting velocity (u_{gl}), all disturbances die out locally. Due to the

erroneous calculation of u_c , gas velocity throughout most of the bronchial tree did not exceed u_{g1} . Accordingly "additional" losses were confined to the upper airway and large bronchi, and were a variable fraction of the kinetic energy of the stream ($\frac{1}{2} \rho u^2$) dependent upon the radius of the bend relative to the radius of the airway. Rohrer solved for the "additional" losses (P_a) using the equation of Weisbach

$$P_a = E \frac{\rho \dot{V}^2}{2 \pi^2 r^4}$$

where E is a constant of bend geometry.

Rohrer's equation for the pressure loss in airways associated with laminar "tubular" flow and "additional" losses due to inertial disturbances may be written:

$$P = \frac{81 \mu \dot{V}}{\pi r^4} + \frac{\rho \dot{V}^2}{2 \pi^2 r^4} \quad (29)$$

This is simplified as follows:

$$P = K_1 \dot{V} + K_2 \dot{V}^2 \quad (30)$$

K_1 has the units of resistance (cm H₂O/lps) and contains gas viscosity and a constant of airway geometry; K_2 has the same dimensions and contains gas density and a constant of bend geometry. When measured P - \dot{V} relationships are plotted as P/\dot{V} against \dot{V} , a straight line relationship is frequently obtained. The slope of this line is K_2 , and the zero flow intercept is K_1 (87).

$$R = K_1 + K_2 \dot{V}$$

Accordingly, when \dot{V} is 1.0 lps, R is the sum of K_1 and K_2 .

Rohrer's equation provides a good description of most airways resistance measurements. Yet a good mathematical description does not necessarily describe the nature of the pressure drop, and several assumptions implicit in the derivation of equation 29 have since proven false. Gaensler (53) pointed out that when u_c is calculated correctly (see Table 2), turbulent flow may be expected during quiet breathing in the upper airway and large bronchi. It may

be argued that the second term of Rohrer's equation can account for the additional losses due to turbulence if the appropriate tubular geometry is included in K_2 . Fry et al. (50) theorized however that for a given airway geometry, the distribution of turbulence in the bronchial tree must change with gas kinematic viscosity and flow rate. The geometric factors contained in K_1 and K_2 change accordingly, making unlikely the possibility that K_1 and K_2 have any physical significance (99). More recent analyses of flow in branched tubes suggest a quite different bronchial $P-\dot{V}$ relationship which is less affected by the distribution of turbulence (113, 119, 121, 146). Furthermore, the venturi tube analogy of upper airways resistance suggests that similar exponents relate pressure drop to gas physical properties and flow rate in extrathoracic and intrathoracic airways (69, 70). It now becomes interesting to recall that Hagen considered the second term of his empirical description of flow in short pipes (eq. 4) to represent the kinetic energy added to the fluid beyond the entrance. This is quite consistent with the present understanding of flow in branched tubes and in a Venturi metre, and raises again a basic theoretical possibility as yet untested. Is the nature of the pressure drop associated with complicated flow patterns through irregular airways geometry correctly described by the sum of viscous losses ($K_1\dot{V}$) and inertial losses ($K_2\dot{V}^2$)?

(2) Upper Airways Resistance. For the upper airway, Rohrer solved equation 29 using published anatomic dimensions of the nostrils, pharynx, glottis and trachea. Because these passages were very irregular in cross section, the hydraulic diameter (see eq. 27) was calculated as the effective diameter for flow. During mouth breathing, the calculated resistance (R_{UAW}) was .61 cm H₂O/lps ($K_1 = .05$, $K_2 = .56$), most of which was due to additional losses across the glottis ($K_1 = .01$, $K_2 = .54$). Though these calculations underestimate the contribution of oropharyngeal resistance (148), their sim-

ilarity with subsequent measurements of R_{Uaw} (14, 44, 64, 69, 148) is remarkable considering that Rohrer thought the flow regime to be laminar. The accuracy may indicate that the flow pattern existing during "tubular" turbulence is quite similar to laminar "tubular" flow when "additional" disturbances are frequent. This possibility is supported by the calculations of Pedley et al. (119, 121) who showed that most of the pressure losses during turbulent flow are due to the blunt velocity profile.

(3) "Bronchiolar" Resistance. Because no published dimensions of the bronchial tree were available, Rohrer measured the lengths and circumferences of airways extending from the trachea to 1 mm diameter bronchioles in a collapsed right human lung. Solution of equation 29 gave K_1 and K_2 values for this "bronchiolar" segment of .11 and .08 cm H₂O/lps respectively. The K_1 value is quite close to the value of .17 cm H₂O/lps estimated by Green (59) from the refined bronchial morphometrics of Weibel (159). Both values are considerably lower than subsequently measured values of .6 cm H₂O/lps (14, 44, 65, 148, 157). This discrepancy has been attributed to the omission of a term for turbulent "tubular" flow (94) but it now seems more likely due to frequent distortions of the parabolic velocity profile in the branching bronchial tree. Rohrer was aware that no uniform equations were derived for velocities between u_c and u_{g1} . Had he been forced to consider bronchial velocities greater than u_{g1} , the relevance of entry length phenomena to airways resistance may not have remained obscure for the next fifty years.

(4) "Lobular" Resistance. For dimensions of airways peripheral to 1 mm bronchioles ("lobular" system), Rohrer relied on published histologic observations. The calculated "lobular" resistance ($K_1 = .25$, $K_2 = .01$) closely resembles values subsequently measured in peripheral airways (61, 82, 84). "Additional" losses were negligible, suggesting to later investigators (59, 63) that they might also be neglected for the total "bronchio-lobular" resis-

tance ($K_1 = .36$, $K_2 = .09$). Accordingly, lobular resistance accounts for more than half of the lower airways resistance (R_{law}), in contrast to subsequent measurements which demonstrate that peripheral resistance accounts for only 10% of R_{law} . This discrepancy is in part due to Rohrer's underestimate of bronchiolar resistance, but must also reflect an underestimate of the number and total cross section of lobular airways relative to bronchiolar airways.

d. Flow Visualization Studies. Rohrer was the first to test his theories concerning flow patterns in branching airways. A machine driven bellows sucked steady air velocities through a glass tube (l - 73cm, d - 1cm) from two daughter tubes (y junction, 45° angle), one of which was filled with ammonium chloride vapor. The average flow rate was varied to a maximum of 1.57 lps ($u = 200$ cm/sec, $Re = 1200$), and a clear separation of vapor and air was observed. From eq. 28, Rohrer had erroneously calculated u_c and u_{gl} to be 2160 cm/sec and 360 cm/sec, so these observations supported his conclusions that turbulence does not occur and eddies do not persist in bronchi during quiet breathing. Subsequent studies (35, 145, 162) examined flow patterns only several diameters downstream from the tube entrance and showed turbulent eddies at lower Re , suggesting that Rohrer might have overlooked this region of his model and therefore underestimated the effect of local disturbances in a frequently branching system.

Gaensler (53) pointed out Rohrer's dimensional error, and calculated u_c for a 21 mm trachea, assuming the Re_c to be 2000. His value of 140 cm/sec ($\dot{V} = 485$ ml/sec) proved higher than observations in subsequent studies.

West and Hughes-Jones (162) perfused segmental bronchi of a hollow airway cast with water marked with dye. During expiration, streamlines wavered in the trachea at the equivalent air flow of 340 ml/sec ($Re = 1360$). Eddies were observed at 670 ml/sec downstream from lobar bronchi, and at 1340

ml/sec downstream from segmental bronchi. During inspiration, turbulence occurred at lower flow rates in all airways, being first observed at 220 ml/sec in the trachea ($d = 17.5$ mm, $Re_c = 1075$). At 670 ml/sec, turbulence extended from trachea to segmental bronchi ($Re = 700$). Dekker (35) visualized the onset of turbulence in twelve excised trachea perfused with steady flow rates of water and dye or air and smoke. The critical Re were similar for water and air, and varied with the diameter of the tracheal inlet. During inspiration the critical flow rates were 380 ml/sec ($Re = 1380$) when the glottis was removed, and 52 ml/sec ($Re = 190$) with the glottis present in the cadaveric position (adduction). Abduction of the cords doubled the critical flow.

These results suggested that critical Re in the human trachea and large bronchi are close to 1290, as suggested by Rohrer. Furthermore, the inlet geometry of the airways produces turbulent eddies when Re exceed about one-sixth of the critical value (Rohrer's u_{gt}) which persist for some distance downstream. Hyatt and Wilcox (65) found evidence supporting similar flow patterns in vivo. From the difference (ΔP) between impact, or total, pressure and lateral pressure they calculated gas velocity at several points across the extra thoracic trachea in human volunteers, from the Bernoulli equation

$$u = \sqrt{2\Delta P/\rho}$$

The velocity profile was blunt at flow rates of 0.5 to 4.5 lps. This is presumably due to tracheal turbulence, although laminar flow with a blunt velocity profile cannot be excluded.

Schroter and Sudlow (145) examined the effect of tube branching on flow patterns of air marked with smoke in perspex models of airways. The branch angle (70°) and diameter/length ratios (1/3.5) were similar to the mean dimensions of airways generations 5 to 20 reported by Horsfield and Cumming (62). Secondary motions were observed to complete at least one helical cycle within three diameters downstream of the branch point at all flow rates (Re .

50 - 4500), and to produce convective dispersion of smoke in the air stream. As an important addition to flow visualization, a hot wire probe was employed to measure the velocity profile for flow through two generations from Re 100 to 1500. The velocity profiles were distorted in a characteristic manner for both inspiratory and expiratory flow, resulting in a uniform distribution of velocity across the section of the tube. This suggested that secondary motions induced by airway branching (and similarly by the glottis) oppose the tendency of fluid momentum to accumulate in the center of the tube, thus tending to maintain a blunt velocity profile in the tracheo-bronchial tree when Re exceed 100. This concept is the major addition to Rohrer's understanding of the flow resistive pressure drop, and its implications are discussed in the following section.

e. Calculation of Bronchial Resistance from Entry Length Theory.

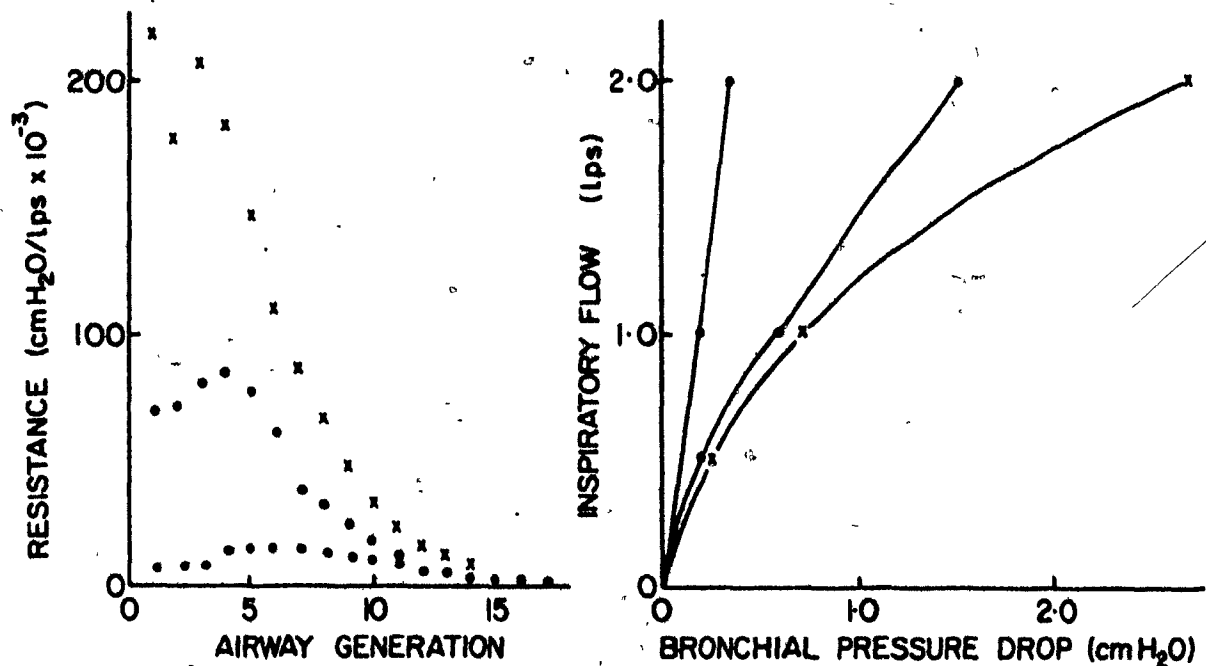
As discussed, Pedley et al. (119, 120, 121) used the measured velocity profiles of Schroter and Sudlow (145) to calculate the pressure drop in their bronchial model. The calculated pressure-flow relations over a tested Re range of 177 - 699 conformed closely to the general equation for boundary layer growth. This suggested a major contribution of entry length phenomena to the inspiratory pressure drop in the bronchial tree, and provided an equation with which to calculate the pressure from Weibel's airway dimensions. Olsen et al. (113) independently concluded that entry length phenomena are important in producing the pressure drop in a different model of airway morphometry. They reasoned that three anatomical features of the bronchial tree disturb the velocity profiles of inspiratory flow, causing the pressure drop to exceed laminar losses by a fraction of the kinetic energy of the gas. These extra losses are interrelated, but can be calculated separately from appropriate equations. The short length of airway segments between branching points relative to their hydraulic diameters accounts for at least 75% of the total

pressure drop in each generation during inspiration (.5 to 2.0 lps). The angle of each bifurcation causes redirection and secondary motion of the flowing gas which account for less than 10% of the total losses per generation. When the branching coefficient exceeds 1.0, additional viscous losses occur due to separation of flow laminae, accounting for 10% or less of the total drop.

The pressure drop per generation of Weibel's model A (159) are compared for an inspiratory flow rate of 1.5 lps in the left panel of figure 1. The results from Pedley et al (120) exceed laminar values by a factor of 10 in larger airways where linear velocities and Re are high. This factor falls off rapidly beyond the 4th generation to less than 2 by generation 8, and R_{law} is about 0.6 cm H₂O/lps. The values of Olsen et al. (113) follow a similar pattern but are about two to three times greater in all generations, and R_{law} is 1.6 cm H₂O/lps. Although the estimated effects of entrance length phenomena are qualitatively similar, the discrepancy in pressure losses when the two approaches are applied to the same airway dimensions is surprising. It is not apparent from the equations published where the discrepancy lies. Assuming the equations are solved correctly, the credibility of the approach of Pedley et al. (120) is enhanced by their experimental verification of the equations employed.

The inspiratory pressure-flow relations calculated for the bronchial tree (carina to alveolus) are compared in the right panel of figure 1. Green (59) and Pedley et al. (120) calculated frictional pressures using the airway dimensions of Weibel's model A. The difference between their values for a given flow indicates the additional energy losses attributed to boundary layer growth. Thus, bronchial resistance (P/\dot{V}) increases with flow rate and at 1.0 lps is three to four times greater than laminar resistance. In the same lung model, Olsen et al. (113) predicted much greater additional losses, so that

FIGURE 1



Left Panel: Resistance to air flow (1.5 lps) per generation of Weibel's model A, calculated from three fluid dynamic theories (see text), \cdot Green (59) \circ Pedley et al (120) \times Olsen et al (113).

Right Panel: Bronchial pressure-flow relationships calculated for Weibel's model by Green (\cdot) and Pedley et al (\circ) and for an effective pathway by Olsen et al (\times) (see text).

their calculated bronchial resistance (1.35 cm H₂O/lps) is eight times greater than Green's value. When they used dimensions of an "effective" pathway in an asymmetric bronchial tree, the pressure drop at 1.0 lps (.7 cm H₂O) was about one-half of their calculated value for Weibel's model. The greater effect of additional losses estimated by Olsen et al. (113) is also present in this "effective" pathway, as indicated by the greater curvature of their P- \dot{V} plots. As a result, these P- \dot{V} relations are more similar to those of Pedley et al. (120) than are the equations employed by the two groups. This suggests a significant effect of the asymmetric branching pattern on bronchial resistance, which has not been directly examined previously. The authors do not discuss this possibility and present little information regarding the construction of the "effective" pathway (113, 146).

Thus there are differences in the effects predicted for entry length phenomena and differences in the airway morphometry to which these concepts are applied. When one also considers the wide range of lower pulmonary resistance among normal subjects (14, 44, 148, 157), it does not seem reasonable to validate either approach on the basis of how closely they simulate published measurements. In this regard the resistance calculations of Green (.17 cm H₂O/lps) are as close to the only published values of lower pulmonary resistance (157) measured in circumstances comparable to Weibel's model (no bronchomotor tone, 75% TLC) as either of the entry length estimates. On the other hand, good theoretical evidence has been presented that entry length phenomena may contribute in an important way to bronchial resistance, and these theories provide an excellent framework for further experiments.

In summary, steady flow through branched tube models of bronchial geometry cause frictional pressure losses three to four times greater than those of laminar flow when Re are as low as 200. The theory of boundary layer growth in branched tubes adequately accounts for the additional pressure

losses, and predicts that bronchial resistance varies as the square root of gas viscosity, density and flow rate. Even larger pressure losses may occur in larger bronchi due to boundary layer turbulence, unsteady flow and wall irregularities. Such losses would cause resistance in central airways to be more dependent on flow rate and gas density, and less dependent on gas viscosity. The low R_e of peripheral airways may minimize the additional losses, and laminar flow may prevail.

3. Observed Effects of Gas Physical Properties and Flow Rate

Gas physical properties were varied in a number of pulmonary mechanics studies (8, 9, 10, 11, 13, 34, 50, 55, 58, 69, 70, 79, 85, 87, 94, 95, 96, 114, 142, 144, 156, 164), and their results were comprehensively reviewed (34, 50, 81, 99). In general, these investigations shared the objective of determining the physical basis of pulmonary resistance by comparing results with predictions based on Rohrer's equation. Excluding earlier studies of historical value, there remain relatively few investigations which contribute observations bearing directly on the nature of pulmonary resistance (50, 69, 70, 85, 87, 94, 156). A remarkable combination of hypotheses, methods, gases and presentation of results complicates comparison between studies to the extent that the extensive literature tends to consist of unrelated observations.

Barach (8, 9, 10) reported marked relief from dyspnoea in several patients with either severe asthma or laryngo-tracheal obstruction when they breathed a gas mixture of 20% O_2 in helium (HeO_2). When subjects breathed quietly through a 3 mm i.d. orifice, the pressure at the mouth decreased from 10.2 to 4.6 cm H_2O when HeO_2 was substituted for air. A similar reduction in pleural pressure excursions were observed in anaesthetized, dogs breathing through an added external

resistance, although no difference was observed when the external resistance was removed. Barach speculated that the 3 fold decrease in gas density during HeO_2 breathing may have little effect in normal subjects where the force required to move gas is small, but may substantially reduce the work of breathing in patients with obstructive lung disease. This insight is correct insofar as the flow regime in the added resistance is density dependent.

Bayliss and Robertson (13) calculated pulmonary viscance from plots of pleural pressure and lung volume obtained in three cats ventilated with air or 20% oxygen in hydrogen (H_2O_2) at 9, 18, and 36 cycles per minute. Although H_2O_2 is only one fourth as dense and 60% as viscous as air, pulmonary viscance was similar on the two gases - except at the highest frequency, where the viscance ratios ($\text{H}_2\text{O}_2/\text{Air}$) were .93, .63 and .77. Using a similar technique, Dean and Vischer (34) observed no difference in the pulmonary viscance of tracheotomized dogs breathing air or HeO_2 . They concluded that if a 3 fold reduction in gas density did not alter viscance, a fully developed laminar parabolic flow regime must exist in the bronchial tree. They pointed out, however, the large component of volume dependent, flow independent "plastic" viscance in their measurements. Presumably the large tidal volumes and low end expired volumes in both of these experiments caused considerable P-V hysteresis, so that the viscous pressure losses of air flow were too small to contribute a detectable difference during foreign gas breathing. McIlroy and Christie (95) measured the tidal volume of excised human lungs ventilated with a constant transpulmonary pressure at 3 and 15 breaths per minute. Because an index of viscous resistance (V_{T3}/V_{T15}) did not change during ventilation of 3 normal lungs with 90% H_2 , they also concluded that most viscance was due to tissue rather than gas flow.

Otis and Bembower (114) used the interruptor technique to measure pressure-flow relations in twenty normal subjects breathing air or HeO₂. Curves were fitted by eye through the P- \dot{V} data for each subject, and mean (\pm SE) resistive pressures for all subjects were determined from these curves at 0.25 lps. increments of flow. When these data were analyzed according to Rohrer, the theoretical P- \dot{V} relations fell within 1 SE of the measured values. Thus K₁ was equal on the two gases according to their similar viscosities, and K₂ on air is three times greater than the HeO₂ values, according to the density ratio of these gases. Although these data were interpreted to support Rohrer's description, the authors pointed out a systematic discrepancy between the measured values and the expressions above. In fact, when the measured values in their Figure 2 are replotted as P/ \dot{V} against \dot{V} , the slopes (K₂) and zero flow intercepts (K₁) give the following expressions;

$$P_{\text{air}} = 2.28 \dot{V} + .57 \dot{V}^2$$

$$P_{\text{HeO}_2} = 1.74 \dot{V} + .29 \dot{V}^2$$

Thus, the best fit to the measured values shows a two fold decrease in K₂ during HeO₂ breathing and a corresponding 20% reduction in K₁. Similar observations were made in three subjects breathing air at reduced ambient pressure, where the same systematic discrepancy between theoretical curves and measurements was evident. The authors reasonably concluded that reduced gas density lowers airways resistance by diminishing pressure losses due to turbulence, although it was not conclusively shown that this reduction conforms to Rohrer's prediction.

Using an esophageal balloon, Fry et al. (50) measured the frictional component of P_L by interruptor technique in subjects breathing air and a mixture of 20% O₂ in argon (A O₂). They reasoned that P_fr was due to tissue viscance and resistance to laminar and

turbulent gas flow.

$$P = K_1 \mu \dot{V} + K_2 \rho \dot{V}^2 + K_3$$

where K_3 is the coefficient of tissue resistance. Since A O_2 was 1.18 times as viscous and 1.33 times as dense as air, the kinematic viscosities differed by only 10%, suggesting a similar distribution of turbulence for the two gases at the same lung volume and flow rate. The constants $K_1 \mu$, and $K_2 \rho$ were obtained by successive differentiation of measured P- \dot{V} curves on each gas. In 18 normal subjects,

$$P_{\text{air}} = 1.50 \dot{V} + .71 \dot{V}^2$$

$$PAO_2 = 1.87 \dot{V} + .99 \dot{V}^2$$

and in 14 patients with emphysema,

$$P_{\text{air}} = 6.04 \dot{V} + 1.87 \dot{V}^2$$

$$PAO_2 = 7.12 \dot{V} + 2.50 \dot{V}^2$$

For both groups, the change in resistance on argon was completely accounted for (within the variability of measurements) by the change in gas physical properties, suggesting that K_3 is negligible. To the extent that the change in pressure on flow interruption measures gas flow resistance only (104), these results do not disagree with other studies demonstrating significant tissue resistance, and validate Rohrer's equation for gases of equal kinematic viscosity.

McIlroy et al (94) measured R_L during single inspirations of pure helium and ethane. The constants K_1 and K_2 were quite different from those predicted from the constants on air. Despite its greater viscosity, helium produced a substantial fall in K_1 , whereas ethane produced no change in K_1 though its viscosity is about half that of air. When air density was increased in a hyperbaric chamber at 4 Ata, both K_1 and K_2 increased in 3 subjects (87).

$$\text{at 1 Ata, } P = 1.27 \dot{V} + .50 \dot{V}^2$$

$$\text{at 4 Ata, } P = 2.37 \dot{V} + 1.17 \dot{V}^2$$

Maio and Fahri (85) measured R_L in another 3 subjects breathing gases of different molecular weight at different ambient pressures. Resistances were quite similar when identical gas densities were produced by different combinations of gas and pressure, and increased with relative gas density (RGD) and flow rate according to the regression,

$$P = .45 (RGD + .63) \dot{V}^{1.6}$$

By substituting appropriate values for RGD and \dot{V} , Rohrer's constants may be calculated for air breathing:

$$\text{at 1 Ata, } P = .28 \dot{V} + .42 \dot{V}^2$$

$$\text{at 4 Ata, } P = .84 \dot{V} + 1.20 \dot{V}^2$$

In both hyperbaric studies, K_1 increased with no viscosity change, and K_2 increased somewhat less than the 4 fold density change. Accordingly, Rohrer's equation did not provide an adequate physical basis for the changes in resistance which occurred with changes in gas kinematic viscosity. This was attributed to an alteration in the distribution of turbulence (50, 94), or to failure of the equation to account for boundary layer growth (120, 121).

In 5 subjects breathing air between 0.5 and 5.2 Ata, Varene et al (156) found R_{aw} to increase according to the exponential equation,

$$R_{aw} = K \rho^{.59}$$

Mean R_{aw} was about 2.5 times greater at 4 Ata (3.91) than at 1 Ata, and this effect was intermediate between the 2.0 and 2.9 fold increases found in similar studies (85, 87) discussed above. The exponent relating gas density to resistance for these data is quite similar to that relating \dot{V} to R_L in the study of Maio and Fahri (85). Thus, the limited data available suggest that resistance varies as the 0.6 power of gas density and flow rate for these conditions. During HeO_2 breathing,

the change in density may have less effect on resistance, as indicated by exponents of 0.3 calculated from the measurements of Grapé et al (58) and Otis and Bembower (114). Such a trend was demonstrated in the upper airway (69, 70), where the complicated fluid dynamics of a Venturi tube provided an adequate explanation. If the bronchial flow regime is similar, the frictional pressure drop would not be explained by the classical flow regimes either alone or in combination, but rather by a continual metamorphosis according to the prevailing Re .

CHAPTER III

INTRAPULMONARY DISTRIBUTION OF INSPIRED GAS

A. Quasi-static Distribution

During quiet breathing, the distribution of ventilation is uneven in the sense that lung regions receive different fractions of the inspired (ΔV) in relation to their end-expiratory volume (V_0). This conclusion is supported by extensive observations of multiple and single breath washouts of tracer gas from the lung and by estimates of regional ventilation by broncho-spirometry and radioactive gas techniques (15, 18, 47, 107). In the majority of multiple breath washout studies, two or more exponentials are required to describe the replacement of lung gas by its diluent (133). Thus, the normal lung washes out as if it consisted of two or more chambers with different $\Delta V/V_0$. Following a slow vital capacity inspiration of oxygen, the expired gas contains progressively less oxygen as expiration proceeds. This must be due either to incomplete mixing within alveoli or to changes in the proportion of total expired gas delivered from regions having different $\Delta V/V_0$. Radioactive gas techniques have demonstrated a vertical gradient of $\Delta V/V_0$ and bronchspirometry has demonstrated a wide range of $\Delta V/V_0$ within a given vertical region. The former is likely due to a gravity dependent gradient of pleural pressure, but little evidence is available to assess the mechanisms proposed to explain the latter.

1. Uneven $\Delta V/V_0$ Between Vertical Lung Regions

a. Different V_0 . The end expiratory volume of lung regions is presumably determined by the local static transpulmonary pressure and the volume-pressure characteristics of the region. In a classic study, Milic-Emili et

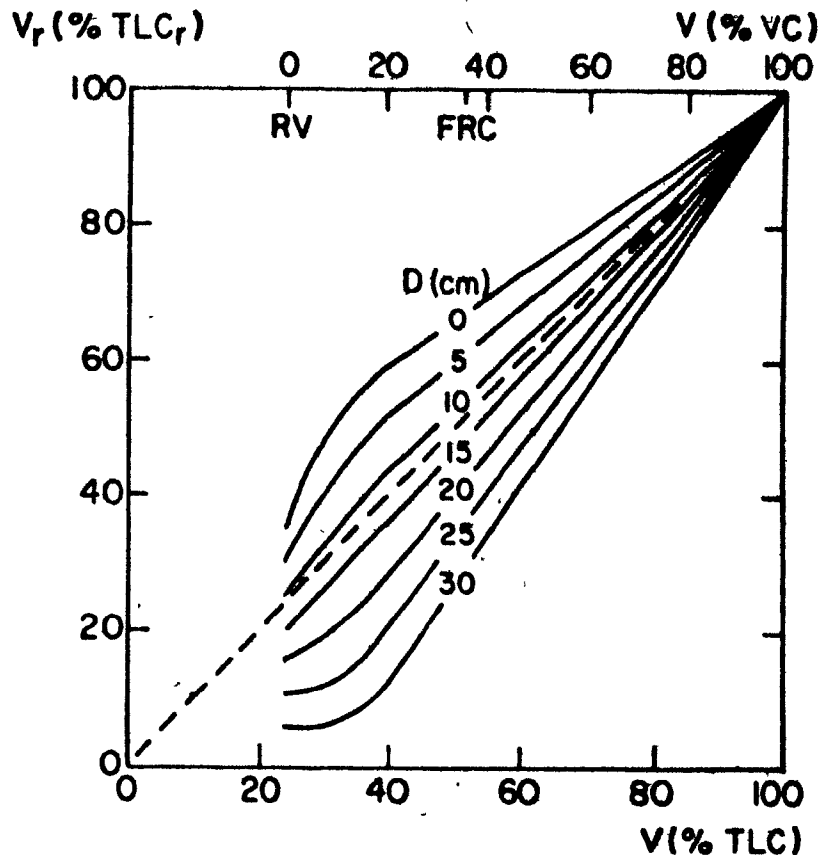
al. (107) demonstrated that upper lung regions are more expanded relative to their total capacities than dependent regions.

Subjects inspired air labelled with radioactive Xenon (^{133}Xe) from residual volume to TLC. During short breath hold periods at 12 to 20 different inspired volumes, gamma radiation was detected with scintillation counters spaced at different distances (D cm) from the lung top. Regional count rates at each lung volume were converted to regional concentrations by repeating the measurements when gas in the lung was equilibrated with a known ^{133}Xe concentration in a closed circuit spirometer (7). Accordingly, regional volume as a percent of regional TLC, V_r (% TLC_r), is the regional concentration at each volume as a percentage of the regional concentration at TLC. When V_r (% TLC_r) was plotted against lung volume as a percent of TLC, upper lung regions were more expanded than lower regions (Fig. 2). Between FRC and TLC, this relationship was described by the mean linear regression equation for all subjects:

$$\text{FRC}_r = 67.5 - 1.188 D \quad (1)$$

Assuming the elastic properties of the lung to be uniform, the vertical gradient of static transpulmonary pressure was calculated for each subject from his gradient of regional expansion and the pressure volume characteristics of his lung. The close agreement of the predicted gradient (0.2 cm H₂O per cm distance down the lung) with direct measurements of the gradient led the authors to conclude that "intrinsic differences in regional static volume/pressure relations contribute little to the nonuniform regional distribution of gas in the lungs" which "appears to result mainly from regional differences in static transpulmonary pressure" (107). At full inspiration, the flat slope of the pressure-volume curves leads to negligible differences in regional expansion due to the relatively small gradient in pleural pressure. As lung volume decreases, the P-V slope becomes steeper, and the same gra-

FIGURE 2



Ordinate: Regional lung volume, expressed as % regional TLC (V_r % TLC_r).
 Abcissa: Overall lung volume, expressed as % TLC and % VC. Each solid line represents a vertical lung region located D cm from the lung top in a seated subject.

Regional lung volume decreases with distance from the lung top, and uppermost regions are about twice as expanded as lowermost regions at RV and FRC. Above 25% VC, the steeper slopes for dependent regions indicate their greater contribution to overall volume change, and the linear relationships for all regions indicate that regional volume change is not sequential. As lung volume is reduced below 25% VC, upper lung regions contribute a progressively greater proportion of overall volume change (after Milic-Emili et al (107)).

dent in transpulmonary pressure causes increasing differences in regional expansion. The vertical gradient in alveolar size was subsequently confirmed by microscopic study of lungs of dogs frozen intact (56).

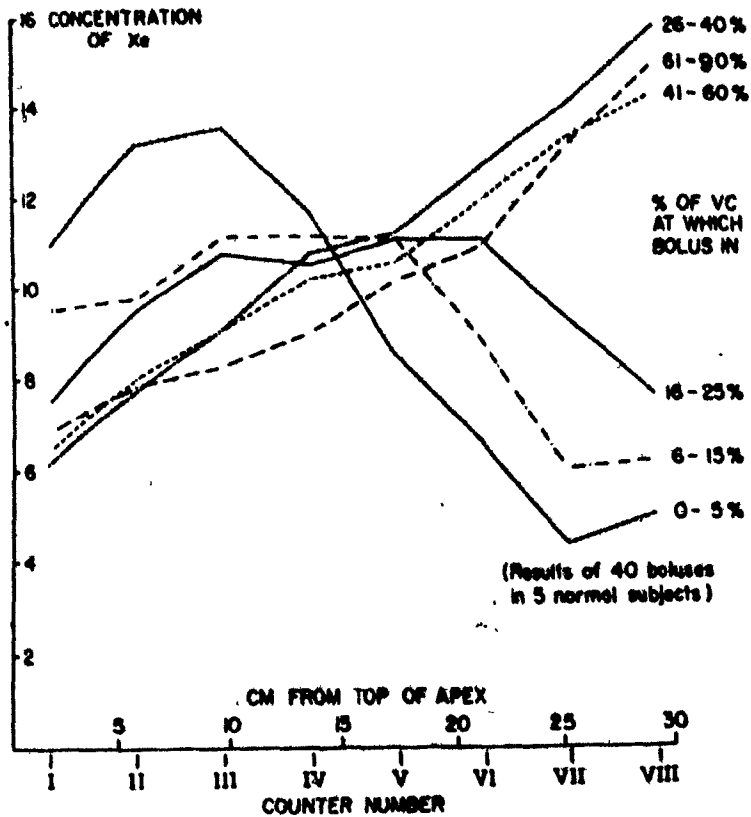
b. Different ΔV . The quasi-static change in volume of a lung region is presumably determined by its volume pressure characteristics and the local change in static transpulmonary pressure (ΔP). Dollfuss et al. (36) studied the vertical distribution of 4 ml bolus of ^{133}Xe injected into the inspire at various lung volumes during a slow vital capacity inspiration. Concentrations at TLC following injection at lung volumes greater than 25% VC showed a systematic gradient from low values at the apex to high values at the base (Fig. 3). The preferential distribution of inspired gas to lung bases is consistent with the regional volume-overall volume plots of Milic-Emili et al. (107), who offered this explanation: "As a result of the less subatmospheric pleural pressure at their level, the lower regions of the lungs lie on a steeper part of the static volume/pressure curve than the upper zones. Therefore, regionally uniform changes in pleural pressure that occur during inspiration produce relatively greater volume changes in lower than in upper regions". Accordingly, there is a systematic difference in lung compliance between regions of different vertical distance from the lung top. The relative compliance of two regions (C_1/C_2) may be calculated from equation 2,

$$C_1/C_2 = (100 - \text{FRC}_1)/(100 - \text{FRC}_2) \quad (2)$$

where FRC_1 and FRC_2 are obtained from equation 1. When regions 1 and 2 are 5 and 30 cms from the lung top respectively, the compliance of the superior region is only 56% of the regional compliance at the lung base.

It is interesting to express the gravity dependent differences in $\frac{\Delta V}{V_0}$ in terms of alveolar differences of nitrogen concentration following a tidal breath of oxygen. Alveolar nitrogen (% N_2) at end inspiration can be calculated from the FRC (V_0) and tidal volume (ΔV) assuming negligible dead

FIGURE 3



Average regional ^{133}Xe concentration (ordinate) measured in eight vertical lung regions (abscissa) following bolus inspiration from different lung volumes.

Above 25% VC, the proportion of ^{133}Xe delivered to vertical lung regions increases with their distance from the lung top, and the ΔV of the lowermost region is about twice that of the uppermost region. This relationship is reversed when inspiration starts at RV (after Dollfus et al (36)).

space.

$$\% N_2 = \frac{V_0}{V_0 + \Delta V} \times 79 \quad (3)$$

Regional FRC (V_{0R}) expressed as a percent TLC_R may be estimated from equation 1. Similarly, the regional tidal volume (ΔV_R) as a $\%$ TLC_R , is estimated from the mean regression equation in table IV of reference 107, rewritten:

$$\Delta V_R = (.667 + .023 D) \frac{\Delta V}{TLC} \% \quad (4),$$

For a tidal volume equal to 10% TLC, equations 1, 3 and 4 may be combined:

$$\% N_2 = \frac{67.5 - 1.188 D}{74.2 - .96 D} \times 79 \quad (5)$$

Solving for the most widely separated regions ($D = 5$ and 30), nitrogen concentrations range from 70% (superior) to 54% (basal). For larger tidal volumes, regional concentrations decrease and their differences increase, so that a tidal volume equal to 20% TLC results in N_2 concentrations of 65% and 44%. Thus, the gravity dependent gradient in pleural pressure accounts for considerable unevenness in the intrapulmonary distribution of inspired gas.

c. Sequential Ventilation. Lung regions having the same $\Delta V/V_0$ may be unevenly ventilated if the dead space (VD), which contains alveolar gas, is distributed differently from the fresh inspired gas ($VD/V_0 \neq \Delta V/V_0$). Regions ventilate sequentially when their fractional contribution to the total change in lung volume varies throughout the respiratory cycle. For quasi-static changes in lung volume, Sutherland et al. (152) demonstrated that vertical regions having widely different $\Delta V/V_0$ will contribute a constant proportion throughout inspiration and expiration if the regional pressure-volume characteristics are uniform and mono-exponential and if the regional changes in transpulmonary pressure are equal. Any departure from these conditions may cause sequential ventilation due to the static pressure-volume characteristics of lung regions. This differs from asynchronous ventilation, which may develop during rapid changes in lung volume, causing a departure from the sta-

tic elastic equilibrium of lung regions. These dynamic events are reviewed in Section B of this Chapter, and are mentioned here only to distinguish them from quasi-static sequential ventilation. It should be noted that asynchronous ventilation may either enhance or diminish sequential ventilation.

Much of the evidence concerning sequential ventilation was obtained from the curve relating expired gas concentration to expired volume. Following a single breath of oxygen, the expired N_2 -volume plot shows four distinct phases: I) a volume usually less than 100 ml containing no N_2 ; II) a similar volume demonstrating a sigmoid-shaped increase in N_2 ; III) a linear increase of 1 to 2% N_2 per litre expired (alveolar plateau); and IV) an increase in the slope of the alveolar plateau as lung volume approaches RV.

(1) Different Pressure-Volume Characteristics

(a) Low Lung Volumes. Rauwerda (129) and Fowler (47) suggested sequential regional filling, such that early-filling regions inspired most of the dead space, which contains nitrogen during oxygen breathing. They concluded that these regions with high nitrogen tensions expired late in expiration giving the characteristic upward slope of the alveolar plateau. This "first in - last out" hypothesis was tested by following an inspiration of oxygen with a further inspiration of air. When the inspiration began at RV, the "first in" regions containing more oxygen were "last out", as evidenced by the downward slope of the alveolar N_2 plateau at end expiration. No reversal of the terminal slope was observed when the experiment was initiated at FRC.

Koler et al. (75) measured the relative expansion of upper and lower lobes with closed circuit bronchspirometry. During an interrupted vital capacity inspiration from RV, upper lobes received more of the early inspire and less of the late inspire than lower lobes. No consistent pattern was demonstrated between lobar contributions to early expiration, but upper lobes

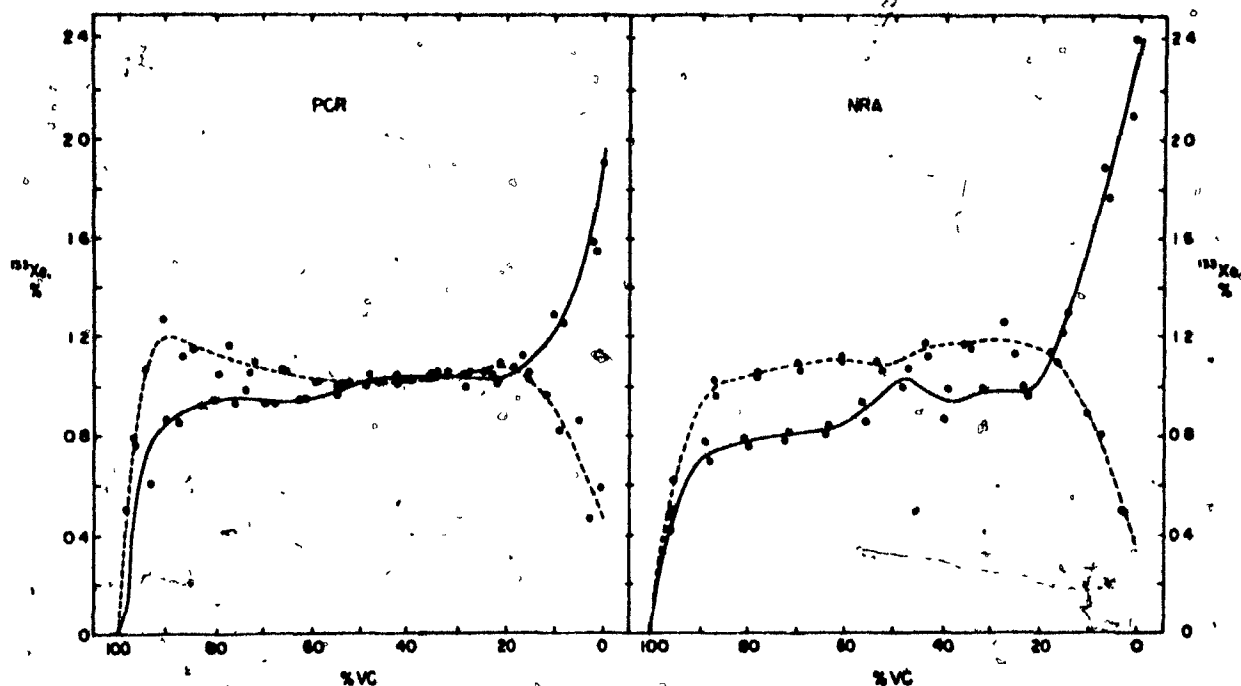
contributed an increased proportion to late expiration. Since lower lobes are dependent in upright and supine man, these observations may be due to the pleural pressure gradient (see below) and offer no conclusive evidence regarding the intrinsic P-V characteristics of lobes at low lung volumes. These results demonstrate interlobar sequential ventilation at low lung volumes, but no evidence is presented to support "first in - last out" sequential ventilation at mid lung volumes.

Radioactive gas techniques have confirmed a gravity dependent inspiratory sequence which occurs only when inspiration is initiated at low lung volumes. Milic-Emili and co-workers (Fig. 2) observed that most of the volume change from RV to 20% VC occurred in superior lung regions, and suggested that dependent airways closed at low lung volumes. When subjects inspired ^{133}Xe boli from RV, regional concentrations were much greater in apical than basal regions (Fig. 3). The slope of the subsequent expired plateau (Fig. 4) increased at about 25% VC (Phase IV) indicating an increase in the proportion of the expirate coming from upper regions. The end expired ^{133}Xe concentration approximated pre-expiratory concentrations in apical regions. When apical regions having high concentrations of tracer were made dependent by inverting the subject prior to expiration, Phase IV sloped downward (Fig. 4). Similar findings in other body positions suggest that the gravity dependent pleural pressure gradient causes closure of basal airways at low lung volumes.

Thus the "first in - last out" units demonstrated in upright normal subjects breathing at low lung volumes reside in apical regions. In considering sequential ventilation during quiet breathing it is important to separate this exclusively low lung volume event from other mechanisms.

(b) Mid-lung Volumes. From the linear relations observed between regional degree of expansion and overall lung volume above 20% VC, Milic-Emili et al (107) concluded that inspiration was not sequential except

FIGURE 4



Expired concentration versus volume curves from two subjects who inhaled ^{133}Xe bolus from RV while standing erect. Unbroken lines represent data gathered when subject expired slowly standing up; dashed lines represent data gathered when subject expired slowly in the head-down position.

At about 20% VC, expired concentration changed abruptly, and values at RV approximated concentrations in the uppermost lung region, indicating gravity dependent sequential emptying of vertical regions at low lung volume.

At higher lung volumes, the upward slope of Phase III (unbroken lines) may be explained if upper regions contribute an increasing proportion of the expirate as lung volume decreases. During head-down expiration, the slope was reduced or reversed, indicating gravity dependent sequential emptying of vertical regions at mid lung volumes. (from Anthonisen et al (2)).

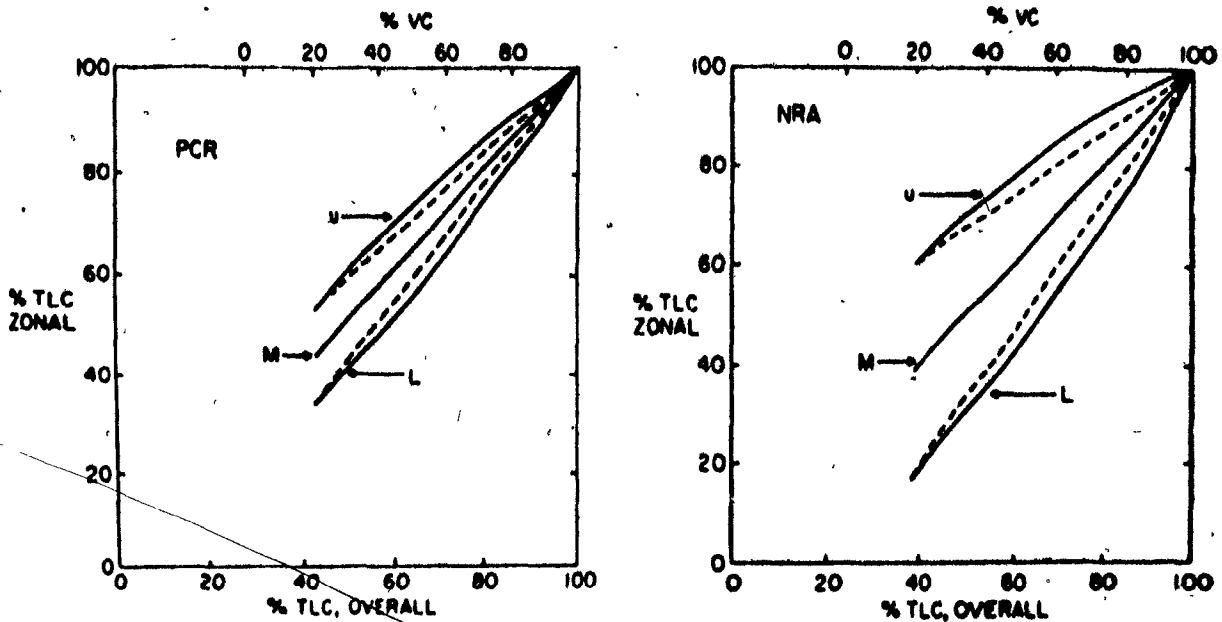
During rapid expiration, Phase III is horizontal, (not shown) indicating that sequential emptying is abolished (72, 108).

at low lung volumes. This relationship was not detectably different when regional expansion was measured by inspiring ^{133}Xe labelled gas to TLC following a slow deflation from TLC, suggesting that the relative rates of emptying of the regions with open airways are probably virtually constant (152).

More sensitive techniques have demonstrated sequential emptying of vertical lung regions. During expiration, Phase III slopes upwards when units with high concentrations are superior, but when these units are made dependent by inverting the subject before expiration, Phase III slopes downwards (2, 26). By combining pre-expiratory regional concentrations with the expired plateaux, Anthonisen et al. (?) calculated that late emptying of superior regions and early emptying of dependent regions departed very little from the emptying pattern observed by Sutherland et al. (Fig. 5). Yet this slight sequential emptying can cause a significant slope of Phase III when vertical concentration differences are large. They concluded that since sequential emptying is gravity dependent, it is not likely due to differences of intrinsic pressure-volume characteristics between lung regions, but rather to volume dependent differences in regional ΔP or to a nonmono-exponential nature of regional P-V curves. Although this conclusion is quite reasonable, it should be noted that the large vertical concentration gradient is not physiological and may obscure intraregional sequential emptying. It follows that the latter is not ruled out as a major contributor to the expired plateau.

The scintillation counters employed in these studies necessarily examine both upper and lower lobes in all but the highest and lowest lung regions (122). Several groups have indirectly estimated lobar pressure-volume characteristics in man. Equal lobar compliances were found in normal subjects when one lobe was blocked and used as a "pressure capsule" to estimate pleural pressure changes per unit volume change measured by closed circuit bronchspirometry in the other lobe (67). Validation of this method was not present-

FIGURE 5



Effect of sequential emptying on regional lung volumes. Ordinates: Regional volume, expressed as % regional TLC. Abscissas: Lung volumes as % TLC. Solid lines (U,M,L) represent emptying patterns of three vertical lung regions required to account for the upward slope of Phase III in Figure 4. Dashed lines represent what upper and lower regional volumes would have been during non-sequential emptying. (after Anthonisen et al (2)).

During rapid expiration, all regions empty along M, indicating that contributions to the expirate from vertical lung regions are not only constant (as with dashed lines), but they are equal (72, 108).

ed and the possibility of local pleural pressure changes over the obstructed lobe (171) makes the interpretation of these results difficult.

In the excised dog lung, slight but significant differences have been observed between the deflation pressure-volume characteristics of upper and lower lobes (43, 48). Upper lobes are more expanded relative to their total capacities than lower lobes. The volume change of upper lobes ($\% \text{ TLC}_u$) exceeds that of lower lobes ($\% \text{ TLC}_l$) between P_L 5 and 0, but is less than lower lobes at higher transpulmonary pressures. The net effect is a smaller $\frac{\Delta V}{V_0}$ in upper lobes above 40% TLC and a relatively greater contribution of upper lobes to late expiration than is predicted above by assuming uniform P-V characteristics.

In the same study, Faridy et al. (43) observed similar results when the degree of lobar expansion ($\% \text{ TLC lobe}$) was measured in relation to overall lung volume ($\% \text{ TLC lung}$) by radioactive gas techniques. Bake et al. (6) used essentially the same techniques to study apical and basal expansion in six supine living subjects. Since gravitational differences were minimal, the striking similarity of their results to those in excised dog lungs suggested different P-V characteristics between human upper and lower lobes. The implications of these findings are a slightly increased vertical gradient of ventilation and "first in - last out" sequential ventilation in the sense that the relative contributions of lower lobes to inspiration and expiration increases with lung volume. Accordingly, these differences would exaggerate the gravity dependent sequence in upright man at mid-lung volumes and minimize it in the inverted position.

(2) Different ΔP . Sequential emptying of parallel units during a quiet expiration may be explained if the change in pressure applied to high $\frac{\Delta V}{V_0}$ units during early expiration exceeds the ΔP of low $\frac{\Delta V}{V_0}$ units and this topography changes with expired volume towards a greater ΔP over the poorly ventilated units. If similar volume dependent inequalities of ΔP occur during

inspiration, "first in" units will inspire a large fraction of the common dead space. This mechanism is not directly investigated by measurements of regional ΔP between end-inspiration and end-expiration, which do not necessarily convey sequential information. A further distinction is necessary between this volume dependent inequality of regional ΔP and time dependent asynchrony of ΔP , the latter being of possible importance only during rapid breathing.

Larger ΔP over lower lung regions were measured with intrapleural needles in the dog (42) and in seated human volunteers (33). Agostoni (1) criticized this "small bubble" method for the distortions introduced by the surface tension of the air-liquid interface and the small radius of curvature of the deformed lung. The "pressure capsule" method (67) also recorded larger ΔP in lower lobes than upper lobes in seated or supine normal subjects during quiet breathing, but these pressures may not reflect local pleural pressure changes associated with normal lobar expansion. Although these methods may be inadequate, the findings of Bake et al (6), explained above by differences in lobar elastic properties, would be equally well explained by a higher ΔP over lower lung regions at mid lung volumes. Schilder et al (143) measured more negative end-expiratory pressures in upper esophageal balloons than in middle and lower balloons in seated subjects, yet observed no significant vertical difference in ΔP during maximal voluntary ventilation. It appears reasonable to conclude that the topography of pleural surface pressure under dynamic conditions is still to be investigated (1).

Thus, sequential ventilation of vertical lung regions occurs at low lung volumes due to closure of dependent airways. When all airways are open, the proportion of a change in lung volume contributed by dependent regions increases as lung volume increases (Fig. 5 solid lines). Accordingly, dead space is preferentially distributed to upper lung regions during

quiet breathing, thereby increasing the nonuniformity of ventilation among vertical lung regions. This effect is necessarily small at mid-lung volumes because dead space is a small proportion of the tidal volume and the amount of sequential ventilation is small. In contrast, airway closure at lower volumes may cause a marked reduction in the ventilation of dependent regions.

2. Uneven $\Delta V/V_0$ Within Small Lung Regions

In a series of N₂ washout experiments during bronchspirometry, Martin, Young and their coworkers have examined the distribution of ventilation within broncho-pulmonary regions. Following a single breath of oxygen, N₂ concentrations were greater in the expirate from upper lobes than from lower lobes, and lobar alveolar plateaux sloped upward and exhibited cardiogenic oscillations (88). The results suggested better ventilation of lower lobes than upper lobes in normal supine man, providing the first localization of parallel compartments having different $\Delta V/V_0$. Since the % N₂ in the expired gas indicates the degree of dilution of alveolar gas by the inspired oxygen, oscillations of N₂ concentration on the lobar plateaux must indicate a range of $\Delta V/V_0$ within each lobe. Finally, the sloping lobar plateaux indicated incomplete diffusive mixing or sequential emptying of parallel units, such that high $\Delta V/V_0$ units contributed a greater proportion to early expiration. These observations and conclusions may be explained by the vertical gradient of pleural pressure, since the lower lobes of supine man are dependent with respect to gravity and the vertical height of lung lobes is substantial. This is a less likely explanation of similar observations at the segmental level, where sloping expired plateaux with cardiogenic oscillations signified intrasegmental uneven ventilation (168). Multiple breath washouts from lobes, segments and subsegments subtended from 3 mm bronchi demonstrated a range of $\Delta V/V_0$ which was as wide as the observed in the whole lung (149). They conclude that hydrostatic forces cannot be a major cause of uneven ventila-

tion, since the mechanical properties of the lung responsible for these differences are as widely distributed in volumes less than 20 ml as they are in the whole lung.

a. Series Inhomogeneity. In the previous discussion, the lung was considered to consist of two or more chambers connected in parallel, each containing gases of uniform concentration. An alternative model considers a proximal well-ventilated space connected in series with a peripheral poorly ventilated space. The different gas concentrations in the two chambers proceed toward equilibrium by molecular diffusion. The question of whether inter-gas diffusion proceeds to completion during the time of a respiratory cycle has been the object of experiment and controversy since the study of Krogh and Lindhard (76). Even if the time for complete diffusional mixing is too short, the concentration differences along a single pulmonary pathway may be abolished by convective mixing of inspired and alveolar gas (42). If mixing by diffusion and convection are incomplete, there exists a gas concentration gradient along each pulmonary pathway, causing the most distal alveolar gas to be less diluted by the inspired gas than when gas concentrations are uniform.

(1) Diffusion in Lung Models. The time required for complete diffusion mixing has been examined by applying the laws governing the process to theoretical lung models. The models are usually based on the morphometry of Weibel (159), which predicts that a tidal volume of 750 ml inspired into the lung with a square front reaches the twentieth generation not more than 2 mm. from the distal end of the alveolar sacs. Rauwerda (129) calculated that a concentration gradient between nitrogen and oxygen is reduced in .38 sec^s to 16% of its original value over a 2 mm distance from the distal surface of his lung model. On the basis of these calculations the possibility of significant series inhomogeneity of ventilation was virtually discarded for

twenty years. Cumming et al. (29) pointed out that the closed proximal end of Rauwerda's model is an unrealistic feature which increases the rate of diffusion mixing in the distal direction. In their model of the airways, a similar concentration difference established 2 mm from the distal end decreased in 1 second to 8% of the initial value, and this gradient was spread over the distal 7 mm of the model. Piiper and Schold (123) transformed this gradient from linear distance to airway volume. They concluded that the concentration differences were abolished in less than 1 second in the distal four generations containing most of the volume. Accordingly, the 8% difference at 1 second was confined to a small airway volume. When LaForce and Lewis (78) examined a model which included alveolar volume, no gradient remained after 0.1 sec in the last three generations containing 60% of the lung volume. They conclude that series inhomogeneity must be insignificant during normal breathing.

The calculations in these studies assume a step concentration difference established at a site within the lung where airway volume is equivalent to the tidal volume. Cumming et al. (31) considered movement of the interface with convective flow during tidal volume cycles of 500 and 1000 ml. The initial concentration gradient spread along the airway during inspiration, and the locus of 50% of the initial concentration proceeded no further than 250 ml down the lung model when the convective flow rate was .67 lps. At this point, molecules moved mouthward by diffusion as fast as convective flow moves them toward the alveoli, so that an assumption which establishes the gradient 500 or 1000 ml within the lung underestimates the time required for diffusive mixing. This concept may considerably alter the relevance of molecular diffusion to uniformity of ventilation distribution. Where earlier considerations placed the interface between inspired and alveolar gas within a very few mm of the gas exchanging surface, it may be located in some peripheral airways beyond which multiple parallel units having different $\Delta V/V_0$ exist.

It follows that molecular diffusion may act to equalize not only stratified concentrations but also parallel inequalities. The authors point out that the critical nature of the boundary condition to these calculations necessitates more accurate estimates of airway morphometry and consideration of the effects of gas mixing by convective diffusion (154), turbulence, and secondary motions at airway bifurcations. As no analysis has defined these conditions satisfactorily, a conclusion about the completeness of gas mixing from model studies is not yet possible.

(2) Diffusion and the Alveolar Plateau. Following a tidal breath of oxygen, expired nitrogen concentrations increase with volume expired in mid-lung regions. The progressive increase in the proportion of gas delivered from poorly ventilated regions may be due to asynchronous emptying of parallel units or to incomplete diffusion mixing in series units. Alternatively, progressive diminution of lung volume due to a respiratory quotient (R) less than 1 may increase the alveolar nitrogen concentration with time. Results of the excellent study of Sikand et al. (147) help to separate the possible mechanisms. Following a 1.5 l inspiration of argon-oxygen, the expired argon/nitrogen ratios (A/N_2) decreased continuously. Since R affects both inert gases equally, these results indicate a rise in expired nitrogen unrelated to pulmonary gas exchange. Dependent lung regions having high $\Delta V/V_0$ contribute a greater proportion of the early expirate (2, 26). Since they also have lower \dot{V}_A/Q ratios than upper regions (7, 160), expired O_2 and CO_2 concentrations must indicate a progressive rise in R if sequential emptying of vertical lung regions is responsible for the alveolar N_2 slope. This change was not observed, and the alveolar slope of A/N_2 decreased with breath hold time, suggesting that series inhomogeneity is the main factor contributing to the alveolar plateau. These results were reasonably simulated in a lung model consisting of three evenly mixed compartments in series. A 1.5 l in-

spirate filled a .3 l dead space, mixed uniformly by convection with alveolar gas in an intermediate 3.0 l chamber, and diffused into a 1.0 l terminal chamber.

It is interesting that the 16% difference between nitrogen concentrations in the upper and lower lung regions do not contribute to the alveolar slope. The majority of evidence supporting gravity dependent sequential emptying (2, 26) was obtained with concentration differences larger by several orders of magnitude than during the conventional single breath test. This suggests that the small amount of regional sequential emptying is not detectable when concentration differences are smaller. Alternatively, the high expiratory flow used may have abolished the sequential emptying of vertical lung regions (72, 108), thereby underestimating its contribution to the alveolar plateau of R during normal single breath. Piiper and Scheid (123) point out that there is no reason for parallel inhomogeneity within small lung regions to correlate with \dot{V}_A/Q inequality as has been argued for the gravity dependent vertical gradients. Accordingly, the results of Sikand et al (147) do not exclude a major contribution to the alveolar N_2 slope by sequential emptying of intraregional parallel units having different $\Delta V/V_0$. Indeed, their experimental results may be alternatively explained by parallel inhomogeneity if different gas concentrations between such parallel units approach equilibrium with breath hold time.

It is generally held that gas mixing during a breath hold occurs by molecular diffusion. Reduction of concentration differences between parallel vertical lung regions during a short breath hold is unlikely. Furthermore, if diffusion proceeds as in most lung model studies from a blunt interface located 2 mm from the distal surface of respiratory units, there is no anatomic basis for parallel units distal to the interface. However, if substantial alveolar gas is present in conducting airways as predict-

ed by Cumming et al. (31) breath-holding may promote uniformity of concentrations in the subtended parallel lung units.

Evidence supporting this possibility is reported by Engel and his colleagues (39, 40), who developed a rapid response technique for continuous measurement of nitrogen concentration (FN_2) in gas sampled through the walls of intrapulmonary airways. During inflation of the lungs of anaesthetized dogs with a constant flow (\dot{V}_I) of oxygen, cardiogenic oscillations of FN_2 were regularly observed in gas sampled from 4 mm (i.d.) airways. Following a two second breath hold, FN_2 in 4 mm airways was 50% of the alveolar concentration (FAN_2), and decreased progressively from these peripheral airways to the lobar bronchi, where FN_2/FAN_2 was less than 10%. At higher \dot{V}_I , the interface between inspired oxygen and alveolar gas was displaced toward the alveoli, whereas lower \dot{V}_I shifted the interface mouthward. As indicated by the reduction of dead space with breath hold time, the mixing between alveolar and inspired gas is much slower in the absence of cardiac activity. The authors conclude that cardiac induced flow oscillations in peripheral airways enhance gas mixing during a breath hold by promoting Taylor diffusion and/or convective mixing. During the subsequent expiration, (L. Engel, personal communication) cardiogenic oscillations of FN_2 occurred in all airways sampled. These were best explained by asynchronous emptying of parallel lung units having different FN_2 . As calculated from the height of expiratory cardiogenic ripples, the range of FN_2 in units subtended from bronchi 4 mm i.d. is reduced during a breath-hold. Such a reduction was not observed at the trachea. These results suggest a role for molecular diffusion in reducing the $\Delta V/V_0$ of peripheral parallel units during a breath-hold. The authors point out that uniformity of parallel unit concentrations is likely enhanced by reexpiration of gas expelled from numerous units and mixed in their common mouthward airway during each cardiac impulse. Similarly, the presence of alveolar gas in con-

ducting airways during the inspiratory phase of quiet respiration limits the range of gas concentrations in subtended parallel units (138).

It therefore appears necessary to modify the existing concept of intra-pulmonary inter-gas diffusion. Perhaps a first approximation of the required change is to partition the intermediate chamber in the model of Sikand et al. (147). The pressure volume characteristics of the two parallel compartments must produce different $\Delta V/V_0$ and sequential emptying such that the well ventilated unit contributes a greater proportion of the early expirate. Young et al. (170) proposed such a model and demonstrated that flow oscillations alter its emptying sequence when the resistances in the parallel pathways are equal (see below). To the extent that perfusion (Q) to each compartment is evenly distributed, $\Delta V/Q$ correlates positively with $\Delta V/V_0$; that is, in the opposite direction to the inverse correlation in gravity dependent units. Intrapulmonary gas mixing between the parallel units reduces the unevenness of ventilation.

Is a distal chamber in series with each parallel chamber required to account for stratification of gas tensions within each parallel unit? Several studies have demonstrated a separation of gases of differing diffusivity during a single breath test (30, 41, 54, 125). Although these results are interpreted as unqualified evidence supporting stratification, the possibility of diffusion among parallel units offers an alternative explanation. In a study by Cummins et al. (30) one litre of a gas mixture containing 40% SF₆ and 20% Ne, was inspired rapidly from FRC and expired at 1.0 lps. The results and interpretation of continuous measurements of ¹³³Xe and Ne during expiration are quite similar to the observations of Georg et al. (54) and Power (125). SF₆ is about seven times more dense than Ne, and, since diffusivity is inversely related to the square root of gas molecular weight (128), the diffusivity of Ne is about 2.7 times that of SF₆. When no end inspiratory pause

was allowed, the expired concentrations of both gases decreased as expiration proceeded. The slopes for each gas differed, in the sense that the Ne/SF₆ ratio increased throughout expiration. After a 5 second end-inspiratory breath hold, the alveolar plateau of Ne/SF₆ was horizontal and the expired ratio was identical to the inspired ratio. The alveolar slopes of each gas may be explained by stratification or by late emptying parallel units having low $\Delta V/V_0$ hence lower SF₆ and Neon concentrations than the earlier emptying parallel units. Assuming no separation of SF₆ and Ne during mass flow, it is argued that the Ne/SF₆ ratio in parallel units must be identical so that asynchronous emptying would give a horizontal Ne/SF₆ plateau. Accordingly, the upward slope of Ne/SF₆ must be due to more rapid diffusion of Ne toward the periphery.

However, to the extent that there is diffusion between parallel units, Ne moves more rapidly than SF₆ along the concentration gradient from the high $\Delta V/V_0$ unit to the low $\Delta V/V_0$ unit. Accordingly, the Ne/SF₆ ratio becomes lower in the early emptying unit, and the expired plateau is explained by sequential emptying of parallel units having different Ne/SF₆. This alveolar slope decreases with breath holding time as both gases equilibrate between the parallel units. The alveolar slope of each gas continued to change between 5 and 30 seconds although the Ne/SF₆ ratio did not, indicating that gas mixing during this interval was equal for Ne and SF₆. Piiper and Scheid (123) point out that this further homogenization is not easily explained by molecular diffusion in pulmonary air spaces, since the change should be different for the two gases. They suggest that gas mixing during this time occurs by diffusion through pulmonary tissue or by convective mixing caused by the mechanical action of the heart. Engel et al. (39) attribute the mechanical mixing action of the heart to Taylor diffusion and convective mixing. They calculated that the effective diffusivity of gases during Taylor diffusion is not related to

the gas molecular weight in the same way as molecular diffusion. In fact, for cardiogenic flow in 6 mm bronchi, both the effective diffusivity and the convective mixing due to secondary motion is greater for SF₆ than for air or helium. Accordingly, the paradox in the results of Cumming et al. (30) may be explained on the basis of continued homogenization of gas tensions among parallel units by a process less sensitive to molecular weight differences.

The slopes of the alveolar plateaux measured at FRC between the 750 and 1250 ml expired were 2.2% with no breath hold and .7% after a 30 sec breath hold (30). The authors conclude that at least two thirds of the plateau reflect incomplete diffusive mixing. It should be noted that this does not limit the contribution of sequential emptying of parallel units to less than one third of the slope, since gas mixing during a breath hold may reduce the slope of the alveolar plateau by diminishing concentration differences among intraregional parallel units. Furthermore, Anthonisen et al. (2) point out that the rapid inspiration and expiration used in this study considerably alter the parallel distribution of ventilation in the sense that concentrations in vertical lung regions are equalized (134) and sequential emptying is abolished (103). As a result, the parallel concentration differences may be much larger during a normal inspiration and expiration.

(3) Diffusion and Gas Exchange. Kvlstra et al. (77) ventilated dogs with hyperbarically oxygenated Ringer solution, and regularly observed differences of 2000 mmHg between inspired and arterial oxygen tensions. In samples taken at increasing distances from the lung in the outflow tube, oxygen tensions were progressively higher and carbon dioxide tensions progressively lower. These observations in conjunction with the much lower diffusivity of oxygen and carbon dioxide in water than in air led the authors to conclude that over all gas transfer was diffusion limited. They simulated these results in a spherical model which allowed diffusion from the centre

through a radius of .85 mm to the gas exchange surface. It was later suggested that the very small dimensions of this diffusion model may be due to more extensive turbulent mixing in the centre of respiratory lobules during water breathing (41).

Although stratification of gas concentrations is of major significance during liquid breathing, the available evidence suggests that this is not true during gas breathing. Martin et al. (92) observed that alveolar-arterial differences of oxygen partial pressures ($A - a_{DO_2}$) were greater in dogs during ventilation with air than with a mixture of 5% O_2 in SF_6 in a hyperbaric chamber at 4.0 Atm (20 x air density). No changes were observed in mixed venous oxygen tension or in percent venous admixture, suggesting that an improved matching of ventilation and perfusion in respiratory units was responsible for the improved gas exchange on SF_6 . They reasoned that gas density is unlikely to change regional perfusion or elastic properties, but may increase regional resistances and convective mixing. They speculate that increased regional resistances may reduce the variations of \dot{V}_A/Q ratios among parallel units as follows. Low \dot{V}_A/Q units are poorly ventilated due to their low compliance during air breathing, but during dense gas breathing, resistances are sufficiently large to alter the parallel distribution of ventilation. If the resistance to low \dot{V}_A/Q units, is less than to high \dot{V}_A/Q units, SF_6 breathing will decrease the variation of \dot{V}_A/Q . It seems that additional conditions must be satisfied before this mechanism explains their results. Among vertical lung regions, low compliance units are located in the superior regions of the lung, and have low $\Delta V/V_0$ and high \dot{V}_A/Q . A shift of ventilation toward these regions and away from dependent regions having low \dot{V}_A/Q can only increase the \dot{V}_A/Q variance. Accordingly, the \dot{V}_A/Q variance responsible for the $A - a_{DO_2}$ must reside within small lung regions where the gravity determined inverse correlation between $\Delta V/V_0$ and \dot{V}_A/Q may not exist. Furthermore, the resis-

tance of peripheral airways supplying parallel units within small lung regions must be density dependent. This is quite possible since Re , as calculated from the data of Ross (137), exceed 1000 in four mm airways when flow of the dense gas is .2 lps.

Molecular diffusivity is about 4.5 times less on the dense gas mixture, which should magnify the effect of gas stratification when compared to air breathing. On the other hand, increased convective mixing of inspired and alveolar gas due to the low kinematic viscosity of the SF₆ mixture may offset the decreased molecular diffusivity (41). The authors were reluctant to accept this explanation since it implies that series inhomogeneity accounted for an A - a DO₂ in excess of 5 mmHg during air breathing. Alternatively, if cardiogenic flow oscillations deliver gas from parallel units into their common airway during quiet breathing, the physical properties of the SF₆ mixture favor mixing by Taylor diffusion and convection (39). Accordingly, the dynamic mixing of the heart may cause a greater reduction in parallel inhomogeneity during ventilation with a high density gas.

Pulmonary gas exchange was measured in normal men breathing dense gas mixtures (46, 117, 139). In five subjects, A - a DO₂ ranged from 4 to 20 mmHg while breathing air at 1 Ata and from 26 to 37 mmHg while breathing 0.9% oxygen in helium at 31.3 Ata (117). The latter gas mixture was 4.4 times as dense as air at normal barometric pressure, and its oxygen partial pressure when inspired (P_IO₂) ranged from 216 to 221. The authors considered that increased P_IO₂ would increase A - a DO₂ due to true shunts, and the increased gas density would impair molecular diffusion and might also cause redistribution of ventilation. In one subject who breathed 1.14% oxygen in helium at 14.6 Ata, the measured A - a DO₂ of 27 mmHg exceeded the value of 19 measured at 1.0 Ata, despite virtually identical values for P_IO₂ and the smaller (2.08) discrepancy in gas density for the two conditions. This same subject was one

of five whose A - a DO₂ was measured while breathing 100% O₂ at .25 Ata (116). In this environment his A - a DO₂ decreased to 8.0 mmHg in accord with the results in other subjects, suggesting a continuous decrease in A - a DO₂ as the fractions of inert gas in the inspirate decreased. Overfield and his co-workers (116, 117) pointed out that if the distribution and magnitude of \dot{V}_A/Q ratios in the lung are constant, the apparent shunt caused by areas with low \dot{V}_A/Q will be minimized by the convergence of gas R lines as the inert gas fraction decreases. They considered this the most probable explanation of the increase A - a DO₂ at 31.3 Ata.

Saltzman et al (139) measured A - a DO₂ in three resting subjects who breathed gas mixtures of O₂ in nitrogen or helium at 1, 4 and 7 Ata. The P_IO₂ remained constant at about 150 mmHg and the gas density ranged from .35 to 7 times the density of air at 1 Ata. Despite the increase in inert gas fraction as ambient pressure increased, an inverse relationship between A - a DO₂ and gas density was evident, especially in two of the subjects. The authors chose to ignore this trend and attempted to explain the failure to demonstrate impaired transfer of oxygen during dense gas breathing. They considered it most likely that stratified inhomogeneity was not a significant factor in pulmonary gas exchange in these conditions. In a subsequent study, Flynn et al (46) reported A - a DO₂ values measured in two healthy subjects immersed to the chin in water. While breathing a mixture of 21% O₂ in helium at 1.15 Ata, A - a DO₂ for the two subjects were 29.4 and 49.1 mmHg. These values decreased to 14.5 and 22.1 respectively when the subjects breathed 1.1% O₂ in helium. P_IO₂ values for the two conditions were about 170 mmHg and the gas at depth was about 4 times more dense than at the surface. Similar reductions in A - a DO₂ at depth were observed during two levels of light exercise.

In conclusion, substantial series inhomogeneity has been demonstrated during saline ventilation. It seems plausible that other investigations

reviewed, generally interpreted as supporting stratification, actually demonstrate incomplete gas mixing in parallel units, the concentrations of which proceed toward equilibrium by cardiac induced Taylor diffusion and convective mixing as well as by molecular diffusion.

b. Parallel Inhomogeneity. Cardiorespiratory and flow induced oscillations observed in gas expired from peripheral lung units are best explained by sequential emptying of intraregional parallel units having substantially different gas concentrations. Such concentration differences are presumably due to variations in the intrinsic stress-strain characteristics of respiratory units, local differences in applied stress, or different distribution of dead space.

The stress-strain characteristics of individual alveolar walls in the cat (52) and man (150, 151) share many of the visco-elastic properties of static P-V curves in the intact lung. Length-tension relationships are non-linear and are different on stretch than on release (hysteresis). The hysteresis increases with the final force and decreases with repeated cycling, associated with an increase in tissue compliance (adaptation). Following a stretch, the force decreases with time (stress relaxation) at a rate proportional to the final force and to the rate of extension. Adaptation and dynamic hysteresis may be explained by the same molecular rearrangement (visco-elasticity) as stress relaxation, whereas the static component of hysteresis (plasto-elasticity) is not. In human lungs, the area of the hysteresis loop is a constant proportion of the area under the length tension curve, reminiscent of the static P-V hysteresis in the whole lung (4). Using a standardized cycling pattern to minimize variations due to stress relaxation and adaptation, Supihara et al. (151) measured the length of tissue at which force first increased with extension (L_0) and plotted length-tension relationships as extension ratio ($\lambda = L/L_0$) against applied stress. The length at infinite stress (L_{max}) was predicted from the length tension curves, and the maximum

extensibility ratio ($\lambda_{max} = L_{max}/L_0$) was calculated. The stress developed at any strain was related to λ_{max} , which is representative of many properties of the tissue. In 170 specimens obtained at autopsy or surgery from 36 lungs, λ_{max} ranged from 1.33 to 2.6. An inverse correlation of λ_{max} with age was found, and λ_{max} was lower at any age in patients with diffuse obstructive lung disease. Within each lung, there was nonuniformity of λ_{max} which was not topographically located and did not exceed the range of means between different lungs (1.48 to 2.2). The authors point out that λ_{max} may decrease due to a reduction in the length of tissue responsible for the "aton" at L_{max} , or due to an increase of L_0 . To the extent that variations in L_0 are responsible for the range of λ_{max} in each lung, there may exist a range of V_0 within small lung regions. Furthermore, the change in stress for a given change in length was greater for a tissue with low λ_{max} . At 25% extension, the stress in a tissue having $\lambda_{max} = 2.0$ is only 20% of that in a tissue with $\lambda_{max} = 1.5$, and this difference becomes larger as the degree of extension is increased. If these results apply in the intact lung, low λ_{max} units having a higher V_0 are less compliant and less ventilated by equal applied stress than high λ_{max} units. The authors speculate that the range of intraregional $\Delta V/V_0$ may be increased by local variations in surface tension or applied pressures.

Robertson et al. (132) described the distortion produced by discrete forces exerted against the pleural surface of excised dog lobes. At applied pressures of 40 and 80 cm H₂O, parenchymal distortions were closely limited to the pleural surface and sharply demarcated from the surrounding parenchyma. They conclude that the lung has mechanisms which localize distortions produced by local pressure changes. It may be argued that these mechanisms stabilize the ventilation patterns of interconnected lung units exposed to unequal applied stresses. The authors also observed considerable variation in the average alveolar dimensions within lobes exposed to a constant transpulmonary

pressure, providing preliminary support for variations in V_0 within lung regions.

Intra-regional differences in V_D/V_0 may occur due to differences in regional airway volumes. In the dog lung, the bronchial path to terminal bronchi exhibits a wide range of lengths and diameters, such that the longer path has the wider diameter (137). As a result, the dead space volume is distributed preferentially to peripheral alveoli. Similar measurements on the human lung indicate the inspired volume required to introduce fresh inspirate into acini subtended from airways with different transit times ranges from 102 to 271 ml (62). Thus, inspiration of 500 ml of oxygen would give alveolar nitrogen concentration differences of about 5% due to dead space ventilation alone.

3. Summary

In quasi-static conditions, vertical unevenness of intrapulmonary ventilation is due to the exposure of lungs with essentially uniform P-V characteristics to a gravity-dependent gradient of pleural surface pressure. At mid-lung volumes superior lung regions are more expanded, hence less compliant, than dependent regions. The preferential distribution of slowly inspired gas to dependent regions is adequately explained by the vertical gradient of compliance. Less conclusive evidence suggests that different lobar P-V curves, different regional ΔP , and sequential ventilation each act to increase the vertical range of $\Delta V/V_0$, although their total contribution is necessarily small. At low lung volumes, ventilation of basal regions is markedly reduced, presumably due to gravity dependent airways closure.

An equally wide range of $\Delta V/V_0$ exists within small lung regions during quiet breathing. Although series inhomogeneity is by far the most prominent cause during saline breathing, the majority of observations in more normal conditions suggest the presence of substantial parallel inequalities of $\Delta V/V_0$. The most plausible explanation is based on variations in stress-

strain characteristics of individual alveolar walls, which suggest that units with high V_0 are less compliant, hence less ventilated, than low V_0 units. The amount of unevenness is substantially reduced by intrapulmonary gas mixing, and an important role of the mechanical action of the heart in this process is suggested.

Thus, the intrapulmonary distribution of ventilation may be described by a series of $V_0/\Delta V$ distribution curves, each representing a vertical lung region. The mean $V_0/\Delta V$ values are calculated from the ratio of equation 1 to equation 4, and the corresponding frequency is estimated from the relative numbers of alveoli in each region (see Table 17). The dispersion of $V_0/\Delta V$ is as wide within each region as for the whole lung, suggesting that intraregional dispersion accounts for most of the uneven ventilation.

B. Dynamic Distribution of Ventilation

When breathing frequency or flow rate is increased, regional ventilation is different from the compliance determined values observed during quasi-static changes in lung volume. This suggests that one or more of the parameters determining the quasi-static distribution is time dependent. The time available for volume change may theoretically influence the completeness of diffusive mixing, the amount of respiratory pressure generated over each lung region, and the degree to which distensible lung units approach elastic

equilibrium with the applied pressure. Most of the studies reviewed in this section employ techniques which are independent of the inter-gas diffusion process. As discussed above, the literature contains little information regarding the topography of dynamic pleural surface pressure. In contrast, a considerable amount of information is available on the role of mechanical time constants of lung regions in determining regional ventilation.

1. Mechanical Time Constants of Pulmonary Units

According to the equation of motion, the pressure applied to lung units is dissipated in friction and stored in elastic distension when inertia is negligible. During slow changes in lung volume, an equal ΔP applied synchronously to two such units causes volume change according to their compliance ($V_1/V_2 = C_1/C_2$). When the volume change is sufficiently rapid, the resistive pressure drop becomes a major proportion of the applied pressure, so that volume change is inversely related to the resistance of the unit ($V_1/V_2 = R_2/R_1$). If the resistance ratio differs from the compliance ratio ($C_1/C_2 \neq R_2/R_1$), there must be a change in the relative distension of the units (V_1/V_2) as breathing frequency or flow rate changes from zero to infinity. Thus, the condition for frequency dependence of ventilation distribution exists when the products of pathway resistance and compliance are not equal ($R_1C_1 \neq R_2C_2$). This product has the dimension of time, and is called the time constant (T) of the pulmonary unit.

Otis et al. (115) considered a single pulmonary pathway to consist of a volume-elastic element having a compliance, C, connected in series with a conducting part having a resistance, R. When a sinusoidal pressure of frequency (f) and amplitude (P_m) is applied across this model, the resultant flow wave leads P_m by a phase angle (A) and the volume change (V_t) is determined by the impedance (Z).

$$\theta = \tan^{-1} \times \frac{1}{\omega RC}$$

$$\text{where } \omega = 2\pi f$$

$$V_t = P_m / \pi f Z$$

$$\text{where } Z = \sqrt{R^2 + \left(\frac{1}{\omega C}\right)^2}$$

Thus, temporal relations between pressure and flow are determined by the time constant and cycle frequency. Also, the limits for impedance as frequency approaches zero and infinity are $\frac{1}{C}$ and R respectively.

When two or more such units are arranged in parallel, the distribution and timing of flow in the separate pathways is determined by the distribution of their impedances. If the time constants for all pathways are equal, their impedances change proportionately with frequency. The behaviour of this system can be duplicated by a single equivalent resistance (R_e) and volume elastic element (C_e). If the parallel time constants are unequal, the impedances of separate pathways do not change proportionately as frequency increases so that a different value of R_e and C_e is required for each frequency.

$$C_e = \frac{\omega^2 (T_2 C_1 + T_1 C_2)^2 + (C_1 + C_2)^2}{\omega^2 (T_1^2 C_2 + T_2^2 C_1) + (C_1 + C_2)} \quad (6)$$

where the subscripts (1, 2) denote the parallel pulmonary pathways. C_e approaches the equal time constant value ($C_1 + C_2$) at low frequencies, but decreases as frequency increases. In effect, a smaller proportion of the total volume is delivered to low RC units as frequency increases because a greater proportion of the applied pressure is used to overcome resistive impedance. In addition, the temporal relations of pressure and flow are different among pathways with unequal time constants, so that flow between parallel units ('pendelluft') may occur.

Thus, Otis et al. (115) demonstrated that time constant inequalities among parallel lung units may cause a fall in pulmonary compliance as breathing frequency increases. Although this must be associated with a predictable

change in the distribution of ventilation among these units, no systematic analysis of this conclusion has been published. The relative tidal volume of a two compartment model may be calculated from equation 6 and 7 of Otis et al. (115), using the equation

$$V_{t1}/V_{t2} = |Z_2|/|Z_1| = \sqrt{R_2^2 + \left(\frac{1}{\omega C_2}\right)^2} / \sqrt{R_1^2 + \left(\frac{1}{\omega C_1}\right)^2} \quad (7)$$

When the solution of this equation is compared with the solution of equation 6 for a range of breathing frequencies, the change of V_{t1}/V_{t2} from the static value ($\omega = 0$) is much greater than the change of C_e from its static value (See Chapter IV). It follows that the absence of frequency dependence of compliance does not necessarily exclude changes in regional ventilation, which may be detected with more sensitive techniques.

2. Effect of Breathing Frequency on the Intrapulmonary Distribution of Ventilation

a. Evidence for Asynchronous Ventilation

(1) In Subjects with Obstructive Lung Disease. In patients with abnormal spirometry and elevated airways resistance diagnostic of chronic obstructive pulmonary disease (COPD), C_{dyn} falls significantly below C_{st} as frequency of breathing increases (81, 99, 100, 115). Multiple breath N_2 washouts were measured (32) with constant tidal volumes in seven such patients at 19 and 31 breaths per minute (bpm). When N_2 % was plotted against breath number, washout during hyperventilation was initially more rapid and subsequently slower than during resting ventilation. At the high frequency, an increased volume was required to reduce expired N_2 to 2.5 and 1.5%, clearance delay percentage was increased, and the distribution of specific tidal volumes indicated an increased number of poorly ventilated alveoli. These results were reasonably simulated by a two compartment mathematical model having time constants of .12 and 1.8 seconds. The effective compliance of such a lung falls from a static

value of 0.3 l/cm H₂O to 0.17 at 19 bpm and only slightly lower (0.15) at 31 bpm. It follows that much larger changes in ventilation distribution may occur at lower frequencies than the resting value of 19 bpm.

Ingram and Schilder (66) measured C_{dyn} and N₂ washouts simultaneously during quiet breathing and at increased frequency (30 - 50 bpm). In five subjects whose washouts did not change, C_{dyn} decreased less than 25%, whereas in five other subjects, N₂ washout was delayed and C_{dyn} fell more than 25%. For several reasons, interpretation of the correlation between frequency dependence of C_{dyn} and ventilation distribution is more complicated in such clinical studies than in the two compartment model discussed above. Among the frequency independent group were three patients with mild Copd whose low C_{dyn} and prolonged washouts during quiet breathing suggest maximal redistribution of resting ventilation. Secondly, in patients with advanced airways obstruction, C_{dyn} may decrease due to phase differences between dead space and parenchyma (100) which have little effect on ventilation distribution. Finally, the complex patterns of change with frequency of both C_{dyn} and N₂ washouts in the simplest two compartment models may be obscured by methodologic errors during measurements in patients. Woolcock et al. (166) assumed that C_{dyn} in normal subjects was independent of frequency, and estimated that a 20% fall from the static value is a detectable abnormality by their technique. The sensitivity of the N₂ washout technique to detect changes in ventilation distribution as frequency increases is diminished by preferential distribution of the common dead space and 'pendelluft' to the short RC units (111, 138, 141).

Although these considerations limit the correlation of frequency dependence between O_{dyn} and nitrogen washout, it is established that both tests of ventilation distribution change significantly when patients with obstructive lung disease increase their breathing rate.

(2) In Subjects with Normal Lung Function. Bouhys et al. (17)

observed no change in nitrogen washout in five normal subjects who breathed similar tidal volumes of oxygen at 10 and 60 bpm. In four healthy subjects who doubled their resting frequency of breathing, Cuttillo et al. (32) noted no significant changes in N_2 washouts. Macklem (81) reviewed numerous studies, and concluded that most normal subjects exhibit a fall in C_{dyn} of less than 20% of the static compliance when frequency is increased to 70 bpm. It therefore appears that the intrapulmonary distribution of ventilation is independent of breathing frequency in normal subjects. Accordingly, the mechanical impedance of parallel pathways is predominantly elastic so that regional filling is determined by regional compliance, and airways resistance does not influence the distribution of ventilation detectable by these techniques.

Among the frequency dependent group in the study of Ingram and Schilder (65) were three "healthy" subjects with normal spirometry who were cigarette smokers with chronic morning cough and/or intermittent episodes of purulent bronchitis. In patients with normal spirometry, pulmonary compliance and airways resistance, Woolcock et al. (166) demonstrated frequency dependence of compliance and concluded that this is a more sensitive test of obstruction in peripheral airways. Macklem (81) summarized the evidence demonstrating that 2 - 3 mm airways are a primary target in many forms of Copd and suggested that peripheral airways obstruction may exist for long periods with little or no abnormality of routine pulmonary function tests. Thus, small airways disease may explain occasional observations of frequency dependence in 'normal' subjects.

b. Factors Promoting Synchronous Ventilation It is probable that RC inequalities do exist within the normal lung (81). The pathway to respiratory units in the posterior basal segment of the lower lobe is much longer and should have higher resistance than the pathway to units near the hilum or

in the apical segments of the upper lobe. According to equation 2 dependent lung regions are about twice as compliant as apical regions at mid-lung volumes. Because lower pulmonary resistance varies inversely with lung volume (14, 157), it seems reasonable to expect resistance in the more expanded upper regions to be less than resistance in the less expanded lower regions. Accordingly, RC discrepancies among vertical regions may differ by more than a factor of two due to the pleural pressure gradient alone. Additional intraregional differences due to random variations of geometry or bronchomotor tone may increase the range of RC discrepancies.

Several mechanisms exist which promote the observed synchronous behaviour of lung units which have different time constants. Macklem and Mead (82) observed that the time constants of parallel units peripheral to 2 mm airways are very short in normal lungs (.01 secs) due to the low values of peripheral resistance. They demonstrated that the frequency at which C_{dyn} decreases below the static value is determined by the absolute magnitude of the time constants as well as their discrepancies. Accordingly, a four fold time constant difference in these pathways causes a fall in C_{dyn} at 100 bpm of only 3%. Although detectable asynchrony between these same units occurs at higher frequency (as $\omega \rightarrow \infty$, $C_e = 50\% C_{st}$), lung gas inertia is expected to influence the results (96). Consequently, lungs with widely discrepant time constants among peripheral pathways may not show significant frequency dependence of C_{dyn} below 100 bpm. When the RC differences are sufficiently large, distribution changes from the compliance determined value, such that the relative volume change of long RC units becomes smaller and later in time than adjacent units with shorter time constants. Due to their different relative distentions, a pressure difference develops between such respiratory units, which has been shown greater than one would predict on the basis of uniform P-V characteristics (102, 105). The extra pressure difference between asynchronous units has been attributed to the interdependence of forces applied

to each through their mutual tissue attachments. The result is pressure tending to restore the volume change of long RC units to their synchronous values. In addition to promoting ventilation through the usual channels, this pressure drives flow through collateral channels which directly connect respiratory units (81).

How effective collateral ventilation and interdependence are in maintaining frequency independence of ventilation distribution in normal subjects cannot be completely assessed by measurements of Cdyn. At infinite frequency when the fall in Cdyn is independent of the absolute values of the parallel time constants, a 2.5 to three-fold discrepancy in time constants is required to cause a 20% fall in Cdyn (See Chapter IV). It follows that the expected vertical difference in RC due to the pleural pressure gradient is not detectable by Cdyn measurements in the absence of factors promoting synchrony. This is true despite the fact that the solution of equation 6 for a 2.5 fold discrepancy at $\omega \rightarrow \infty$ gives a change of tidal volume distribution (V_{t1}/V_{t2}) of 250%.

In summary, most subjects with normal routine pulmonary function tests do not exhibit a change in dynamic compliance or nitrogen washouts as breathing frequency increases. Accordingly, the parallel distribution of ventilation is essentially determined by the elastic properties of lung units in healthy subjects at rest and exercise (101). However, these tests do not directly measure the volume change of pulmonary units, and the literature does not indicate how much change in the relative tidal volumes of parallel units must occur before the available tests become abnormal.

3. Effect of Flow Rate on Ventilation Distribution

a. Expiratory Flow As discussed above, asynchronous emptying of vertical lung regions occurs at low expiratory flow rate (\dot{V}_e), such that upper lung regions contribute a progressively greater proportion of the expirate

as lung volume decreases. Accordingly, the alveolar plateau of a single expiration slopes upward when upper regional concentration exceeds that in lower lung regions. Although several earlier studies (12, 15, 18, 47, 74, 136) of the effect of \dot{V}_e on the slope of the alveolar plateau produced conflicting results, it is now clear that the sequence of regional emptying is altered.

Jones and Clarke (72) measured argon concentration in the expirate of ten subjects who inhaled 100 ml of argon at RV followed by a vital capacity breath of air. The amount of argon in the last litre of the expirate and the upward slope of phase III progressively diminished as \dot{V}_e increased, suggesting earlier emptying of upper lung regions. They concluded that regional emptying is influenced by regional resistance at increased \dot{V}_e . As discussed above, the slopes of phase III and IV slope downwards when subjects are inverted prior to a slow expiration. Clarke et al. (26) observed less sequential emptying as \dot{V}_e was increased in inverted subjects, suggesting that in both positions the lung regions which are superior with respect to gravity empty progressively earlier as \dot{V}_e is increased. Accordingly, the gradient in pleural surface pressure plays an important role in the reduction of sequential emptying between vertical lung regions when \dot{V}_e is increased.

Expired ^{133}Xe concentrations were measured in 7 subjects who inhaled bolus from RV, thereby establishing a vertical concentration gradient measured at TLC (108). During slow expiration, the expired concentration progressively increased to a value at RV which was similar to the concentration in apical regions. During a rapid expiration, more ^{133}Xe was expired at high volumes and less at low volumes, giving a horizontal alveolar plateau. The contribution of stratification to these changes was minimized by a 15 second pre-expiratory breath hold at TLC. In two subjects who expired at

several flow rates, these changes were progressive, supporting the contention that factors unique to maximum expiratory flow are not the explanation. Thus, vertical lung regions contribute a constant proportion of the expirate throughout a forced expiration. Recalling that sequential emptying during a slow expiration departs only slightly from the plot of V_r (% TLC_r) against lung volume (% TLC), shown in Figure 5, the changes in emptying sequence with \dot{V}_e required to flatten the expired plateau are very small. By reinspiring to TLC following an expiration interrupted at a series of lung volumes, regional end expiratory volumes were determined (108). The vertical gradient of regional expansion observed at all lung volumes following a slow expiration was not present above 30% VC following a forced expiration. Accordingly, the volume changes of vertical lung regions are not only synchronous, but they are equal. This distinction is illustrated in Figure 5, where the slow emptying of upper and lower regions follow line u and l, but during maximum expiratory flow, both regions empty along line M, indicating a much greater effect of \dot{V}_e on the emptying pattern than can be inferred from expired plateaux.

Millette et al. (108) offered these explanations. Because of regional compliance differences due to pleural pressure gradient, lower regions change volume more than upper ones for a given static ΔP . If maximum effort abolished this gradient, differences in emptying rate would be diminished. This is not the explanation, since Martin et al. (91) subsequently showed that low \dot{V}_e achieved by maximal effort through a high external resistance did not alter the quasi-static emptying sequence. As they point out, these observations do not exclude transient asynchrony of ΔP during forced expiratory effort, which could alter the emptying sequence over a much larger part of the vital capacity at high \dot{V}_e than at low \dot{V}_e . Alternatively, if the time constants of upper regions are relatively short

due to their low compliance, an equal dynamic ΔP applied to both regions may increase the emptying rate of upper regions more than lower.

Young et al (170) reported that when subjects voluntarily produce expiratory flow oscillations following a tidal breath of oxygen, oscillation of N_2 and CO_2 concentrations are observed on the alveolar plateau. When these concentrations were corrected for transit time from the lobar bronchi and sampling delay, the N_2 oscillations were in phase and the CO_2 oscillations were 180° out of phase with the flow oscillations. Thus, units emptying at increased flow rates have relatively low $\frac{\Delta V}{V_0}$ and high $\frac{\dot{V}_A}{Q}$, characteristic of upper lobes and regions. Because the flow oscillations were small ($< .1$ lps), they reasoned that differences in compartmental resistance could not account for these differences. As an alternative, they proposed a model with 2 compartments having different pressure volume characteristics and the same V_0 , such that equal applied pressure causes the low ΔV unit to contribute a greater proportion of the expirate as lung volume decreases. From the equation of motion of the lungs, they derived a first order differential expression for flow into either compartment as a function of overall flow rate.

$$2 \frac{dV_1}{dt} = \frac{dV}{dt} + \frac{-f_1 (V_1) + f_2 (V_2)}{R}$$

where V is lung volume, equal to $V_1 + V_2$

V_1 is volume of compartment 1, and f_1 its elastance

V_2 is volume of compartment 2, and f_2 its elastance

R is the resistance to compartment 1

Graphical solution for step changes in expiratory flow rate (dV/dt) showed alterations in the emptying sequence of the two compartments which caused increases in expired N_2 concentrations synchronous with increased flow rate. Although this model was proposed as an alternative to a time constant model,

the equation is identical to one derived by Pedley et al (122, eq. 7) to explain the effect of RC discrepancies on distribution of inspired flow. As discussed below, a model with discrepant time constants will transiently depart from compliance determined filling and emptying when flow rate is changed. When an indicator is distributed during the transient, a change in the sequence of compartment emptying is readily detectable.

In conclusion, the sequential quasi-static emptying of vertical lung regions is progressively diminished as \dot{V}_e increases. At maximum \dot{V}_e , emptying of vertical lung regions is synchronous and is not determined by regional compliance alone. This departure from compliance determined emptying can occur at much lower \dot{V}_e , and may be explained by unequal regional time constants or by an asynchronous regional ΔP .

b.) Inspiratory Flow

Robertson et al (134) demonstrated that a bolus of ^{133}Xe inspired maximally from mid-lung volume is equally distributed to superior and dependent lung regions. They suggested that the distribution of a rapid bolus is theoretically determined by the regional resistances, and concluded that if regional ΔP are equal, apical and basal resistances are approximately equal. Martin et al (90) assumed that regional filling during maximal inspiration is resistance determined, and calculated the regional time constant ratios as follows. The ratio of count rates at TLC between upper and lower regions is proportioned to their compliance ratio, C_u/C_l , following a slow inspiration of ^{133}Xe boli from FRC, and inversely proportioned to their resistance ratio (R_l/R_u) following a rapid inspiration. The time constant ratio, obtained by dividing the slow count rate ratio by the fast ratio, $(C_u/C_l)/(R_l/R_u)$, decreased as vertical distance between the regions increased. Accordingly, regional time constants increase progressively

with distance from the lung top in a very similar manner to regional compliance, suggesting that regional resistances at mid-lung volumes are equal.

Using an electrical analogue, Macklem (81) showed that if maximal inspiration is analogous to a square wave pressure change and superior and dependent lung regions are analogous to two resistor-capacitor circuits in parallel, then the distribution of volume to the two regions at the instant the pressure is applied is inversely proportional to the regional resistances and is independent of the common resistor. Because it takes a finite time to administer a rapidly inhaled bolus, the regional distribution by this analysis is not necessarily resistance determined but may be a function of the regional time constants which include the common resistor. This could account for the inability to demonstrate higher concentrations of ^{133}Xe in the apex than in the base when apical resistance was expected to be less than basal resistance.

Pedley et al (122) considered the theoretical effect of gravity induced time constant inequalities on the distribution of constant inspiratory flow between upper and lower lobes in erect man. Their analysis examines the transient departure from elastic equilibrium caused by a step change of flow in the lung, and is analogous to the application of a constant current to the electrical analogue discussed by Macklem (81). In contrast to a square wave voltage (or pressure), the response of the parallel units to constant current (or flow) is independent of the common resistor, which merely provides a time invariant pressure drop. From the equation of motion, they derive an expression for the lobar distribution of flow (eg. 10, ref. 122) which may be rewritten:

$$\frac{\dot{V}_u}{\dot{V}_l} = \frac{C_u + \frac{T_l - T_u}{R_u + R_l} \exp^{-Bt}}{C_l - \frac{T_l - T_u}{R_u + R_l} \exp^{-Bt}}$$

where the subscripts (u, l) denote upper and lower lobes, C is compliance, R is resistance, T is their product (RC), t is time, and B is $(C_u + C_l)/C_u C_l (R_u + R_l)$. The instant flow begins ($t = 0$), the total impedance to flow is resistive, and lobar flow is inversely proportional to lobar resistance ($\lim_{t \rightarrow 0} \frac{\dot{V}_u}{\dot{V}_l} = \frac{R_l}{R_u}$). In the other extreme, relative lobar filling is determined by lobar compliance ($\lim_{t \rightarrow \infty} \frac{\dot{V}_u}{\dot{V}_l} = \frac{C_u}{C_l}$).

If R_l/R_u is not equal to C_u/C_l ($T_u \neq T_l$), lobar distribution changes with time from R_l/R_u to C_u/C_l .

Using estimated values for lobar compliance and resistance, they calculated the effect of inspired flow rate on lobar distribution of various inspired volumes. When P - \dot{V} and P - V characteristics were linear, a greater fraction of the inspirate was distributed to lower lobes at low flow rates ($C_u < C_l$) because they were less expanded, hence more compliant, due to the vertical gradient in pleural pressure. As flow increased, the fraction of the inspirate going to upper lobes increased until at very high flows, lobar distribution was equal ($R_u = R_l$). Non-linear pressure flow relations exaggerate the effects of time constant inequalities, and cause the distribution of a given inspired volume to approach the resistance determined value at a lower \dot{V}_l . Conversely, non-linear pressure-volume relations tend to maintain compliance determined distribution. The distribution ratio is also affected by allowing lobar resistance to vary with lobar expansion in the same way as pulmonary resistance varies with lung volume. In this

case, R_1 is greater than R_u , and V_u/V_1 approaches a value more discrepant from the quasi-static distribution, causing preferential distribution of inspired volume to upper lobes at high inspiratory flow rates. This latter case was theoretically considered most representative of lung events.

It follows that if time constant inequalities are responsible for the effect of inspiratory flow rates on vertical distribution of inspired gas, a characteristic pattern of change will occur. At low flow rates, regional distribution will be according to regional compliances. As flow rate increases, a greater proportion of the inspired gas will be delivered to short time constant regions. This change with flow will at first be rapid and then progressively diminish until at high flows distribution is resistance determined and essentially independent of further increases of flow rate. A compliance determined distribution may be maintained to high flow rates if RC discrepancies are small and the time course of the transient is short relative to the time taken for the volume to be distributed. Furthermore, collateral ventilation and interdependence of lung regions may oppose any departure from compliance determined distribution.

CHAPTER IV

EXPERIMENTS

A. The Effect of Gas Physical Properties and Flow Rate on Canine Lower Pulmonary Resistance

1. Introduction

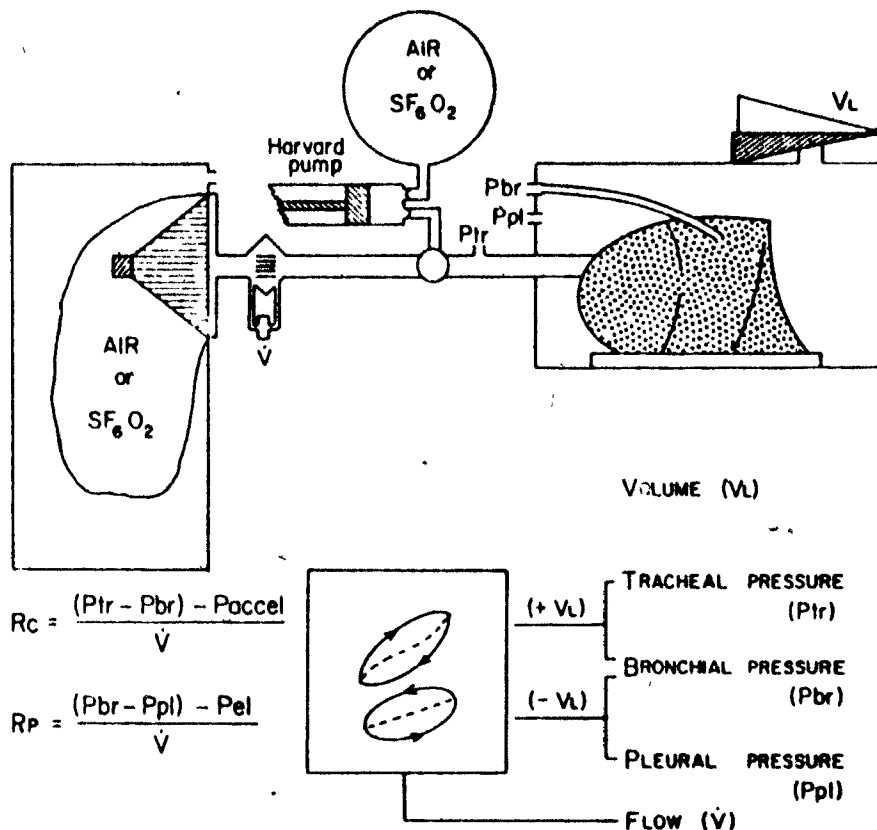
Contemporary understanding of the nature of airways resistance is based primarily on the investigation of Rohrer (135). Recent theoretical studies, supported by measurements in airway models, emphasize previously overlooked disturbances of boundary layers as a major cause of resistance to bronchial flow (113, 119, 120, 121, 145). According to the theory of boundary layer growth, Pedley et al (119, 120) predicted that lower pulmonary resistance (R_{lp}) varies as the square root of gas viscosity, density and flow rate. This study was designed to test this hypothesis by comparing predicted with observed effects of gas physical properties and flow rate on resistance in central and peripheral segments of the lower pulmonary airways in anaesthetized dogs. It has been suggested that the underlying physical basis of Rohrer's equation as applied to the bronchial tree is not theoretically sound (50, 94, 113, 120). As these arguments are not conclusive, a second aim of this study was to test Rohrer's equation in the same way.

2. Methods

a. Experimental Procedure. Mongrel dogs were anesthetized with chloralose urethane. The chest was widely opened by a sternum splitting operation and the trachea cannulated. A retrograde catheter with a 4.0 mm bell was placed in the right middle lobe according to the

technique of Macklem and Mead (82). The dogs were paralyzed with succinyl choline, artificially ventilated, and placed in a volume displacement plethysmograph from which lung volume was obtained. Flow was measured with a small NIL pneumotachygraph attached to the tracheal cannula. Lateral tracheal pressure (P_{tr}) was sampled with a pizometer ring on the tracheal cannula, and pressure at the lung surface (P_{pl}) was estimated by a catheter lying free in the plethysmograph. Pressures were measured with Sanborn 267 B and 268 B transducers. Prior to each measurement of resistance, the lung was fully inflated (P_L 30 cm H_2O) and allowed to deflate to predetermined transpulmonary pressures. The lungs were then oscillated at 4 cps by a loudspeaker powered by a sine wave generator so that peak to peak flow approximated 2 lps. The pressure differences of catheter bell (P_{br}) from P_{pl} and P_{tr} were simultaneously displayed against flow on a cathode ray oscilloscope (Fig. 6). The resulting pressure-flow loops from the peripheral and central airways were closed by electrically subtracting the elastic and accelerative components of the pressure. Flow, and the components of the peripheral pressure (P_p) and central pressure (P_c) which were in phase with flow were recorded on a 4-channel Sanborn Poly Viso (Fig. 7). Flow rate was then reduced to 1 lps and another recording was obtained. After at least 3 measurements at each of two lung volumes (Table 4) a gas mixture of 20% oxygen in sulfur-hexafluoride (SF_6) was connected to the inlet of the Harvard pump. The bag sealed to the loudspeaker (Fig. 6) was evacuated and refilled with SF_6 , and the resistance measurements were repeated. As it was not possible to obtain sinusoidal flow oscillations much higher than 1.0 lps on the dense gas, SF_6 measurements were made at 1.0 and 0.5 lps in all animals. When these were completed, the cervical vagi were cut and the measurements were repeated on SF_6 and air.

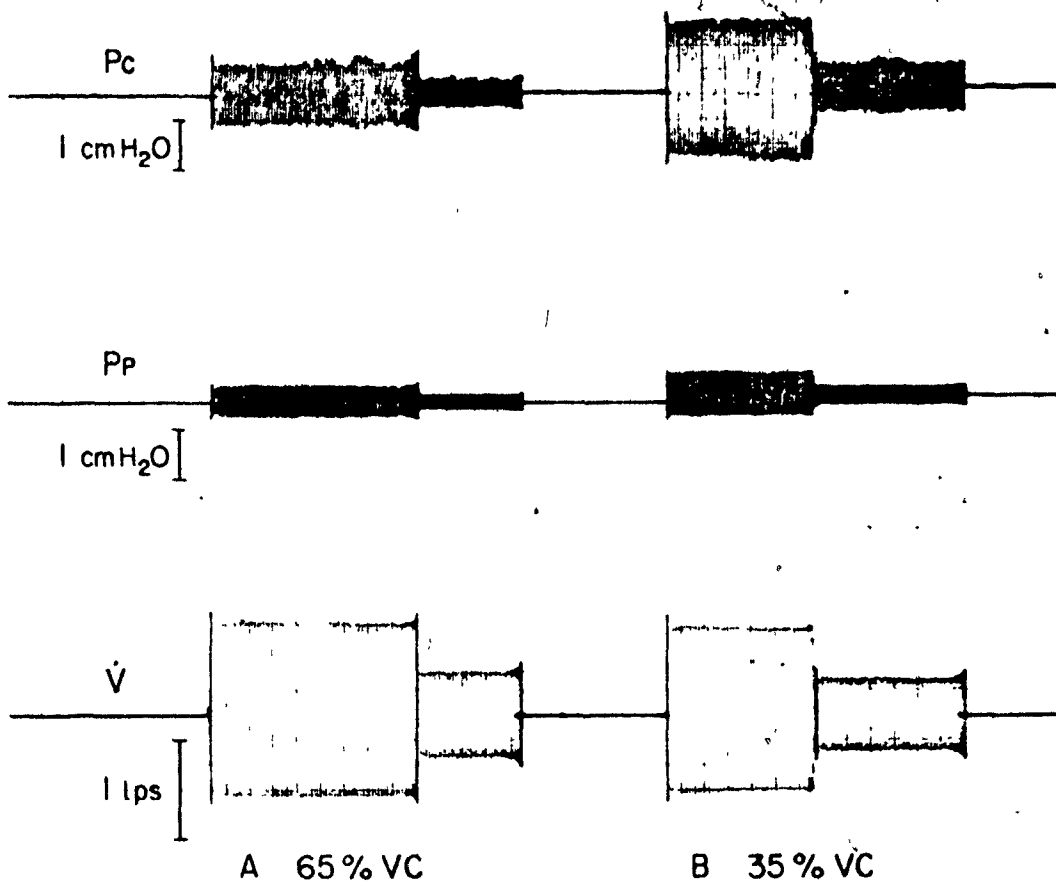
FIGURE 6



Schematic diagram of experimental apparatus.

Anaesthetized dogs in a body plethysmograph (upper right) were ventilated by Harvard pump or oscillated by a loudspeaker (upper left) with either air or SF₆O₂. During oscillation, the differential pressures in central ($P_{tr} - P_{br}$) and peripheral ($P_{br} - P_{pl}$) airways were displayed against flow (lower middle), and the resulting P-V loops (solid lines) were closed (dashed lines) as indicated.

FIGURE 7



Photograph of Poly viso recording of \dot{V} and the central (P_c) and peripheral (P_p) pressures in phase with flow (corresponding to dashed lines on oscilloscope in Figure 6) during forced oscillation at two lung volumes.

TABLE 4Lung Volumes and Catheter Position During Resistance Measurements

<u>Expt. No.</u>	<u>VC l.BTSP</u>	<u>% VC</u>		<u>RETROGRADE CATHETER SITE</u>			
		<u>HIGH</u>	<u>LOW</u>	<u>D (cm)</u>	<u>d(mm)</u>	<u>G</u>	<u>Re</u>
1	2.13	57	29	7.0	4.4	6	116
2	2.00	68	36	10.0	3.3	12	64
3	1.60	59	34	9.0	3.0	12	58
4	2.12	68	35	7.6	4.2	11	105
5	1.33	63	30	10.6	3.5	17	67
6	1.70	69	31	11.5	3.5	15	67
7	1.90	68	36	13.5	3.5	15	59
8	1.50	69	35	10.8	3.8	12	75

D = distance from carina

d = airway diameter

G = airway generation

Re = average Re for air oscillations at 1 lps (see text)

TABLE 5

Arterial Blood Gas Tensions

Expt. No.	PaO ₂		PaCO ₂		pH	
	Air	SF ₆	Air	SF ₆	Air	SF ₆
1	95	101	23	28	7.41	7.34
2	88	96	32	38	7.40	7.30
3	69	76	35	51	7.37	7.23
4	70	62	30	46	7.33	7.22
5	88	83	36	42	7.34	7.28
6	85	90	37	40	7.35	7.32
7	100	111	41	38	7.29	7.30
8	91	52	38	56	7.38	7.27
Mean ± sd	86± 11	84± 11	34± 6	42± 9*	7.36± .04	7.29± .05*

* denotes difference from corresponding air value ($p < .01$)

Static pressure-volume curves of the lung were recorded throughout the experiment and no major changes were noted. Blood samples were drawn from indwelling femoral artery catheters during air and SF₆ ventilation for determination of PO₂, PCO₂, pH and bicarbonate concentration (Table 5).

At the end of the experiment, the animals were exsanguinated. The lungs were excised and air dried for ten days while distended at a transpulmonary pressure of 20 cms H₂O. The gross morphometry of the airway was determined by cutting along a thread from the trachea to its attachment on the catheter bell. At each branch point, generation number, airway diameter and length from the carina were recorded (Table 4). Presumably these values differ from those during the experiment due to changes with lung volume and bronchomotor tone.

b. Data Analysis. Central and peripheral resistances were calculated from the Sanborn tracings by dividing P_c and P_p by flow. Note that peak flows of 1.0 lps constitute 0.5 lps inspiratory and expiratory flow. No attempt was made to separate inspiratory and expiratory resistances.

Rohrer's descriptive equation for airway resistive pressure losses (135) was expressed for airways resistance:

$$R = K_1 + K_2 V \quad (1)$$

Using the two resistance values and flow rates, simultaneous equations were solved for K₁ and K₂, where K₂ is the change in resistance per unit change in \dot{V} . The sum of K₁ and K₂ is equivalent to the resistance at 1.0 lps. Since measurements were made on both gases during flow oscillations approximating 1 lps, the sum of Rohrer's constants is nearly identical to the measured resistance. A second equation describing the

flow resistive pressure drop in branched tubes modelled on bronchial morphometry has recently been put forward by Pedley et al (120, 121).

The equation may be written in terms of resistance

$$R = K (\rho \mu)^{.5} \dot{V}^{.5}$$

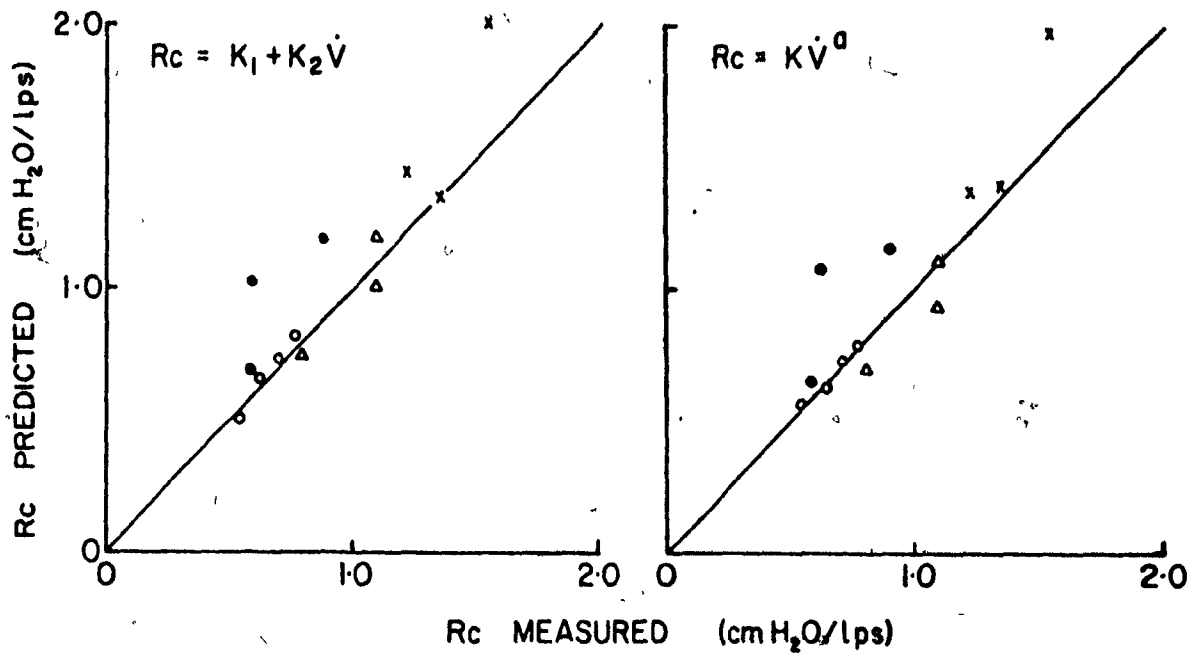
and expressed in the general form

$$R = K (\rho \mu)^n \dot{V}^a \quad (2)$$

Using the two resistance values and flow rates, simultaneous equations were solved for the exponent 'a' on each gas. This value expresses the change in resistance with flow assuming an exponential pressure-flow relationship. Similarly simultaneous equations were solved for the exponent 'n', using the known density-viscosity products for air and SF6 and the resistance measured on each gas.

Since measurements on air were not made at flow oscillations of .5 lps, we attempted in experiments 2 and 8 to validate equations 1 and 2 over this flow range. Resistances were measured at .5, 1.0 and 2.0 lps during air oscillations and Rohrer's constants and the exponent 'a' were calculated in the usual manner from the higher pair of flow rates. These values were then used to predict the resistance values at .5 lps, which are compared in Fig. 8 with the resistance measured at .5 lps during that maneuver. There is a reasonably close approximation of all values to the line of identity, with a suggestion of better fit for equation 1 than equation 2. These data suggest that the use of different flow rates for the two gases introduced no systematic error to either the estimated value of resistance at 1.0 lps when the actual flow rate was not exactly so, or to the calculated values of K_1 , and K_2 and 'a'. In experiments 2 and 8, two flow sequences were used (highest to lowest and vice versa), and no significant trend was noted in the resistances measured or constants calculated, suggesting that flow sequence did not influence airways resistance. In experiments 1-3, $P_{tr} - P_{pl}$ was also displayed against flow,

FIGURE 8



Values of R_c measured during air oscillations at 0.5 lps (abscissa) versus R_c predicted from values measured at 1 and 2 lps according to equation 1 (left ordinate) and equation 2 (right ordinate).

Expt. 2	65% VC ○	35% VC △
Expt. 8	65% VC ●	35% VC ×

and the resulting loop was closed by adjusting the frequency of oscillations. The resonant frequency was slightly greater at 65% VC, where it averaged 5.2 cps on air and 2.8 cps on SF₆. No systematic differences were observed on either gas between the resistance values at pulmonary resonance and the corresponding values measured at 4 cps. Thus the latter values presumably reflect lower pulmonary resistance at all lower frequencies.

For practical reasons, the order of gas exposure was not randomized. To exclude systematic variations of resistance with time, the resistance measurements on both gases were repeated following the first SF₆ measurements in experiments 7 and 8. No significant difference or trend was observed between the duplicate determinations. Accordingly, all measurements were used to calculate the mean values of each parameter, and an estimate of experimental variability was obtained. Table 6 presents the coefficients of variation from these two experiments. No systematic change is noted between lung volumes. The variability of resistance measurements averaged 15 and 22% in central and peripheral airways respectively, whereas the calculated constants exhibited 2.5 to ten times greater variability.

Statistical significance of results was assessed by the paired comparison *t* test, and the level of significance was taken as $p < .05$. For each lung volume and airway segment before and after vagotomy, several parameters (R , K_1 , K_2 , 'a') were tested for differences between their air and SF₆ values. The constants K_2 , 'a' and 'n' were each tested for differences in their values between central and peripheral airways.

c. Calibration Techniques. The pneumotachygraph was calibrated for each gas using the experimental apparatus. Air blown into the chamber enclosing the loudspeaker displaced either air or SF₆ from the bag through the pneumotachygraph into the plethysmograph. The change of plethysmograph

TABLE 6

Coefficients of Variation*

<u>% VC</u>	<u>Gas</u>	<u>Expt.</u>	<u>K₁</u>	<u>K₂</u>	<u>R_c</u>	<u>K₁</u>	<u>K₂</u>	<u>R_p</u>	
68	Air	7	.32	.86	.17	.65	2.54	.35	
		8	.26	.24	.11	.20	.79	.06	
	SF ₆	7	.36	.63	.29	.28	.80	.19	
		8	.58	.40	.11	.23	1.70	.12	
35	Air	7	.59	.40	.13	.32	8.40	.37	
		8	.24	1.12	.11	.73	1.45	.27	
	SF ₆	7	.35	.23	.13	.47	.42	.19	
		8	.43	.41	.15	.62	1.45	.19	
	Mean			.39	.54	.15	.48	2.20	.22

*The corresponding mean values for each parameter are listed in Tables 10 and 11.

volume with time over a constant and linear range of the spirometer transducer provided an accurate measurement of flow rate. The pressure drop across the pneumotachygraph was linearly related to air flow to 2.5 lps. The pressure-flow plot for SF6 was curvilinear, the pressure drop being about 10% less than air at 0.5 lps and equal to air at 1.0 lps. When a large Fleisch pneumotachygraph (No. 4) which was linear to 2 lps for the SF6 mixture was used, the pressure drop for SF6 was 14.5% less than for air flow. This value is assumed to represent the difference in gas viscosity between air and SF6 (104), suggesting that the pneumotachygraph used in the experiment was non-linear even at .5 lps for SF6.

In a separate calibration procedure air or SF6 was oscillated at 4 cps across the pneumotachygraph between the bag in the loudspeaker and a second bag in the plethysmograph. The actual flow rate was calculated from the volume excursion (V_T) according to the equation

$$\dot{V} = 2 \pi f V_T$$

where f is the oscillation frequency. The calibration curves for both gases were not different from steady flow conditions and SF6 flow values were corrected using this calibration curve. The frequency response of the pressure recording systems were adequate for phase and amplitude to 7 cps. for both gases in simulated experimental conditions.

d. Calculation of Gas Physical Properties and Reynold's Numbers.

During forced oscillations, the composition of the flow gas presumably approaches alveolar fractions (.74 inert gas, .14 O₂, .06 CO₂, .06 H₂O). Using data from the Handbook of Chemistry and Physics, the density of the air and SF6 mixtures were computed to be 1.12 and 4.27 g/L x 10⁻³ respectively. The viscosity of such an air mixture is 1.87 x 10⁻⁴ poise (135). As discussed above, SF6 was found 14.5% less viscous than air at room

temperature. If the change in viscosity produced by heat, water vapor and gas exchange is similar for both mixtures, the viscosity of SF6 was 1.60×10^{-4} poise. Thus, the SF6 mixture is 3.8 times as dense and .855 times as viscous as air, giving it a density-viscosity product 3.2 times greater than for air.

Reynold's numbers were calculated at the catheter site from the equation

$$R_e = d \rho u / \mu$$

where d (cm) is airway diameter and u is linear velocity (cm/sec.). According to Ross (137), linear velocity in a given airway of the dog lung may be estimated:

$$U = .145 \dot{V}T A^{.25} / D^{.5}$$

where $\dot{V}T$ is flow rate in the lung (ml/sec), A is the cross sectional area (mm^2) of that airway and D is its distance from the carina. For sinusoidal oscillations, the average flow is the root mean square of the flow amplitude, of which half is inspiratory and half expiratory. The velocity equation was simplified and solved for mean velocity during 1 lps oscillations for each lung studied

$$U = 48.4 (d/D)^{.5}$$

Using these values, average R_e were calculated for air oscillations (Table 4). During SF6 oscillations at the same flow rate, R_e increase by a factor of 4.5 (relative $\rho / \mu = 3.8 / .855$). Thus R_e are similar during .5 lps SF6 oscillations and 2 lps air oscillations.

3. Results

Lower pulmonary resistance (R_{lp}) was partitioned in eight dogs (Table 7) in the region of FRC (about 35% VC) and at a higher lung volume (about 65%). At FRC, R_{lp} increased from 1.56 during air breathing to 2.34

9/
TABLE 7

Effect of Gas Physical Properties and Flow Rate on R_{1p}

A. Pre Vagotomy

<u>65% VC</u>	<u>K_1</u>	<u>K_2</u>	<u>R_{1p}</u>	<u>t_a'</u>	<u>t_n'</u>
Air	.77	.18	.95	.14	
SF ₆ Measured	.85	.60 ⁺⁺	1.45 ⁺⁺⁺	.34 ⁺⁺	.37
SF ₆ Predicted 1	.66	.67	1.33		
2			1.72	.50	.50
<u>35% VC</u>					
Air	1.27	.29	1.56	.15	
SF ₆ Measured	1.28	1.06 ⁺⁺	2.34 ⁺⁺⁺	.37 ⁺	.35
SF ₆ Predicted 1	1.09	1.10	2.19		
2			2.80	.50	.50

B. Post Vagotomy

<u>65% VC</u>	<u>K_1</u>	<u>K_2</u>	<u>R_{1p}</u>	<u>t_a'</u>	<u>t_n'</u>
Air	.61	.08	.69	.10	
SF ₆ Measured	.86	.15	1.01 ⁺⁺⁺	.10	.32
SF ₆ Predicted 1	.56	.38	.94		
2			1.35	.50	.50
<u>35% VC</u>					
Air	.64	.11	.75	.12	
SF ₆ Measured	.91	.23	1.14 ⁺⁺⁺	.16	.36
SF ₆ Predicted 1	.55	.42	.97		
2			1.35	.50	.50

Mean values for individual experiments listed in Tables 10-13.

The SF₆ predicted values were calculated from equations 1 and 2 (See text).
+ ($p < .05$), ++ ($p < .01$) and +++ ($p < .001$) denote differences from the corresponding air values.

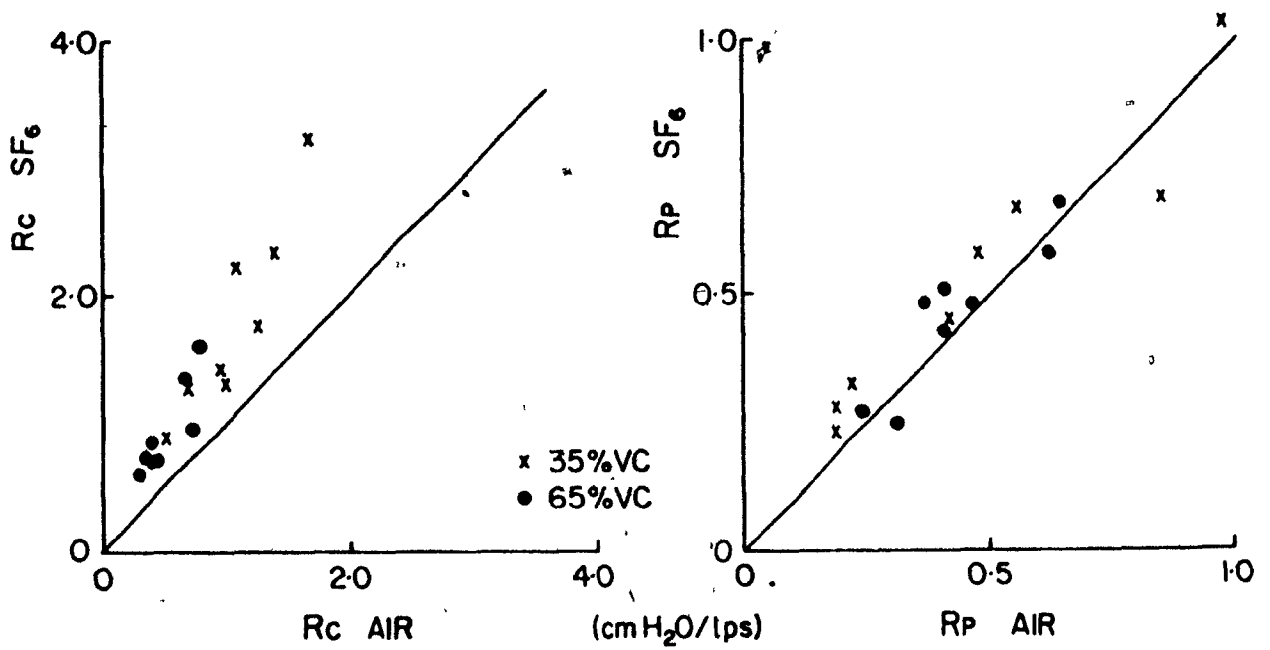
For definitions of other symbols, see text.

during ventilation with SF6. At the higher lung volume R_{lp} was reduced on both gases, and a significant difference was again observed between air (.95) and SF6 (1.45). After vagotomy, R_{lp} measured in seven dogs was markedly reduced at FRC, and the reduction in resistance as lung volume increased was no longer evident. The effects of gas physical properties were similar to the prevagotomy results, as R_{lp} increased from .75 and .69 during air breathing to SF6 values of 1.14 and 1.01 at 35 and 65% VC respectively.

The results in Table 8 reveal that almost all of the change in R_{lp} associated with changes in gas and lung volume occurred in central airways (proximal to 4 mm bronchi). This is illustrated in Fig. 9, which plots the partitioned resistance values before vagotomy during air breathing (abscissa) against the corresponding values for SF6 (ordinate). For the central airways (Left Panel) all points for both lung volumes lie above the line of identity, and R_c is approximately doubled during SF6 breathing. At FRC, R_c increased from 1.08 on air to 1.81 during SF6 breathing. As indicated by the separation of crosses and dots, R_c decreased on both gases at the higher lung volume, and SF6 resistance (.96) remained greater than air resistance (.52). The exponent 'n' relating resistance to gas physical properties was .44 at FRC and .56 at the higher lung volume.

In contrast, the points comparing peripheral resistance (Figure 9 - Right Panel) cluster more closely about the line of identity, and the symbols denoting different lung volumes are not clearly separated. No significant differences were observed between mean R_p values during ventilation with air and SF6 at either lung volume. Accordingly, values of the exponent 'n' were much lower, indicating that resistance in peripheral airways is virtually independent of gas density.

FIGURE 9



Comparison of resistance at 1 lps between air (abscissa) and SF₆ (ordinate) for central (left panel) and peripheral (right panel) airways. The line of identity is drawn (see text).

TABLE 8

Effect of Gas Physical Properties on Partitioned Resistance

<u>% VC</u>		<u>Pre Vagotomy</u>		<u>Post Vagotomy</u>	
		<u>R_c</u>	<u>R_p</u>	<u>R_c</u>	<u>R_p</u>
65	Air	.52±.19	.44±.14	.35±.07	.34±.09
	SF6	.96±.33 ⁺⁺⁺	.46±.15	.58±.16 ⁺⁺	.44±.08 ⁺⁺
	'n'	.56±.14	.04±.12 ^{***}	.36±.23	.16±.12 [*]
35	Air	1.08±.37	.49±.30	.54±.13	.22±.12
	SF6	1.81±.75 ⁺⁺⁺	.55±.27	.87±.24 ⁺⁺⁺	.27±.12
	'n'	.44±.13	.13±.15 ^{**}	.36±.20	.19±.30

++ (p < .01) and +++ (p < .001) denote difference from corresponding air values.

* (p < .05), ** (p < .01) and *** (p < .001) denote differences from corresponding R_c values.

For definitions of other symbols, see text.

Similar features are noted after vagotomy (Table 8). R_c increases significantly from .54 (35% VC) and .35 (65%VC) during air breathing to .87 and .58 at corresponding lung volumes during SF6 breathing, giving an exponent 'n' of .36 in each case. Peripheral resistance is much less affected by the change in gas physical properties, and the exponent 'n' is significantly lower than in central airways.

R_c increased with flow rate at both lung volumes as indicated by the values of K_2 (Table 9). Before vagotomy ventilation with SF6 caused a four to five-fold increase in K_2 which completely accounted for the increase in R_c on the dense gas. When an exponential P-V relationship described by equation 2 was assumed, the exponent 'a' increased from .22 and .26 on air at 35% and 65% VC respectively to .46 and .56 on SF6 at the corresponding lung volumes. Similar changes were noted after vagotomy.

In comparison with the results in central airways, values for K_2 and 'a' in peripheral airways are markedly reduced on both gases at both lung volumes before and after vagotomy (Table 9), indicating that R_p is virtually independent of flow rate. Furthermore, neither K_2 nor 'a' increase with gas density.

The constants calculated from each experiment are presented in Tables 10-13. Resistance values in each airway segment for each tested condition of lung volume and bronchomotor tone may be obtained by summing the corresponding values of K_1 and K_2 . The mean results presented above may be summarized as follows. At both lung volumes before and after vagotomy, R_c increased significantly with gas ($\rho\mu$) products and flow rate, whereas R_p was not influenced by either.

TABLE 9Effect of Flow Rate on Partitioned ResistanceA. Pre Vagotomy

<u>% VC</u>		<u>R_c</u>		<u>R_p</u>	
		<u>Air</u>	<u>SF6</u>	<u>Air</u>	<u>SF6</u>
65	K ₁	.39 _± .14	.37 _± .32	.38 _± .13	.48 _± .21
	K ₂	.12 _± .12	.58 _± .39 ⁺⁺	.06 _± .05	.02 _± .11 ^{***}
	a	.26 _± .19	.56 _± .40 [†]	.17 _± .11	.02 _± .21 ^{***}
35	K ₁	.85 _± .27	.92 _± .38	.42 _± .25	.36 _± .17
	K ₂	.22 _± .20	.89 _± .46 ⁺⁺⁺	.07 _± .13	.18 _± .22 ^{***}
	a	.22 _± .18	.46 _± .08 ⁺⁺	.11 _± .28	.20 _± .30 [*]

B. Post Vagotomy

<u>% VC</u>		<u>R_c</u>		<u>R_p</u>	
		<u>Air</u>	<u>SF6</u>	<u>Air</u>	<u>SF6</u>
65	K ₁	.28 _± .13	.32 _± .09	.33 _± .11	.54 _± .22 [†]
	K ₂	.07 _± .07	.26 _± .13 ⁺⁺	.01 _± .04	-.11 _± .18 ^{***}
	a	.25 _± .29	.44 _± .11	.03 _± .19	-.19 _± .25 ^{***}
35	K ₁	.42 _± .17	.62 _± .22	.23 _± .14	.29 _± .15
	K ₂	.12 _± .06	.25 _± .07	-.01 _± .05 [*]	-.02 _± .07 ^{**}
	a	.28 _± .15	.30 _± .19	.04 _± .35	-.08 _± .33 [*]

+ (p < .05), ++ (p < .01) and +++ (p < .001) denote differences from corresponding air value.

* (p < .05), ** (p < .01) and *** (p < .001) denote differences from corresponding R_c value.

For definitions of other symbols, see text.

TABLE 10

Partitioned Resistance at 65% VC Pre Vagotomy

A. Central Airways

Expt. No.	K_1		K_2		'a'		'n'
	Air	SF6	Air	SF6	Air	SF6	
1	.45	.34	-.04	.52	-.10	.51	.64
2	.62	-.25	.10	1.22	.16	1.24	.26
3	.35	.69	.04	.04	.14	.04	.54
4	.31	.27	.07	.50	.26	.67	.61
5	.34	.18	.12	.55	.36	.73	.40
6	.16	.40	.13	.22	.49	.39	.65
7	.45	.78	.24	.54	.34	.33	.56
8	.46	.55	.33	1.05	.47	.58	.61

B. Peripheral Airways

Expt. No.	K_1		K_2		'a'		'n'
	Air	SF6	Air	SF6	Air	SF6	
1	.58	.55	.04	.03	.09	0	-.06
2	.36	.39	.11	.09	-.22	.20	.04
3	.32	.67	.07	-.19	.22	-.30	.18
4	.42	.52	-.01	-.01	-.04	0	.19
5	.28	.23	.03	.02	.11	.10	-.19
6	.19	.16	.06	.11	.31	.38	.07
7	.36	.56	.05	-.13	.21	-.18	.04
8	.51	.75	.14	-.07	.24	-.07	.04

TABLE 11Partitioned Resistance at 35% VC - Pre Vagotomy

A. Central Airways

<u>Expt. No.</u>	<u>K₁</u>		<u>K₂</u>		<u>'a'</u>		<u>'n'</u>
	<u>Air</u>	<u>SF6</u>	<u>Air</u>	<u>SF6</u>	<u>Air</u>	<u>SF6</u>	
1	.79	.76	-.10	.52	-.08	.39	.53
2	.89	1.02	.38	.73	.35	.43	.28
3	.53	.47	.01	.43	.02	.46	.47
4	.72	.67	.26	.65	.31	.55	.26
5	.83	.78	.13	.66	.19	.41	.35
6	.72	1.28	.37	.95	.38	.37	.62
7	.91	.74	.49	1.61	.39	.61	.45
8	1.44	1.66	.24	1.56	.22	.44	.56

B. Peripheral Airways

<u>Expt. No.</u>	<u>K₁</u>		<u>K₂</u>		<u>'a'</u>		<u>'n'</u>
	<u>Air</u>	<u>SF6</u>	<u>Air</u>	<u>SF6</u>	<u>Air</u>	<u>SF6</u>	
1	.85	.40	0	.29	0	.39	-.18
2	.17	.29	.06	.04	.39	.12	.31
3	.41	.52	.01	-.07	0	-.13	.06
4	.24	.10	.24	.48	.51	.66	.16
5	.22	.29	-.03	-.06	-.23	-.21	.20
6	.24	.26	-.03	.02	-.16	.03	.25
7	.54	.33	-.02	.34	-.05	.42	.15
8	.67	.66	.31	.38	.39	.31	.05

TABLE 12

Partitioned Resistance at 65% VC Post Vagotomy

A. Central Airways

Expt. No.	K_1		K_2		$'a'$		$'n'$
	Air	SF6	Air	SF6	Air	SF6	
1	.47	.28	-.08	.25	-.30	.56	.22
2	.41	.45	.04	.21	.13	.40	.28
4	.30	.28	.06	.16	.22	.43	.15
5	.27	.40	.12	.17	.36	.24	.27
6	.14	.19	.11	.28	.53	.52	.46
7	.24	.28	.07	.20	.25	.38	.32
8	.14	.34	.14	.55	.55	.55	.83

B. Peripheral Airways

Expt. No.	K_1		K_2		$'a'$		$'n'$
	Air	SF6	Air	SF6	Air	SF6	
1	.45	.51	-.04	-.01	-.15	-.02	.15
2	.27	.58	.08	-.11	.29	-.38	.21
4	.27	.42	.03	.06	.13	.16	.13
5	.31	.42	-.02	-.12	-.23	-.27	.02
6	.18	.42	.04	-.05	.19	-.10	.38
7	.32	.42	-.02	-.01	-.05	-.15	.23
8	.48	1.03	.03	-.50	.06	-.59	.03

TABLE 13Partitioned Resistance at 35% VC Post Vagotomy

A. Central Airways

Expt. No.	K_1		K_2		$'a'$		$'n'$
	Air	SF6	Air	SF6	Air	SF6	
1	.40	.39	0	.23	0	.45	.32
2	.76	.64	.12	.34	.18	.43	.08
4	.33	.41	.08	.12	.26	.29	.18
5	.55	1.01	.14	-.07	.25	-.09	.32
6	.35	.77	.20	.27	.43	.22	.46
7	.26	.46	.14	.31	.39	.34	.47
8	.29	.63	.16	.56	.42	.45	.70

B. Peripheral Airways

Expt. No.	K_1		K_2		$'a'$		$'n'$
	Air	SF6	Air	SF6	Air	SF6	
1	.26	.34	.02	.04	.10	.14	.22
2	.26	.19	-.06	-.01	-.18	-.08	-.08
4	.28	.37	-.03	-.07	-.18	-.58	.13
5	.26	.30	-.05	-.12	-.38	-.41	-.11
6	.06	.15	.01	.06	.29	.24	.79
7	.04	.10	.07	.06	.66	.28	.27
8	.43	.55	-.01	-.08	-.01	-.15	.08

4. Discussion

These results demonstrate a significant increase in R_{lp} during ventilation with SF6. Arterial oxygen tensions were not different on the two gases. The small but significant increase in P_{aCO_2} during SF6 ventilation may decrease airways resistance in dogs due to vagally mediated bronchodilation thus opposing the observed increase in resistance. A quantitatively similar effect of SF6 and R_{lp} was observed after vagotomy, tending to exclude this and other vagally mediated reflexes as a cause of the observed increased resistance. It is most likely that the increase in resistance is due to the change in gas physical properties. For a laminar flow regime, resistance to periodic flow exceeds steady flow resistance at higher frequencies, and this difference is greater with gases of lower kinematic viscosity (25, 167). It is argued in appendix 1 (P. 211) that because boundary layers are thin throughout the bronchial tree, resistance measured at 4 cps is not different from steady flow resistance during ventilation with either air or SF6. Accordingly, the observed effects of gas physical properties and flow rate on lower pulmonary resistance are relevant to conditions of quiet breathing.

Information regarding the physical basis of airways resistance in central and peripheral segments of the bronchial tree is provided by the results of the partitioned studies. Peripheral resistance was not significantly affected by gas density or flow rate, which may be explained by a fully developed laminar flow regime in these airways. Alternatively, the effect of gas density and flow rates on non-laminar flow may be masked by a significant contribution of pulmonary tissue resistance (R_{ti}) to R_p . Pulmonary tissue does not behave as a flow resistance but as a non-ideal elastic element exhibiting pressure volume hysteresis (3). The area of the static hysteresis loop is the resistive work (W) done on lung tissue

per breath and can be converted to R_{ti} using the equation (110):

$$R_{ti} = \frac{2 W_t}{\pi^2 V_T^2}$$

where t is the period of a respiratory cycle. Furthermore, the hysteresis area is a constant fraction (.12) of the product of tidal volume x elastic pressure (4). In this experiment, the average inflationary compliance was 80 ml/cm H₂O and the tidal volume during resistance measurement at 1 lps was 40 ml, giving a calculated hysteresis area of 2.4 gram cm, and a value for R_{ti} of .08 cm H₂O/lps. Since the mean values for R_p were .44 and .49, R_{ti} contributes a small proportion of the measured resistance in peripheral airways. Thus, the failure to demonstrate a significant effect of gas density and flow rate upon R_p is best explained by a fully developed laminar flow regime in these airways.

A quite different flow regime must exist in central airways where the resistance increased significantly with gas density and flow rate. At both lung volumes, the exponents 'n' relating R_c to gas physical properties are close to 0.5. Similar values of exponents 'a' relate R_c to flow rate during SF₆ breathing. These observations support the hypothesis that boundary layer growth accounts for a major component of flow resistance in central airways. Opposing this conclusion is the finding that during air breathing the exponent 'a' is considerably lower than 0.5. This may be explained if boundary layer growth effects are prominent up to and beyond the retrograde catheter site during SF₆ breathing, but during air breathing, fully developed parabolic velocity profiles exist in airways contributing significantly to R_c . According to equation 5 in Pedley et al (119), the pressure drop in their airway model became equal to the laminar pressure drop when $R_e = 33$. During air breathing, R_e at the catheter site averaged 85 when flow oscillations are 1.0 lps (Table 4). Given the errors in applying these estimates, this value is not inconsistent with a fully developed laminar

profile in airways some generations proximal to the catheter site. Since these airways (4 to 8.0 mm) account for the major resistance in the dog (84), the exponent 'a' may be markedly diminished. On the other hand, R_e at the same site and flow rate during SF6 breathing average 380, and are conceivably high enough to promote significant boundary layer disturbances throughout the central airway. Accordingly, the measurements of lower pulmonary resistance can be explained by boundary layer growth in central bronchi and laminar flow in peripheral airways. The transition between these flow regimes during quiet breathing oscillates about the 4 mm airways according to the prevailing R_e .

Alternatively, these results may be explained by a continual metamorphosis of the flow regime along the tracheo-bronchial tree. Jaeger and Mathys (69, 70) pointed out the fluid dynamic similarity between the human upper airway and a Venturi metre. In both, the pressure drop at low R_e is entirely viscous, but as R_e increase, inertial disturbance account for an increasing proportion of the pressure drop. The exponent 'a' relating resistance to flow increases progressively with R_e from values of 0 at $R_e < 10$ to 1.0 at $R_e > 10^4$. The energy equations describing laminar flow, boundary layer growth, turbulent flow, and orifice flow fall on this relationship (Table 1, P.19) according to the general equation:

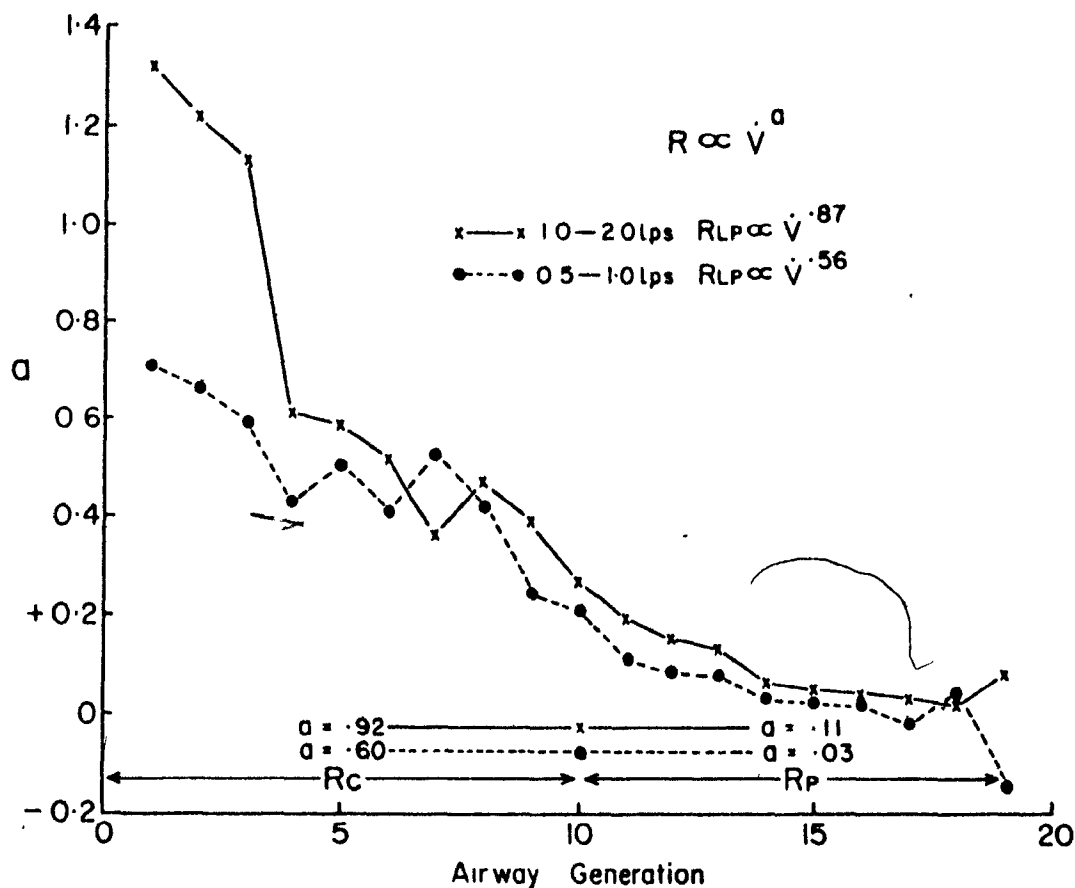
$$R = C \dot{V}^{-a} \rho^a \mu^{1-a} \quad (3)$$

In the lower pulmonary airways, R_e progressively diminish as gas flows peripherally at a given rate. To the extent that the Venturi metre fluid dynamics operate in the bronchial tree, the additional pressure losses due to inertial disturbances at each bifurcation will cause a large 'a' in central airways and a small 'a' peripherally. According to equation 3, there will be a corresponding large 'n' with less effect of gas viscosity

centrally, and a small 'n' in peripheral airways.

This concept is supported by the theoretical study of Olsen et al (113). They calculated the resistive pressure drops per generation of a human airway model at 3 flow rates. Values of the exponent 'a' were calculated from their results and are plotted per generation in Fig. 10. The exponent decreases progressively as flow proceeds peripherally. Furthermore, for all but two generations, the exponent calculated for the higher pair of flow rates is greater than that calculated for the lower pair. These observations illustrate the theoretical dependence of the exponent 'a' upon R_e in the bronchial tree. The effect of this concept on the interpretation of our results is demonstrated by a consideration of Fig. 10. Between inspiratory flow rates of 0.5 and 1.0 lps, (broken line) R_{1p} varies as $\dot{V}^{.56}$. From this observation, it is reasonable to conclude that boundary layer growth effects account for most of the lower pulmonary resistance. Partitioning R_{1p} with a catheter in the tenth airway generation reveals that R_c is similarly related to flow ($R_c \propto \dot{V}^{.60}$) but that R_p is virtually flow independent ($R_p \propto \dot{V}^{.03}$). Now the additional conclusion that the peripheral flow regime is laminar is supported. However, to interpret the partitioned results as indicating different uniform flow regimes in central and peripheral airways would miss additional information. In the central airways the exponent 'a' decreases from 0.75 in the trachea to 0.25 in generation 9. The former value is consistent with turbulence, (see Table 1) whereas the latter may indicate that a parabolic velocity profile is re-established within the length of generation 9 after being distorted at the bifurcation. Finally, this mechanism suggests that due to the lower R_e , the exponent 'a' will be lower in each generation during air breathing than during SF6 breathing. It follows that the overall exponent in central

FIGURE 10



Exponent 'a' versus airway generation.

Resistances per generation were calculated from pressure losses at three flow rates (Tables 1-3 in Olsen et al (113)), and used to solve equation 2 for 'a' between .5 and 1 lps and between 1 and 1.5 lps. Values of 'a' were similarly obtained for total (RLP), central (R_c) and peripheral (R_p) airways from the summed pressure losses in each segment (113). For discussion, see text.

airways in the present experiment may be significantly lower for air than for SF₆ in the same way as the value of 'a' decreases in Fig. 10 from .92 at the higher pair of flow rates (hence higher R_e) to .60 at the lower pair.

The equation for boundary layer growth considerably overestimates the measured values of 'a' and 'n' in the total bronchial tree. Thus, the prediction of Pedley et al is less accurate than that of Rohrer for R_{lp} in dog lungs (see Table 7). This does not necessarily contradict Pedley et al, whose prediction was based on the morphometry of the human lung. It appears from this study that laminar flow occurs at higher R_e in the dog lung than in a human airway model, where resistance considerably exceeds that calculated for laminar flow when R_e are as low as 200 (119). Other differences aside, if a smaller ratio of R_p to R_{lp} exists in the human lung than was observed in this study (.3 to .5), the exponents for the total airway would approach those observed in central airways where they are quite consistent with the prediction of Pedley et al.

According to Rohrer (135), the flow resistive pressure drop in pulmonary airways is the sum of losses due to laminar flow and additional losses due to inertial disturbances of the fluid in the irregular conducting system. The former pressures are proportioned to flow rate by a factor (K_1) containing gas viscosity and the geometry of the airway segment conducting laminar flow. The additional losses are related to the square of flow by another factor (K_2) containing gas density and the geometry of the airway responsible for the inertial disturbances. Fry et al (50) pointed out that the distribution of turbulence along the bronchial pathway is similar for two gases only when their kinematic viscosities are similar. In these conditions, K_1 and K_2 vary as gas viscosity and density respectively so that the effect of gas physical

properties on resistance is predictable from Rohrer's equation (50, 94). For gases of differing kinematic viscosity, these constants are not so related to physical properties, presumably because the geometric factor of each constant changes with the distribution of turbulence (50). Accordingly, although experimentally determined pressure flow curves are adequately described, Rohrer's constants are not believed to account for the physical events responsible for airway resistance (94).

It is surprising then that predictions of R_{1p} on SF6 from Rohrer's constants during air breathing ($K_1 \times .855 + K_2 \times 3.8$) are within 10% of the measured values (Table 7). Before vagotomy, the changes in K_1 and K_2 from air to SF6 are similar to Rohrer's prediction. Even after vagotomy, where the predicted change in these constants is less accurate, it would not be reasonable to reject Rohrer's equation in view of the wide range of error inherent in determining K_1 and K_2 (see Tables 6 & 9). Several earlier studies show Rohrer's equation to predict adequately the change in resistance when gases of differing kinematic viscosity were studied (85, 156), and it is questionable whether other reports (94, 114) are justified in rejecting the equation. Perhaps there is a valid physical basis underlying Rohrer's equation which is compatible with the theory of boundary layer growth. This theory states that the parabolic velocity profile of Poiseuille flow is disturbed at each bifurcation (145) and energy in addition to laminar losses is used to accelerate core molecules as the velocity profile is re-established downstream (113). These additional losses are proportioned to the square of flow by a factor, analogous to Rohrer's K_2 , containing the geometry of the bifurcation and gas density. Pedley et al (120, 121) point out that most of the resistance by which turbulent flow exceeds laminar is due to the blunt velocity profile. Accordingly, turbulence in branching airways does not grossly alter the pressure drop, since a blunt profile already exists in the absence of turbulence. It follows that a predictive

equation based on laminar losses for the entire bronchial tree and additional losses due to inertial disturbances may provide not only a description of lower airways resistance but a physical explanation as well. In this regard, it is noteworthy that a correct mathematical description of Rohrer's equation by equation 2 requires the exponent 'a' to increase with flow rate, a feature compatible with both the fluid dynamic principles reviewed above and the frequent observation that Rohrer's constants provide a good description of airway pressure-flow relationships.

5. Summary and Conclusions

Lower pulmonary resistance (R_{1p}) was partitioned at two flow rates (\dot{V}) in anaesthetized dogs during ventilation with air and with a gas mixture (SF₆-O₂) having 3.8 x the density (ρ) and .86 x the viscosity (μ) of air. In airways peripheral to 4 mm bronchi, resistance (R_p) was independent of gas physical properties and flow rate. When the equation $R = K (\rho \mu)^n \dot{V}^a$ was solved using resistances measured in central airways, the exponents 'n' and 'a' each approximated a value of 0.5. These results indicate that fully developed parabolic velocity profiles exist in peripheral airways, so that the entire viscous pressure losses are described by the Poisseuille equation. In central airways where Reynold's numbers (R_e) are much greater, frequent inertial disturbances of the velocity profile cause additional pressure losses which are adequately described by the equation of boundary layer growth. It is likely that these two flow regimes are not discrete but undergo a continual metamorphosis from predominantly inertial pressure losses to completely viscous losses as R_e decrease between trachea and alveoli. Primarily because R_p accounted for 30 - 50% of R_{1p} , the boundary layer growth equation overestimated the effects of gas physical properties and flow rate on lower pulmonary resistance. Rohrer's equation more accurately predicted these effects, and it is suggested that there may be a physical basis underlying its adequate mathematical description of these pulmonary pressure-flow relationships.

B. The Effect of Gas Physical Properties and Flow Rate on Human Lower Pulmonary Resistance.

1. Introduction

In the previous section, the relationship of canine lower pulmonary resistance with gas physical properties and flow rate was described and compared with theoretical equations developed by Rohrer (135) and Pedley et al (119, 120, 121). Using a similar approach, this study attempts to elucidate the fluid dynamics underlying human lower pulmonary resistance.

2. Methods

Lower pulmonary resistance was measured in 3 volunteer laboratory personnel. An esophageal balloon (length 10 cm, circumference 3.5 cm) was positioned in the lower third of the esophagus. Under local anaesthesia and aseptic technique, a #18 gauge medicut was inserted between the second and third tracheal rings. The intratracheal position was adjusted under fluoroscopy to give the smallest angle with respect to the axis of flow and to ensure that the catheter did not move during respiration. The esophageal balloon and tracheal needle were connected to opposing ports of a Sanborn 268 B differential pressure transducer. The subject was seated in an Emerson volume displacement body plethysmograph (98) and breathed through a Fleisch No. 4 pneumotachygraph coupled to a Sanborn 270 transducer. A two way breathing valve (Warren E. Collins High Velocity double J) was connected in series with the pneumotachygraph, and the inspiratory line was connected to one of three gas mixtures consisting of 21% oxygen in helium, nitrogen or sulfur hexafluoride. After three minutes of open circuit breathing, punctuated by several vital capacity breaths, the subject inspired to

total lung capacity, expired to his predetermined FRC and began to breath rapidly (100 bpm) and shallowly (< 300 ml) for about 30 seconds. This manoeuvre was repeated three times on each gas, and air measurements were repeated before and after each foreign gas. Measurements were also obtained at a lower lung volume (FRC -1 litre) in two subjects breathing air and SF₆. In one subject (LE), FRC measurements were repeated on air and SF₆ after an intravenous injection of 1.2 mg atropine.

Signals proportional to flow, pressure, and lung volume were recorded on a Sanborn Poly Viso and stored on magnetic tape. To analyse the data, flow and pressure signals were led from the tape to a storage oscilloscope (Tektronix No. 564) and the resulting pressure-flow loop was closed by subtracting from the pressure a signal proportional to lung volume (104). The closed loops were traced and lower pulmonary resistance (R_{1p}) was calculated at $\pm .25$ and $\pm .50$ lps taking account of the measured difference in gas viscosities (see below). Using R_{1p} values at two flow rates, the equation $R_{1p} = K_1 + K_2 \dot{V}$ was solved for K_1 and K_2 , and the equation $R_{1p} = K (\rho \mu)^n \dot{V}^a$ was solved for the exponent 'a' on each gas. Similarly, the exponent 'n' was calculated using the different density-viscosity products and the corresponding differences in R_{1p} between pairs of different gases (e.g. helium-air and air-SF₆).

Using a technique described above (p. 93), the pneumotachygraph was found linear to 2 lps on all gas mixtures used. For a given flow rate, the flow signal for the helium mixture was 12% greater and that for the SF₆ mixture was 14.5% less than for air. These differences are presumably due to the different viscosities of the gases. Gas densities, calculated as outlined previously (p. 95) gave values for helium

and SF₆ mixtures of .39 and 3.8 respectively times that of air. Thus, the corresponding density-viscosity products relative to air were .43 (helium) and 3.24 (SF₆).

Errors in the measurement of lateral tracheal pressure are due to angulation of the needle with respect to the axis of flow (yaw) and to acceleration of gas between trachea and alveolus. If yaw is constant, the resulting errors in inspiratory and expiratory resistance are equal and opposite, and so may be ignored when R_{1p} is calculated for both phases of respiration.

3. Results

Considerable cardiac artefact was encountered in the pressure-flow loops recorded from all subjects. By replaying the recorded signals repeatedly, it was possible to obtain for each tested condition three to ten closed P - \dot{V} loops from breaths apparently free from cardiac artefact. When the mean values for R_{1p} for each subject were compared (t-test) between gas mixtures, R_{1p} increased (p < .05) from helium to air and from air to SF₆ (Table 14). At FRC, the exponent 'n' averaged 0.35 for all subjects. At the lower volume, the effect of gas physical properties was greater in LW and less in LE, giving a similar average value for 'n' (0.31). After atropine, R_{1p} increased from 0.45 cm H₂O/lps on air to .75 on SF₆ ('n' = 0.45).

The P - \dot{V} curves were generally a linear. Between \pm .25 at \pm .5 lps, values of the exponent 'a' for all subjects (Table 14) averaged 0.16 at FRC, and were considerably lower than the corresponding 'n' values. This was also true at the lower lung volume, and after atropine the P - \dot{V} curves were linear ('a' = 0). In addition, a tendency for 'a' to increase with gas density was apparent. This relationship was explored in more

TABLE 14

Effect of Gas Physical Properties and Flow Rate on Human R_{lp} *

A: FRC

<u>Subject</u>		<u>Helium</u>	<u>'n'</u>	<u>Air</u>	<u>'n'</u>	<u>SF6</u>
PD	$R_{lp}(\pm Sd)$	1.05(.18)	.31	1.53(.16)	.57	3.38(.10)
	'a'	.14		.22		.48
	K_2	.20		.44		1.90
LW	$R_{lp}(\pm Sd)$.64(.14)	.30	.88(.15)	.30	1.34(.11)
	'a'	0		.13		.22
	K_2	0		.14		.38
LE	$R_{lp}(\pm Sd)$.39(.15)	.36	.60(.16)	.27	.87(.14)
	'a'	.14		0		.11
	K_2	.06		0		.12

B: FRC-1 litre

<u>Subject</u>		<u>Air</u>	<u>'n'</u>	<u>SF6</u>
LW	$R_{lp}(\pm Sd)$	1.34(.14)	.45	2.25(.10)
	'a'	.10		.11
	K_2	.18		.34
LE	$R_{lp}(\pm Sd)$	1.17(.12)	.16	1.43(.12)
	'a'	.09		0
	K_2	.12		0

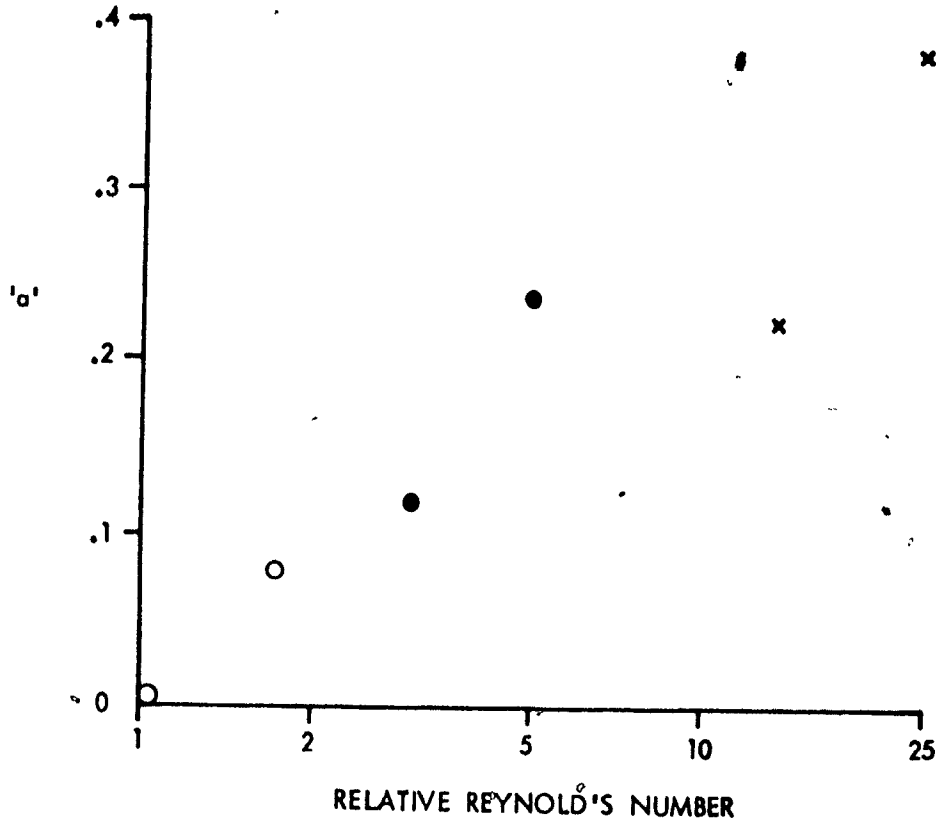
*Lower pulmonary resistance in cm H₂O per lps.

detail for subject LW, whose flow excursions allowed the calculation of R_{1p} at $\pm .75$ lps. A second value of 'a' was calculated for each gas at the higher pair of flow rates (.5 to .75 lps). Although 'a' values increased with flow rate on each gas, a single value for K_2 adequately described the pressure drop at the three flow rates. The exponent 'a' also increased with gas density, and a good correlation was obtained when 'a' was plotted against a relative R_c scale (Fig. 11).

4. Discussion

The measured values of R_{1p} during air breathing are similar to previously reported values (14, 44, 65, 157). Of these studies, only Ferris et al (44) mention the $P - \dot{V}$ contour which was essentially linear. In this study, linear $P - \dot{V}$ curves were noted in one subject (LE) during air breathing whereas other curves were noticeably ailinear. A review of several papers which examined the effect of gas physical properties on human pulmonary (50, 85, 87, 94, 114) and airways (156) resistance revealed that both vary as the 0.5 to 0.6 power of gas density. Jaeger and Mathys (69, 70) observed that upper airways resistance was related to gas density by a higher power (about .8), so R_{1p} is expected to be less affected by gas density than the total airway. In a model of the human bronchial tree, the resistive pressure losses were completely described by calculations based on the growth of boundary layers (119). Applying the equation of boundary layer growth to human bronchial morphology, Pedley et al (120, 121) predicted that R_{1p} varies as the square root of gas density, viscosity and flow rate (eq. 2, P.91). In the dog lung, the exponents relating R_{1p} to gas physical properties ('n') and flow rate ('a') were considerably less than predicted.

FIGURE 11



The relationship between Reynold's number and exponent 'a' in lower pulmonary airways. Ordinate: Exponent 'a' calculated from R_{1p} values measured in LW at .25, .50 and .75 lps on helium (O), air (●) and SF₆(x) Abscissa: Log scale of relative Reynold's number, expressed as the average value calculated for the lower and higher pair of flow rates for each gas mixture. Absolute R_e calculated for generation 5 of Weibel's lung model are 50 times greater than the relative values.

The effects of gas physical properties and flow rate upon human R_{lp} appear quite similar to those in the dog. The exponent 'n' is less than that predicted by Pedley et al, suggesting that a flow regime less dependent on gas density and flow rate than boundary layer growth must account for a substantial portion of human lower pulmonary resistance. In the canine lung, laminar flow was demonstrated in airways peripheral to 4 mm bronchi, which accounted for 30 to 50% of R_{lp} . In more central airways, the equation of boundary layer growth adequately described the observed effects of gas physical properties and flow rate upon resistance. Laminar flow in peripheral airways accounting for a similar proportion of human R_{lp} is one possible explanation of these results. Alternatively, pulmonary tissue resistance (R_{ti}) may obscure an entirely adequate description of lower airways resistance (R_{law}) by the equation of boundary layer growth. Marshall and Dubois (86) reported an average value for R_{ti} of .21 cm H₂O/lps measured at FRC in 12 healthy adults during a rapid shallow breathing manoeuvre quite similar to that used in this study. When this value was subtracted from R_{lp} and the exponents recalculated for R_{law} , the values of 'n' were much closer to that predicted by Pedley et al (Table 15). Accordingly, these results do not exclude the possibility that the equation of boundary layer growth adequately describes the pressure-flow relationship of the human bronchial tree.

One finding opposing this possibility is the increase of the exponent 'a' with gas density and flow rate (Fig. 11). This observation supports the theoretical dependence of 'a' upon R_c discussed in Section A, and so suggests that the bronchial flow regime is not constant. Rather it undergoes a continual metamorphosis, in which the relationship between resistance, gas physical properties and flow rate change according to

TABLE 15

Exponents Relating Gas Physical Properties and Flow Rate to R law *

<u>Subject</u>	<u>$\frac{1}{a}$</u> <u>Helium</u>	<u>$\frac{1}{n}$</u>	<u>$\frac{1}{a}$</u> <u>Air</u>	<u>$\frac{1}{n}$</u>	<u>$\frac{1}{a}$</u> <u>SF6</u>
PD	.18	.54	.30	.75	.52
LW	0	.53	.16	.45	.27
LE	.26	.92	0	.45	.14

* Resistance in lower airways estimated by subtraction of R_{ti} from R_{lp} .

(See text).

equation 3 (P.109). During quiet breathing ($\dot{V} = .4$ lps), R_e between lobar bronchi (1000) and 2 mm airways (50) are in the range where boundary layer growth accounts for almost all of the pressure drop ($'a' = .5$). Outside these R_e limits, there is a tendency toward turbulent or laminar flow. At high R_e , turbulent eddies cause added inertial pressure losses, which alter the exponents according to equation 3 toward an $'a'$ value of 1 (for classical turbulence, $'a' = .75$). When R_e are low, the parabolic velocity profiles may be re-established within each generation, so that a portion of the pressure drop per generation is entirely viscous and the exponents change according to equation 3 toward an $'a'$ value of zero. Thus, when R_e are large, as with SF₆ breathing at $\pm .75$ lps, values of $'a'$ in each generation increase, and central airways having larger initial $'a'$ values account for a greater proportion of R law (Fig.11, $'a' = .35$). When R_e are small, as with helium breathing at $\pm .25$ lps, the $'a'$ values per generation are reduced and the peripheral airways having smaller initial $'a'$ values account for a greater proportion of R law (Fig. 11, $'a' = 0$). Accordingly, the results of this study may be interpreted to support a variable flow regime in the bronchial tree in which boundary layer growth is the principle cause of airways resistance.

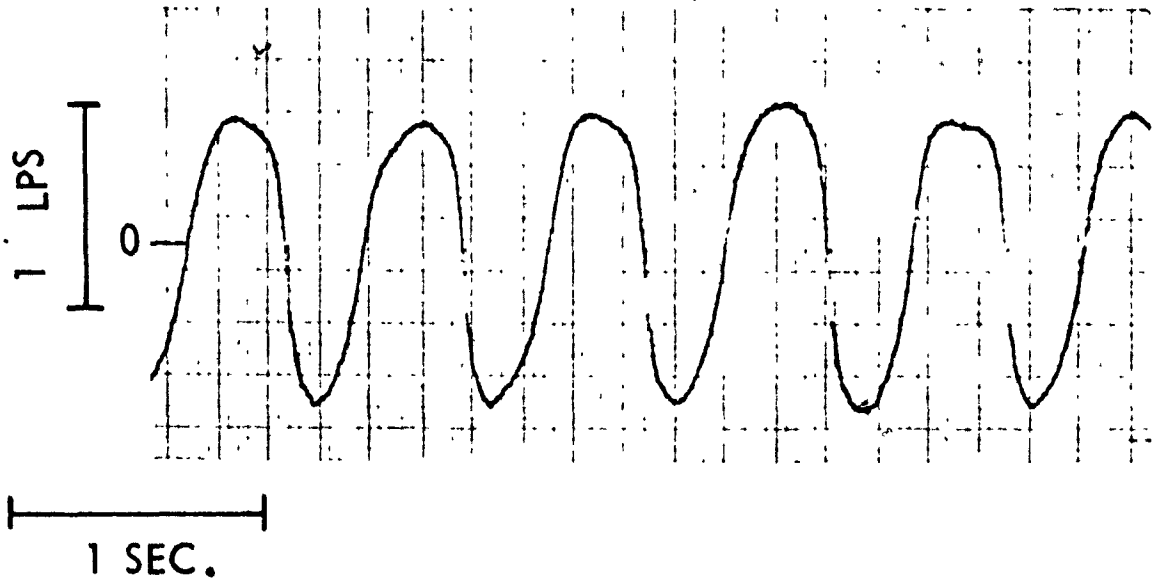
A further objection to this interpretation is the observation that $'a'$ values, even when corrected for R_{ti} , are less than one half the values predicted by Pedley et al. Furthermore, since gas density was the predominant change in physical properties, $'n'$ must be at least as small as $'a'$ to be compatible with equation 3. The discrepancy between observed values of $'n'$ and $'a'$ suggests a peculiar flow regime in which the exponent relating resistance to flow is less

than that relating resistance to density. One possible explanation is the effect of periodic flow upon resistance in frequently branching tubes. As previously described, resistance to periodic flow exceeds resistance to steady flow when the dimensionless term, B , exceeds 1.

$$B = (2 \omega x / u_0)^{.5} \quad (4)$$

where ω is angular frequency, x is distance from the bifurcation and u_0 is core velocity. Thus, the tendency for oscillations to raise resistance above the steady flow value increases as flow rate decreases. Furthermore, the panting manoeuvre often exhibits the highest frequency components at the onset of inspiration and expiration (Fig. 12). Solving equation 4 for a frequency of 4 cps, values of B in the 2 to 8 mm airways of Weibel's lung model (159) are less than 1 when flow exceeds 200 ml/sec, but at 100 and 50 ml/sec, B is equal to 1.4 and 2 respectively. To the extent that these effects exist in the bronchial tree, the $P - \dot{V}$ curves are linearized and values of 'a' underestimate the inertial contribution to bronchial resistance. Because B is independent of gas physical properties, 'n' is unaffected when periodic flow causes added resistance. In such conditions, 'a' becomes less than 'n' and equation 3 no longer describes bronchial resistance. Furthermore, Rohrer's equation is also invalidated, since inertial losses are underestimated by the $P - \dot{V}$ curvilinearity (K_2). Accordingly, failure to predict the effect of gas physical properties in this study does not disprove the underlying physical basis of Rohrer's equation during steady flow.

Clearly, human lower pulmonary resistance is not adequately described by equations for laminar, entry length, turbulent or orifice flow regimes. This was also observed in the upper airway where the variable flow regime of a venturi metre best described the measured

FIGURE 12

Flow oscillations during panting at 80 bpm, illustrating higher frequency components in early inspiration and early expiration. See text for discussion.

resistance (69). Since the general equation underlying this and other classical flow patterns (Equation 3) may also describe bronchial resistance to steady flow, it conceivably provides the best description of human airways resistance. This possibility may be tested by comparing resistance measured on gases having different physical properties with corresponding predictions calculated from equation 3 using 'a' values measured during air breathing in steady flow conditions.

5. Summary and Conclusions

Lower pulmonary resistance (R_{lp}) was measured in three healthy volunteers breathing mixtures of 21% oxygen in helium, nitrogen and SF_6 . R_{lp} increased with gas density ($\rho\mu$) and flow rate (\dot{V}), indicating that bronchial flow is non-laminar. Solution of the equation $R_{lp} = K (\rho\mu)^n \dot{V}^a$ gave 'n' values of about 0.3, and even lower values of 'a'. Thus, R_{lp} is not adequately described by the equation of boundary layer growth. Although tissue resistance may obscure an adequate description of airways resistance by this equation, the observed dependence of 'a' upon Reynold's number suggests a non-uniform bronchial flow regime. To the extent that periodic flow linearized the P- \dot{V} relationships, these results are compatible with the general equation $R = K \dot{V}^a \rho^a \mu^{1-a}$, where 'a' reflects the inertial disturbances of flow.

C. The Effect of Flow Rate on the Regional Distribution of Inspired Gas

1. Introduction

The distribution of slowly inspired gas among vertical lung regions is determined by the regional lung compliance (36, 107). Anthonisen and his co-workers (89, 90, 134) observed that boli of ^{133}Xe rapidly inspired from mid lung volumes are not distributed according to regional compliance, and suggested that during rapid inspiration, regional ventilation is determined by regional resistance. The theoretical analysis of this possibility has recently been extended (81, 122), and Pedley et al (122) have calculated from the mechanical time constants of upper and lower lobes detailed patterns of redistribution of lobar ventilation as inspiratory flow increases. The present investigation attempts to answer several questions by determining the pattern of change in regional ventilation as flow rate increased. These questions are: At what flow rate does the regional distribution change from its compliance determined value; by how much does it change when flow rates are very high; is the pattern of redistribution adequately explained by the mechanical time constants of lung regions; if so, is the regional ventilation at high flow rates determined by regional resistances?

2. Methods

a. Experimental Procedure. The vertical distribution of gas inspired over a wide range of flow rates was measured with a modification of the ^{133}Xe technique described by Dollfuss et al (36).

TABLE 16

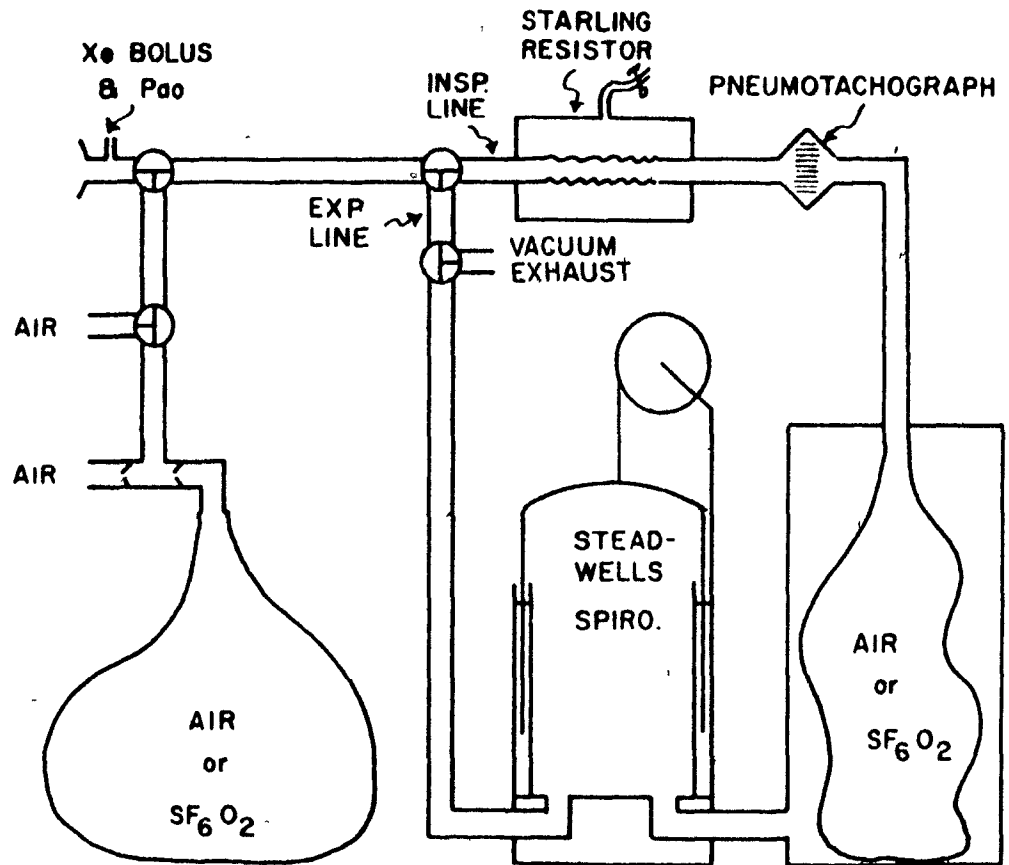
Physical Characteristics and Lung Volumes

Subject	Age (yrs)	Height (cm)	Weight (kg)	TLC (l.BTSP)	FRC/TLC %	RV/TLC %
PD	33	172	82	6.6	53	14
MG	25	178	83	6.5	55	23
JH	36	180	76	7.6	48	23
SI	24	172	60	6.4	48	17
AJ	33	190	83	8.5	49	27
LW	29	180	80	8.8	52	22
AZ	30	176	77	7.0	50	23

Seven healthy male laboratory personnel who were familiar with respiratory manoeuvres were studied (Table 16). Two were moderate cigarette smokers (PD and MG). Each subject sat in a chair with support for his head, arms and back, breathing room air through a mouthpiece. After inspiring to total lung capacity (TLC), he was switched into the breathing circuit (Fig. 13) and expired a measured volume to functional residual capacity (FRC). A 2 to 4 ml bolus of ^{133}Xe (2 mCi) was injected with a syringe into the mouthpiece during a short (3-5 sec) breath hold at FRC. The subject then inhaled forcibly to TLC at various constant inspiratory flow rates determined by a Starling resistor (see below). At TLC, regional count rates were recorded during a 20 sec breath hold. The subject's position with respect to the chest counters was carefully checked and adjusted throughout each study by means of marks on the anterior thorax and a fixed pin point light source. After six to ten different flow rates were studied with two or three boli each, the subject was switched to a separate closed spirometer circuit containing ^{133}Xe in air (7). Once ^{133}Xe concentration was equilibrated between the spirometer and the lungs, regional count rates at TLC were recorded during several 20 second breath hold periods.

Regional count rates were measured by six scintillation counters facing each lung and positioned in slit collimators mounted horizontally behind the subject's chest. The most apical pair of counters were positioned about 5 cm below the lung apices, and the others at 5 cm intervals down the lung. Inspiratory flow was measured by a Fleisch No. 4 pneumotachygraph coupled to a 270 Sanborn differential pressure transducer.

FIGURE 13



Schematic diagram of breathing apparatus. See text.

The flow recording system was linear for air to 8.0 lps. The flow signal was electrically integrated to give an accurate measurement of the initial 300 ml inspired volume. Pressure at the mouth (P_{ao}) was estimated by a Sanborn 267B differential pressure transducer. Flow, integrated flow and P_{ao} were simultaneously recorded on a four channel Sanborn Poly Viso. Inspired and expired volumes were obtained from the spirometer kymograph. A signal from a potentiometer attached to the spirometer and the outputs from the scintillation counters were stored on tape.

The regional count rates were replayed from the tape together with the volume signal from the potentiometer. The following equation was used to calculate regional ventilation per alveolus ($\dot{V}_r(\text{alv})$) for 12 lung regions:

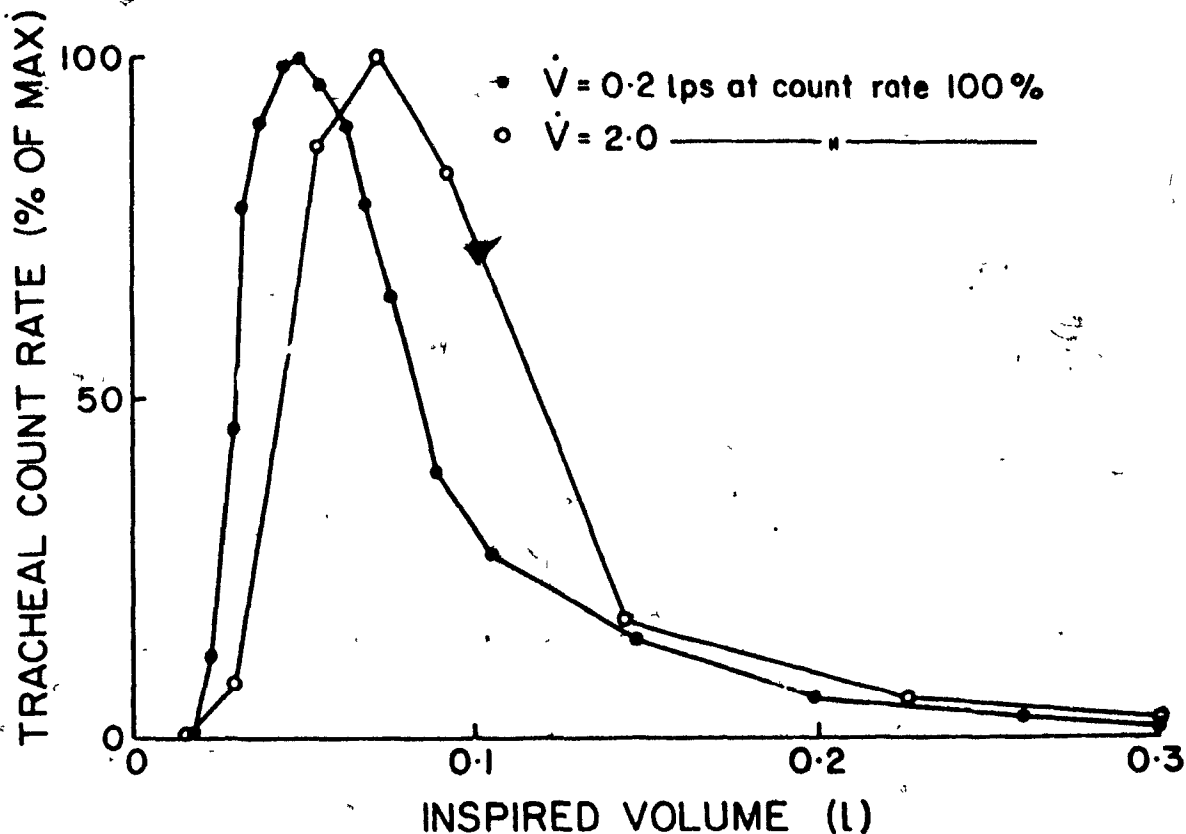
$$\dot{V}_r(\text{alv}) = \frac{CR_r(\text{bolus}) \times \sum CR_r(\text{eq})}{CR_r(\text{eq}) \times \sum CR_r(\text{bolus})} \times 100$$

where $CR_r(\text{bolus})$ is the regional count rate at TLC after inhalation of the bolus and $CR_r(\text{eq})$ is the corresponding regional count rate after equilibration (background counts are subtracted). Thus, $\dot{V}_r(\text{alv})$ is expressed as a percentage of the mean ventilation of all 12 regions.

In four subjects, several boli were administered when the subject and breathing circuit were equilibrated with a mixture of 20% oxygen in sulfur hexafluoride (SF_6). This gas mixture is about four times as dense and .85 times as viscous as air, and approximately doubled the lower pulmonary resistance measured in two of the subjects (PD and LW, Table 14). During SF_6 measurements a calibration curve was used to correct flow recordings for gas viscosity and non-linearity.

b. Preliminary experiments In order to interpret the results, it was necessary to know over which part of the tidal volume the bolus was distributed to the various lung regions. For a given flow rate, the time taken for a ^{133}Xe bolus to be vertically distributed will depend on the airway volume between the injection site and the lobar bronchi as well as the volume of inspire that is labelled by the bolus. In a preliminary series of experiments, these parameters were estimated in two subjects under the same experimental conditions as described above. A scintillation counter with horizontal slit collimation was positioned in front of the extra thoracic trachea, below the cricoid cartilage. During inspiration, count rate and flow (pneumotachygraph) were simultaneously recorded on a four-channel Sanborn Poly Viso. The analogue rate meter had a time constant of 3 msec and the recorder a 90% response time of 8 msec. Tracheal count rate was replotted against integrated flow, so that the area under each curve represented the amount of injected tracer (Fig. 14). In both subjects, at all flow rates (.2 to 4 lps), 40 ml (S.D. = 8 ml, n = 12) was inspired before 5% of the ^{133}Xe bolus was counted and 135 ml (S.D. = 40 ml, n = 12) was inspired when 75% of the tracer had passed the counter. Adding 46 ml for the airway volume between tracheal counter and the lobar bronchi (159), approximately 100 ml is inspired before the leading edge of the bolus reaches the first point of vertical distribution, and the distribution of the next 100 ml is measured by the bolus technique. Although the trailing count rates usually spread over a larger volume as flow rate increased, this flow dependent component constituted less than 25% of the inspired tracer.

FIGURE 14



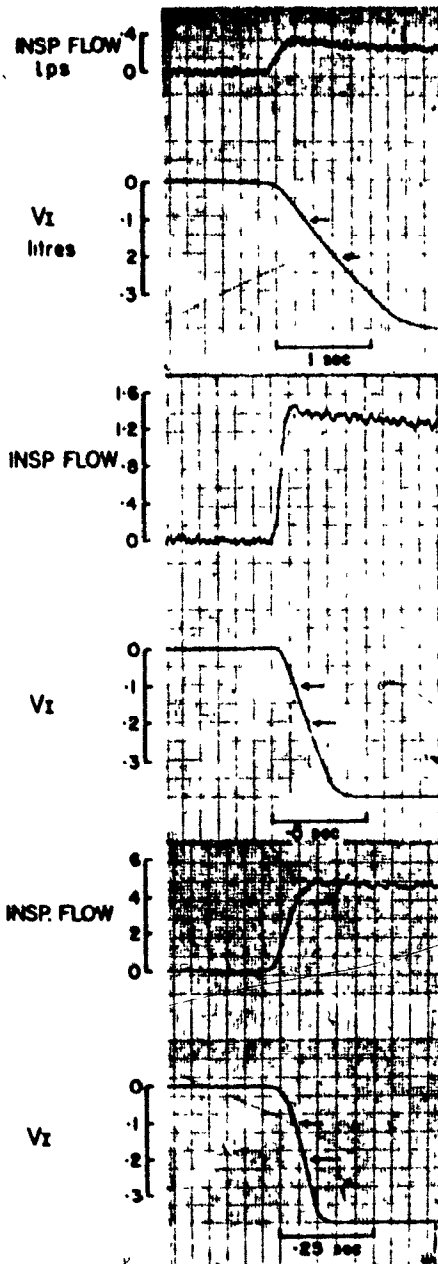
Volume distribution of 2 ml ^{133}Xe bolus injected at mouthpiece and measured in extra-thoracic trachea during inspirations at 0.2 and 2.0 lps. Ordinate: tracheal count rate, expressed as % of peak count rate during that breath. Abscissa: inspired volume in litres. Area under curves indicate that most tracer is distributed in volume inspired between 40 and 130 ml from start of breath.

To enable subjects to reach high flow rates before 100 ml was inspired, and yet to maintain constant flow during distribution of the bolus, a modified Starling resistor was constructed. A tube of thin latex rubber (length 4.0 cm, diameter 2.5 cm) was enclosed in an airtight lucite box (22 x 12 x 12 cm). When the box pressure was atmospheric, progressive lowering of pressure at the outlet of the box caused proportional increases in flow rate until, at about 4 lps, the latex tube became visibly compressed and further reductions in outlet pressure caused no further increase in flow. The maximal flow rate could be changed in a reproducible manner by adding (or removing) measured volumes of air to the box. When this device was inserted in the inspired line of a low resistance bag-in-box breathing circuit (Fig. 13) the subjects could usually increase inspiratory flow to 4 lps in less than 50 msec ($\ddot{V} = 80 \text{ lps}^2$) and hence reach a constant flow before the bolus was distributed at this and all lower flow rates (Fig. 15). To reach higher flow plateaux prior to bolus distribution, some subjects inspired against a closed stopcock, which was suddenly opened.

3. Results

In each study, the range of \dot{V}_I about the mean value for multiple determinations was less than 15%. The pre-inspiratory lung volume varied less than 100 ml from FRC for 95% of all boli inhaled. Variation of alveolar gas decompression due to P_{ao} differences between boli was less than 50 ml and P_{ao} was virtually constant during the distribution of each bolus.

FIGURE 15



Representative records of inspiratory flow rate (lps) and inspired volume (l) from three bolus inhalations in subject J.H. Arrows indicate the second 100 ml inspired at .3, 1.4 and 4.2 lps.

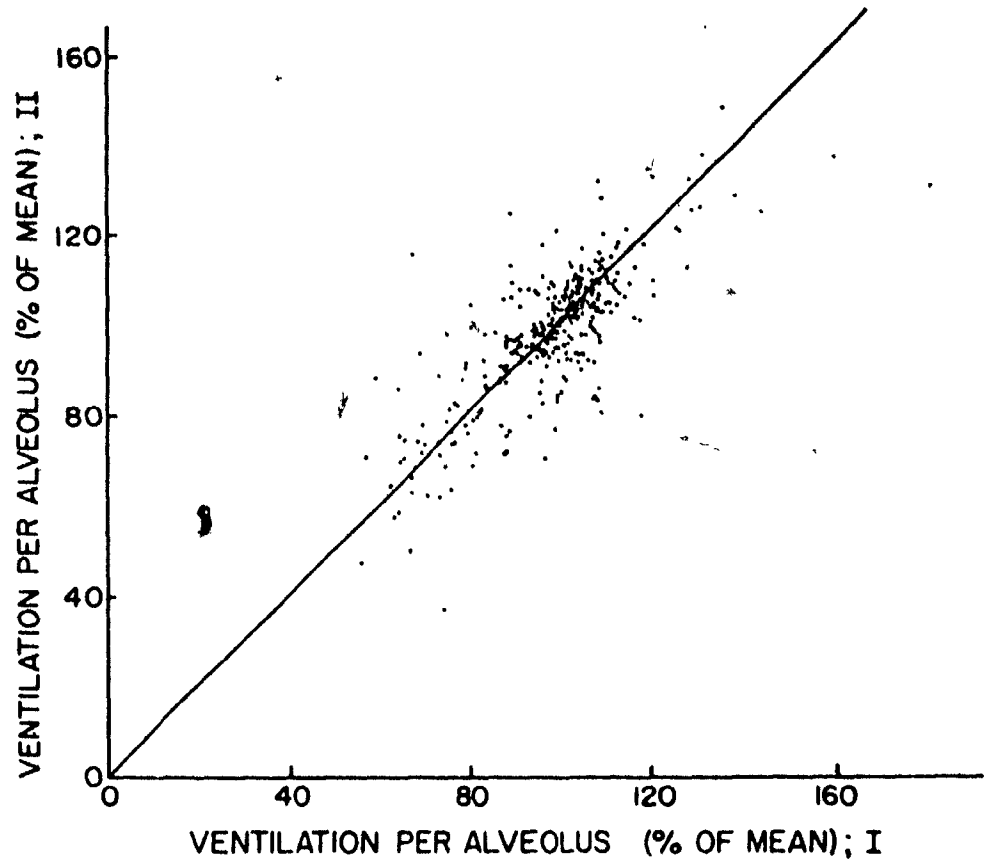
No systematic differences between $\dot{V}_r(\text{alv})$ of right and left lungs were observed, and only mean values for each vertical lung region are presented. The sum of count rates during equilibration is considered to represent total lung volume, so the proportion of count rates in each vertical region indicates the proportion of lung examined (Table 7). To illustrate the methodologic variation, Fig. 16 plots the results of duplicate determinations of $\dot{V}_r(\text{alv})$ for seven subjects and six regions. Similar variation was observed when each region was considered separately.

The effect of inspiratory flow rate on the $\dot{V}_r(\text{alv})$ of the uppermost and lowermost regions in one subject (AZ) are shown in Fig. 17. Each dot represents one measurement and the average values for similar flow rates are connected as illustrated. From such curves, values of $\dot{V}_r(\text{alv})$ were read at the same six flow rates for all subjects and lung regions. Flow rates were chosen which were close to those obtained in all subjects. The mean (\pm SE) values of $\dot{V}_r(\text{alv})$ for all subjects are plotted against flow rate in Fig. 18. As flow rate increased, $\dot{V}_r(\text{alv})$ increased to apical regions (5 and 10 cm from lung top) and decreased to basal regions (25 and 30 cm), whereas middle lung regions (15 and 20 cm) were less affected. Most of the redistribution of ventilation occurred between 0.1 and 1.5 lps, and Fig. 19 shows the ventilation distribution down the lung for these two flow rates. The vertical gradient of $\dot{V}_r(\text{alv})$ was reduced at 1.5 lps. Significant differences ($P < .01$) were observed in the two apical and two basal lung regions.

The vertical inequality of ventilation may be expressed by the upper to lower ventilation ratio (V_U/V_L) defined as the ratio between $\dot{V}_r(\text{alv})$ of the two uppermost regions (5 and 10 cm) to the two lowermost regions (25 and 30 cm). Figure 20 illustrates V_U/V_L against inspiratory flow rate for each subject. At low flow rates, apical

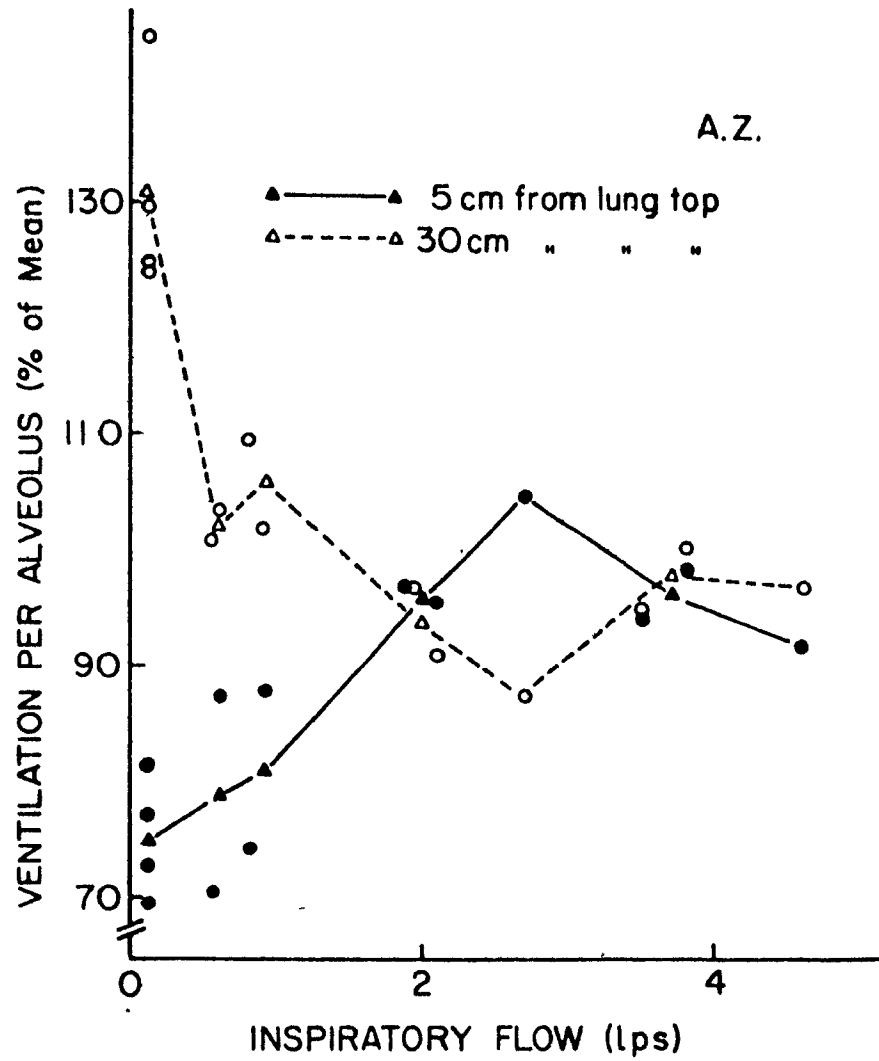
TABLE 17Regional Counts at Equilibration (% of Total)

D(cm)	5	10	15	20	25	30
Mean	9.1	14.8	18.0	20.1	19.8	18.2
\pm S.D.	1.8	1.9	.85	1.2	1.4	2.9

FIGURE 16

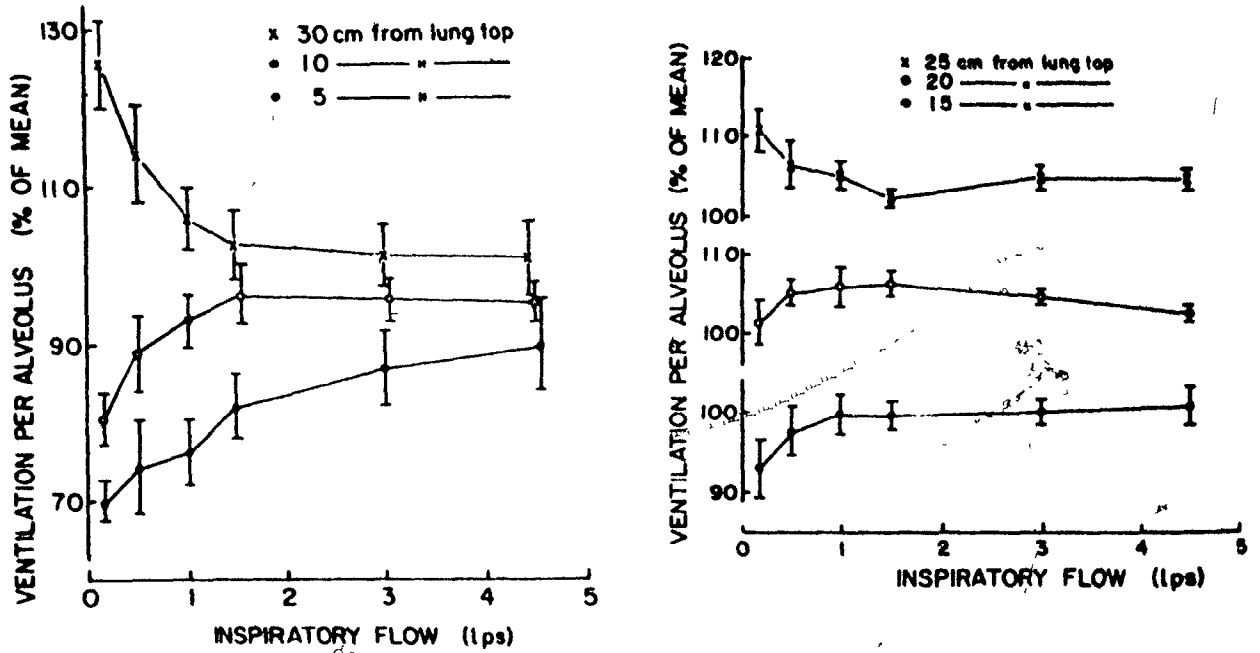
Plot of duplicate measurements of \dot{V}_T (alv) for all subjects and counter positions. I and II denote temporal sequence. The line of identity is shown.

FIGURE 17



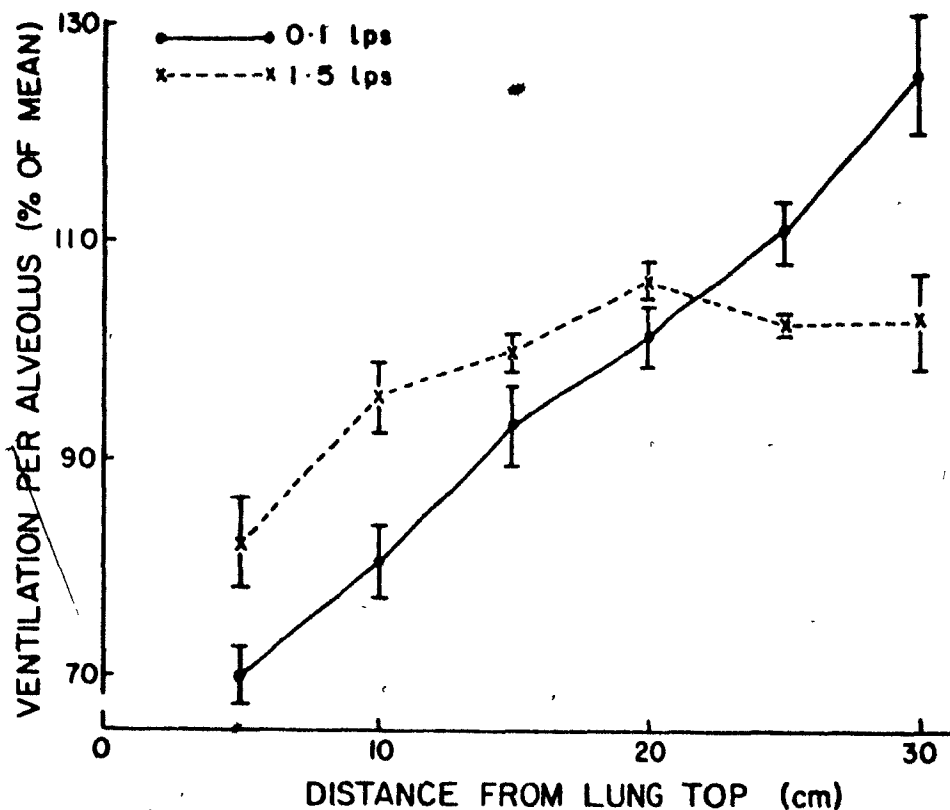
\dot{V}_R (alv) in the upper and lower lung regions plotted against \dot{V}_I (lps) for fourteen ^{133}Xe boli in one subject. Triangles denote mean \dot{V}_R (alv) of several boli inspired at similar \dot{V}_I .

FIGURE 18



Mean \pm SE \dot{V}_R (alv) for 7 subjects, at 6 vertical lung regions, against \dot{V}_I (lps)
(see text).

FIGURE 19



Mean \pm SE \dot{V}_R (alv) for seven subjects plotted against the counter distance from the lung top during quasi-static inspiration and at 1.5 lps. Differences of mean \dot{V}_R (alv) between these flow rates are significant ($p < .01$) for counter positions 5, 10, 25 and 30 cm from the top of the lung. Higher \dot{V}_I did not significantly change \dot{V}_R (alv) in any lung region from its 1.5 lps value.

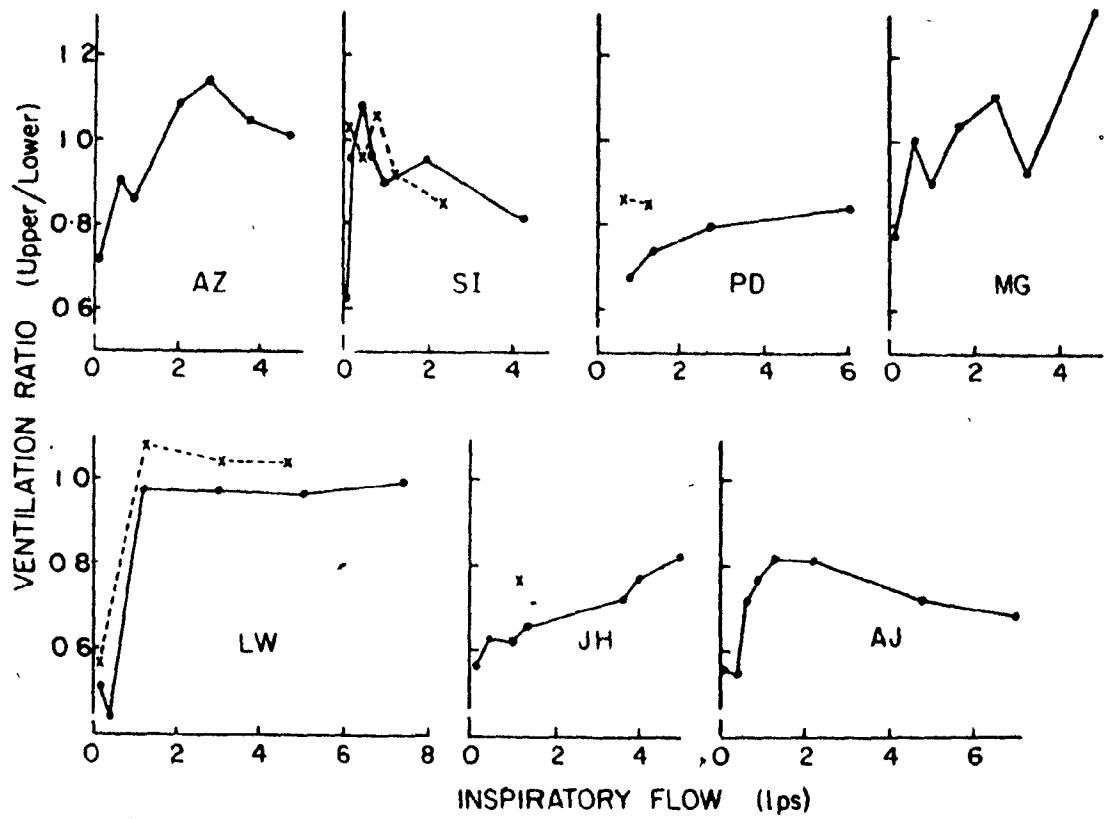
regions were less ventilated than basal regions, and as flow rate increased, ventilation distribution became more uniform, although there was considerable variability among the individual patterns of redistribution. Three subjects appeared to change continually with flow rates, whereas three others showed maximal values at low flow rates. Ventilation ratios during SF_6 breathing were either higher or not different from air values at comparable flow rates.

Figure 21 summarizes the results, and plots average (\pm SE) upper to lower ventilation ratios against inspiratory flow rate. During quasi-static inspirations ($\dot{V}_I < 0.2$ lps) the average apical respiratory unit received about .65 of the ventilation to the average basal unit. This ratio increased with flow rates in a curvilinear manner, rapidly at first to .76 at 0.5 lps, .81 at 1.0 lps and .88 at 1.5 lps, and then more slowly to .90 and .93 at 3.0 and 4.5 lps, respectively. When V_U/V_L was calculated in the same way, using only the uppermost (5 cm) and lowermost (30 cm) regions, a similar pattern was observed. Mean V_U/V_L for the same six \dot{V}_I values were .56, .65, .72, .80, .86 and .89. For 10 cm and 25 cm regions, mean V_U/V_L were .73, .85, .89, .94, .92 and .92.

4. Discussion

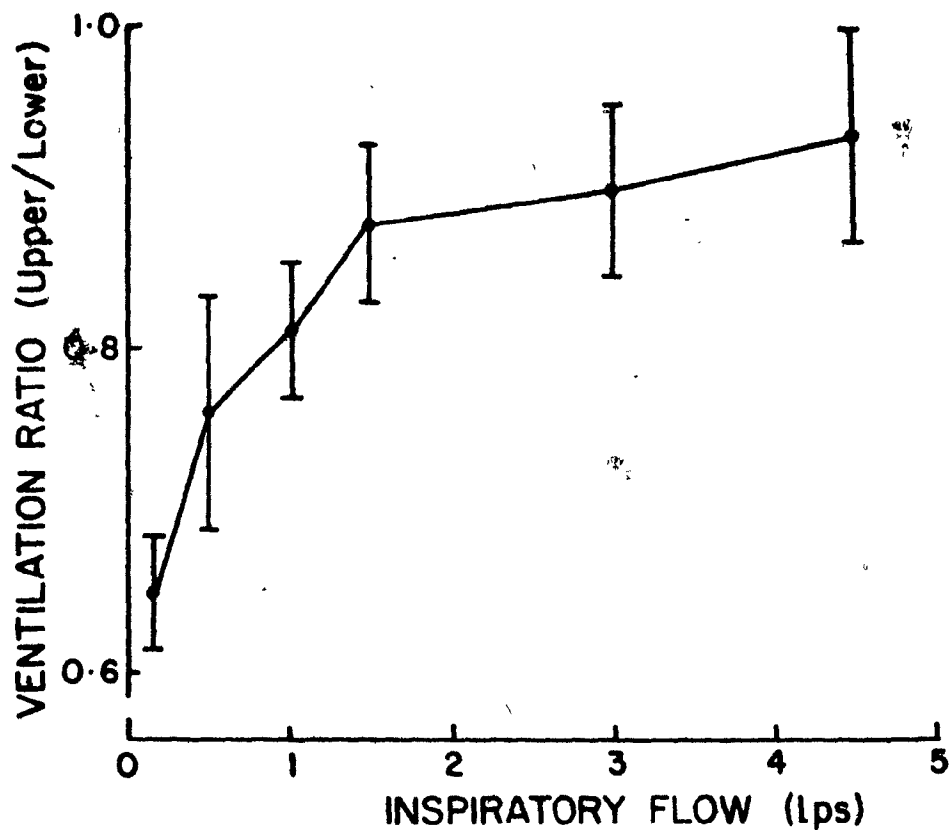
Throughout these experiments, considerable care was taken to maintain the position of subjects constant relative to the scintillation counters, and the effects of random count variations were minimized by using boli not less than 2 mCi. Despite these precautions, there was substantial variability of $\dot{V}_r(\text{alv})$ determinations (Fig. 16, 17). Because the methodologic variations are large, interpretations are confined largely to the mean results.

FIGURE 20



Ventilation ratio (V_U/V_L) of average \dot{V}_R (alv) for the upper two regions' ($D = 5$ and 10 cm) to the average \dot{V}_R (alv) of the lower two regions ($D = 25$ and 30 cm) plotted against \dot{V}_I . ●—● air; X----X SF6.

FIGURE 21



Mean \pm SE V_U/V_L for 7 subjects plotted against \dot{V}_I . See text.

It is established that regional alveolar filling is determined by regional compliance during quasi-static inspirations from FRC (36, 107). The compliance determined ventilation of lung regions may be calculated from measurements of regional volumes during static conditions (107).

$$V_U/V_L = (100 - FRC_U) / (100 - FRC_L) \quad (5)$$

where FRC_U and FRC_L are the regional volumes at FRC of upper and lower zones respectively, each expressed as a percent of its regional volume at TLC. The mean regional FRC values for regions 7.5 and 27.5 cm from the lung top previously reported (107, Table 3) give a V_U/V_L value of 0.64. In the present study the ventilation ratio for the same upper and lower zones was 0.65 as determined from the regional distribution of ^{133}Xe boli at $\dot{V}_I < .2$ lps (Fig. 19, 21). It is therefore concluded that at these flow rates, the bolus technique measures the compliance determined ventilation distribution, and accordingly the compliance ratio for these regions (C_U/C_L), is 0.65.

Robertson et al (134) observed that rapid inspiration altered the distribution of ^{133}Xe boli from the quasi-static values by reducing basal concentrations and increasing concentrations in apical regions. At 0.3 lps, V_U/V_L ranged from 0.50 to 0.77, but at about 4 lps the ratio increased to values between 0.71 and 1.21. The present study (Fig. 20, 21) confirms and extends these observations, and demonstrates an interesting pattern of redistribution. At 0.5 lps regional filling is no longer determined by regional compliance alone, and this alteration increases progressively to 1.5 lps. However, with further increase in flow the distribution remains relatively constant. This distribution pattern can be due to regional differences of time constants or applied pressure. The general pattern of redistribution in Fig. 21 closely resembles the theoretical response of a two compartment lung model having

different regional time constants (122).

a. Lung Model Studies. To pursue this similarity quantitatively, values for regional compliance and resistance were chosen, and equation 10 of Pedley et al (122) was modified to solve for the regional distribution appropriate to the present experimental conditions (see Appendix 3 Equation 13). It is assumed that the whole lung can be modelled as if it consisted of two parallel compartments, i.e. the upper two and lower two lung regions studied.

(1.) Choice of Values.

The preliminary experiments demonstrated that a bolus volume of approximately 100 ml reached the first regional branch after 100 ml were inspired. Since \dot{V}_I was rapidly attained and held constant during bolus distribution, equation 13 is solved for the time interval, t_1 to t_2 , where $t_1 = \frac{100 \text{ (ml)}}{\dot{V}_I \text{ (ml/sec)}}$ and $t_2 = 2 t_1$. Accordingly this solution gives the upper to lower distribution of the second 100 ml of the inspire for each \dot{V}_I .

At very low \dot{V}_I ($t_1 \rightarrow \infty$), V_U/V_L equals C_U/C_L . Compliance values of 0.098 (C_U) and 0.151 (C_L) were chosen, to approximate normal pulmonary compliance (.25 l/cm H₂O) as well as the experimental value of C_U/C_L (.65). At high \dot{V}_I ($t_2 \rightarrow 0$), V_U/V_L approaches R_L/R_U . Macklem (81) demonstrated that for a step change in pressure, regional resistances are not the only relevant resistance to flow in parallel units because the relative pressure applied to the parallel units at any time after t_0 is influenced by the common resistor (e.g., airway from mouth to lobar bronchi). However, when a square wave of flow is applied, the common resistor merely provides a constant pressure drop such that the

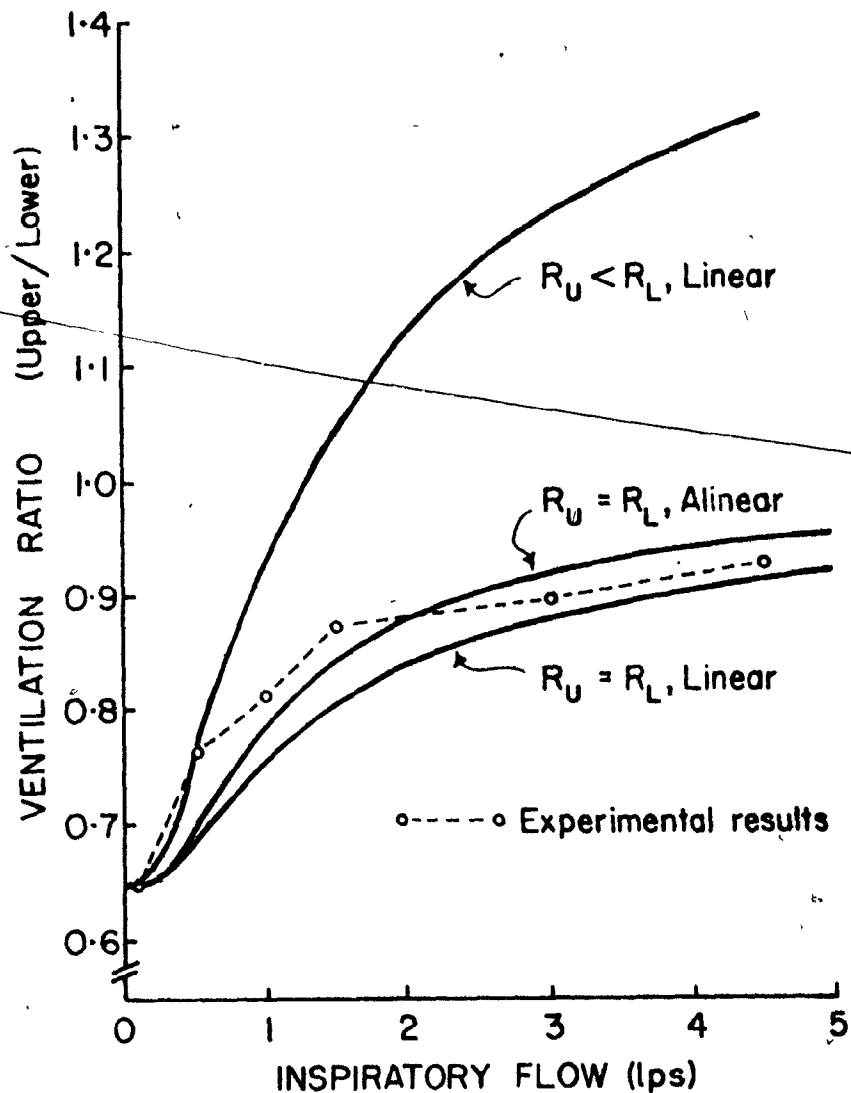
pressure difference between lobar bronchi and pleura is adequate to maintain constant flow. In this model, the common resistor does not influence parallel distribution, and R_L/R_U may be estimated from Fig. 21 which shows that with increasing \dot{V}_I , the mean V_U/V_L approaches a value between .9 and 1.0. Accordingly, the normal lower pulmonary resistance at FRC of .6 cm H₂O/lps (14, 44, 157) was divided equally between the two regions ($R_U = R_L = 1.2$ cm H₂O/lps). A prediction for non-linear bronchial P- \dot{V} relations was also calculated¹ by allowing regional resistances to vary as the square root of flow rate and gas density. Nonlinearity of P-V characteristics is not expected to influence the distribution over small volume changes (case 4, ref. 122).

(2.) Comparison with Results.

The solutions to equation 9 for these values are plotted in Fig. 22. When regional P- \dot{V} relations are linear ventilation distribution changes from the static value as flow rate increases in a curvilinear manner quite similar to the mean experimental results. When regional resistances increase with flow, the predicted curve moves up and to the left (as in case 2, ref. 122), which is even closer to the experimental results. A four-fold increase in gas density moves the predicted line further upward, so that SF₆ breathing should cause a large redistribution of the bolus at low flow rates (Fig. 23). This prediction is confirmed

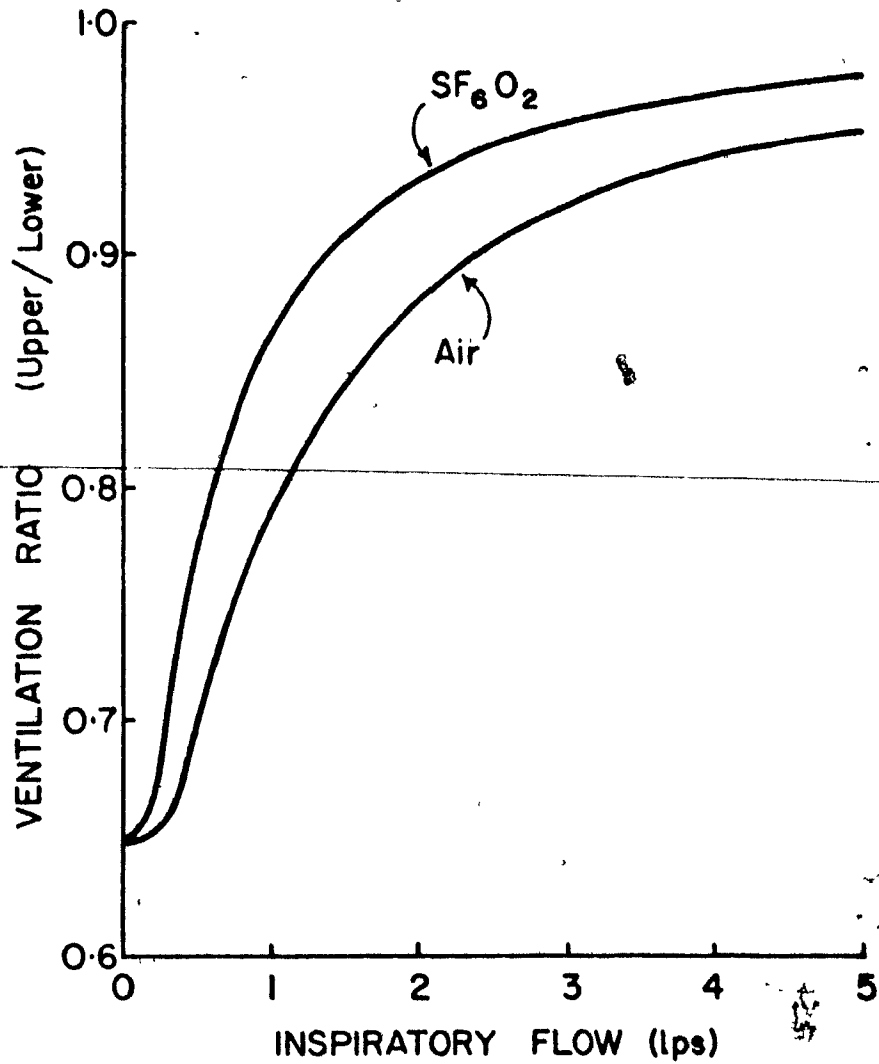
¹The ailinear results were obtained by substituting $R_{u,1} = K_{u,1}(\dot{V}_{u,1})^{.5}$ into equation 7 of Pedley et al. (122) and solving it by the Runge-Kutta method using the IBM system/360 Scientific Subroutine RKGS on the McGill University computer. The constants $K_{u,1}$ were equivalent to the linear resistance values for air at 1.0 lps, and were increased by a factor of two for SF₆. The subroutine RKGS calculated V_u and V_l at 99 points in the bolus interval and the output subroutine calculated the ratio of average regional flows to give the upper to lower ventilation ratio.

FIGURE 22



V_U/V_L plotted against step \dot{V}_I applied to lung models consisting of two parallel compartments having different compliance values ($C_U = .098$ l/cm H₂O, $C_L = .151$ l/cm H₂O) and the following resistance values: Lower curves - $R_U = R_L = 1.2$ cm H₂O/lps and independent of \dot{V}_I ; middle curve - as above, but resistances equal $1.2 \dot{V}_I^{.5}$; upper curve - $R_U = 1.1$ cm H₂O/lps, $R_L = 1.7$ cm H₂O/lps. Open circles and dashed line indicate the mean experimental results from Figure 18.

FIGURE 23



V_U/V_L of nonlinear lung model having equal resistances, plotted against step \dot{V}_I of air or SF₆. The difference between the curves is due to the increase in regional resistance values during SF₆ breathing, where $R_U = R_L = 2.4 \dot{V}_I^{-0.5}$.

in subjects PD and JH and is not contradicted in SI and LW (Fig. 20) whose V_U/V_L ratios change at such low flow rates that it is not clear whether the ratios increase at lower flow rates on SF_6 than on air.

(3.) Assumptions and Limitations.

(a.) Inertia is negligible. Lung gas accounts for most of the measured pulmonary inertance (.01 cm H₂O/lps²) during active ventilation, and about 70% of this value is attributed to gas in the extra thoracic airways (96). Since flow rates were constant during the distribution of the boli, inertance in the parallel pathways must contribute negligibly to regional impedance to flow.

(b.) Regional ΔP Values are equal. The observed redistribution of ventilation can be produced by asynchrony of regional pressure changes, in the sense that pressure applied to upper regions (ΔP_u) increases more rapidly than that applied to lower regions (ΔP_l). These regional pressures do not include frictional or inertial losses in the common pathway, and therefore contribute only a fraction of the change in transpulmonary pressure (ΔP_L) at higher flow rates. Accordingly, small differences in ΔP_L between upper and lower regions may reflect large differences between ΔP_u and ΔP_l . Using balloons placed at three levels in the intrathoracic esophagus, Schilder et al (143) measured ΔP_L during quiet breathing and maximal voluntary ventilation, and reported no systematic difference between levels. This and other studies (33, 67) do not provide sufficient evidence to exclude small differences between ΔP_L applied to upper and lower regions. Preliminary results of an attempt to investigate this question (see below) demonstrate that ΔP_l exceeds ΔP_u at 4 lps, suggesting a force opposing the observed redistribution of ventilation at increased flow rate.

(c.) Lobar P-V and P- \dot{V} Characteristics are Equal. The determination of $\dot{V}_R(\text{alv})$ in vertical lung regions necessarily examines both upper and lower lobes in all but the uppermost ($D = 5$ cm) and lowermost ($D = 30$ cm) counters (122). Differences in the pressure-volume characteristics of upper and lower lobes exist in the dog (43, 48) and are suggested by indirect experiments in man (6, 67). Differences may also exist between lobar resistances. Such differences may cause the upper and lower lobes in the same vertical slice to respond quite differently to changes of \dot{V}_I . This may be assessed by comparing the V_U/V_L ratios for vertical regions containing only upper ($D = 5$ cm) and lower ($D = 30$ cm) lobes with the corresponding V_U/V_L ratios from regions thought to include both lobes ($D = 10$ and 25 cm). At flow rates $< .2$ lps, the ratios (see results) differ according to the difference in vertical distance, and are close to the values predicted from equation 5. The patterns of redistribution with increasing \dot{V}_I are quite similar and both appear to approach a high flow asymptote of about 1.0. Thus, possible differences in the lobar mechanical properties are not apparent in this study, indicating that each compartment of the model may reasonably be described by a single R and C value.

(d.) Experimental Flow Patterns are Square Waves. The experimental flow patterns departed slightly from the step increase assumed in the model (Fig. 15). Mathematical analysis of the effect of this rise-time on ventilation distribution in the model proved difficult so an electrical analogue of the model was constructed (see Appendix 2). When a step current, analogous to a step \dot{V}_I was applied to the network, the parallel distribution followed the linear mathematical model closely.

When current was allowed initially to increase linearly with time, analogous to our volume acceleration of 80 lps^2 , followed by a constant current, the distribution was not detectably different from a true step response.

It is therefore concluded that the observed regional distribution of inspired gas may be explained by time constant differences among parallel pathways to different lung regions having equal non-linear regional resistances and unequal compliances. Two surprising conclusions arise directly from this interpretation of our data: 1) that regional resistances are equal, and 2) that regional ventilation is influenced by regional resistance at very low flow rates.

b. Equality of Regional Resistances. Lower pulmonary resistance has been shown to vary inversely with lung volume (14, 157). As upper lung regions are more expanded than dependent regions, it seems reasonable to expect R_U to be less than R_L (81, 122, 134). A quantitative prediction on this basis (Appendix 2) gave values for $R_U = 1.1 \text{ cm H}_2\text{O/lps}$ and $R_L = 1.7 \text{ cm H}_2\text{O/lps}$. The upper solid curve in Fig. 22 represents the solution of equation 13 for these values. The predicted change in distribution considerably exceeds the experimental values above 0.5 lps. If regional resistances are dependent on regional expansion, what factors may act to maintain the distribution ratio closer to the quasi-static value than predicted?

Intrinsic differences of geometry (e.g. length, diameter, bronchomotor tone) may cause resistance in upper regions to exceed dependent airways resistance at equal regional expansion. This possibility might be explored by repeating the study in supine subjects. Even if regional geometry is similar, resistance to upper regions may be increased due to the change in flow direction. The pressure loss due to a bend (P_b)

may be estimated from the equation of Weisbach, quoted by Rohrer (135):

$$P_b = E \frac{\rho \dot{V}_I^2}{2 g A^2}$$

where ρ is gas density in grams/cm³, \dot{V}_I in cm³/sec, A is the total cross section of airways where redirection occurs in cm², g is 980 cm/sec², and E is an empirical factor equal to 0.2 for 90° bends when the daughter radius is one to two parent radii. From Weibel (159), pathways to upper regions bend about 90° relative to lower pathways at generations 2 to 5 ($A = 2.0$ cm²). Accordingly, P_b values are .03, .27, and .6 cm H₂O at 1.0, 3.0 and 4.5 lps, respectively. In effect these values diminish the pressure driving flow to upper regions, and may account for reductions of .15% and 20% from the predicted V_U/V_L at 3.0 and 4.5 lps. A third possibility is that intrapulmonary airways are sufficiently distended at high inspiratory flow rates to minimize the effect of the pleural pressure gradients on relative regional resistances (134). However, even at 4.5 lps, the dynamic transmural pressure of these airways cannot exceed the static value by more than 3 cm H₂O when R_{1p} is 0.6 cm H₂O/lps. This is unlikely to alter the relative distensions of regional airways significantly.

As discussed above, differences in the dynamic pressures applied to upper (ΔP_u) and lower (ΔP_l) lung regions have not been ruled out. Assuming $R_U < R_L$ as in Fig. 22, the difference in regional ΔP that would give the experimental values in Fig. 21 may be calculated for high flow rates when regional ventilation is determined by regional resistance, e.g. $\dot{V}_u = P_u/R_u$. When \dot{V}_I was 4.5 lps, V_U/V_L was .93, so P_u is 2.4 cm H₂O (2.2 lps x 1.1 cm H₂O/lps) and P_l is 3.9 cm H₂O (2.3 lps x 1.7 cm H₂O/lps). Thus, a 1.5 cm H₂O difference in the regional ΔP may account for more than a 40% reduction in the ventilation ratio. At 1.5 and 3.0 lps, ΔP differences of .6 and 1.1 cm H₂O would give the observed values of V_U/V_L

when regional resistances are dependent on regional expansion. This possibility was tested in one subject. Two esophageal balloons matched for frequency response characteristics were positioned 28 and 39 cm from the nose, and their differential pressure was estimated by a Sanborn 267B transducer. At FRC, pressure in the upper balloon was 2 cm H₂O more negative than in the lower balloon. During several rapid inspirations from FRC, the lower balloon consistently recorded a greater ΔP (mean 2.3 cm H₂O) than the upper balloon when \dot{V}_I was 4 to 5 lps. No pressure difference was observed during comparable inspiratory efforts against a closed airway.

Occlusion of a lobar bronchus is associated with a local increase in the effective ΔP applied to that lobe during ventilation (67, 171). Zidulka et al (171) suggested that with obstruction there is local interaction between the chest wall and lung, resulting in forces tending to expand the obstructed lobe. It may be argued that in the present experiment the lower lung regions are relatively obstructed at high \dot{V}_I , in the sense that their rate of inflation relative to upper regions is slower than during compliance determined ventilation ($\dot{V}_I < .2$ lps). Inasmuch as the chest wall overlying upper and lower regions resists elastic deformation, a greater ΔP will tend to develop over dependent zones as V_U/V_L increases with \dot{V}_I , driving more flow to lower regions than predicted for equal ΔP . Such a mechanism promotes compliance determined filling of widely separated lung regions having different time constants when the major regional impedance is resistive. This is analogous to the mechanical interdependence of adjacent lung segments (102, 105).

Thus, several mechanisms may act to diminish the redistribution of ventilation as flow increases. Whatever the cause, the lung

does behave as if the regional resistances were equal and were the principal determinants of regional distribution of inspired gas at V_T 1.5 lps.

c. Effects of Regional Resistances on Regional Ventilation in Normal Subjects. In most normal subjects, multiple breath nitrogen washouts do not change with frequency (17, 32) and dynamic pulmonary compliance (C_{dyn}) falls by less than 20% of the static value (C_{st}) up to 70 breaths per min (81). Mead (101) concluded that the parallel distribution of ventilation is essentially determined by the elastic properties of lung units in healthy subjects at rest and during exercise. The data presented in this study indicates that regional resistances do influence the distribution of inspired gas at low flow rates. Are these findings and conclusions compatible?

Otis et al (115) considered a single pulmonary pathway to consist of a volume elastic element having compliance, C , connected in series with a conducting part having resistance, R . When a sinusoidal pressure of frequency, f , and amplitude, P_m , is applied across this model, the resulting volume change (V_T) is determined by the impedance (Z). As frequency approaches zero, pathway impedance approaches $1/C$, and, at the other extreme ($f \rightarrow \infty$), impedance is due only to resistance. When two or more units with equal time constants are connected in parallel, their impedances change proportionately as frequency increases. The behaviour of this system may be duplicated by a single equivalent resistance (R_e), and compliance (C_e). If the parallel time constants are unequal, pathway impedances do not change proportionately and a different value for R_e and C_e is required at each frequency. As frequency increases, C_e decreases associated with a reduction in the tidal volume of the long RC unit (s).

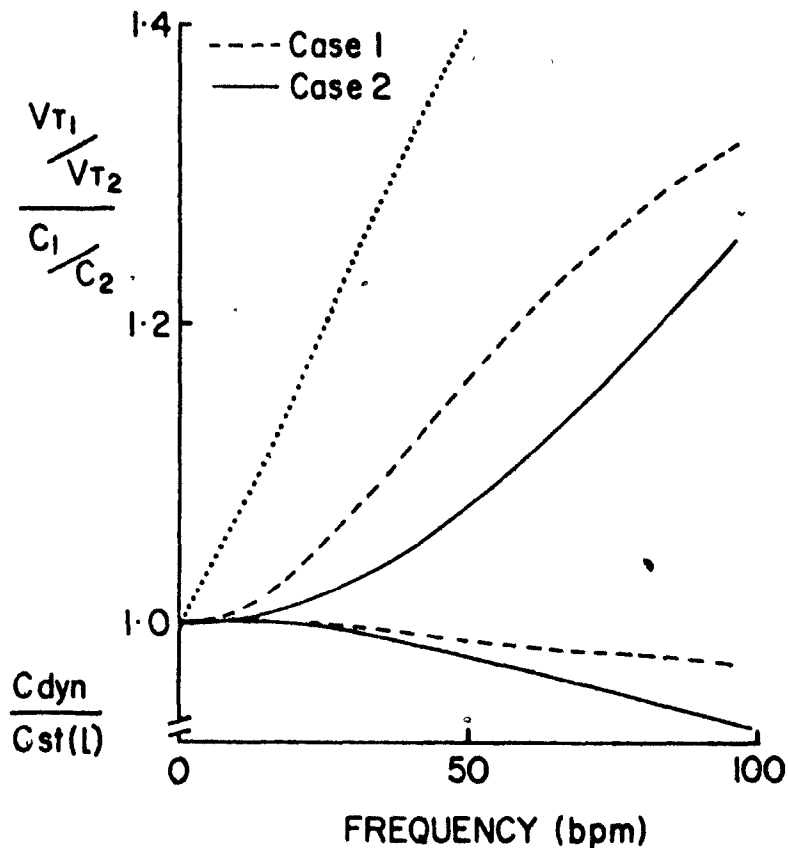
The tidal volume ratio of the compartments may be calculated from equations 6 and 7 of Otis et al (115).

$$V_{T1}/V_{T2} = |z_2|' / |z_1| = \sqrt{R_2^2 + \frac{1}{(\omega C_2)^2}} / \sqrt{R_2^2 + \frac{1}{(\omega C_1)^2}}$$

where $|z|$ is the vector impedance and ω is the angular velocity equivalent to $2\pi f$. The corresponding value for C_{dyn} may be obtained from their equation 13. The values of R and C from our linear model were chosen to examine the gravity dependent asynchrony between upper and lower lung regions during sinusoidal breathing. Figure 24 plots the results (case 1) as the fractional change from the static value ($f = 0$) as frequency increases. At 100 breaths per minute (bpm) C_{dyn} has fallen by 3%, whereas the change in ventilation ratio is ten times greater. When the total sinusoidal volume change was 500 ml, the relative distribution of the second 100 ml inspired from FRC (dotted line) represents the hypothetical regional distribution of a ^{133}Xe bolus administered at FRC.² Its distribution is much more frequency dependent than the whole tidal volume, and this effect may be magnified by an earlier bolus injection. This emphasizes the increased sensitivity to RC discrepancies of a test which labels a small part of the early inspirate. Furthermore the effects of frequency on intrapulmonary distribution of ventilation

² This curve was computed from the flow-time patterns calculated for each compartment in case 1 from manipulation of equations given in Otis et al (115). The time interval for the second 100 ml inspired was divided into ten equal periods, the instantaneous flow ratio (\dot{V}_1/\dot{V}_2) was calculated for each, and the average \dot{V}_1/\dot{V}_2 approximates the ventilation ratio.

FIGURE 24



The change in relative tidal volumes (V_{T1}/V_{T2}) of two compartments of simple lung models (left ordinate) compared with the corresponding change in compliance (C_{dyn}) of the model (right ordinate), plotted against sinusoidal breathing frequency (abscissa). Both ordinate values are expressed as fraction of static value ($f = 0$). The mechanical properties of the two models illustrated are as follows:

- Case 1 - $R_U = R_L = 1.2$ cm H₂O/lps; $C_U = .1$ and $C_L = .15$ l/cm H₂O
- Case 2 - $R_U = .2$ and $R_L = .8$ cm H₂O/lps; $C_U = C_L = .1$ l/cm H₂O

The dotted line represents the calculated distribution of the second 100 ml inspired from FRC during sinusoidal breathing in Case 1.

as assessed by multiple breath washout will be obscured by preferential distribution of the common dead space to the short time constant units and pendelluft (111, 141). Neglecting these factors, the differences in turnover rate between compartments must exceed 30% before nitrogen clearance techniques detect a difference (111). It follows that frequency independence of \dot{C}_{dyn} or nitrogen washout does not exclude changes in the regional distribution of inspired gas.

This is equally true for intraregional distribution among peripheral lung units having different time constants. Macklem and Mead (82) pointed out that in the normal lung, the resistance of peripheral pathways is low, so that elastic impedance predominates at high breathing frequencies even in the presence of four-fold time constant discrepancies. Woolcock et al (166) assumed that \dot{C}_{dyn} of normal lungs is independent of frequency, and estimated that a 20% fall from the static value is a detectable abnormality by the present technique of \dot{C}_{dyn} measurement. Case 2 of Fig. 24 illustrates for such peripheral units ($R_2C_2 = 4 R_1C_1$) that although \dot{C}_{dyn} decreases by only 7% at 100 bpm, the ventilation ratio changes by 30%. When R_2 was increased ($R_2C_2 = 10 R_1C_1$) so that a detectable fall in \dot{C}_{dyn} was observed (25% at 100 bpm), the ventilation ratio changed by 100%. It is therefore implicit in the analysis of Otis et al (115), though perhaps not generally recognized, that ventilation distribution may be quite frequency dependent when \dot{C}_{dyn} is not. As a result, the intrapulmonary distribution of inspired gas is influenced by regional resistances in normal subjects at rest and during exercise. If this is true, the test for frequency dependence of \dot{C}_{dyn} may be particularly useful in detecting abnormalities of peripheral resistance because it is insensitive to the effects of normal time constant variations. For example, the vertical difference in

regional time constants ($R_L C_L = 1.5 R_U C_U$) responsible for the change in ventilation distribution observed in this study causes only a 7% fall in C_{dyn} as theoretical breathing frequency approaches infinity.³ The results of similar calculations (Fig. 25) show that RC differences must exceed a factor of 2.5 to 3.0 before C_{dyn} falls abnormally. Therefore, the widely held concept that normal lungs behave synchronously so that ventilation distribution is uninfluenced by frequency is no longer tenable. As a corollary of this conclusion, the forces of interdependence among lung units must operate continuously in normal subjects.

As discussed, the proportion of sinusoidal ventilation distributed to parallel units having different time constants changes when pathway resistance contributes significantly to pathway impedance: A step change in flow causes impedance to shift from purely resistive at

³ According to Otis et al (115), the dynamic compliance of a two compartment lung model as frequency of sinusoidal oscillation approaches infinity is given by the equation:

$$\lim_{\omega \rightarrow \infty} C_{dyn} = \frac{(R_2 C_2 C_1 + R_1 C_1 C_2)^2}{(R_1 C_1)^2 C_2 + (R_2 C_2)^2 C_1}$$

If $R_1 C_1 / R_2 C_2 = x$, this equation can be solved for the following two conditions.

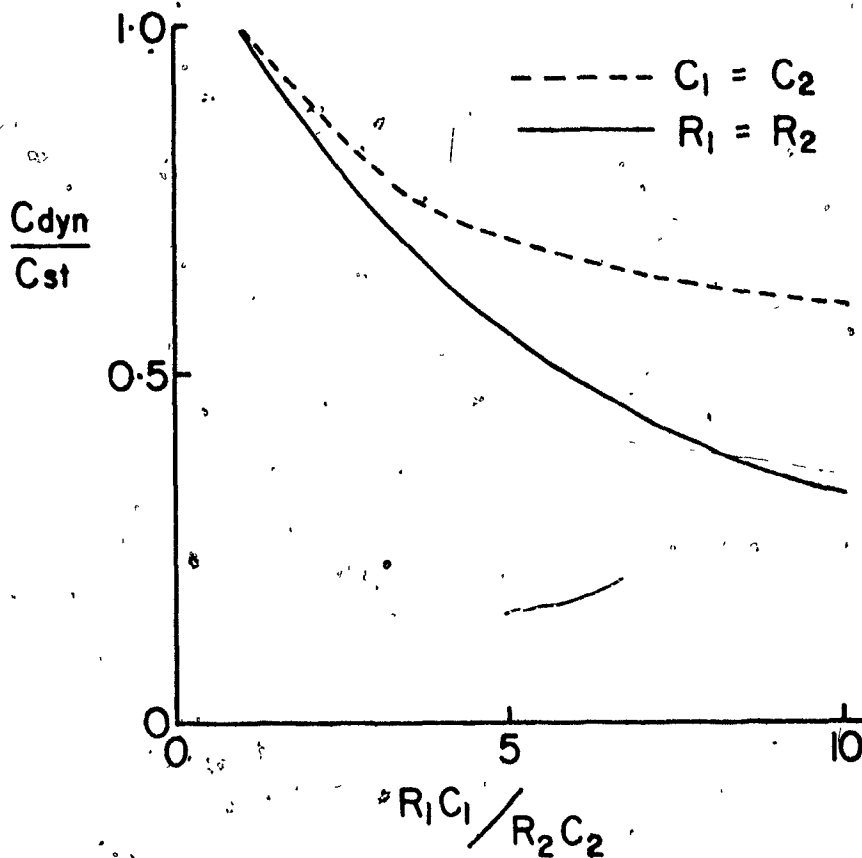
$$(1) \quad C_1 = C_2, \text{ so } R_1 = x R_2 \\ \text{then } C_{dyn} = C_1 (1 + x)^2 / (1 + x^2) \\ \text{and } C_{dyn}/C_{st} = (1 + x)^2 / 2(1 + x^2)$$

As the time constant ratio increases, C_{dyn} approaches 50% of the static value.

$$(2) \quad R_1 = R_2, \text{ so } C_2 = x C_1 \\ \text{then } C_{dyn} = (4 x C_1) / (1 + x) \\ \text{and } C_{dyn}/C_{st} = 4 x / (1 + x)^2$$

As the time constant ratio increase, C_{dyn} approaches zero.

FIGURE 25



Ordinate: Calculated dynamic compliance of a two compartment lung model at infinite cycling frequency, expressed as a fraction of static compliance (C_{dyn}/C_{st}). Abscissa: Ratio of time constants of the two compartments ($R_1 C_1/R_2 C_2$).

For a given RC difference, C_{dyn} is more frequency dependent when the difference is due to compliance (lower curve) than to resistance (upper curve). To cause a 20% reduction in C_{dyn} , $R_1 C_1/R_2 C_2$ must be 2.5 to 3.0 even at infinite frequency.

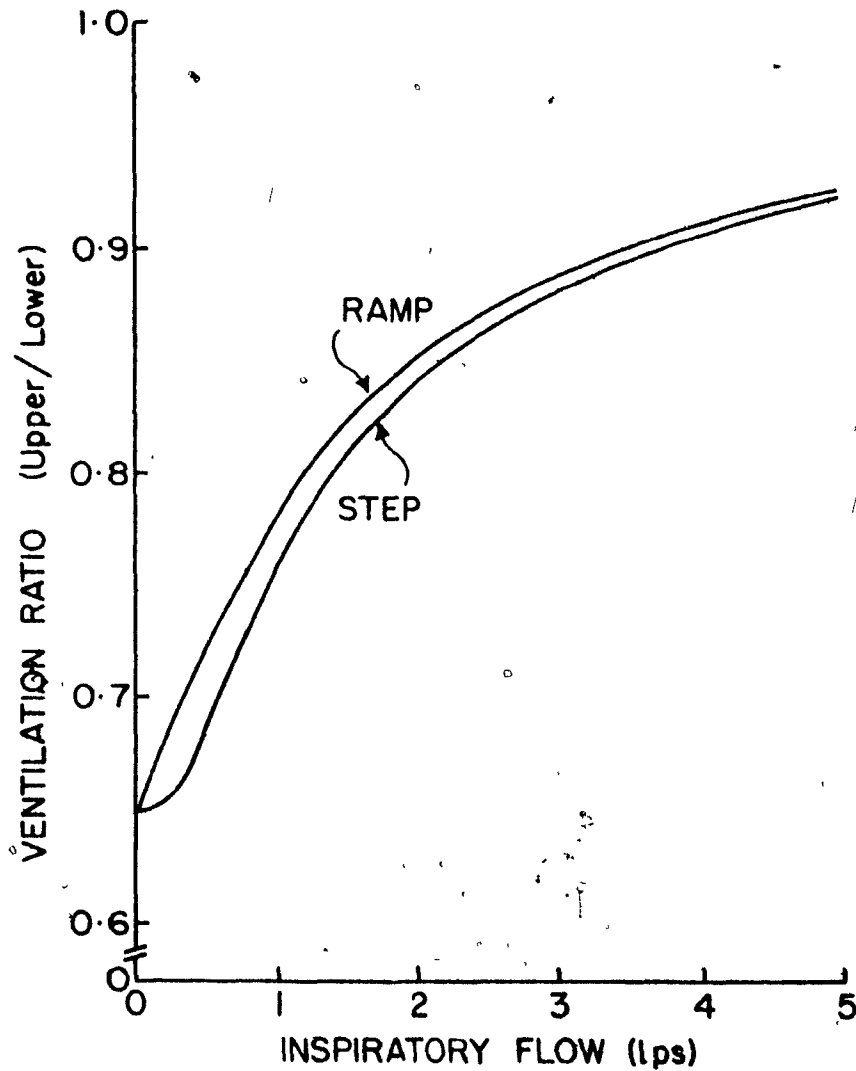
$t = 0$ to purely elastic a fraction of a second later. The distribution of a tracer delivered during the transient differs considerably from its distribution after the transient, and is therefore a very sensitive indicator of time constant discrepancies. Young et al (170) observed oscillations of nitrogen and CO_2 concentrations produced in the expirate by normal subjects who voluntarily varied expiratory flow rate following a tidal inspiration of oxygen. Because the imposed flow oscillations did not exceed 100 ml/sec, they reasoned that regional resistances could not be responsible for the variations in emptying sequence of lung units with flow rate. As an alternative to the time constant explanation of Otis et al (115), they proposed an explanation also based on a mechanical two-compartment model having different pressure volume characteristics and equal resistances. From the equation of motion of the lungs, they derived a differential equation expressing the relative volume changes of the two compartments as a function of overall flow rate. Graphical solution of this equation for small flow oscillations demonstrated transient variations in emptying sequence which simulated the observed oscillations of expired gas tension. It can be shown that this differential expression is identical to equation 7 of Pedley et al (122), and accordingly its solution is identical to equation 13 used in this study to explain our results by time constant discrepancies.

Thus, flow oscillations cause a transient departure from the elastic equilibrium of lung units having different mechanical time constants. The duration of the transient is determined by the mechanical properties of the units, so the amplitude of the imposed flow change only determines the amount of gas distributed during the transient. Even small changes in flow cause readily detectable alterations in ventilation distribution if an appropriate tracer is distributed during the transient.

One such example is the transient flow oscillations imposed on the lung by the beating heart (163). The resulting asynchronous emptying of peripheral lung units having different time constants (82) and gas concentrations (149) may produce the cardiogenic oscillations in gas concentrations observed in the expirate from lung lobes and segments (39, 40, 168). This distinction between continuous and discontinuous flow-time profiles may explain the increased unevenness of ventilation observed when normal subjects doubled their inspiratory flow rate while keeping tidal volume and frequency constant during multiple breath nitrogen washout (169), in contrast to other studies (17,32) which demonstrated no change in ventilation distribution when breathing frequency was increased.

The results in this study support this explanation for step increases in inspiratory flow. This flow pattern was chosen to minimize inertial effects and variations of flow rate during the bolus distribution, but it is not a physiologic breathing pattern in man except during exercise. During quiet breathing the time course of early inspiratory flow more closely resembles a ramp starting from an end expiratory pause. When a ramp current was applied to the electronic analogue, distribution departed even further from the compliance-determined value at low flow rates (.2 to 1.5 lps), than during application of a step current. The equation for a ramp increase in flow is derived in Appendix 2, and solution of equation 20 for V_U/V_L showed a similar shift of the bolus toward upper regions as during step flow (Fig. 26). For low flow rates, distribution is even more flow sensitive during ramp flow, indicating that the observations in Fig. 21 can reasonably be extended to most physiologic breathing patterns. This is supported

FIGURE 26



V_U/V_L of linear model, against \dot{V}_I applied as a step (lower curve) and as a ramp (upper curve), showing that the regional distribution of ventilation is even more sensitive to flow rate when the flow increases with time.

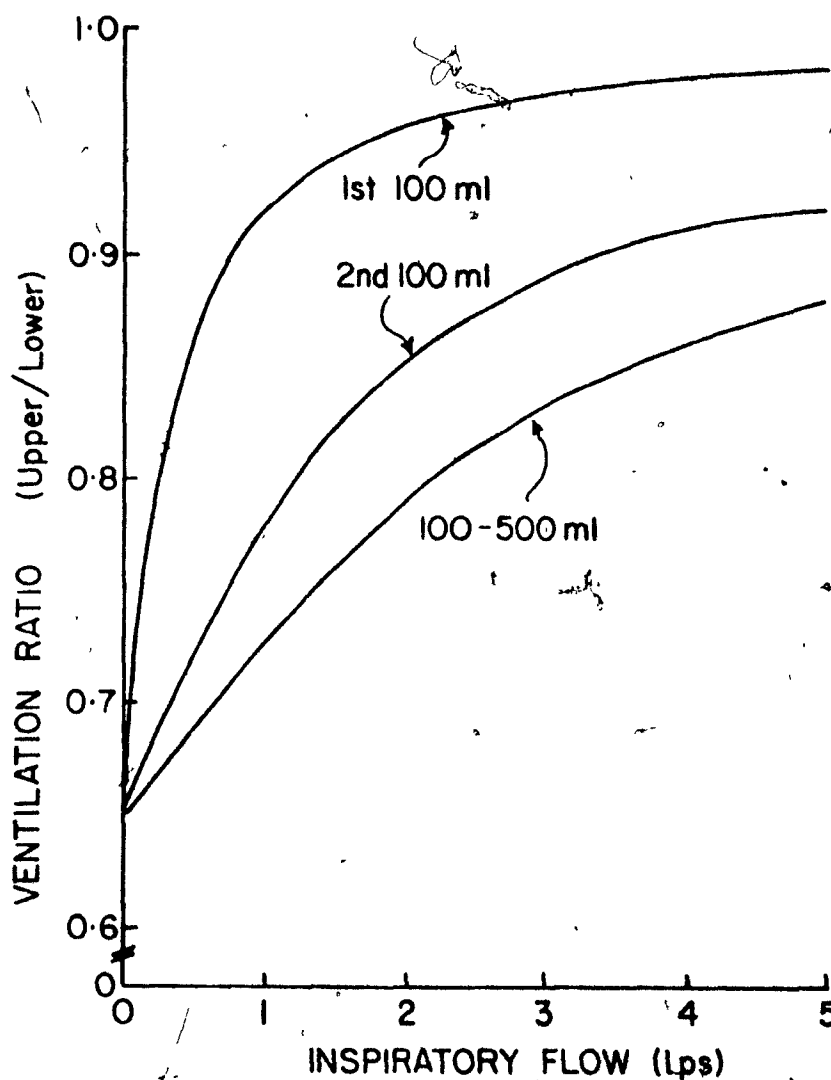
by the similarity of these results to those of Robertson et al (134), whose flow rates increased during bolus distribution.

Some predictions from this model exposed to ramp flow are presented in Fig. 27. The common dead space (1st 100 ml) appears to be almost equally distributed at flow rates as low as 0.5 lps. One consequence is that short RC units will inspire a greater proportion of the common dead space during resting ventilation than would be expected from their compliance. Larger inspired volumes are less influenced by flow rate and only approach an equal regional ventilation above 5.0 lps. This change in tidal ventilation distribution explains the observations of Bryan et al (21) that ventilation per unit volume became uniform in exercising subjects. Finally, dense gas breathing, as in hyperbaric environments, does not considerably alter the intrapulmonary distribution of ventilation (Fig. 23).

5. Summary and Conclusions

The regional distribution of the second 100 ml of gas inspired from FRC by sitting subjects was measured at flow rates (\dot{V}_I) of .1 to 4.5 lps. At $\dot{V}_I < .2$ lps, dependent lung regions were better ventilated than superior regions in accord with the vertical gradient of lung compliance. As \dot{V}_I increased, the labelled inspirate was progressively redirected toward upper lung regions until all regions were about equally ventilated at 1.5 lps. Further increases in \dot{V}_I caused little further change in relative regional ventilation. This pattern of change in regional ventilation closely resembled the distribution of flow in a

FIGURE 27



V_U/V_L against ramp \dot{V}_I for linear model. Upper curve represents dead space distribution. Middle curve is ^{133}Xe bolus distribution. Lower curve is tidal volume distribution (see text).

simple lung model consisting of two parallel compartments having different compliances and equal non-linear resistances.

It is therefore concluded that regional time constant differences are responsible for the observed change in distribution of inspired gas with flow rate. Accordingly, the lung behaves as if regional resistances were equal and so independent of regional expansion. If regional resistances are inversely related to regional volume, the absence of greater apical than basal ventilation at high \dot{V}_I may be due, among other explanations, to a greater dynamic ΔP applied to the long time constant (lower) region.

This greater pressure may be generated by the interdependence between lung and chest wall, such that a departure from the static elastic equilibrium of lung regions is opposed. In spite of forces promoting elastic equilibrium, these results indicate that regional resistances influence intrapulmonary distribution of inspired gas during quiet breathing in healthy subjects. This was not recognized previously because other tests of ventilation distribution e.g. frequency dependence of dynamic compliance and nitrogen washout, are less sensitive indicators of time constant discrepancies.

D. The Influence of Regional Concentration Differences on the Expired Concentration vs Volume Relationship.

1. Introduction

A considerable body of evidence suggests that airways in dependent lung regions close at low lung volume (2, 26, 36, 107, 152). When pre-expiratory concentrations of a tracer gas differ between superior and basal lung regions, the lung volume at which airways close may be detected by a change in the expired gas concentration (2, 26, 36, 47, 129). Despite a great deal of investigation into the mechanisms underlying "airways closure" and its detection by single breath techniques, little information is available regarding the influence of regional concentration differences upon the detection of "closing volume".

To investigate this question, a range of post-inspiratory regional concentrations were produced by varying the flow rate at which ^{133}Xe boli were inhaled, and the subsequent expired concentration-volume records were examined.

2. Methods

As described in the preceding section, labelled boli were inhaled from FRC at various constant flow rates, and ^{133}Xe concentration was measured in six vertical lung regions during a breath hold at total lung capacity. The subjects then expired to residual volume (RV) through an orifice ($d = 3 \text{ mm}$, $l = 18 \text{ mm}$) at virtually constant low flow rates ($< .25 \text{ lps}$) into a spirometer (Fig. 13). Expired ^{133}Xe count rate was continuously monitored by a shielded scintillation counter mounted over a plastic cuvette and connected to a digital rate meter. The cuvette

was 2.5 cm from the mouthpiece and had a washout volume of 250 ml. The output of the rate metre drove the ordinate of an x-y recorder and the signal from a potentiometer on the spirometer drove the abscissa. In this way, a plot of expired count rate against expired volume was obtained for each ^{133}Xe bolus inhaled by the seven subjects. A line of visual best fit was drawn through the 'alveolar plateau' of each curve, and the lung volume (% VC) at which the expired count rate dropped below the plateau (phase IV) was determined. In addition, the count rate at residual volume was expressed as a fraction of the counts at mid expiration, e.g. expired count rate (RV/.5VC).

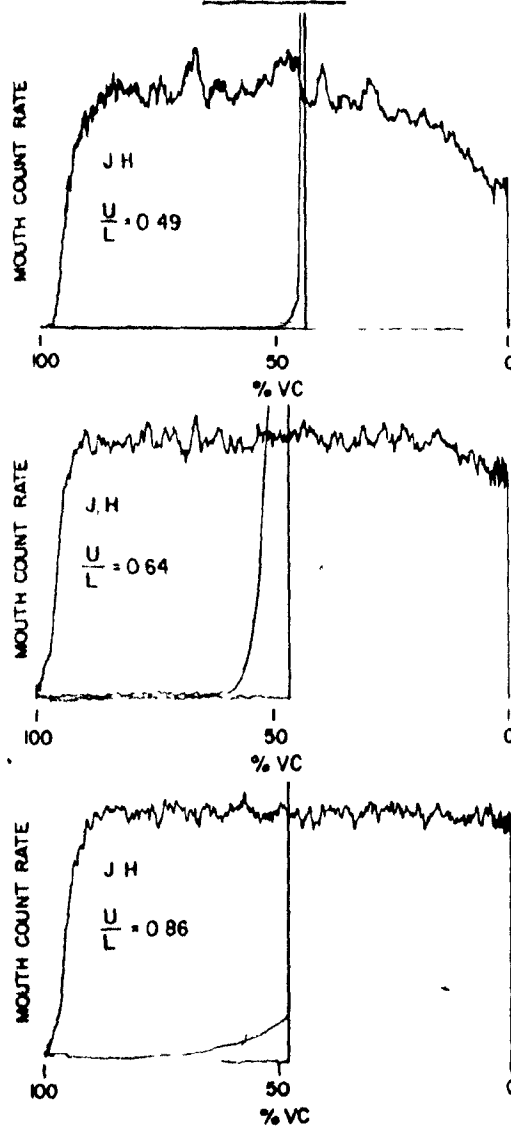
3. Results

The relationship between expired concentration and volume was recorded for 99 ^{133}Xe boli inhaled by seven subjects. The alveolar plateaux were essentially horizontal above 25% VC (Fig. 28). At lower lung volumes, there was a downward slope in forty-four of the records, and the corresponding upper to lower concentration ratio (U/L) was less than 0.8 in forty of these. The ratio, U/L, was less than .8 in only eleven of the remaining records, which showed no change in slope and consequently had no detectable Phase IV (Fig. 28 lower panel). When U/L was small, expired count rates at RV were much less than at 50% VC and Phase IV was detected at about 25% VC. At higher values of U/L, the expired count rate ratio (RV/.5VC) increased and Phase IV was detected at a lower lung volume. The former trend was significant in all subjects (Fig. 29), giving a linear regression for the entire group ($r = .71$, $p < .001$):

$$\text{Expired count rate ratio (RV/.5VC)} = .38 \text{ U/L} + .61.$$

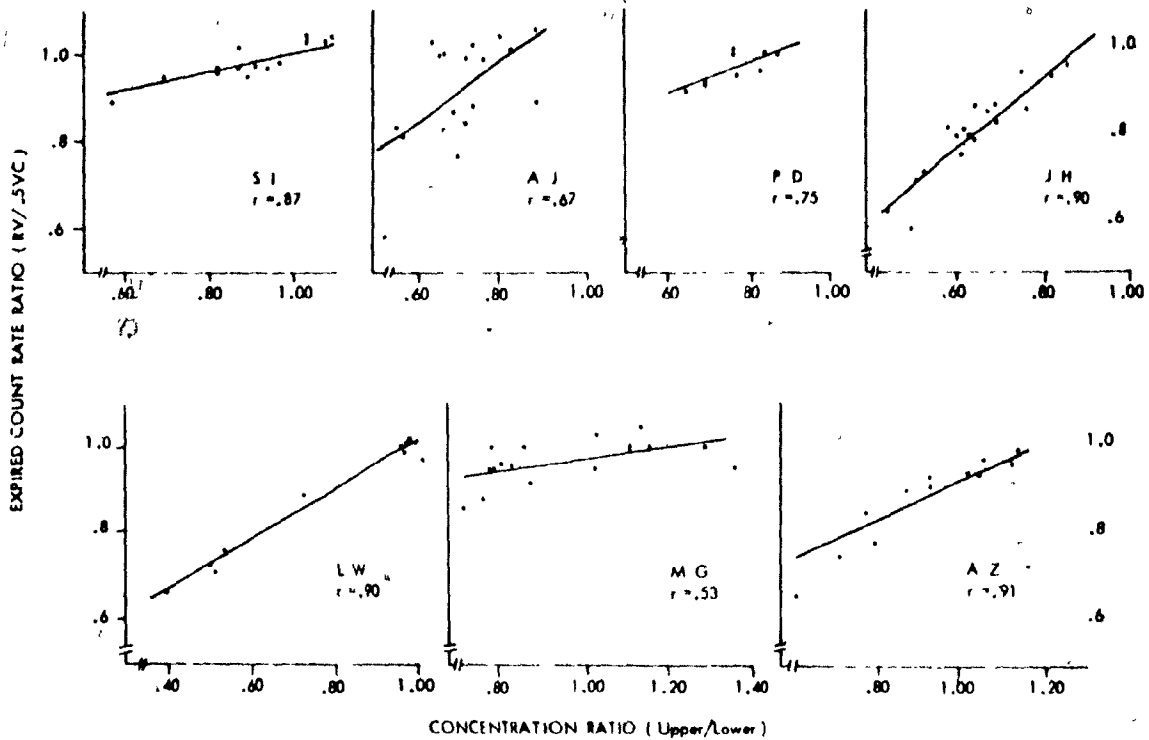
The relationship between Phase IV (% VC) and U/L was significant in five

FIGURE 28



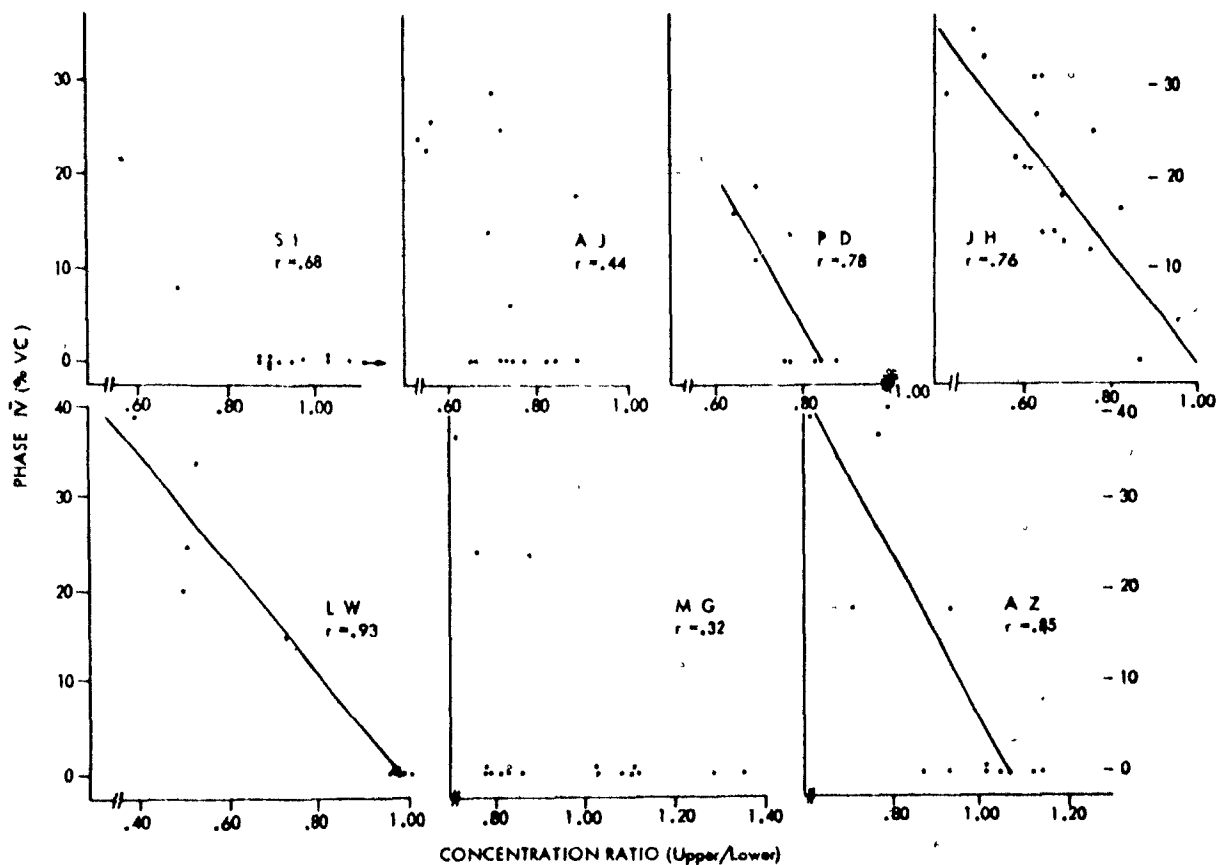
Mouth count rate vs lung volume, recorded during three vital capacity expirations in subject J.H. The insert, U/L , denotes pre-expiratory ratio of ^{133}Xe concentrations in two uppermost to two lowermost regions. (For discussion, see text).

FIGURE 29



Relationship between expired count rate ratio (RV/.5VC) and pre-expiratory upper to lower concentration ratio. Regression lines are significant ($p < .05$) for all subjects, indicating that end expired gas came from upper regions.

FIGURE 30



Relationship between Phase IV (%VC) and upper to lower concentration ratio (U/L). For $U/L > .8$, Phase IV was rarely detected, giving a preponderance of values at 0 %VC. Regression lines were significant ($P < .05$) for 5 subjects, though significance is questionable in subject SI due to skew distribution.

of the seven subjects (Fig. 30). According to the linear regression equation ($r = .60$, $p < .001$)

$$\text{Phase IV (\%VC)} = 46 - 44 \text{ U/L}$$

Phase IV was detected for all subjects at 24% VC when lower regional concentrations were twice those in upper regions ($\text{U/L} = .5$) and was virtually zero when U/L was one.

4. Discussion

Following a single breath of foreign gas, the expirate exhibits an abrupt change in concentration (Phase IV) as lung volume approaches RV (36, 47, 129). In upright subjects, radioactive gas techniques demonstrated preferential ventilation of apical regions by gas inspired from RV (36, 107, 152). During the subsequent expiration, the end expired gas resembled the post-inspiratory concentration in apical regions, whereas concentrations in mid expiration were similar to post inspiratory concentrations in middle lung regions (2, 134). Similar methods demonstrated for inverted and lateral body positions that upper lung regions were preferentially ventilated and contributed a substantial proportion of the terminal expirate in several different body positions (2). Accordingly, Phase IV may be explained by gravity dependent "airways closure" in basal lung regions in the presence of apex to base concentration differences.

In this study, post-inspiratory regional concentration changed as a function of inspiratory flow rate. During the subsequent expiration, the mechanisms causing dependent airways to close were presumably identical in a given subject. Thus the changes observed in Phase IV (%VC) must be due to the associated change in regional concentration unless the inspiratory flow rate altered some other factor contributing to the expired curves. Martin et al (89) reported evidence suggesting that intraregional

ventilation distribution differed between slow and rapid inspiration. To the extent that sequential emptying of intraregional units having different concentrations contribute to Phase IV, the results in Figure 30 may not be due to changes in regional concentration alone. This is unlikely in at least three subjects (JH, LW, AZ), where the steep slope relating expired count rate ratio (RV/.5VC) and post-inspiratory concentration ratio indicates that apical regions contribute a greater proportion of end expiratory gas following all inspiratory flow rates. Accordingly, regional concentration differences likely account for the terminal portion of the expired curves. It is concluded that although dependent airways close at the same lung volume, the "closing volume" as detected by Phase IV (%VC) varies systematically according to the apex to base concentration differences. Airways closure goes undetected by the ^{133}Xe technique when apical and basal concentrations differ by less than a factor of 1.25 ($U/L = .8$). At a factor of 2, Phase IV is detected at 24% for the entire group. Though not tested in this study, higher concentration differences are presumably associated with no further increase in Phase IV, since this value is the upper limit of normal for "closing volume" for this age group.

These findings may affect the determination of "closing volume" by each of the two common techniques and their variations. When a bolus of indicator gas is inspired slowly ($< .3$ lps) from RV, apical concentrations exceeded those at the lung base by a factor of five to ten (2, 36, 108, 134). Following maximal inspiratory flow rates, this difference becomes 2:1 or less, and Phase IV on the subsequent expired plateaux are apparent only at a lower lung volume if at all (2). In one subject who was studied at several flow rates (2), essentially all

of the concentration change had occurred by 1.7 lps, and no flow rates were studied between .3 and 1.7 lps. Accordingly, apex to base ratios less than 2:1 may occur in subjects where inspiratory flow rate exceeds .3 lps. Similar reductions in vertical concentration differences occur readily with this technique when the pre-inspiratory lung volume is much greater than RV (36). To the extent that small regional concentration differences exist, "closing volume" may be underestimated.

The second, or "resident gas", technique measures expired nitrogen concentration following a vital capacity inspiration of oxygen. The regional nitrogen fraction may be estimated from the regional RV (RV_r) expressed as a fraction of the regional TLC (TLC_r). According to Milic-Emili et al (107),

$$RV_r/TLC_r = .38 - .89 D$$

where D is the distance (cm) from lung top. When corrected for the nitrogen fraction in the resident gas (.79), the solution of this equation for regions 7.5 and 27.5 cms from the lung top gives alveolar nitrogen fractions of .32 (upper) and .15 (lower), hence a 2:1 concentration gradient. It should be noted that this is a mean gradient, and four of nine subjects in their study (107) had apex/base ratios less than this mean value, thus falling in the range where Phase IV (%VC) underestimates the volume at which airways close. Even smaller concentration differences exist following inspiratory capacity breaths of O_2 , when apical nitrogen concentrations calculated from the mean regression relating FRC_r/TLC_r to D averaged 1.68 x basal concentration (107). Although such resident gas techniques give smaller differences in regional concentration, these differences are not altered by variations in pre-inspiratory lung volume or flow rate.

Gravity dependent sequential emptying of vertical lung

regions caused an upward slope of Phase III when upper concentrations were about ten times greater than those in lower lung regions (2, 26). The horizontal Phase III observed in the present study may be explained if regional emptying is not sequential enough to cause a significant slope of Phase III when the concentration ratio is 2:1 (see Figure 28). Since this ratio is not larger following a breath of oxygen, the upward slope of the resident gas technique is probably due to sequential emptying of intraregional lung units having different concentrations. To the extent that alveoli are of equal size at TLC, there must be an intraregional range of alveolar size (V_0) at FRC. This has been observed in dogs (132), and may be related to a corresponding range of stress-strain characteristics observed among individual alveolar walls obtained from small lung segments (52, 150, 151). Such measurements in the human lung (151) indicated that units with high V_0 are less distensible, hence less ventilated (ΔV), than the more compliant units with low V_0 . These P - V differences are identical to regional differences attributed to the pleural pressure gradient (107), so both models may explain the sloping Phase III when low $\Delta V/V_0$ units contribute a greater proportion of the expirate as lung volume decreases. If intraregional units are responsible for a sloping N_2 plateau in conditions where regional concentration differ by a factor of 2, either the concentration difference or the amount of sequential emptying within small lung regions must exceed that between vertical lung regions. In this light, the horizontal Phase III in this study also indicates that intraregional compliances are equal at FRC.

5. Summary and Conclusions

Seven healthy subjects inhaled ^{133}Xe bolus from FRC at various flow rates, and ^{133}Xe concentration in vertical lung regions was measured at TLC. The ratio (U/L) between concentrations in upper and lower regions ranged from 0.4 to 1.2. For $U/L < .5$, the expired count rate was constant from 90% to about 25% VC where it decreased abruptly (Phase IV) to values at RV much less than at mid expiration (.5 VC). As U/L increased, the expired count rate ratio (RV/.5 VC) increased and Phase IV (%VC) decreased according to the relationships:

1. $RV/.5\text{ VC} = .38\ U/L + .61\ (P < .001)$

2. $\text{Phase IV (\% VC)} = 46 - 44\ U/L\ (P < .001)$

These results indicate 1) that concentration differences between vertical lung regions were responsible for the terminal portions of all expired curves; and 2) that "closing volume" is systematically underestimated when these concentrations differ by less than a factor of 2. Accordingly, regional concentration differences are a potential source of variation in "closing volume" as estimated by resident gas techniques ($U/L \div 2$), or by RV bolus techniques when pre-inspiratory volume or inspiratory flow rate are not controlled. The observed horizontal Phase III may be explained if emptying of vertical regions is not sufficiently sequential to cause a slope when U/L is 2. Thus, the sloping alveolar plateau of resident gas techniques is probably due to sequential emptying of intraregional units having different concentrations.

E. The Effect of Increased Gas Density on Pulmonary Gas Exchange in Man.1. Introduction

Pulmonary gas exchange in liquid breathing dogs is limited by slow diffusion of respiratory gases through the dense fluid (77). Similar impairment of gas exchange was not observed when gas density was increased in a hyperbaric environment (19, 46, 92, 117, 139, 140). In fact, an inverse correlation between gas density and the alveolar-arterial difference for oxygen ($A-a)DO_2$) was demonstrated in dogs (92). A similar trend observed in man (139) suggests that the pulmonary exchange of oxygen may improve as gas density increases. To study this possibility without introducing large variations of inert gas fraction or time between gas mixtures, resting gas exchange was measured at 1 Ata in subjects breathing air and a dense gas.

2. Methods

Pulmonary gas exchange was measured in seven healthy male laboratory personnel 27 to 42 years of age. After an indwelling catheter was inserted percutaneously into the brachial artery, each subject lay supine and breathed through a two way valve. The inspiratory inlet was connected by short wide bore tubing to a balloon containing a mixture of about 21% oxygen in nitrogen (air) or sulfur hexafluoride (SF_6). Expired gas was collected in a 120 l. chain compensated spirometer which was emptied following an initial 30 minute period of quiet air breathing. Measurements were made from records and samples collected during the subsequent three minutes (A_1). The inspired mixture was then switched and the procedure was repeated on SF_6 . A third set of measurements were obtained 30 minutes after the inspired line was switched back to air (A_2).

During each collection period, two samples of arterial blood were drawn slowly and anaerobically into cold 10 ml syringes containing approximately 0.1 ml of heparin solution. The syringes were capped and kept on ice until the time of analysis, which was always within 30 minutes of collection. Blood gas tensions were measured in duplicate using Radiometer electrodes (P_{aO_2} type E5046, P_{aCO_2} type E5036, and pH unit type E5021a with pH metre type 27). Gas was continuously sampled at the mouthpiece by a rapid response CO_2 analyzer (Beckman LB-1) and the average end tidal value during the collection period was taken to represent alveolar CO_2 (P_{ACO_2}). At the end of the collection period, samples of inspired and mixed expired gas were withdrawn in duplicate from the balloon and the spirometer into 50 ml glass syringes sealed with 3 way stopcocks and lubricated with lithium chloride. Each gas sample was analyzed in triplicate for the mole fraction of oxygen (F_{IO_2} , F_{EO_2}) and carbon dioxide (F_{ECO_2}) by the micro-Scholander technique. Inspired oxygen was corrected (F_{IO_2c}) for R, and the average inspired and expired fractions were converted to partial pressures (P_{IO_2} , P_{EO_2} , P_{ECO_2}) at BTPS by multiplying by dry ambient barometric pressure (P bar -47). Minute ventilation and respiratory frequency were obtained from the spirometer record. Ventilation was corrected to BTPS or STPD using measured values of temperature and ambient pressure.

In one subject (CB), the study was repeated after a second catheter was positioned under fluoroscopy in the main pulmonary artery. Samples of mixed venous blood were drawn simultaneously with the arterial samples, and were analyzed as described. Oxygen content in arterial (CaO_2) and mixed venous (CvO_2) blood were estimated from a standard dissociation curve using measured values of PO_2 , PCO_2 , pH, temperature,

and hemoglobin. Cardiac output (Q_T) and percent venous admixture (Q_{va}/Q_T) were calculated. In the other subjects, blood pressure, pulse rate and temperature were recorded intermittently.

In a preliminary study, the accuracy of blood and gas analyses were assessed, and instrumental alterations due to SF_6 were examined. Because it is based on specific absorption of oxygen and CO_2 , Scholander gas analysis was presumably unaffected by the change in inert gas. This assumption was supported by failure to detect absorption of pure SF_6 by either solvent. Twelve test gas mixtures were prepared, containing by Scholander analysis, oxygen (5, 10 or 15%) and CO_2 (4 or 6%) in inert gas (N_2 or SF_6). Samples of fresh whole venous blood (20 ml) were added to 100 ml heparinized round bottomed flasks immersed in a temperature controlled ($37^\circ C$) water bath. While the flasks rotated (60 rpm) the blood was exposed to a steady flow (.3 lpm) of each test gas for 30 minutes (blood gas tensions were stable after 25 minutes). Gas tensions in tonometered blood were measured and compared with the corresponding values in the tonometer gas. The electrodes were calibrated with gas mixtures having partial pressures of O_2 and CO_2 which were lower (S 1), approximately equal, and higher (S 3) than those in the measured blood sample (S 2). During each measurement, readings were made in the sequence S 1, S 2, S 3, S 2, S 1, and were repeated if electrode drift exceeded 2 mm Hg.

Blood oxygen tensions were consistently low, and the average tonometer factor (1.030 , $sd \pm .005$) was not different between N_2 or SF_6 mixtures. Whereas measured values of CO_2 in N_2 tonometered blood were stable after 2 minutes exposure to the electrode, SF_6 prolonged this period to 4 minutes. Furthermore, even at 4 minutes, the blood

CO₂ values were consistently lower by 2 mm Hg than the SF₆ tonometer gas, in contrast to equal blood and gas PCO₂ values for N₂ mixtures. The output of the LB-1 was adequately linearized between 30 and 45 mm PCO₂, and measured all test gases within 2% of the Scholander value. There was no systematic error in the determination of CO₂ in SF₆ mixtures, and the 90% response times (\approx 100 msec) to step changes in CO₂ concentration were similar for N₂ and SF₆ mixtures.

On the basis of these results, the electrodes were calibrated as described during each experiment. The average PaO₂ values were multiplied by 1.03, and 2 mm Hg was added to average PaCO₂ values during SF₆ breathing. The observed variation in measurements during the preliminary study indicated an instrumental error of about 2 mm Hg in the experimental determinations of PaO₂, PaCO₂ and PACO₂. The variations in triplicate Scholander analysis ranged less than .5 mm Hg from the mean, indicating a smaller error in the measurement of inspired and mixed expired gas tensions. The measured values and the parameters of gas exchange calculated from equations listed below were compared between gas mixtures (A 1 vs SF₆ vs A 2 and A 1 vs A 2) by paired t analysis. The following parameters were computed:

$$FIO_2 c = FIO_2 (FEN_2 / FIN_2)$$

$$\dot{V}O_2 = (FIO_2 c - FEO_2) \dot{V}E \text{ (STPD)}$$

$$\dot{V}CO_2 = FECO_2 \cdot \dot{V}E \text{ (STPD)}$$

$$R = \dot{V}CO_2 / \dot{V}O_2$$

$$PAO_2 = PIO_2 - PACO_2 (FIO_2 c + \frac{1 - FIO_2 c}{R})$$

$$VD/\dot{V}T = (PaCO_2 - PECO_2) / PaCO_2$$

$$Q_T = \dot{V}O_2 / (CaO_2 - C\bar{V}O_2)$$

$$Q_{va}/Q_T = (CcO_2 - CaO_2) / (CcO_2 - C\bar{V}O_2)$$

3. Results

The measured and calculated parameters of pulmonary gas exchange are presented in tables 18 and 19. Due to a slightly lower oxygen fraction in the SF₆ mixture, P_{IO}₂ was about 3 mm Hg lower than in air. Despite the lower P_{IO}₂, P_aO₂ increased from air to SF₆ and decreased again when the subjects resumed air breathing. Accordingly, SF₆ breathing caused a small but highly significant (P<.01) reduction in the inspired to arterial difference for oxygen. The calculated ideal alveolar oxygen tensions reflected the F_{IO}₂ differences between gas mixtures. Thus, mean (A-a) D_O₂ decreased from 12.4 to 7.0 during SF₆ breathing (P<.01) and increased again to 13.34 (P<.01) when air breathing resumed. Values of R were high on both gas mixtures, and were not systematically different between gases. P_aCO₂ increased during SF₆ breathing with no associated change in minute ventilation, breathing pattern or CO₂ production. No systematic change was noted in heart rate, blood pressure, or arterial concentrations of HCO₃⁻ between gas mixtures. During the second study in CB (Table 20), (A-a) D_O₂ was again reduced by 10 mm Hg despite slightly lower values of cardiac output and mixed venous oxygen content during SF₆ breathing.

4. Discussion

The pulmonary exchange of oxygen improved during dense gas breathing. These results confirm a similar trend noted in three subjects breathing different gas mixtures between 1 and 8.5 Ata (139). In that study, increments in gas density produced by increased ambient pressure were associated with increased inert gas fractions. Since (A-a) D_O₂ increases with inert gas fraction (116, 117), the inverse



TABLE 18

Results of Gas and Blood Analysis

		<u>CB</u>	<u>LB</u>	<u>SB</u>	<u>MG</u>	<u>AL</u>	<u>HL</u>	<u>LW</u>	<u>Mean (+ Sd)</u>
V _e	A 1	6.50	4.71	5.20	6.95	7.23	6.00	7.34	6.28 (1.02)
	SF6	6.29	4.70	7.13	6.52	6.40	5.94	7.19	6.32 (.84)
	A 2	7.08	4.34	7.90	7.74	5.84	7.82	7.26	6.83 (1.34)
f	A 1	13.0	6.7	13.7	8.5	13.0	16.0	14.7	12.2 (3.4)
	SF6	13.0	9.3	7.7	6.8	10.0	11.3	15.0	10.4 (2.9)
	A 2	13.7	7.7	11.7	7.0	12.0	18.7	16.0	12.4 (4.2)
P _I O ₂	A 1	147	148	146	147	144	149	147	147 (2)
	SF6	144	147	144	144	140	145	144	144 (2)
	A 2	147	148	146	147	144	149	147	147 (2)
P _E O ₂	A 1	118	114	120	112	118	119	120	117 (3)
	SF6	115	113	118	111	114	121	116	115 (3)
	A 2	120	113	125	117	115	121	119	119 (4)
P _E CO ₂	A 1	27	33	25	32	27	25	26	28 (3)
	SF6	27	28	28	29	29	24	26	27 (2)
	A 2	27	33	22	29	28	25	26	27 (3)
P _a CO ₂	A 1	38	40	38	40	41	39	37	39.0 (1.4)
	SF6	42	46	38	41	42	39	39	41.0 (2.7)
	A 2	38	42	32	38	41	39	37	38.1 (3.2)
P _a O ₂	A 1	84	97	92	96	96	97	98	94.3 (4.9)
	SF6	89	98	104	98	98	99	98	97.7 (4.4)
	A 2	88	98	96	98	95	96	96	95.3 (3.4)

TABLE 19

The Effect of Gas Density on Pulmonary Gas Exchange

Subject	VO ₂ (ml. STPD)			R			A-a D _O 2			VD/VT (%)		
	A 1	SF6	A 2	A 1	SF6	A 2	A 1	SF6	A 2	A 1	SF6	A 2
CB	221	246	195	.93	.90	1.02	24	14	22	29	36	29
LB	185	188	178	.97	.81	.91	10	6	9	19	39	21
SB	166	228	204	.91	1.06	1.03	17	6	21	34	26	32
MG	286	262	273	.89	.85	.96	7	3	11	20	29	24
AL	229	194	201	1.02	1.12	.92	10	7	8	33	31	32
HL	207	158	247	.82	1.00	.93	9	8	12	36	38	36
LW	229	244	239	.97	.89	.91	10	5	11	30	33	30
Mean	218	217	219	.93	.95	.95	12.4	7.0	13.4	29	33	29
± Sd	38	38	34	.07	.11	.05	6.0	3.5	5.7	7	5	5

TABLE 20

Gas Density and Gas Exchange During
Cardiac Catheterization

	<u>Air</u>	<u>SF6</u>		<u>Air</u>	<u>SF6</u>
\dot{V}_e	6.73	6.94	$\dot{V}O_2$	254	270
f	13.4	13.0	R	.78	.75
PIO ₂	144	140	(A-a)DO ₂	32	22
PEO ₂	111	106	VD/VT	26	32
PECO ₂	26	26	CvO ₂	14.2	13.8
PaCO ₂	35	38	QT	4.9	4.7
PaO ₂	72	76	Qva/QT	11	7
PvO ₂	36	35			

relationship between (A-a) DO_2 and gas density was potentially obscured. The results were interpreted to demonstrate no deterioration of gas exchange over a wide range of gas densities, most likely due to an insignificant contribution of stratified inhomogeneity to (A-a) DO_2 . In dogs breathing 5% oxygen in SF_6 at 4 Ata, (A-a) DO_2 were significantly lower than values measured during air breathing at 1.0 Ata in spite of the greater inert fraction (92). The authors considered a number of possible explanations for the reduced (A-a) DO_2 , and excluded changes in cardiac output, mixed venous oxygen content, respiratory quotient, breathing pattern, "airways closure", and distribution of pulmonary perfusion. They concluded that their results were compatible with a reduced variation in ventilation-perfusion ratios (\dot{V}_A/Q) due to density induced alterations in series or parallel ventilation distribution.

In this study, a number of possible causes of improved gas exchange are also unlikely. "Airways closure" usually occurs below FRC in young supine subjects, and there is no other reason to expect changes during SF_6 breathing in cardiovascular parameters contributing to (A-a) DO_2 , e.g. $\text{C}\dot{V}\text{O}_2$, Q_T , Q_S/Q_T , and pulmonary perfusion distribution. This was supported by direct measurements in one subject (Table 3) and in others by the absence of systematic variations of heart rate or blood pressure between gases. No systematic changes in R were observed, and the parallel improvement of inspired-arterial differences for oxygen excludes a spurious improvement in (A-a) DO_2 due to calculation of alveolar oxygen tension. The high values of R are possibly due to the non-fasting state of the experimental subjects, so that occasional values of $R > 1$ may be attributed to minor errors in gas analysis. On the other hand, rigorous rejection of all studies in which $R > 1$ does not alter the results. Ventilation tended to be slower and deeper on SF_6 ,

but these differences were not significant. Furthermore, (A-a) DO_2 also decreased in subjects with smaller tidal volumes and increased frequency during dense gas breathing. Accordingly, the improved pulmonary exchange of oxygen during SF_6 breathing is likely due to a favourable change in ventilation distribution, such that \dot{V}_A/Q variance is diminished.

The static distribution of inspired gas among parallel lung regions is determined by the regional elastic properties (107). During a rapid volume change, ventilation distribution changes if regional time constants are different (115). Such asynchronous behaviour occurs during quiet breathing, and is enhanced by SF_6 breathing if regional resistances are density dependent (see sec. C.4). Dynamic redistribution of ventilation among vertical lung regions acts to increase (A-a) DO_2 , because upper lung regions having high \dot{V}_A/Q become better ventilated at the expense of lower lung regions having low \dot{V}_A/Q . To explain these results, gas density must cause a shift of ventilation from well ventilated lung units having high \dot{V}_A/Q to poorly ventilated units having low \dot{V}_A/Q . Within small lung regions considerable non-uniformity exists in ventilation (149), elastic properties (151), and alveolar size (132). Furthermore, there is no reason to expect parallel inhomogeneity within peripheral lung segments to correlate with \dot{V}_A/Q as has been demonstrated for vertical lung regions (160). If the well ventilated units also have longer time constants, SF_6 breathing reduces the contribution of intraregional \dot{V}_A/Q variance to (A-a) DO_2 . It should be noted that during quiet breathing the volume redistributed during the transient departures from the static distribution is necessarily small, and occurs primarily at the onset of flow (see appendix 3 C and Fig. 27). Thus, the effect

on gas concentrations is minimized by redistribution of dead space (111, 138, 141).

Marked series inhomogeneity of gas tensions occurred in liquid ventilated dogs, presumably because the rate of gas transfer by molecular diffusion is inversely related to the square root of fluid density (77). At least two mechanisms may explain paradoxical improvement of oxygen transfer when intergas diffusion is retarded by SF₆. Proximal portions of gas exchange units are better perfused than distal portions in some species (130, 131, 158). If stratified perfusion causes high \dot{V}_A/Q distally and low \dot{V}_A/Q proximally during air breathing, increased gas stratification on SF₆ would reduce series \dot{V}_A/Q variance. Alternatively, Farhi speculated that bulk mixing of inspired and alveolar gas occurs during inspiration and increase with gas density (41). If proximal bulk mixing predominates over peripheral impaired diffusion, gas stratification may be reduced on SF₆. Engel et al subsequently observed in dogs that the interface between inspired and alveolar gas was spread in transit from trachea to 4 mm bronchi (40). The volume in which inspired gas was distributed ahead of the mean interface increased by only 15 ml, and inspired gas was only a small fraction of this volume. They concluded that a negligible fraction of the tidal volume was mixed mechanically with alveolar gas in the bronchial tree. If these results apply to the human airway, it is unlikely that enhanced bulk mixing during SF₆ breathing significantly reduces series inhomogeneity. Furthermore, the latter explanation of these results requires that series inhomogeneity account for at least one-half of the (A-a) DO₂ during air breathing. Other than inconclusive studies of diffusion in lung models (31), the principal evidence supporting series inhomogeneity comes from expired concentration vs volume curves demonstrating 1) diminishing concentration

differences during a breath hold and ii) separation of gases having different diffusivities (30, 54, 125, 147). Traditionally, equilibration or separation of gas tensions in peripheral lung regions is attributed to molecular diffusion in a series system. To the extent that mixing occurs between peripheral parallel lung units, these results are not an unqualified demonstration of gas stratification.

Engel et al measured nitrogen concentration (FN_2) in gas sampled through the walls of canine intrapulmonary airways. During inflation of the lungs with oxygen, cardiogenic oscillations of FN_2 were regularly observed in 4 mm airways (40). After a two second breath hold, FN_2 was 50% of the alveolar fraction (FAN_2) in 4 mm bronchi and decreased progressively in mouthward airways to 10% of FAN_2 in lobar bronchi (38). During the subsequent expirations, the amplitude of cardiogenic oscillations of FN_2 decreased with breath hold time (39). They concluded that ventilation varies considerably within parallel lung units subtended from peripheral airways, and that gas mixing among these units reduces the inhomogeneity of gas tensions. Mixing was much faster in the presence of cardiac motion, suggesting a dynamic component attributed to convective diffusion and eddies secondary to cardiac induced flow oscillations. These mechanisms promote mixing of gas expelled by cardiac impulses from peripheral parallel units into the common mouthward airway, so that reexpiration of the common 'dead space' tends to reduce their concentration differences. Additional mixing by "pendelluft" occurs to the extent that time constant differences contribute to the cardiac induced sequential behaviour of parallel units (111, 141). Since increased gas density promotes convective diffusion, convective mixing and asynchronous ventilation, SF_6

breathing diminishes alveolar concentration differences between parallel peripheral lung units. A corresponding reduction in \dot{V}_A/Q variance accounts for the observed reduction in (A-a) DO_2 .

This mechanism implies that parallel inhomogeneity within peripheral lung units contributes a large proportion of the normal (A-a) DO_2 , and that the mixing action of the heart is a potent mechanism reducing this value. The mechanical properties underlying such intraregional inhomogeneity of ventilation were described by a simple 2 compartment model (39, 170). The different P-V characteristics of the compartments cause different alveolar size (V_0) at mid lung volume such that high V_0 units have less ventilation (ΔV). These differences conform to variations in stress-strain characteristics of individual alveolar walls within small lung regions (52, 151). The predicted variations in alveolar size are supported by measurements in dogs (132), and the intraregional dispersion of $\Delta V/V_0$ values is as large as their dispersion between vertical lung regions (39, 149). The P-V characteristics also predict sequential ventilation, such that high V_0 units having low $\Delta V/V_0$ contribute an increasing proportion of the total volume change as lung volume decreases. Furthermore, asynchronous ventilation due to lower time constants in these units exaggerates the sequential behaviour.

A slight increase in $PaCO_2$ occurred during SF_6 breathing. Because the mechanism of SF_6 -electrode interaction was unknown, this trend was not completely convincing. Nevertheless, elevated $PaCO_2$ during dense gas breathing was previously described and attributed to increased work of breathing or central respiratory depression (18, 55, 79, 118, 140). In this study, $\dot{V}O_2$ and $\dot{V}CO_2$ are quite similar on air

and SF₆. This was not surprising since the 2 - 3 fold increase in airways resistance expected during SF₆ breathing (85, 87, 156) is unlikely to alter the work of resting ventilation, which is predominantly elastic. SF₆ produced CNS symptoms (light headedness, retarded mentation, mood lability), and total ventilation was slightly reduced between A2 and SF₆. However, PaCO₂ increased between A1 and SF₆ despite equal ventilation, presumably due to the increased V_D/V_T. This agrees with the concept that V_D/V_T depends on diffusion of alveolar gas into airways, but opposite changes of this ratio and of (A-a) DO₂ are surprising. Similar observations by Martin et al (92) suggest that gas density acts differently on the pulmonary exchange of O₂ and CO₂. Since SF₆ retards inter-gas diffusion of O₂ and CO₂ about equally, the discrepancy possibly arises from the greater effect of \dot{V}_A/Q variance on (A-a) DO₂ than on V_D/V_T. As discussed, greater dynamic gas mixing during SF₆ breathing reduced the parallel range of alveolar gas tensions, thereby opposing any tendency of impaired oxygen diffusion to increase (A-a) DO₂. Due to the linear CO₂-blood dissociation curve, diminished parallel inhomogeneity has less effect on V_D/V_T, so impaired molecular diffusion near gas exchanging surfaces increased the 'alveolar' dead space. Alternatively, the explanation of reduced (A-a) DO₂ based on stratified perfusion provides a similar explanation for a corresponding increase in V_D/V_T.

5. Summary and Conclusions

Pulmonary gas exchange was measured in 7 resting supine subjects breathing air or a dense gas mixture containing 21% O₂ in SF₆. Mean \pm sd values of (A-a) DO₂ decreased from 12.4 \pm 6.0 on air to 7.0 \pm 3.5 on SF₆ (p < .01), and increased again to 13.4 \pm 5.7 when air breathing resumed (p < .01). No differences occurred between gases for $\dot{V}O_2$, R, \dot{V}_e , f, HR or BP,

and the improved oxygen transfer could not be attributed to changes in Q_T or $\overline{C\dot{V}O_2}$ in the one subject in which they were measured. These results are best explained by an altered distribution of ventilation, such that the \dot{V}_A/Q variance was reduced. Although the distribution of inspired gas may be influenced by differences in density dependent time constants of parallel units, two other explanations are thought more likely. To the extent that stratified perfusion contributes to (A-a) DO_2 during air breathing, impaired inter-gas diffusion on SF_6 may improve the series matching of \dot{V}_A and Q . Alternatively, SF_6 promotes cardiogenic gas mixing between peripheral parallel units having different concentrations, and a corresponding reduction in \dot{V}_A/Q variance conceivably accounts for the reduced (A-a) DO_2 . Both mechanisms allow observed increases in $PaCO_2$ and V_D/V_T during dense gas breathing. Accordingly, intraregional \dot{V}_A/Q variance accounts for about one half of the resting (A-a) DO_2 in healthy supine young men.

F. Exercise Ventilatory Mechanics at Increased Ambient Pressure.

1. Introduction

Expiratory flow rates during heavy exercise in healthy people are much lower than their maximum expiratory flow rates (\dot{V}_{max}) at comparable lung volumes (112). In patients with obstructive lung disease, expiratory flow during quiet breathing approaches or equals \dot{V}_{max} (60, 124, 153), so that attempts to meet added ventilatory requirements become limited by the dynamic compression of intrathoracic airways (124). Since values of \dot{V}_{max} at mid lung volumes are inversely related to the square root of air density in healthy subjects (164), their exercise ventilation may become limited by airways compression at increased ambient pressure. This study was designed to examine this possibility by measuring the inter-relationships among pleural pressure, air flow, and lung volume during maximum exercise in hyperbaric conditions.

2. Methods

To define pressure, flow and volume relationships at the onset of flow limitation, expiratory iso-volume pressure-flow (IVPV) curves were constructed at five lung volumes (90, 75, 60, 50 and 25% of vital capacity) and at five ambient pressures (1.0, 2.0, 4.0, 7.0 and 10.0 Ata). From each curve, P_{Lmax} , defined as the lowest transpulmonary pressure giving maximum flow, was determined, and these values were plotted against lung volume (V_L). The $P_{Lmax}-V_L$ lines were superimposed on transpulmonary pressure-volume loops measured during exercise in the same environmental condition. Since expiratory pressures greater than P_{Lmax} do not increase flow because they compress intrathoracic airways (51, 103, 127), the presence of expiratory flow limitation during exercise

can be detected. In this condition, expiratory flow rates are equivalent to the maximum expiratory flow rate and ventilation is equivalent to the maximum breathing capacity (MBC).

a. IVPV Relationships at Rest. Two healthy laboratory personnel familiar with respiratory manoeuvres sat on the floor of a hyperbaric chamber. At each simulated depth, they performed a series of graded vital capacity (VC) expirations varying from a very slow breath out to one of maximum speed and effort. From recordings of lung volume, flow rate and transpulmonary pressure, the flow rates as the subject passed through a given lung volume were plotted against the simultaneous values of transpulmonary pressure. A smooth line was drawn through these points, and P_{Lmax} was determined by visual inspection of the IVPV curve.

Flow and volume signals were obtained from a wedge spirometer (Med. Science Electronics Model 270) and were not influenced by increased gas density. The spirometer resistance was less than 1 cm H₂O/lps at all depths. A time delay of 40 msec. in the signals from the spirometer was corrected during construction of IVPV curves. A differential pressure transducer (Sanborn 267B) estimated the difference between lateral pressure in the mouthpiece and pressure in an esophageal balloon (length 10 cm, circumference 4 cm). The lateral oral pressure tap and the esophageal balloon were connected to the transducer by identical polyethylene catheters (length 90 cm, i.d. .15 cm). During measurements, the balloon was positioned in the lower esophagus and inflated with 1.5 ml air. When the recording system was exposed to atmospheric pressure, the recorded pressure in the balloon was zero over a range of balloon volumes from 0.5 to 6.0 ml. The volume displacement coefficient measured at 1 Ata was .017 ml/cm H₂O. At all experimental depths, the 90% response time of the pressure recording system was less than 10 msec.

The signals proportional to transpulmonary pressure, flow and volume were simultaneously recorded on a 4 channel Sanborn Poly Viso. Flow and volume signals were also displayed on the ordinate and abscissa of a storage oscilloscope, and the maximum perimeter flow-volume curve was copied at each depth. At ambient pressures greater than 2 Ata, this curve was not different from the flow volume curve of a single maximal effort expiration.

b. Exercise Studies. Three (ACB) and four (LW) levels of exercise were attempted at each depth on a mechanical bicycle ergometer (Monark). To minimize time at depth, subjects proceeded from lightest to heaviest work load without interruption. Exercise duration was five minutes for the first level of exercise and decreased by one minute at each successive level. During the last minute at each work load, the subjects breathed from the box to the bag of a bag-in-box system (capacity 150 l) through short wide bore (i.d. 2") tubing connected by a two-way breathing valve (Warren E. Collins High Velocity Double J). At the beginning and end of this period, vital capacity manoeuvres were performed to establish the end expiratory position (EEP). The wedge spirometer was connected in series with the box, and recorded lung volume (V_L) and air flow (\dot{V}) during exercise. Taking account of the fixed time lag, this system accurately measured a sinusoidal volume input for phase and amplitude to 120 cycles/minute at all depths. A potentiometer was mechanically linked to the wedge bellows to record ventilation. Transpulmonary pressure (P_L) was measured as described above. Signals proportional to P_L , \dot{V} , V_L and ventilation were simultaneously recorded on a 4 channel Sanborn Poly Viso and a bipolar EKG was recorded separately. Pressure-volume and flow-volume loops were reconstructed from the written record.

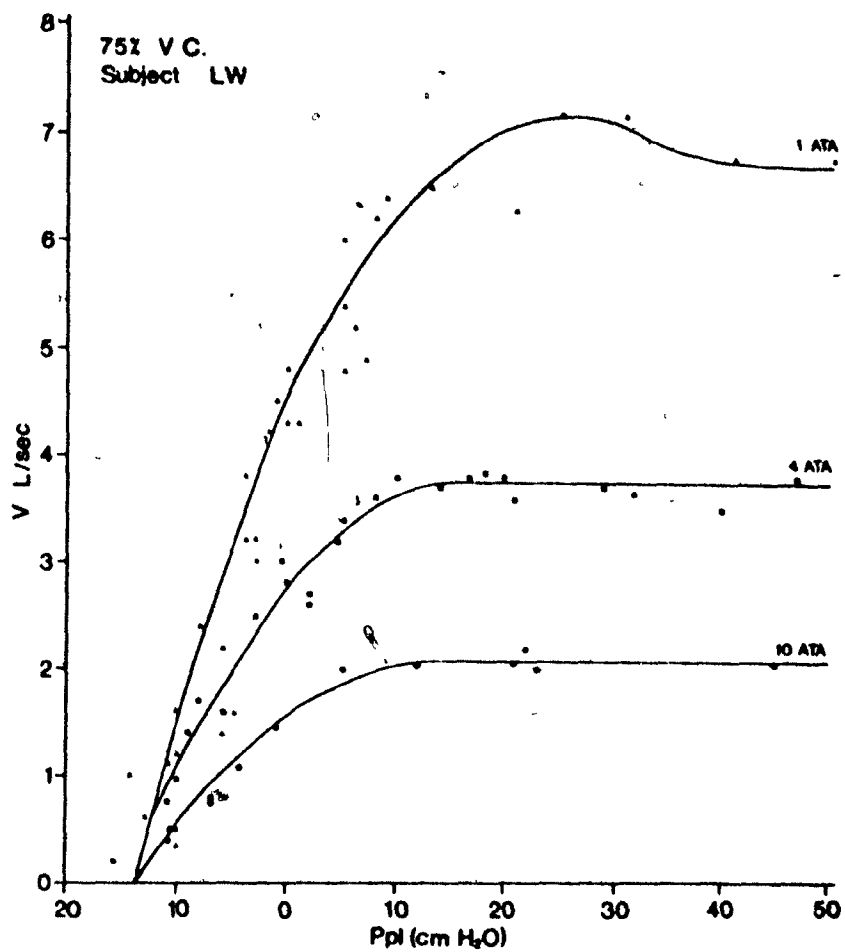
Samples of chamber air during exercise and mixed expired gas from the bag following each exercise period were collected in duplicate and analyzed at 1 Ata for CO_2 and O_2 by the micro-Scholander technique. The product of gas fractional composition and dry barometric pressure gave the partial pressure for these samples. Oxygen consumption was calculated from minute ventilation and expired gas composition. Mean alveolar CO_2 tension (PA_{CO_2}) was calculated from the Bohr equation using tidal volume, expired CO_2 tension, and the subjects' anatomic dead space measured separately for similar volume conditions, using the single breath technique described previously (165).

3. Results

As ambient pressure increased, \dot{V}_{max} and the initial slopes of the IVPV curves decreased at each lung volume (Fig. 31 and Table 21). Above 50% VC, P_{Lmax} decreased as ambient pressure increased, so that the reduction in P_{Lmax} with lung volume was much less at depth than at 1.0 Ata (Fig. 32). Static elastic recoil pressures were unaffected by hyperbaric conditions, and the slopes of maximum flow-static recoil (MFSR) curves decreased as ambient pressure increased (Fig. 33).

During maximum exercise at 1.0 and 2.0 Ata, P_{Lmax} and \dot{V}_{max} exceeded the expiratory transpulmonary pressures and flow rate respectively (Fig. 34 and 35, upper panels). At 4.0 Ata P_{L} exceeded P_{Lmax} and flow was equal to \dot{V}_{max} over most of the expired volume (middle panels). Expiratory flow limitation occurred at progressively lower flow rates at greater depths (lower panels), where there were corresponding reductions in minute ventilation, maximum oxygen uptake and heart rate, as well as elevated values of PA_{CO_2} and end expiratory position (Tables 22 and 23).

FIGURE 31



Expiratory pressure-flow curves at 75% VC in one subject at 1, 4, and 10 Ata. As gas density increased, maximum flow (V_{max}) and the lowest pressure giving maximum flow ($P_{L,max}$) decreased.

TABLE 21

Flow Rates⁺ and Resistances^{*} at Expiratory Flow Limitation

<u>XVC</u>	<u>AMBIENT PRESSURE (ATA)</u>								
	<u>1</u>		<u>2</u>		<u>4</u>		<u>10</u>		
	<u>ACB</u>	<u>LW</u>	<u>ACB</u>	<u>LW</u>	<u>ACB</u>	<u>LW</u>	<u>ACB</u>	<u>LW</u>	
90	\dot{V}_{max}	8.8	10.4	6.6	6.8	4.2	4.8	2.6	2.6
	R _{us}	2.4	1.9	3.0	3.0	4.8	4.2	7.7	7.7
	R _{ds}	7.1	5.6	8.8	6.7	10.8	8.6	15.3	13.0
75	\dot{V}_{max}	6.8	7.2	5.0	5.6	3.5	3.8	1.8	2.1
	R _{us}	2.1	1.8	2.8	2.3	4.0	3.4	8.0	6.2
	R _{ds}	7.3	5.1	8.9	6.1	10.5	8.0	15.3	13.2
50	\dot{V}_{max}	3.8	5.5	3.3	5.0	2.3	3.1	1.5	1.8
	R _{us}	1.6	1.6	1.8	1.8	2.6	2.9	4.0	5.1
	R _{ds}	7.0	4.5	9.5	6.7	13.3	9.5	17.7	15.4
25	\dot{V}_{max}	1.8	3.1	1.5	2.6	1.1	1.8	0.6	0.9
	R _{us}	0.6	1.6	0.7	1.9	0.9	2.8	1.7	5.6
	R _{ds}	6.6	5.5	8.9	6.9	11.1	10.0	20.7	18.2

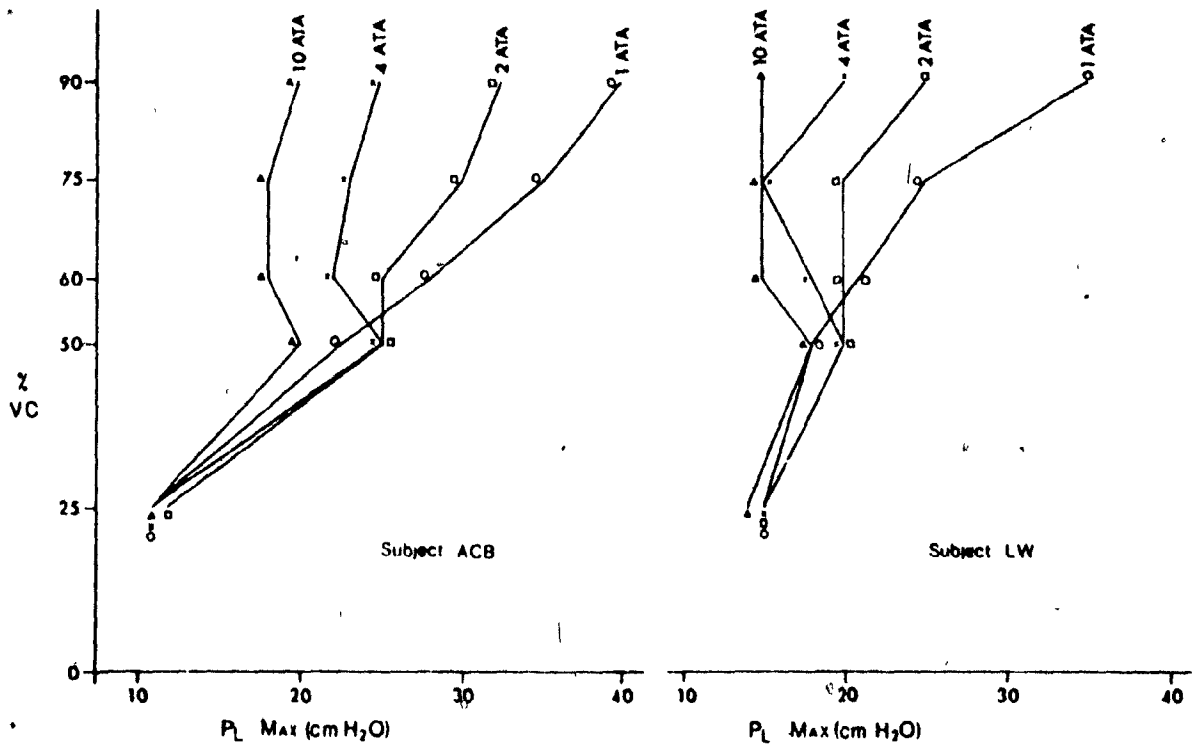
+ Maximum expiratory flow rates (\dot{V}_{max}) in litres/second

* Calculated at the onset of flow limitation in cm H₂O/lps

R_{us} - total resistance upstream from EPP = $P_{st}(1)/\dot{V}_{max}$

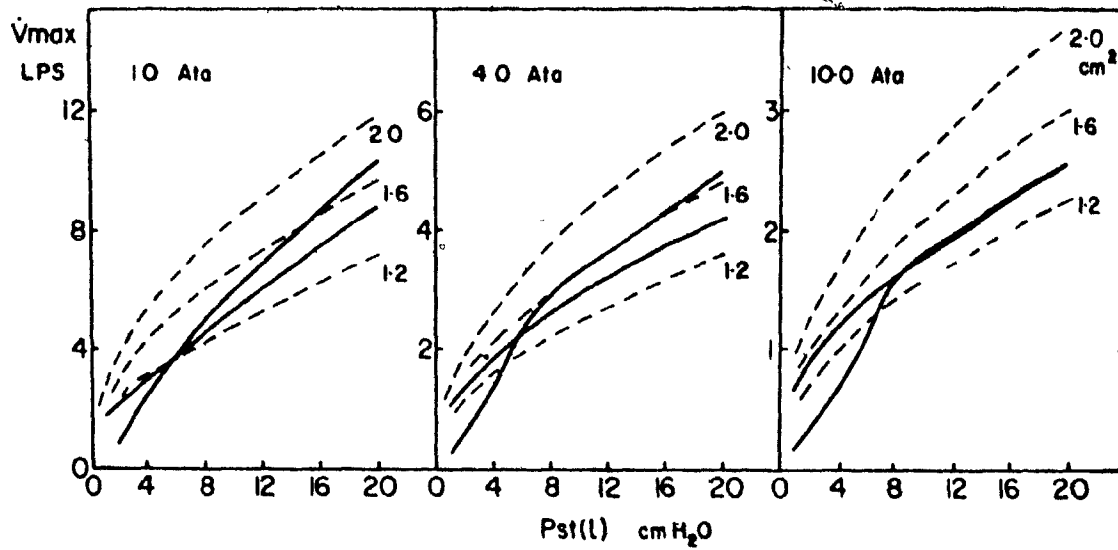
R_{ds} - frictional resistance downstream from EPP = $(P_{Lmax} + P_{ca'})/\dot{V}_{max}$

FIGURE 32



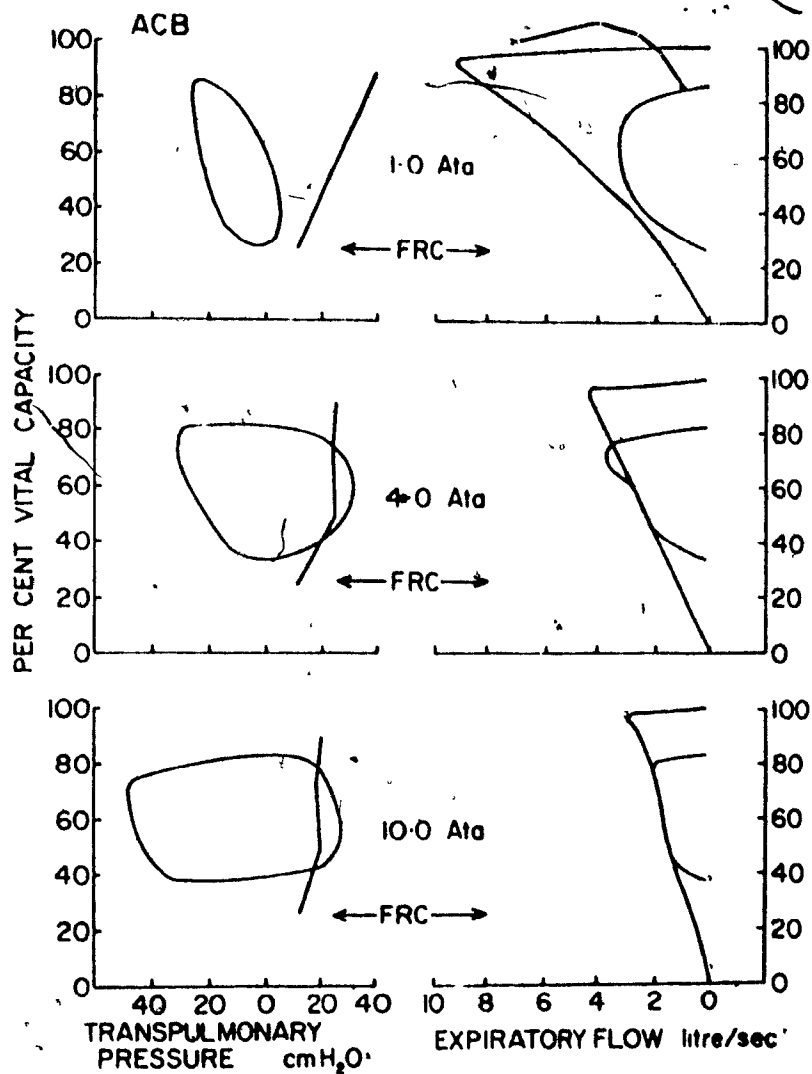
Relationship between lung volume and $P_{L,max}$ in two subjects at 1, 2, 4, and 10 Ata.

FIGURE 33

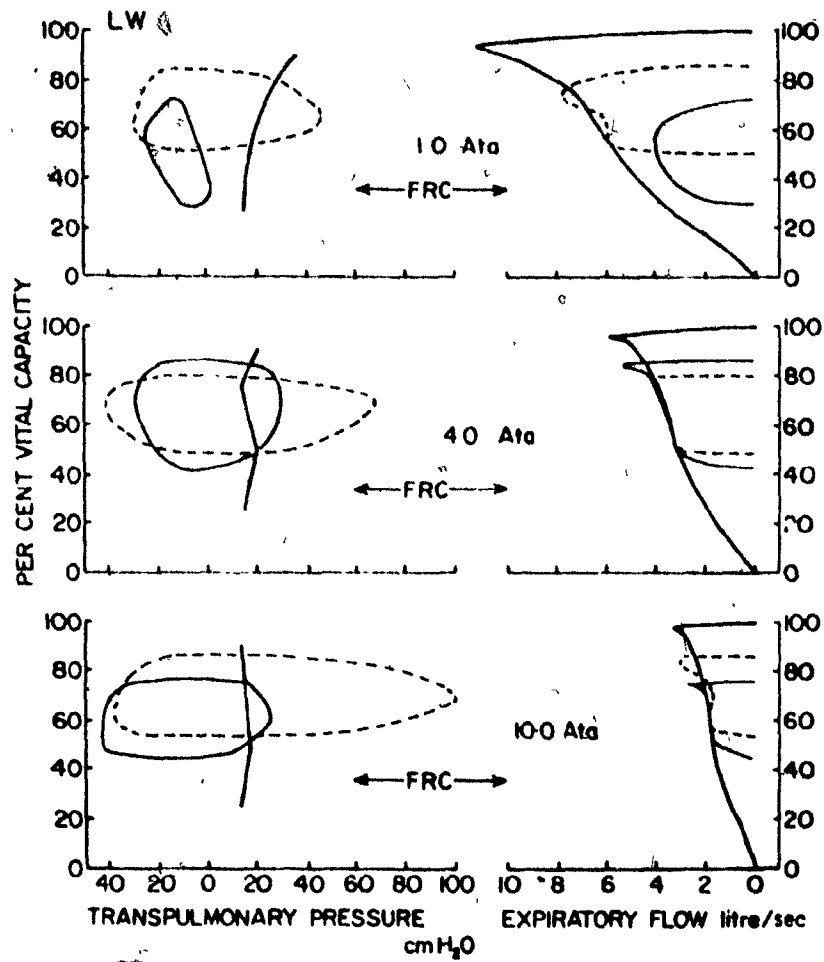


Maximum flow-static recoil relationships (solid lines) in two subjects at 1, 4 and 10 Ata. The broken lines represent isopleths of Pca calculated for EPP areas of 1.2, 1.6 and 2.0 cm².

FIGURE 34



Relationships of transpulmonary pressure (left abscissa) and expiratory flow (right abscissa) to lung volume (ordinates) during maximum exercise at 1, 4 and 10 Ata in one subject. Resting FRC and $P_{L\max}$ -volume lines are indicated (for discussion, see text).

FIGURE 35

Legend as in Figure 34, except broken lines indicate pressure-volume and flow volume relationships during maximum voluntary ventilation at rest.

TABLE 22

Cardio-Respiratory Parameters During Exercise (ACB)

<u>WORK LOAD</u> (Kgm. M./Min)		<u>AMBIENT PRESSURE (ATA)</u>			
		<u>1</u>	<u>4</u>	<u>7</u>	<u>10</u>
450	VE	74	70	65	52
	PA _{CO2} (PI _{CO2})	37	43 (2)	47 (3)	63 (4)
	$\dot{V}O_2$	1.7	1.8	1.8	1.7
	EEP	0.95	1.10	1.25	1.55
	HR	130	130	125	120
600	VE	97	88	66	
	PA _{CO2}	35	39 (3)	52 (3)	
	$\dot{V}O_2$	2.2	2.3	1.9	
	EEP	0.90	1.15	1.50	
	HR	145	150	140	
900	VE	120	86		
	PA _{CO2}	34	51 (4)		
	$\dot{V}O_2$	3.1	2.8		
	EEP	0.84	1.40		
	HR	175	175		

VE - Minute ventilation in litres (BTPS).

PA_{CO2} - partial pressure (mm.Hg) of CO₂ in alveolar gas.

PI_{CO2} - P_{CO2} in the inspired gas.

$\dot{V}O_2$ - Minute oxygen consumption in litres (STPD).

EEP - End expiratory lung volume in litres (BTPS) above RV.

HR - Heart rate in beats per minute.

TABLE 23

Cardio-Respiratory Parameters During Exercise (L.W.)

<u>WORK LOAD</u>		<u>AMBIENT PRESSURE (ATA)</u>			
(Kgm. M./Min)		<u>1</u>	<u>4</u>	<u>7</u>	<u>10</u>
450	VE	57	61	47	49
	PA _{CO2}	37	41	39	49 (6)
	$\dot{V}O_2$	2.5	2.7	2.7	2.9
	EEP	2.3	2.7	3.1	3.0
	HR	130	135	125	120
900	VE	92	84	61	56
	PA _{CO2}	34	39 (6)	50 (4)	54 (7)
	$\dot{V}O_2$	3.6	3.6	3.5	3.3
	EEP	2.0	2.7	3.2	3.7
	HR	160	150	150	155
1200	VE	110	100	74	
	PA _{CO2}	36	39 (6)	50 (4)	
	$\dot{V}O_2$	3.9	4.0	3.6	
	EEP	2.0	3.2	3.9	
	HR	175	170	165	
1500	VE	140	112		
	PA _{CO2}	34	45 (8)		
	$\dot{V}O_2$	4.4	4.2		
	EEP	1.8	3.8		
	HR	185	180		

For definition of parameters, See Table 22.

4. Discussion

a. IVPV Relationships at Rest. The driving pressure of \dot{V}_{max} at the onset of flow limitation is the difference between mouth (P_{ao}) and alveolar (P_{Blv}) pressures. According to Mead et al (103), the airway during forced expiration may be divided into two segments by points where the lateral intraluminal pressures are equal to the pleural pressure. In the segment upstream from these equal pressure points (EPP), the static elastic recoil of the lung ($P_{st}(l)$) is the driving pressure of \dot{V}_{max} so that MFSR curves define the upstream resistance (R_{US}). The configuration of MFSR curves is determined by the relative contribution of friction (P_{fr}) and convective acceleration (P_{ca}) to the upstream pressure drop. At high lung volumes where convective acceleration accounted for more than 80% of R_{US} , the cross sectional area of EPP (AEPP) was accurately estimated from the shape of the MFSR curves as follows. Several isopleths were drawn through values of \dot{V}_{max} and P_{ca} calculated from the Bernoulli equation for different AEPP.

$$P_{ca} = \frac{\rho \dot{V}_{max}^2}{2g \text{ AEPP}^2}$$

The isopleth which was similar to the MFSR curves indicated the AEPP.

In this study, the configuration of MFSR curves closely approximated isopleths of AEPP equal to 1.4 cm^2 at all depths for subject ACB and 1.7, 1.6, and 1.4 cm^2 at 1, 4 and 10 Ata respectively for subject LW (Fig. 33). These values of AEPP are similar to those estimated at 1 Ata by Mead et al (103) and are compatible with the location of EPP in the second or third airway generation. Since airway cross section distal to the third generation increases rapidly (159), these results suggest no significant upstream movement of EPP as gas density increased. Despite a relatively fixed geometry of the upstream segment,

R_{US} increased in a non-linear manner with gas density (Table 21). A logarithmic plot of these parameters was adequately described by a straight line, the slope of which is the exponent 'n' of the equation $R_{US} = K \rho^n$. The exponents were .48 (A.C.B.) and .50 (L.W.), indicating that R_{US} was proportional to the square root of gas density. This finding agrees with previous observations and is consistent with a major contribution of convective acceleration to the upstream pressure drop (164).

The downstream segment extends from EPP to the airway opening, and P_L is the pressure driving \dot{V}_{max} through these airways (103). Accordingly, P_{Lmax} is the downstream pressure drop at the onset of flow limitation. It should be noted that P_{Lmax} represents the downstream frictional pressure drop only if expired gas velocities are equal at EPP and airway opening. As described in Appendix 4 (P. 221) substantial downstream frictional loss in excess of P_{Lmax} occurred in this study because the area of mouthpiece (A_{ao}) was much greater than A_{EPP} . This pressure (P_{ca}) was calculated for each lung volume and gas density, so that the sum of P_{ca} and P_{Lmax} divided by \dot{V}_{max} represents the downstream resistance (R_{ds}) at the onset of flow limitation (Table 21). When these values for R_{ds} were plotted against gas density using logarithmic scales, slopes of .40 (ACB) and .45 (LW) were obtained. As discussed, similar density dependence of upstream resistance is due primarily to convective acceleration. Since R_{ds} was corrected for convective acceleration, these exponents relating resistance to density likely reflect a turbulent flow regime in which the relationship $R \propto \rho^{.43}$ is expected (164). This conclusion is compatible with the high Reynold's numbers in large airways at \dot{V}_{max} .

b. Exercise Studies. During a breathing cycle, the $P_{Lmax}-V_L$ line indicates the onset of expiratory flow limitation. If P_L exceeds P_{Lmax} , this portion of the corresponding pressure-volume loop is mechanically inefficient, in the sense that the increased work of breathing does not result in increased ventilation. Olafsson et al (112) demonstrated that most normal subjects did not develop pressures exceeding P_{Lmax} or flow rates equal to \dot{V}_{max} during exhausting exercise to maximum heart rates. Because the mechanical properties of the lung were unchanged during maximum exercise they reasoned that P_{Lmax} values determined at rest are not likely different during exercise. At 1.0 and 2.0 Ata in the present study, minute ventilation exceeded 100 l/min. during exhausting exercise to maximal heart rates. The exercise pressure-volume and flow-volume loops differed considerably from the corresponding P_{Lmax} and \dot{V}_{max} values, suggesting that considerable further increases in ventilation were possible. This was confirmed in subject LW, who breathed on his flow volume curve and generated values of P_L greater than P_{Lmax} while performing a maximum breathing capacity of 225 l/min (See Fig. 35, upper panel). These observations are in close agreement with the findings of Olafsson et al, who concluded that ventilation remains efficient and is not limited by the mechanical properties of the lung during maximum exercise in normal subjects.

Potter et al (124) described a quite different pattern in patients with obstructive lung disease whose lower values of P_{Lmax} and increased airways resistance caused expiratory flow limitation at lower values of ventilation. The limit of exercise tolerance was associated with a submaximal heart rate, excessive expiratory pressure, and flow rates equal to \dot{V}_{max} . They concluded that exercise capacity was limited by the deranged ventilatory apparatus in these patients. Similarly, in our normal subjects, expiratory pressures exceeded P_{Lmax} during

maximum exercise at 4 Ata and expiratory flow rates became equal to \dot{V}_{max} . At 7 and 10 Ata, this evidence of dynamic airways compression occurred at lower levels of exercise, minute ventilation, $\dot{V}O_2$ and heart rate. At these latter depths, expiratory flow limitation was observed 10 and 20 seconds after the work load was increased. Subjects continued exercise for 30 to 60 seconds beyond this point but neither completed the usual duration at that level due to severe choking dyspnea. In these circumstances, expiratory pressures did not exceed P_{Lmax} by more than 15 cms H_2O . In contrast expiratory pressures during MBC manoeuvres at 4, 7 and 10 Ata were much greater even though the MBC was not different from the maximal exercise ventilation. The elevated PA_{CO_2} values during maximal exercise at 7 and 10 Ata contrast with the hypocapnia during exercise at 1 Ata and support the notion of ventilatory insufficiency at depth.

These results demonstrate that maximal aerobic capacity is limited by dynamic compression of intrathoracic airways in normal subjects breathing air at depths in excess of 4 Ata. This occurs primarily because the density of a gas flowing mouthward through the narrowing cross section of intrathoracic airways considerably reduces the flow rate at which the airways become unstable. It is a quite different mechanism from that limiting exercise in normal subjects breathing less dense gases, when ventilatory capacity exceeds the requirements of maximal oxygen carrying capacity and tissue oxygen uptake. It also differs from exercise limitation imposed by external resistive loads. In these circumstances respiratory muscles maintain ventilation by generating additional pressure to a maximal excursion of 100 cm H_2O (23), yet dynamic airway compression does not occur. Presumably, fatigue of respiratory muscles plays a more important role in limiting

exercise during external loading than in this study, where expiratory pressures in excess of 15 cms H₂O were rarely observed. In this regard, it is possible that considerably greater expiratory effort is generated when flow can be increased but is not generated when expiratory flow is effort independent. Perhaps neural reflexes from compressed airways limit further effort, and contribute directly to the sensation of dyspnea.

The mechanism of exercise limitation demonstrated in this study is similar to that observed in patients with obstructive lung disease. Potter et al (124) suggested that the observed reductions of P_Lmax handicaps these patients in that flow limitation occurs at lower expiratory effort. It is equally tenable that exercise ventilation in patients is primarily limited by upstream events (loss of elastic recoil or peripheral airways obstruction) which lower MEFR to levels required to satisfy their metabolic requirements. Then the reduced P_Lmax is a consequence of the reduced maximal flow in relatively normal extra-thoracic airways (see Appendix 4, P. 223). There may be no difference in the control of expiratory efficiency between health and obstructive lung disease, in that the same inefficiency is demonstrated in both states when ventilatory requirements exceed expiratory capacity.

Several features of the submaximal work loads are of added interest. At 1 Ata, the end expiratory position (EEP) tended to decrease at higher exercise levels, but the opposite trend was observed at increased ambient pressure. For a given exercise level, EEP increased progressively with depth, especially when dynamic airways compression was observed. Presumably, expiratory effort is insufficient to expel the tidal volume within the time available at that frequency. These changes may compensate for flow limitation in the sense that increased

values of \dot{V}_{max} and ventilation are achieved at higher lung volumes. One price paid for this improvement is a greater inspiratory elastic work.

The gas exchange estimates at depth are complicated by CO_2 accumulation in the hyperbaric chamber. Inspired CO_2 tensions, measured during the last minute of exercise at each level, are recorded in Tables 22 and 23 adjacent the corresponding PA_{CO_2} value. Despite this limitation, it is reasonably safe to conclude from these results that alveolar hypoventilation accompanied the decrease in minute ventilation as depth increased at each work load. In previous studies (19, 68, 79, 140), CO_2 accumulation at depth was observed and attributed to respiratory depression or to the increased work of breathing dense gas.

A recent study demonstrated that the mechanical power output of the respiratory system in response to CO_2 stimulation was not different at 1, 4 and 7 Ata, although the ventilation achieved was progressively reduced due to the increased frictional work of breathing dense gas (L. Wood and A.C. Bryan, unpublished observations). This explanation was previously proposed to account for similar changes in CO_2 response curves during external resistance loading (106). To the extent that the complicated respiratory stimuli from of a given level of exercise cause a fixed inspiratory power at all depths, exercise ventilation must decrease as gas density increases.

5. Summary and Conclusions

Transpulmonary pressure, lung volume and flow rate were recorded in two healthy subjects performing graded exercise between 1 and 10 Ata. At simulated depths greater than 4 Ata, exercise was terminated by severe choking dyspnea at levels of work, oxygen consumption, heart rate and

ventilation significantly lower than during maximum exercise at 1 Ata. Comparison of exercise ventilatory mechanics with corresponding MEFV and IVPV curves demonstrated that the reduced aerobic capacity was associated with maximum ventilation. This occurred because increased gas density reduced the expiratory flow rate at which flow limiting transmural pressures develop across intrathoracic airways. At each level of submaximal exercise, end-expiratory position and alveolar CO_2 tension increased with ambient pressure due primarily to the density dependence of airways resistance. In these respects, healthy subjects breathing dense gas resemble patients with obstructive lung disease.

G. APPENDIX1. The Effect of Periodic Flow on Airways Resistance

In conditions of steady laminar flow through a single conducting element, velocities near the centre of the tube exceed those near the wall. When the pressure driving flow is sinusoidally oscillated at increasing frequencies, core flow eventually begins to lag the applied pressure due to the inertia of central molecules. In such circumstances, a greater proportion of the flow occurs near the walls where the shear rate is high, so that total flow per unit pressure decreases relative to steady flow conditions. The magnitude of this disturbance of the boundary layer relative to its steady flow thickness may be calculated according to Womersley (167) from the equation

$$a = r\sqrt{\omega/\nu} \quad (6)$$

where r is tube radius (cm), ω is angular frequency (sec^{-1}) and ν is gas kinematic viscosity (cm^2/sec). When the dimensionless parameter a exceeds a value of 1, oscillatory resistance exceeds that during steady flow. By this analysis, sinusoidal breathing at 10 cycles per minute causes a significant increase over resistance to steady laminar flow in the trachea and large bronchi (25).

However, the boundary layer of flow in frequently branching tubes is much less than the tube radius. According to Schroter and Sudlow (145) equation 6 may be rewritten to solve for an analogous parameter, B by substituting boundary layer thickness ($r\delta$) for radius.

$$B = r\delta\sqrt{\omega/\nu} \quad (6a)$$

Boundary layer thickness for a given steady flow rate may be estimated according to Pedley et al, (119).

$$r \delta = (2 \mu x / \rho U_0)^{.5} \quad (7)$$

where x is the axial distance (cm) downstream from the bifurcation, and U_0 is the gas velocity (cm/sec) in the core of the tube (e.g. outside the boundary layer). Assuming $U_0 = \bar{U}$, equations 6a and 7 are combined to give

$$B = (2 \omega x A / \dot{V})^{.5} \quad (8)$$

where A is the cross sectional area (cm^2) of the tube and $\dot{V} = A \cdot \bar{U}$. Since $r \delta \ll r$ for most of the bronchial tree (119), the assumption $U_0 = \bar{U}$ introduces only a slight underestimation of B . Note that equation 8 must be replaced by equation 6 when $r \delta = r$. A comparison of these two equations reveals that the effect of periodic flow on resistance in frequently branching tubes differs in several respects from its effect on resistance to fully developed laminar flow. The term, B , is independent of gas physical properties. In a given airway generation, B varies inversely as the square root of flow rate, and increases with distance from the bifurcation. Thus, those parameters which increase bronchial resistance by promoting a thin boundary layer also cause this resistance to be less affected by flow oscillations.

The solution of equation 8 for 2 to 8 mm airways in Weibel's lung model ($A \cdot x \approx 4$) allows several predictions of the effect of periodic flow on bronchial resistance (Table 2). At $\pm .5$ lps, resistance is uninfluenced by frequency ($B < 1$) to 10 cps. At 4 cps, $B < 1$ when $\dot{V} > .2$ lps, but at 50 and 100 ml/sec, values of B are 2 and 1.41 respectively.

Accordingly, the resistance measurements reported in sections A and B are equivalent to steady flow resistance if equation 8, derived from a human airway model, applies to the bronchial tree in living human and dog lungs. The similarity of R_{lp} measurements at 4 cps and at resonant frequency confirms this prediction for the dog (see Section A.3). It should be noted that if equation 8 slightly underestimates the effect of periodic flow on human bronchial resistance, P-V curves during oscillation would be more linear than during steady flow, and the effect of flow rate ($K_2, 'a'$) on resistance to steady bronchial flow would be underestimated (see Section B.4). In man, total pulmonary resistance is independent of frequency to 5 cps, and decreases slightly at higher frequencies due to parallel RC inequalities (81). Since asynchronous ventilation is greater during dense gas breathing (see Section C.4), the effect of gas density on bronchial resistance may be underestimated at higher breathing frequencies.

2. Estimate of Regional Resistance From Regional Lung Expansion

In order to make a quantitative prediction, a linear relationship between lower airway conductance (G_{law}) and over-all lung volume was defined by zero conductance at minimal air volume (20% TLC) and 1.67 ($G_{law} = 1/0.6$) at FRC (50% TLC). Thus % TLC = $18 G_{law} + 20$. This regression closely approximates published relationships between lower pulmonary resistance (R_{lp}) and lung volume (157), where R_{lp} is about .6 cm H₂O/lps at 50% TLC. For each compartment in a two-compartment model in parallel, % TLC_r = $36 G_{law} + 20$. Combining this latter equation with the mean relationship between regional expansion at FRC and distance (D cms) down the lung, (ref. 21 Table 3) the following equation was found: $G_{law} = 1.32 - 0.033 D$. Thus knowing the distance down the lung for each of the two compartments the corresponding resistances could be calculated.

However, as airways to upper (7.5 cm) and lower (27.5 cm) regions diverge essentially from the hilum, the pertinent distances will be closer to the hilum than to the corresponding regions. Values approximately one half way along the paths were arbitrarily considered to represent the mean effect of regional expansion on resistance. Thus, $R_u = 1.1 \text{ cm H}_2\text{O/lps}$ ($D = 12.5 \text{ cm}$) and $R_l = 1.7 \text{ cm H}_2\text{O/lps}$ ($D = 22.5 \text{ cm}$).

3. Distribution of Inspired Gas in a Two-Compartment Lung Model

a. Constant flow. Neglecting inertia, the distribution of a constant flow (\dot{V}_s) to each of two parallel visco-elastic pathways of a lung model (Fig. 36) may be calculated according to equation 10 of Pedley et al (122).

$$\dot{V}_{su}(t) = \dot{V}_s \frac{C_u}{C_u + C_l} + \dot{V}_s A \exp^{-Bt} \quad (9)$$

where

$$A = (R_l C_l - R_u C_u) / (R_u + R_l) (C_u + C_l)$$

$$B = (C_u + C_l) / C_u C_l (R_u + R_l)$$

u, l denote upper and lower compartments

C is the compliance of the volume elastic elements (l/cm H₂O)

R is the resistance of the parallel conducting parts (cm H₂O/lps)

and $\dot{V}_{su}(t)$ is the instantaneous flow (lps) in the upper pathway at a time, t seconds, after the start of \dot{V}_s (lps).

The instantaneous flow in the lower compartment, $\dot{V}_{sl}(t)$ is similarly:

$$\dot{V}_{sl}(t) = \dot{V}_s \frac{C_l}{C_u + C_l} - \dot{V}_s A \exp^{-Bt} \quad (10)$$

The volume of the upper compartment as a function of time ($V_{su}(t)$) is obtained by integrating equation 9 and assuming $\dot{V}_{su}(0) = 0$:

$$V_{su}(t) = \dot{V}_s \left[\frac{C_u t}{C_u + C_l} - \frac{A(\exp^{-Bt} - 1)}{B} \right] \quad (11)$$

and similarly for the lower compartment:

$$\dot{V}_{sl}(t) = \dot{V}_s \left[\frac{C_1 t}{C_u + C_l} + \frac{A(\exp^{-Bt} - 1)}{B} \right] \quad (12)$$

The distribution ratio of gas to the two compartments between time t_1 and t_2 is then given by:

$$\frac{V_{su}}{V_{sl}} = \frac{V_{su}(t_2) - V_{su}(t_1)}{V_{sl}(t_2) - V_{sl}(t_1)} \quad (13)$$

which can be solved using equations 11, 12 and known values for t_2 and t_1 .

b. Ramp flow. Equation 9 may be normalized for a unit step flow input and written:

$$\dot{V}_{su}(t) = \frac{C_u}{C_u + C_l} + A \exp^{-Bt} \quad (14)$$

The unit step response is integrated to determine the response to a unit ramp flow input (\dot{V}_r). For any ramp input of slope $M \text{ lps}^2$, we multiply our result by M .

$$\dot{V}_{ru}(t) = M \int_0^t \left[\frac{C_u}{C_u + C_l} + A \exp^{-Bt} \right] dt \quad (15)$$

where $\dot{V}_{ru}(t)$ is the instantaneous flow in the upper pathway in response to a ramp flow input. Also $\dot{V}_{ru}(0) = 0$, so

$$\dot{V}_{ru}(t) = M \left[\frac{C_u t}{C_u + C_l} - \frac{A(\exp^{-Bt} - 1)}{B} \right] \quad (16)$$

Similarly the flow response in the lower compartment ($\dot{V}_{rl}(t)$) is given by

$$\dot{V}_{rl}(t) = M \left[\frac{C_l t}{C_u + C_l} + \frac{A(\exp^{-Bt} - 1)}{B} \right] \quad (17)$$

The volume of the upper compartment as a function of time ($V_{ru}(t)$) is found by integrating equation 16 and assuming $V_{ru}(0) = 0$:

$$V_{ru}(t) = M \left[\frac{C_u t^2}{2(C_u + C_l)} + \frac{A}{B^2} (\exp^{-Bt} + Bt - 1) \right] \quad (18)$$

and similarly the volume of the lower compartment ($V_{r1}(t)$) is:

$$V_{r1} = M \left[\frac{C_1 t^2}{2(C_u + C_1)} - \frac{A(\exp^{-Bt} + Bt - 1)}{B^2} \right] \quad (19)$$

The distribution ratio of gas to the two compartments between time t_1 and t_2 is then given by:

$$\frac{V_{ru}}{V_{r1}} = \frac{V_{ru}(t_2) - V_{ru}(t_1)}{V_{r1}(t_2) - V_{r1}(t_1)} \quad (20)$$

Equation 20 was solved for the distribution of the second 100 ml in our model, using equations 18 and 19 and the following values of M , t_1 and t_2 . M was determined for each flow rate, defined as the average flow (\bar{V}) during the bolus distribution.

$$\begin{aligned} \dot{V}_r &= Mt \\ \text{so } \bar{V} &= M \frac{(t_1 + t_2)}{2} \\ \text{and } M &= \frac{2\bar{V}}{t_1 + t_2} \quad (21) \\ \text{also } V_r &= \frac{Mt^2}{2} \end{aligned}$$

Therefore, the time t_1 for the first 100 ml to enter is $\sqrt{.2/M}$ and t_2 for the first 200 ml to enter is $\sqrt{.4/M}$ or $\sqrt{2} t_1$. Substituting in equation 21:

$$M = 3.4343 \bar{V}^2$$

It should be noted that this value of M is specific for the distribution of the second 100 ml inspired, and M must be recalculated to solve for the distribution of other portions of the inspirate.

The solutions for equation 13 and 20 are compared in Fig. 26 and discussed in Section C 4. As $t_2 \rightarrow 0$ of equation 20, then $(t_2 - t_1)$ approaches zero as well. Accordingly, equation 20 can be written using partial differentials.

$$\lim_{t \rightarrow 0} \frac{V_{ru}}{V_{rl}} = \frac{\frac{dV_{ru}}{dt} \cdot dt}{\frac{dV_{rl}}{dt} \cdot dt} = \frac{\dot{V}_{ru}}{\dot{V}_{rl}} \quad (22)$$

The limit of equation 22 as $t \rightarrow 0$ is found by substituting in equations 16 and 17 and using l'Hospital's rule, which yields

$$\lim_{t \rightarrow 0} \frac{V_{ru}}{V_{rl}} = \frac{R_l}{R_u}$$

Comparison of equation 16 with equation 11 and of equation 17 with equation 12 reveals that their only difference is the dimension of the constant, M . That is, the flow response to a ramp flow input is of the same form as the volume response to a step input. Therefore,

$$\frac{\dot{V}_{ru}}{\dot{V}_{rl}} = \frac{V_{su}}{V_{sl}}$$

It follows that the limit of equation 13 as $t \rightarrow 0$ is identical to the limit of equation 20. The limits of these same equations as $t \rightarrow \infty$ are obtained from equations 11 and 12,

$$\lim_{t \rightarrow \infty} \frac{V_{su}}{V_{sl}} = \frac{C_u}{C_l}$$

and from equations 18 and 19,

$$\lim_{t \rightarrow \infty} \frac{V_{ru}}{V_{rl}} = \frac{C_u}{C_l}$$

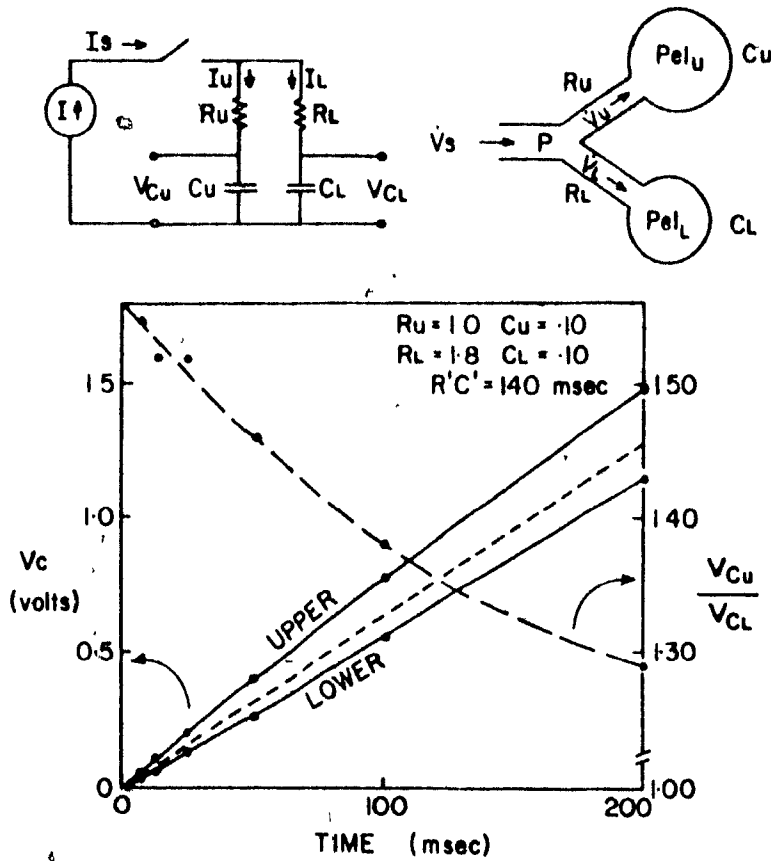
Accordingly, the distribution of both step and ramp flow is proportional to compliance as $t \rightarrow \infty$ and inversely proportional to resistance as $t \rightarrow 0$ (see Figure 26).

c. Experimental flow. The mathematical description of the experimental flow-time pattern observed during the experiments described in Section C ($M = 80 \text{ lps}^2$ followed by a constant flow) was difficult, so an electrical analogue of the lung model was constructed. In addition to providing the solution, analysis of the response of the analogue proved instructive regarding the mechanism of parallel distribution of gas inspired during a change in \dot{V}_I . The analogue studied is schematically illustrated in Fig. 36 adjacent to the corresponding mechanical lung model. Upper and lower pulmonary pathways are analogous to

two-resistor (R) - capacitor (C) circuits in parallel. When the switch is closed ($t = 0$), a current (I) analogous to a flow (\dot{V}) is applied to the network, and the charge (Q) on each capacitor at any time after t_0 is analogous to the volume change of each region. This may be calculated from the measured voltage across each capacitor (V_C), since $Q = V_C \cdot C$. The parallel capacitors are approximately equal and have the equivalent mechanical dimension of .1 l/cm H₂O. The parallel resistors are unequal and scaled to the equivalent mechanical dimensions of 1.0 (R_u) and 1.8 (R_l) cm H₂O/lps. The lower panel of Fig. 36 illustrates the response of the network to a constant current input (I_s), so the following description and explanation are completely analogous to the response of the lung model to a constant flow.

Upon closure of the switch, V_{cu} (upper solid line) increases more rapidly than V_{cl} (lower solid line). Both lines are curvilinear, the upper being concave and the lower being convex to the time axis, such that each becomes parallel to the dashed line of identical filling at about 500 msec. (not shown in figure). Thus, the ratio of the voltages in the parallel circuits (broken line) is initially about 1.8 and decreases with time to approach a value of 1.0 beyond 500 msec. The parallel distribution of a portion of the charge distributed between t_1 and t_2 is given by the ratio: $(V_{cu}(t_2) - V_{cu}(t_1))/(V_{cl}(t_2) - V_{cl}(t_1))$. In mechanical units, the distribution of the second .1 litre inspired at a constant flow of 2 lps occurs between 50 msec. ($t_1 = .1$ litres/2lps) and 100 msec. ($t_2 = .2$ litres/2lps). From Fig. 36, the distribution ratio is $(.8 - .4)/(.56 - .26)$ or 1.33. At .2 lps ($t_1 = 500$ msec.) the parallel increase in V_{cu} and V_{cl} gives a distribution ratio of 1.0. Thus, more of the bolus is distributed to the upper region at 2 lps than at .2 lps.

FIGURE 36



Schematic diagram of an electrical analog (upper left) of a two compartment lung model (upper right). Each parallel pathway in the lung model consists of a conducting element having resistance (R_U , R_L) in series with a volume elastic element having compliance (C_U , C_L). These are analogous to two electronic resistance-capacitor circuits arranged in parallel. Upon closure of the switch, a constant current, I_s , analogous to a constant flow (\dot{V}_s), is applied to the network.

The measured response is plotted in the lower panel: left ordinate is voltage on the equal capacitors, analogous to volume change in the two compartments of the lung model; right ordinate is the ratio of circuit voltages, analogous to the ratio of regional volume changes; and time following the switch closure is on the abscissa. Initially, regional current is inversely proportional to regional resistance, but this transient departure from elastic equilibrium decays according to the time constant, $R'C'$, until current is distributed according to the regional capacitors. (For full description, see appendix).

This response of the network, hence of the lung model, is explained as follows. Before the switch is closed, the parallel circuits are balanced ($V_{Cu} = V_{C1}$). The instant the switch is closed, I_s divides according to the parallel resistors, so that $I_u = 1.8 I_l$. Accordingly, V_{Cu} transiently increases more rapidly than V_{C1} , and the voltage drop across R_u decreases relative to that across R_l . This is equivalent to saying that I_u decreases with time until $I_u = I_l$. Thereafter, I_s is equally divided according to the equal capacitors, which subsequently fill synchronously. Thus, a dynamic balance of the parallel circuits is established where V_{Cu} exceeds V_{C1} . The time constant of the transient is $R'C'$, where R' is the addition of R_u and R_l in series and C' is equivalent capacitance of C_u and C_l in series. Thus, $R'C'$ is the time constant of a transient current from C_u through R_u and R_l to C_l , and is the reciprocal of B in equations 9 - 19. What is actually happening in mechanical terms is a transient overinflation of the upper region that elevates Pe_{lu} above Pe_{ll} . This pressure difference redistributes the inflow away from the upper region toward the lower region.

Although the transient duration is independent of \dot{V}_I , \dot{V}_I influences the time it takes for a bolus to reach the lobar bronchi. For a given average \dot{V}_I , this time is longer for a ramp than for a constant flow. Since this gives more time for the exponential terms in equation 18 to die out, one might expect the ramp response to reach the compliance determined limit at lower flows than the step response. However, results from the model prove the opposite (Fig. 26), presumably because the rising flow of the ramp input continuously applies a new driving level to the system. Although the transient terms of equation 18 die out exponentially, the $\frac{MAT}{B}$ -terms do not. These components represent the response to the changing drive and result in the distribution of ventilation being slightly

more flow sensitive than during constant flow conditions. Since our experimental flow-time profile was a combination of a ramp and a step, the response of the model to that profile was not detectably different from the constant-flow response for the values used.

4. Frictional Resistance to Flow Downstream from EPP

As discussed in Section F 4, the airway during forced expiration is divided by EPP into upstream and downstream segments (103). Resistance in these segments may be calculated as the ratio to \dot{V}_{max} of P_{st} (1) (R_{us}) and P_l (R_{ds}). Implicit in the considerations of Pride et al (127) is a further partitioning of the downstream segment into 1) a length extending mouthward from the site of airway instability (flow limiting segment - FLS) and 2) and a length between EPP and FLS in which lateral intraluminal pressure becomes negative with respect to pleural pressure by an amount equal to the threshold of elastic stability (P_{tm}') of the airway (Fig. 37). At the onset of flow limitation, the downstream driving pressure (P_{Lmax}) is the sum of P_{tm}' and the resistive pressure drop (P_d') from the FLS to airway opening. Accordingly, the inverse slope of the relationship between P_{Lmax} and V_{max} is the resistance (R_d') downstream from FLS, and the zero flow intercept is P_{tm}' , (provided P_{tm}' does not change with lung volume).

As shown in Fig. 38, the same linear relationships exists between P_{Lmax} and \dot{V}_{max} at all depths, indicating values for P_{tm}' of about 10 cm H₂O. These values are consistent with previous estimates of P_{tm}' (127). The fact that downstream resistance was apparently independent of gas density and flow rate implies a laminar flow regime. This is quite surprising since R_e in large airways during \dot{V}_{max} are exceptionally high. One possible explanation is that because $A_{ao} \gg A_{EPP}$, P_{Lmax} underestimates the frictional losses downstream from EPP by the amount of pressure stored in gas velocity at EPP and converted to lateral pressure

as gas decelerates. This pressure (P_{ca}') was calculated for each lung volume and gas density as follows:

$$P_{ca}' = (\rho \dot{V}_{max}^2 / 2g) (1/A_{EPP}^2 - 1/A_{ao}^2)$$

The sum of P_{ca}' and P_{Lmax} is plotted against \dot{V}_{max} in Figure 39, illustrating the expected increase in downstream frictional resistance (R_{ds}) with gas density.

The model provides one explanation for the relationship between P_{Lmax} and V_L . As lung volume decreases, P_{st} (1) decreases with lung volume so that \dot{V}_{max} decreases even if R_{us} is independent of volume (103). To the extent that EPP remain in second or third generation airways from 75 to 25% VC, there is unlikely to be any major change in P_{tm}' or R_d' . Since $P_d' = \dot{V}_{max} \times R_d'$, there will be a reduction in P_d' corresponding to the reduction in \dot{V}_{max} . It is less evident why P_{Lmax} decreases at the same lung volume as gas density increases, but several explanations are considered. i.) Because \dot{V}_{max} is inversely related to the square root of air density, any flow regime in the downstream segment having less density dependence will result in a smaller P_d' . Consider as an extreme example a laminar flow regime.

$$P_d' = K \mu \dot{V}_{max}$$

where K is a constant containing geometry of the downstream segment.

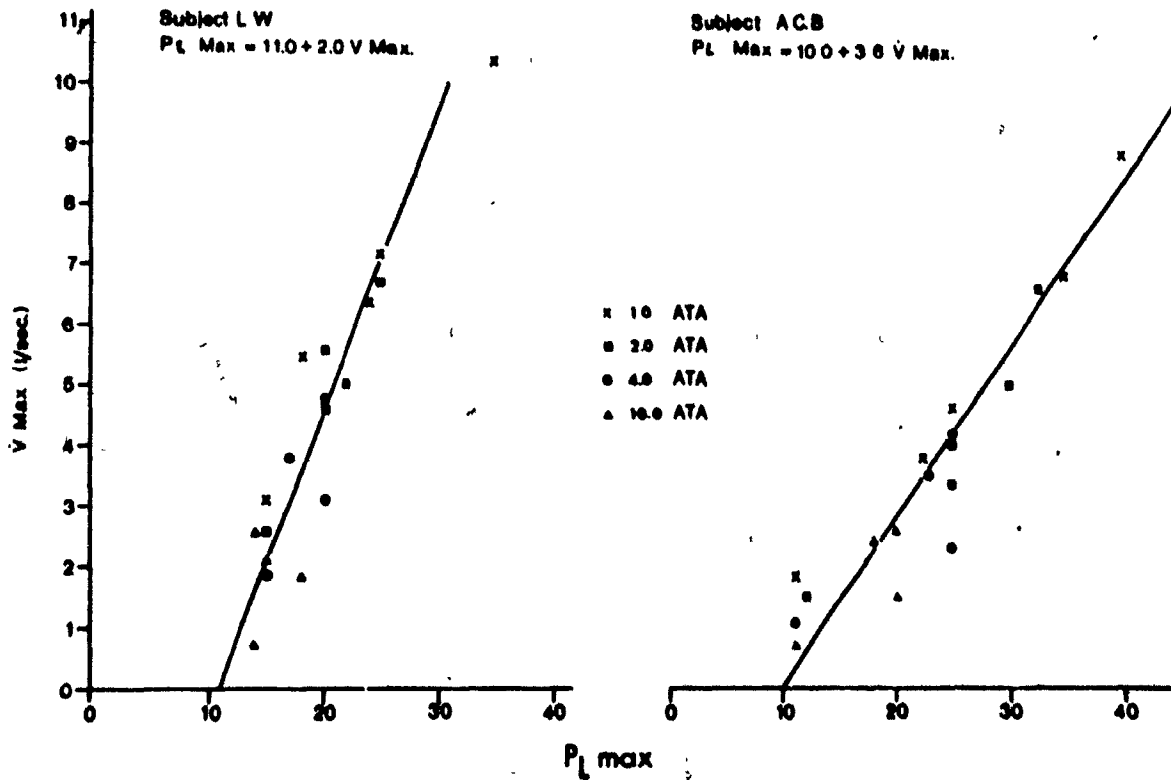
When \dot{V}_{max} decreases at increased ambient pressure, P_d decreases accordingly.

At the opposite extreme is orifice flow,

$$P_d' = K \rho \dot{V}_{max}^2$$

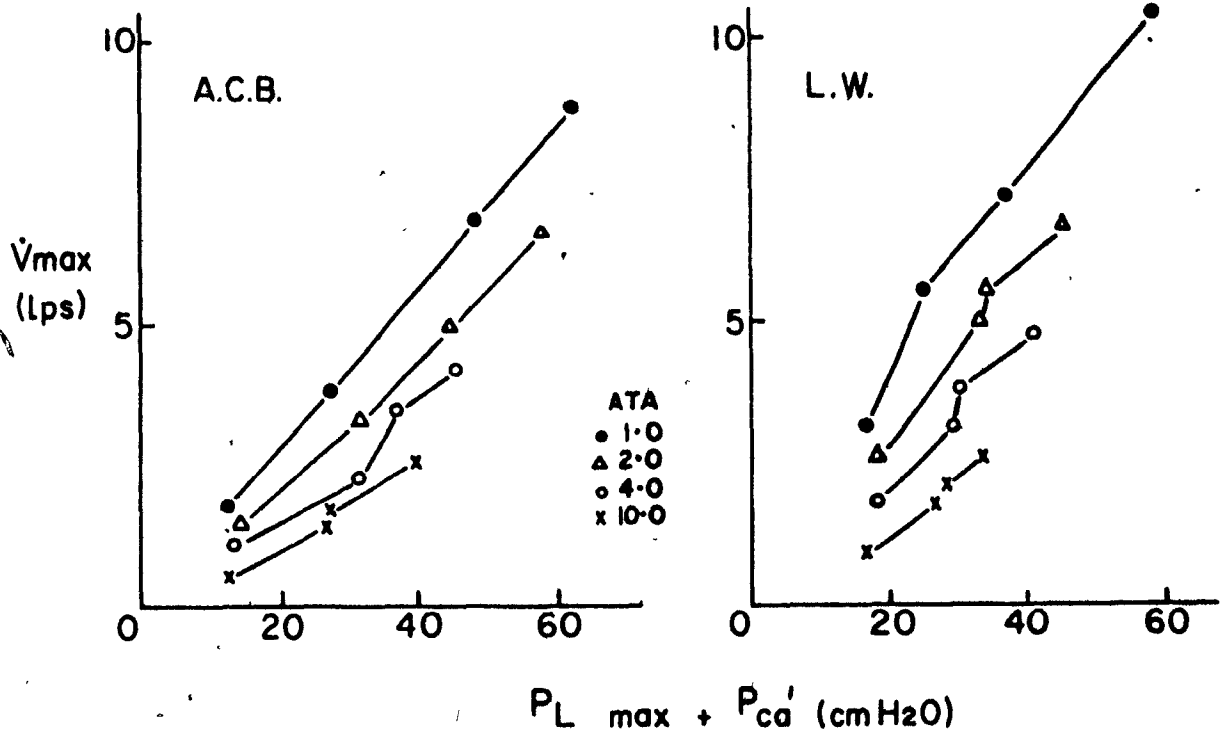
Now when \dot{V}_{max} is reduced by the square root of gas density, P_d' remains constant. For intermediate flow regimes, e.g. turbulence, P_d' must decrease as gas density increases. ii.) If EPP move downstream as depth

FIGURE 38



Relationship between \dot{V}_{max} and $P_{L \text{ max}}$ for 2 subjects at 1, 2, 4, and 10 Ata. Values at each ambient pressure obtained from IVPV curves for 90, 75, 50 and 25% VC. Regression lines ($p < .01$) are drawn (for discussion, see text).

FIGURE 39



Relationship between \dot{V}_{max} and downstream flow resistive pressure drop ($P_{L \max} + P_{ca}'$). Values are identical to those in Figure 38 except for correction of $P_{L \max}$ with P_{ca}' (for discussion, see text).

increases, the downstream segment shortens and P_d is reduced. (iii.) P_{tm} may be reduced as ambient pressure increases due to alterations in bronchial tone. It is not clear from this study which of these mechanisms is operative.

CHAPTER VCONCLUSIONS

Lower pulmonary resistance increased with gas density and flow rate because the frequently branching pattern of the bronchial tree prevents growth of laminar boundary layers. In the dog, this mechanism of flow resistance predominates in the segment proximal to 4 mm airways, but in peripheral airways where $Re < 100$, gas flow is laminar. Rather than two discrete flow regimes, it is likely that flow patterns undergo a continual metamorphosis as Re decrease between trachea and alveoli. Accordingly, airways resistance is not described by any single fluid dynamics equation, but may be explained by the general equation, $R = K \dot{V}^a \rho^a \mu^{1-a}$, where 'a' reflects the proportion of inertial to viscous pressure losses and varies between 1 and zero according to Re . To the extent that periodic flow increased R_{1p} , neither the general equation nor Rohrer's equation were definitively tested.

The pattern of regional redistribution of inspired gas with flow rate supports an explanation based on regional time constant differences. By increasing parallel time constants through its effect on lower pulmonary resistance, greater gas density increased the flow dependence of regional ventilation. The dynamic departure of lung regions from their static elastic equilibrium appears to be opposed by forces generated through the mechanical interaction of lung and chest wall. Since it occurred at flow rates as low as 0.5 lps, such dynamic redistribution accounts for a considerable change from the compliance determined ventilation of vertical lung regions during quiet breathing. Similar flow dependence of gas distribution likely occurs between parallel units of peripheral lung segments.

Regional concentration differences influence the expired concentration vs volume relationship such that "closing volume" is systematically underestimated when $U/L < 2$. Since the alveolar plateau was horizontal when $U/L = 2$, its upward slope following a single breath of oxygen probably represents sequential emptying of parallel intraregional units having concentration differences $> 2:1$. To the extent that all alveoli are the same size at TLC, the different concentrations probably arise from intraregional variations in alveolar size at FRC.

Gas density improved the pulmonary exchange of oxygen by reducing intraregional \dot{V}_A/Q variance. Although the distribution of inspired gas may be influenced by differences in density dependent time constants of parallel units, two other explanations are thought more likely. Impaired inter-gas diffusion on SF_6 may increase stratification of alveolar oxygen concentrations, thereby matching stratified perfusion. Alternatively, by enhancing mechanisms responsible for intraregional cardiogenic gas mixing, greater gas density may reduce parallel inhomogeneity of gas tensions.

Maximum exercise is limited by expiratory compression of intrathoracic airways in healthy subjects breathing air at depths in excess of 4 Ata. This occurs primarily because the increased density of gas flowing mouthward through a diminishing cross-sectional area reduces the flow rate at which flow limiting transmural pressures develop across the airways. During submaximal exercise, CO_2 retention develops as gas density increases because a greater proportion of the work of breathing is required to overcome flow resistance. In these two aspects healthy subjects breathing dense gas resemble patients with obstructive lung disease.

BIBLIOGRAPHY

1. Agostoni, E. Mechanics of the pleural space. *Physiol. Rev.* 52:57-128, 1972.
2. Anthonisen, N.R., P.C. Robertson, and W.R.D. Ross, Gravity dependent sequential emptying of lung regions. *J. Appl. Physiol.* 28:589-595, 1970.
3. Bachofen, H. Lung tissue resistance and pulmonary hysteresis. *J. Appl. Physiol.* 24:296-301, 1968.
4. Bachofen, H. and J. Hildebrandt. Area analysis of pressure-volume hysteresis in mammalian lungs. *J. Appl. Physiol.* 30:493-497, 1971.
5. Bachofen, H. and M. Scherrer. Lung tissue resistance in healthy subjects and in patients with lung disease, In: Airway Dynamics, edited by A. Bouhuys, Springfield, Ill.: Thomas, 1970, pp. 123-134.
6. Bake, B., J. Bjure, G. Grimby, J. Milic-Emili, and N.J. Nilsson. Regional distribution of inspired gas in supine man. *Scand. J. Resp. Dis.* 48:189-196, 1967.
7. Ball, W.C., P.B. Stewart, L.G.S. Newsham, and D.V. Bates. Regional pulmonary function studied with xenon¹³³. *J. Clin. Invest.* 41:519-531, 1962.
8. Barach, A.L. The effects of inhalation of helium mixed with oxygen on the mechanics of respiration. *J. Clin. Invest.* 15:47-61, 1936.
9. Barach, A.L. The use of helium in the treatment of asthma and obstructive lesions in the larynx and trachea. *Ann. Int. Med.* 9:739-765, 1936.
10. Barach, A.L. The therapeutic use of helium. *J.A.M.A.* 107:1273-1280, 1936.
11. Barnett, T.B. Effects of helium and oxygen mixtures on mechanics during airway constriction. *J. Appl. Physiol.* 22:707-713, 1967.
12. Bashoff, M.A., R.H. Ingram, Jr., and D.P. Schilder. Effect of expiratory flow rate on the nitrogen concentration vs. volume relationship. *J. Appl. Physiol.* 23:895-901, 1967.
13. Bayliss, L.E. and G.W. Robertson. Visco-elastic properties of the lungs. *Quart. J. Exptl. Physiol.* 29:27-46, 1939.
14. Blide, R.W., H.D. Kerr, and W.S. Spicer, Jr. Measurement of upper and lower airway conductance in man. *J. Appl. Physiol.* 19:1059-1069, 1964.

15. Bouhuys, A. Distribution of inspired gas in the lungs, In: Handbook of Physiology, edited by W.O. Fenn and H. Rahn. Washington, D.C.: Am. Physiol. Soc. 1964, sect. 3, vol. 1, pp. 715-733.
16. Bouhuys, A. and B. Jonson. Alveolar pressure, air flow rate and lung inflation in man. *J. Appl. Physiol.* 22:1086-1100, 1967.
17. Bouhuys, A., S. Lichtneckert, C. Lundgen and G. Lundin. Voluntary changes in breathing pattern and N₂ clearance from the lungs. *J. Appl. Physiol.* 16:1039-1042, 1961.
18. Bouhuys, A. and G. Lundin. Distribution of inspired gas in the lungs. *Physiol. Rev.* 39:731-750, 1959.
19. Bradley, M.E., N.R. Anthonisen, J. Vorosmarti, and P.G. Linaweaver. Respiratory and cardiac responses to exercise in subjects breathing helium-oxygen mixtures at pressures from sea level to 19.2 atmospheres. In: Underwater Physiology, edited by C.J. Lambertsen, New York: Academic Press, 1971, pp. 325-337.
20. Briscoe, W.A. and A.B. DuBois. The relationship between airway resistance, airway conductance and lung volume in subjects of different age and body size. *J. Clin. Invest.* 37:1279-1285, 1958.
21. Bryan, A.C., L.G. Bentivoglio, F. Beerel, H. Macleish, A. Zidulka, and D.V. Bates. Factors affecting regional distribution of ventilation and perfusion in the lung. *J. Appl. Physiol.* 19:395-402, 1964.
22. Butler, J., C.G. Caro, R. Alcalá, and A.B. Dubois. Physiological factors affecting airway resistance in normal subjects and in patients with obstructive respiratory disease. *J. Clin. Invest.* 39:584-591, 1960.
23. Gerretelli, P., S. Sikand, L. Farhi. Effect of increased airway resistance on ventilation and gas exchange during exercise. *J. Appl. Physiol.* 27:597-600, 1969.
24. Cherniack, R.M. and D.P. Snidal. The effect of obstruction to breathing on the ventilatory response to CO₂. *J. Clin. Invest.* 35:1286-1290, 1956.
25. Chow, C. and Y. Lai. Alternating flow in the trachea. *Resp. Physiol.* 16:22-32, 1972.
26. Clarke, S.W., J.G. Jones, and D.H. Glaister. Change in pulmonary ventilation in different postures. *Clin. Sci.* 37:357-369, 1969.
27. Clarke, S.W., J.G. Jones, and D.R. Oliver. Resistance to two-phase gas-liquid flow in airways. *J. Appl. Physiol.* 29(4):464-471, 1970.
28. Cumming, G. Gas mixing efficiency in the human lung. *Resp. Physiol.* 2:213-224, 1967.

29. Cumming, G., J. Crank, K. Horshfield, and I. Parker. Gaseous diffusion in the airways of the human lung. *Resp. Physiol.* 1:58-74, 1966.
30. Cumming, G., K. Horshfield, J.G. Jones, and D.C.F. Muir. The influence of gaseous diffusion on the alveolar plateau at different lung volumes. *Resp. Physiol.* 2:386-398, 1967.
31. Cumming, G., K. Horshfield, and S.B. Preston. Diffusion equilibrium in the lungs examined by nodal analysis. *Resp. Physiol.* 12:329-345, 1971.
32. Cutillo, A., E. Ombroni, and S. Delgrossi. Effect of respiratory frequency on the distribution of inspired gas in normal subjects and in patients with chronic obstructive lung disease. *Am. Rev. Resp. Dis.* 105:756-767, 1972.
33. Daly, W.J. and S. Bondurant. Direct measurement of respiratory pleural pressure changes in normal man. *J. Appl. Physiol.* 18:513-518, 1963.
34. Dean, B. and M.B. Visscher. The kinetics of lung ventilation. *Am. J. Physiol.* 134:450-468, 1941.
35. Dekker, E. Transition between laminar and turbulent flow in the human trachea. *J. Appl. Physiol.* 16:1060-1064, 1961.
36. Dollfuss, R.E., J. Milic-Emili, and D.V. Bates. Regional ventilation of the lung, studied with boluses of ¹³³Xenon. *Resp. Physiol.* 2:234-246, 1967.
37. DuBois, A.B., S.Y. Botelho, and J.H. Comroe, Jr. A new method for measuring airway resistance in man using a body plethysmograph: Values in normal subjects and in patients with respiratory disease. *J. Clin. Invest.* 35:327-335, 1956.
38. Engel, L.A., H. Menkes, L.D.H. Wood, G. Utz, J. Joubert, and P.T. Macklem. Gas mixing during breathholding studied by intrapulmonary gas sampling. *J. Appl. Physiol.* 35:9-17, 1973.
39. Engel, L.A., G. Utz, L.D.H. Wood and P.T. Macklem. Ventilation distribution in anatomical lung units. *J. Appl. Physiol.* In press.
40. Engel, L.A., L.D.H. Wood, G. Utz, and P.T. Macklem. Gas mixing during inspiration. *J. Appl. Physiol.* 35:18-24, 1973.
41. Farhi, L. Diffusive and convective movement of gas in the lung. In: Circulatory and Respiratory Mass Transport, edited by G.E.W. Wolstenholme and J. Knight. London: Churchill, 1969, pp. 277-293.
42. Farhi, L., A.B. Otis, and D.F. Proctor. Measurement of intrapleural pressure at different points in the chest of the dog. *J. Appl. Physiol.* 10:15-18, 1957.

43. Faridy, E.E., R. Kidd, and J. Milic-Emili. Topographical distribution of inspired gas in excised lobes of dogs. *J. Appl. Physiol.* 22:760-766, 1967.
44. Ferris, B.G., Jr., J. Mead, and L.H. Opie. Partitioning of respiratory flow resistance in man. *J. Appl. Physiol.* 19:653-658, 1964.
45. Finucane, K.E., B.A. Egan, and S. V. Dawson. Linearity and frequency response of pneumotachographs. *J. Appl. Physiol.* 32:121-126, 1972.
46. Flynn, E.T., H.A. Saltzman, and J.K. Summitt. Effects of head-out immersion at 19.18 Ata on pulmonary gas exchange in man. *J. Appl. Physiol.* 33:113-119, 1972.
47. Fowler, W.S. Intrapulmonary distribution of inspired gas. *Physiol. Rev.* 32:1-20, 1952.
48. Frank, N.R. A comparison of static volume pressure relations of excised pulmonary lobes of dogs. *J. Appl. Physiol.* 18:274-278, 1963.
49. Fry, D.L. Physiologic recording by modern instruments with particular reference to pressure recording. *Physiol. Rev.* 40:753-788, 1960.
50. Fry, D.L., R.V. Lbert, W.W. Stead, and C.C. Brown. Mechanics of pulmonary ventilation in normal subjects and in patients with emphysema. *Am. J. Med.* 16:80-97, 1954.
51. Fry, D. L. and R.E. Hyatt. Pulmonary mechanics. A unified analysis of the relationship between pressure, volume and gas flow in the lungs of normal and diseased human subjects. *Amer. J. Med.* 29:672-689, 1960.
52. Fukaya, H., C.J. Martin, A.C. Young, and S. Katsura. Mechanical properties of alveolar walls. *J. Appl. Physiol.* 25:689-695, 1968.
53. Gensler, E.A., J.V. Maloney, and V.O. Bjork. Bronchspirometry II - Experimental observations and theoretical considerations of resistance breathing. *J. Lab. and Clin. Med.* 39:935-953, 1952.
54. Georg, J., N.A. Lassen, K. Mellemegaard, and A. Vinther. Diffusion in the gas phase of the lungs in normal and emphysematous subjects. *Clin. Sci.* 29:525-532, 1965.
55. Glauser, S.C., E.M. Glauser, and B.F. Rusy. Gas density and the work of breathing. *Resp. Physiol.* 2:344-350, 1967.
56. Glazier, J.B., J.M.B. Hughes, J.E. Maloney, and J.B. West. Vertical gradient of alveolar size in lungs of dogs frozen intact. *J. Appl. Physiol.* 23:694-705, 1967.
57. Gomez, D.M., W.A. Briscoe, and G. Cumming. Continuous distribution of specific tidal volume throughout the lung. *J. Appl. Physiol.* 19:683-692, 1964.

58. Grape, B., E. Channin, and J.M. Tyler. The effect of helium oxygen mixtures on pulmonary resistances in emphysema. *Am. Rev. Resp. Dis.* 81:823-829, 1960.
59. Green, M. How big are the bronchioles? *St. Thom. Hosp. Gazette.* 63:136-139, 1965.
60. Grimby, G. and J. Stiksa. Flow-volume curves and breathing patterns during exercise in patients with obstructive lung disease. *Scand. J. Clin. Lab. Invest.* 25:303-313, 1970.
61. Hogg, J.C., P.T. Macklem, and W.M. Thurlbeck. Site and nature of airway obstruction in chronic obstructive lung disease. *New Engl. J. Med.* 278:1355-1360, 1968.
62. Horsfield, K. and G. Cumming. Morphology of the bronchial tree in man. *J. Appl. Physiol.* 24:373-383, 1968.
63. Horsfield, K. and G. Cumming. Functional consequences of airway morphology. *J. Appl. Physiol.* 24:384-390, 1968.
64. Hyatt, R.E. and R.E. Wilcox. Extrathoracic resistance in man. *J. Appl. Physiol.* 16:326-330, 1961.
65. Hyatt, R.E. and R.E. Wilcox. The pressure-flow relationships of the intrathoracic airway in man. *J. Clin. Invest.* 42:29-39, 1963.
66. Ingiam, R.H., Jr. and D.P. Schilder. Association of a decrease in dynamic compliance with a change in gas distribution. *J. Appl. Physiol.* 23:911-916, 1967.
67. Ishikawa, K., C.J. Martin, and A.C. Young. Pressure-volume studies on lung lobes in man. *J. Appl. Physiol.* 19:823-826, 1964.
68. Jarrett, A.S. Alveolar carbon dioxide tension at increased ambient pressures. *J. Appl. Physiol.* 21:158-162, 1966.
69. Jaeger, M.J. and H. Matthys. The pattern of flow in the upper human airways. *Resp. Physiol.* 6:113-127, 1968-69.
70. Jaeger, M.J. and H. Matthys. The pressure flow characteristics of the human airways. In: Airway Dynamics, edited by A. Bouhuys, Springfield, Ill.: Thomas, 1970, pp. 21-32.
71. Jaeger, M.J. and A.B. Otis. Measurement of airway resistance with a volume displacement plethysmograph. *J. Appl. Physiol.* 19:813-820, 1964.
72. Jones, J.G. and S.W. Clarke. The effect of expiratory flow rate on regional lung emptying. *Clin. Sci.* 37:343-356, 1969.

73. Jonson, B. Pulmonary mechanics in normal men studied with the flow regulator method. Scand. J. Clin. Lab. Invest. 25(4): 363-373, 1970.
74. Kjellmer, I., L. Sandquist, and E. Berglund. 'Alveolar plateau' of the single breath nitrogen elimination curve in normal subjects. J. Appl. Physiol. 14:105-108, 1959.
75. Koler, J.J., A.C. Young, and C.J. Martin. Relative volume changes between lobes of the lung. J. Appl. Physiol. 14:345-347, 1959.
76. Krogh, A. and J. Lindhard. On the average composition of the alveolar air and its variations during the respiratory cycle. J. Physiol. (London). 47:431-445, 1914.
77. Kylstra, J.A., G.V. Paganelli, and E.H. Lanphier. Pulmonary gas exchange in dogs ventilated with hyperbarically oxygenated liquid. J. Appl. Physiol. 21:177-184, 1966.
78. LaForce, R.C. and B.M. Lewis. Diffusional transport in the human lung. J. Appl. Physiol. 28:291-298, 1970.
79. Lanphier, E.H. Influence of increased ambient pressure upon alveolar ventilation. In: Proceedings of the Second Symposium on Underwater Physiology, edited by C.J. Lambertsen and L.J. Greenbaum, Jr., Washington, D.C.: Natl. Acad. Sci. - Natl. Res. Council, 1963, pp. 124-133.
80. Levison, H. and R.M. Cherniack. Ventilatory cost of exercise in chronic obstructive pulmonary disease. J. Appl. Physiol. 25:21-27, 1968.
81. Macklem, P.T. Airways obstruction and collateral ventilation. Physiol. Rev. 51:368-436, 1971.
82. Macklem, P.T. and J. Mead. Resistance of central and peripheral airways measured by a retrograde catheter. J. Appl. Physiol. 22:395-401, 1967.
83. Macklem, P.T. and J. Mead. Factors determining maximum expiratory flow in dogs. J. Appl. Physiol. 25:159-169, 1968.
84. Macklem, P.T., A.J. Woolcock, J.C. Hogg, J.A. Nadel, and N.J. Wilson. Partitioning of pulmonary resistance in the dog. J. Appl. Physiol. 26:798-805, 1969.
85. Maio, D.A. and L.E. Farhi. Effect of gas density on mechanics of breathing. J. Appl. Physiol. 23:687-693, 1967.
86. Marshall, R. and A.B. DuBois. The measurement of viscous resistance of the lungs of normal man. Clin. Sci. 15:161-170, 1956.

87. Marshall, R., E.H. Lanphier, and A.B. DuBois. Resistance to breathing in normal subjects during simulated dives. *J. Appl. Physiol.* 9:5-10, 1956.
88. Martin, C.J. and A.C. Young. Lobar ventilation in man. *Am. Rev. Tuberc.* 73:330-337, 1956.
89. Martin, R.R., N.R. Anthonisen, and M. Zutter. Flow dependence of the intrapulmonary distribution of inspired boluses of ^{133}Xe in smokers and non-smokers. *Clin. Sci.* 43:319-329, 1972.
90. Martin, R.R., J.E. Wilson, W.R.D. Ross, and N.R. Anthonisen. Detection of unequal time constants in the lung by ^{133}Xe technique. *Bull. de Physio-Path. Resp.* 7:291-298, 1971.
91. Martin, R.R., J.E. Wilson, W.R.D. Ross, and N.R. Anthonisen. The effect of added external resistance on regional pulmonary filling and emptying sequence. *Can. J. Physiol. Pharmacol.* 49:406-411, 1971.
92. Martin, R.R., M. Zutter, and N.R. Anthonisen. Pulmonary gas exchange in dogs breathing SF_6 at 4 Ata. *J. Appl. Physiol.* 33(1): 86-92, 1972.
93. Matthews, C.M.F. and C.T. Dollery. Interpretation of ^{133}Xe lung wash-in and wash-out curves using an analogue computer. *Clin. Sci.* 28:573-590, 1965.
94. McIlroy, M.B., J. Mead, N.J. Selverstone, and E.P. Radford, Jr. Measurement of lung tissue viscous resistance using gases of equal kinematic viscosity. *J. Appl. Physiol.* 7:485-490, 1955.
95. McIlroy, M.B. and R.V. Christie. A post-mortem study of the visco-elastic properties of normal lungs. *Thorax.* 7:291-295, 1952.
96. Mead, J. Measurement of inertia of the lungs at increased ambient pressure. *J. Appl. Physiol.* 9:208-212, 1956.
97. Mead, J. Control of respiratory frequency. *J. Appl. Physiol.* 15:325-336, 1960.
98. Mead, J. Volume displacement body plethysmograph for respiratory measurements in human subjects. *J. Appl. Physiol.* 15:736-740, 1960.
99. Mead, J. Mechanical properties of lungs. *Physiol. Rev.* 41:281-330, 1961.
100. Mead, J. Contribution of compliance of airways to frequency-dependent behavior of lungs. *J. Appl. Physiol.* 26:670-673, 1969.
101. Mead, J. The distribution of gas flow in lungs. In: Circulatory and Respiratory Mass Transport, edited by G.E.W. Wolstenholme and J. Knight. London: Churchill, 1969, pp. 204-209.

102. Mead, J., T. Takishima, and D. Leith. Stress distribution in lungs: A model of pulmonary elasticity. *J. Appl. Physiol.* 28:596-608, 1970.
103. Mead, J., J.M. Turner, P.T. Macklem, and J.B. Little. Significance of the relationship between lung recoil and maximum expiratory flow. *J. Appl. Physiol.* 22(1):95-108, 1967.
104. Mead, J. and J.L. Whittenberger. Physical properties of human lungs measured during spontaneous respiration. *J. Appl. Physiol.* 5:779-796, 1953.
105. Menkes, H., D. Lindsay, L. Wood, A. Muir, and P.T. Macklem. Interdependence of lung units in intact dog lungs. *J. Appl. Physiol.* 32:681-686, 1972.
106. Milic-Emili, J. and J.M. Tyler. Relation between work output of respiratory muscles and end-tidal CO₂ tension. *J. Appl. Physiol.* 18(3):497-504, 1963.
107. Milic-Emili, J., J.A.M. Henderson, M.B. Dolovich, D. Trop, and K. Kaneko. Regional distribution of inspired gas in the lung. *J. Appl. Physiol.* 21:749-759, 1966.
108. Millette, B., P.C. Robertson, W.R.D. Ross, and N.R. Anthonisen. Effect of expiratory flow rate on emptying of lung regions. *J. Appl. Physiol.* 27:587-591, 1969.
109. Murphy, T.M., W.H. Clark, I.P.B. Buckingham, and W.A. Young. Respiratory gas exchange in exercise during helium-oxygen breathing. *J. Appl. Physiol.* 26(3):303-307, 1969.
110. Nisell, O. and L. Ehrner. The resistance to breathing determined from time-marked respiratory pressure volume loops. *Acta Med. Scand.* 161(6):427-436, 1958.
111. Nye, R.E. Theoretical limits to measurements of uneven ventilation. *J. Appl. Physiol.* 16:1115-1124, 1961.
112. Olatsson, S. and R.E. Hyatt. Ventilatory mechanics and expiratory flow limitation during exercise in normal subjects. *J. Clin. Invest.* 48:564-573, 1969.
113. Olson, D.E., G.A. Dart, and G.F. Filley. Pressure drop and fluid flow regime of air inspired into the human lung. *J. Appl. Physiol.* 28(4):482-494, 1970.
114. Otis, A.B. and W.C. Bembower. Effect of gas density on resistance to respiratory gas flow in man. *J. Appl. Physiol.* 2:300-306, 1949.
115. Otis, A.B., C.B. McKerrow, R.A. Bartlett, J. Mead, M.B. McIlroy, N.J. Selverstone, and E.P. Radford. Mechanical factors in the distribution of pulmonary ventilation. *J. Appl. Physiol.* 8:427-443, 1956.

116. Overfield, E.M. and J.A. Kylstra. Distribution component of alveolar-arterial oxygen pressure difference in man. *J. Appl. Physiol.* 27:634-636, 1964.
117. Overfield, E.M., H.A. Saltzman, J.A. Kylstra, and J.V. Salzano. Respiratory gas exchange in normal men breathing .9% oxygen in helium at 31.3 Atm. *J. Appl. Physiol.* 27:471-475, 1969.
118. Parker, D.C. and E. Nagel. The effects of breathing a high density gas upon carbon dioxide elimination. In: Underwater Physiology, edited by C.J. Lambertsen, New York: Academic Press, 1971, pp. 379-384.
119. Pedley, T.J., R.C. Schroter, and M.F. Sudlow. Energy losses and pressure drop in models of human airways. *Resp. Physiol.* 9:371-386, 1970.
120. Pedley, T.J., R.C. Schroter, and M.F. Sudlow. The prediction of pressure drop and variation of resistance within the human bronchial airways. *Resp. Physiol.* 9:387-405, 1970.
121. Pedley, T.J., R.C. Schroter, and M.F. Sudlow. Flow and pressure drop in systems of repeatedly branching tubes. *J. Fluid. Mech.* 46:365-383, 1971.
122. Pedley, T.J., M.F. Sudlow, and J. Milic-Emili. A non-linear theory of the distribution of pulmonary ventilation. *Resp. Physiol.* 15:1-38, 1972.
123. Piiper, J. and P. Scheid. Respiration: Alveolar gas exchange. *Annu. Rev. Physiol.* 33:131-154, 1971.
124. Potter, W.A., S. Olafsson, and R.E. Hyatt. Ventilatory mechanics and expiratory flow limitation during exercise in patients with obstructive lung disease. *J. Clin. Invest.* 50:910-919, 1971.
125. Power, G.G. Gaseous diffusion between airways and alveoli in the human lung. *J. Appl. Physiol.* 27:701-709, 1969.
126. Prandtl, L. and O.G. Tietjens. Applied Hydro and Aeromechanics. New York: Dover Publications, 1957, pp. 1-85.
127. Pride, N.B., S. Permutt, R.L. Riley, and B. Bromberger-Barnea. Determinants of maximal expiratory flow from the lungs. *J. Appl. Physiol.* 23:646-662, 1967.
128. Radford, E.P. The physics of gases. In: Handbook of Physiology, edited by W.O. Fenn and H. Rahn. Washington, D.C.: Am. Physiol. Soc., 1964, sect. 3, vol. 1, pp. 125-152.
129. Rauwerda, P.E. Unequal ventilation of different parts of the lung and the determination of cardiac output. PhD thesis, State Univ. Groningen, Groningen, Netherlands, pp. 152, 1946.

130. Read, J. Stratified pulmonary blood flow: Some consequences in emphysema and pulmonary embolism. *Brit. Med. J.* 2:44-46, 1969.
131. Read, J. Redistribution of stratified pulmonary blood flow during exercise. *J. Appl. Physiol.* 27:374-7, 1969.
132. Robertson, C.H., D.L. Hall, and J.C. Hogg. A description of lung distortion due to localized pleural stress. *J. Appl. Physiol.* 34:344-50, 1973.
133. Robertson, J.S., W.E. Siri, and H.B. Jones. Lung ventilation patterns determined by analysis of nitrogen elimination ratio; use of the mass spectrometer as a continuous gas analyzer. *J. Clin. Invest.* 29:577-590, 1950.
134. Robertson, P.C., N.R. Anthonisen, and D. Ross. Effect of inspiratory flow rate on regional distribution of inspired gas. *J. Appl. Physiol.* 26:438-443, 1969.
135. Rohrer, F. Der strömungswiderstand in den menschlichen atemwegen und der einfluss der unregelmässigen verzweigung des bronchial systems uaf den atmungsverlauf in verschifdenen lungenbezirken. *Arch. ges. Physiol.* 162:225-299, 1915.
136. Roos, A., H. Dahlstrom, and J.P. Murphy. Distribution of inspired air in the lungs. *J. Appl. Physiol.* 7:645-659, 1955.
137. Ross, B.B. Influence of bronchial tree structure on ventilation in the dog's lung as inferred from measurements of a plastic cast. *J. Appl. Physiol.* 10:1-14, 1957.
138. Ross, B.B. and L.E. Farhi. Dead-space ventilation as a determinant in the ventilation-perfusion concept. *J. Appl. Physiol.* 15(3): 363-371, 1960.
139. Saltzman, H.A., J.V. Salzano, G.O. Blenkarn, and J.A. Kylstra. Effects of pressure on ventilation and gas exchange in man. *J. Appl. Physiol.* 30(4):443-449, 1971.
140. Salzano, J., D.C. Rausch, and H.A. Saltzman. Cardiorespiratory responses to exercise at a simulated seawater depth of 1,000 feet. *J. Appl. Physiol.* 28(1):34-41, 1970.
141. Saranoff, I. and G.E. Emmanuel. The effect of pendelluft and dead space on nitrogen clearance: Mathematical and experimental models and their application to the study of the distribution of ventilation. *J. Clin. Invest.* 46:1683-1693, 1967.
142. Schilder, D.P., A. Roberts, and D.L. Fry. Effect of gas density and viscosity on the maximal expiratory flow-volume relationship. *J. Clin. Invest.* 42(11):1705-1713, 1963.

143. Schilder, D.P., A. Roberts, J.C. Greenfield, Jr., and D.L. Fry. Regional distribution of intraesophageal pressure in normal and emphysematous subjects. *J. Appl. Physiol.* 20:209-214, 1965.
144. Schiller, I.W., F.C. Lowell, M.T. Lynch, and W. Franklin. The effect of helium-oxygen mixtures on pulmonary function in asthmatic patients. *J. Allergy*, 26:11-15, 1955.
145. Schroter, R.C. and M.F. Sudlow. Flow patterns in models of the human bronchial airways. *Resp. Physiol.* 7:341-355, 1969.
146. Sekihara, T., D.E. Olsen, and G.F. Filley. Airflow regimes and geometrical factors in the human airway. In: Proc. 11th Aspen Emphysema Conference. Washington, D.C.: U.S. Public Health Service, 1968, pp. 103-113.
147. Sikand, R., P. Cerretelli, and L.B. Fahl. Effects of \dot{V}_A and \dot{V}_A/Q distribution and of time on the alveolar plateau. *J. Appl. Physiol.* 21:1331-1337, 1966.
148. Spann, R.W. and R.E. Hyatt. Factors affecting upper airway resistance in conscious man. *J. Appl. Physiol.* 31:708-712, 1971.
149. Suda, Y., C.J. Martin, and A.C. Young. Regional dispersion of volume to ventilation ratios in the lung of man. *J. Appl. Physiol.* 24:480-485, 1970.
150. Sugihara, T., J. Hildebrandt, and C.J. Martin. Viscoelastic properties of the alveolar wall. *J. Appl. Physiol.* 33:93-98, 1972.
151. Sugihara, T., C.J. Martin, and J. Hildebrandt. Length-tension properties of the alveolar wall in man. *J. Appl. Physiol.* 30:874-878, 1971.
152. Sutherland, P.W., T. Katsura, and J. Milic-Emili. Previous volume history of the lung and regional distribution of inspired gas. *J. Appl. Physiol.* 25:566-574, 1968.
153. Takishima, T., G. Grimby, W. Graham, R. Knudson, P.T. Macklem, and J. Mead. Flow-volume curves during quiet breathing, maximum voluntary ventilation, and forced vital capacities in patients with obstructive lung disease. *Scand. J. Resp. Dis.* 48:384-393, 1967.
154. Taylor, G. Dispersion of soluble matter in solvent flowing slowly through a tube. *Proc. Roy. Soc. Lond.* A219:186-203, 1953.
155. Tsunoda, S., A.C. Young, and C.J. Martin. Emptying pattern of lung compartments in normal man. *J. Appl. Physiol.* 32:644-649, 1972.
156. Varene, P., J. Timbal, and C. Jacquemin. Effect of different ambient pressures on airways resistance. *J. Appl. Physiol.* 22:699-706, 1967.

157. Vincent, N.J., R. Knudson, D.E. Leith, P.T. Macklem, and J. Mead. Factors influencing pulmonary resistance. *J. Appl. Physiol.* 29:236-243, 1970.
158. Wagner, P., J. McRae, and J. Read. Stratified distribution of blood flow in secondary lobule of the rat lung. *J. Appl. Physiol.* 22:1115-1123, 1967.
159. Weibel, E.R. Morphometry of the Human Lung. New York: Academic Press, 1963, pp. 151.
160. West, J.B. Regional differences in gas exchange in the lung of erect man. *J. Appl. Physiol.* 17:893-898, 1962.
161. West, J.B., J.B. Glazier, J.M.B. Hughes, and J.E. Maloney. Pulmonary capillary flow, diffusion ventilation and gas exchange. In: Circulatory and Respiratory Mass Transport, edited by G.E.W. Wolstenholme and J. Knight. London: Churchill, 1969, pp. 256-272.
162. West, J.B. and P. Hughes-Jones. Patterns of gas flow in the upper bronchial tree. *J. Appl. Physiol.* 14:753-759, 1959.
163. West, J.B. and P. Hughes-Jones. Pulsatile gas flow in bronchi caused by the heart beat. *J. Appl. Physiol.* 16:697-702, 1961.
164. Wood, L.D.H. and A.C. Bryan. Effect of increased ambient pressure on flow-volume curve of the lung. *J. Appl. Physiol.* 27(1):4-8, 1969.
165. Wood, L.D.H., Sarah Pritchard, T.R. Weng, K.A. Krueger, A.C. Bryan, H. Levison. Relationship between anatomic dead-space and body size in health, asthma and cystic fibrosis. *Am. Rev. Resp. Dis.* 104:215-222, 1971.
166. Woolcock, A.J., N.J. Vincent, and P.T. Macklem. Frequency dependence of compliance as a test for obstruction in small airways. *J. Clin. Invest.* 48:1097-1106, 1969.
167. Wormersley, J.R. Oscillatory motion of a viscous liquid in a thin walled elastic tub. *Phil. Mag. Ser. 7*, 46:199-221, 1955.
168. Young, A.C. and C.J. Martin. The sequence of lobar emptying in man. *Resp. Physiol.* 1:372-381, 1966.
169. Young, A.C., C.J. Martin, and T. Hashimoto. Can the distribution of inspired gas be altered? *J. Appl. Physiol.* 24:129-133, 1968.
170. Young, A.C., C.J. Martin, and W.R. Pace, Jr. Effect of expiratory flow patterns on lung emptying. *J. Appl. Physiol.* 18:47-50, 1963.
171. Zidulka, A., M. Demedts, and N.R. Anthonisen. Lobar obstruction in dog lungs. *Fed. Proc.* 31:321, 1972. (Abstract)